CRANFIELD UNIVERSITY

T SPARKS

FLUID MIXING IN ROTOR/STATOR MIXERS

BIOTECHNOLOGY CENTRE

PhD

1996.

CRANFIELD UNIVERSITY

BIOTECHNOLOGY CENTRE

PhD

1992 - 1995

T SPARKS

FLUID MIXING IN ROTOR/STATOR MIXERS

Supervisor: Prof. D. E. Brown

Dec 1996

This thesis is submitted in partial fulfilment for the degree of doctor of philosophy

ABSTRACT

An industrial rotor-stator mixer was fitted into a flow loop to carry out overall power balance, flow visualisation and residence time distribution experiments. These were performed on various rotor-stator geometries and a half-scale unit.

The overall power measurements showed that a large amount of power was given to the fluid by the rotor and estimates of the local turbulent energy dissipation rate per unit mass, ε, were made using these data. It was found that the pumping efficiency of rotor-stator mixers is ~10 to 20% and an expression for the motor power (when the flow rate is controlled) was found.

The flow pattern was characterised by a high tangential velocity in the rotor followed by an abrupt transformation to radial flow through the stator. It was suggested that the kinetic energy of the fluid in the rotor is transformed to pumping, friction and turbulence in the stator and that this is the region of greatest importance for mixing.

The residence time distribution is characterised by a region of plug flow in series with a region of mixed flow. The flow through the volute has a dominant effect on the overall residence time distribution and the RTD is insensitive to operating condition (flow rate, rotor speed) or geometry.

The knowledge gained from the above experiments was used to design diazo-coupling experiments (a mixing-sensitive competitive chemical reaction with well known kinetics) such that they gave qualitative information (e.g. best feed position) and quantitative information (e.g. turbulent energy dissipation rate) on the performance of a rotor-stator mixer. ε was found to be proportional to the power given the fluid by the rotor and estimates for ε of order 500 W kg^{-1} were made using a micro-mixing model.

TABLE OF CONTENTS

Variable Print Quality

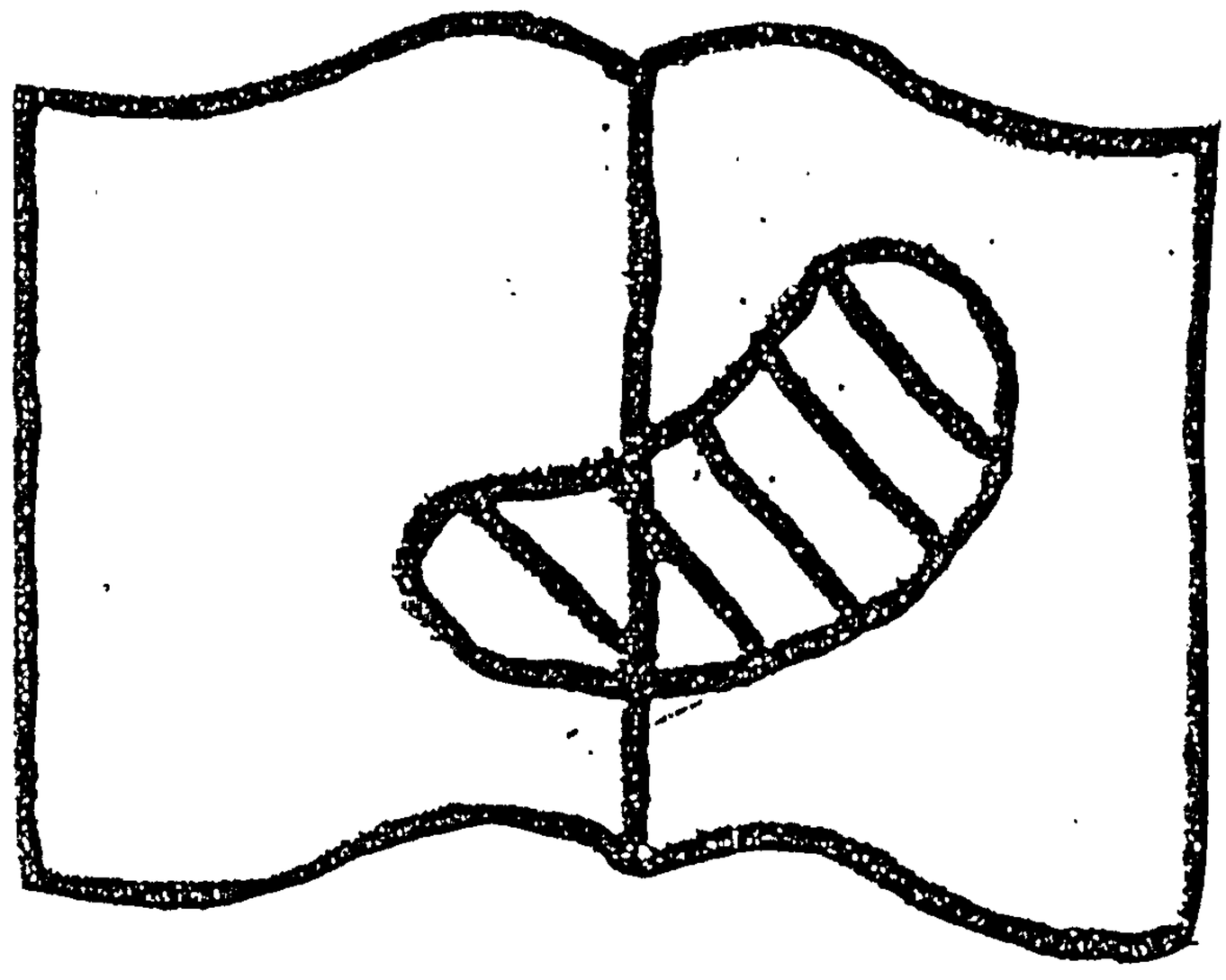

LIST OF FIGURES

LIST OF PLATES

LIST OF TABLES

NOTATION

Symbol	Meaning	Units
a	flow rate ratio	-
A	open area	m^2
A	species A	
B	species B	
C	species C	
C	exit concentration	-
c_i	concentration of species i	$mol.m^{-3}$
c_{B0}	initial concentration of B	$mol.m^{-3}$
C_i	dimensionless concentration of species i	-
d	light path	m
D	molecular diffusivity	$m^2.s^{-1}$
D	rotor diameter	m
Da	Damkohler number	-
E	engulfment rate	s^{-1}
E	rotor thickness	m
$E(k)$	spectral density of energy of wave number k	m^3s^{-1}
f	an exponent	-
$F(k)$	spectral density of concentration of wave number k	mol^2m^{-5}
g	an exponent	-
h	an exponent	-
k	reaction rate constant	$m^3.mol^{-1}.s^{-1}$
k	wave number of an eddy	m^{-1}
K	disc friction coefficient	-
L_0	initial scale of segregation	m

n	number of teeth on the rotor	-
n_{i0}	initial number of moles of species i	-
N	rotor speed	s^{-1}
m	mass of a fluid element	kg
P_{SHAFT}	shaft power	W
P_{PUMP}	pumping power	W
P_{MECH}	mechanical power losses	W
P_{DISC}	disc friction power losses	W
P_{LEAK}	leakage (recirculation) power losses	W
$P_{HYDRAULIC}$	hydraulic power losses	W
P_{STATIC}	static power losses (pressure drop)	W
P_{FLUID}	power supplied to the fluid by the rotor	W
Po	power number	-
Pn	power number	-
Q	flow rate	$l.s^{-1}$
Q	species Q	
R	species R	
Sc	Schmidt number	-
S	species S	
T	species T	
T	dimensionless time	-
t_D	diffusive mixing time	s
t_E	engulfment time	s
t_{MESO}	meso-mixing time	s
u	inlet pipe velocity	$m.s^{-1}$
v_{TIP}	rotor tip speed	$m.s^{-1}$
v_{RADIAL}	nominal radial velocity	$m.s^{-1}$
V	volume	m^3
V_P	volume of plug flow	m^3

V_M	volume of mixed flow	m^3
X	product distribution	-
X_Q	selectivity of Q	-
X_S	selectivity of S	-
X_B	volume fraction of B	-
Z_0	initial value of X_B	-
α	age of a fluid element in a reactor	-
β	reaction rate factor	-
Δp	differential pressure	Pa
ε	turbulent energy dissipation rate per unit mass	$W.kg^{-1}$
ϵ	molar absorbance coefficient	
η	pumping efficiency	-
η_{TURB}	turbulence efficiency factor	-
η'_{TURB}	turbulence efficiency factor (referring to statci losses)	-
θ	dimensionless time	-
Λ	shaft torque	N.m
λ	wavelength	m
λ_B	Batchelor micro-scale	m
λ_K	Kolmogorov micro-scale	m
ξ	stoichiometric ratio	-
σ	stoichiometric ratio	-
μ	dynamic viscosity	$kg.m^{-1}.s^{-1}$
ρ	density	$kg.m^{-3}$
τ	nominal residence time	s
Φ	power per unit mass	$W.kg^{-1}$
Φ'	power per unit mass due to static losses	$W.kg^{-1}$

ACKNOWLEDGEMENTS

I would like to thank the members of my support panel, for their indispensable support and guidance - Professor Don Brown, Mr Andrew Green and Dr Martyn Pendlebury. I learned a great deal from each of them.

I would also like to thank: Silverson Machines limited, who supplied the test unit; many of my colleagues at BHR Group, for their support, advice and encouragement; in particular Rahul Dogra, Ming Zhu, Joe Hannon, Steve Ruszkowski and Steve Hearn; John Brown, for his help with the experimental work; Pete Huckle and Bryan Atkinson who made the perspex casing and many of the rotor-stator units; the members of the HILINE project and Professor John Bourne.

Finally, I would like to thank my family; Naomi, who inspired me to start, and Lily, who arrived last year and did her best to stop me from finishing this thesis.

CHAPTER 1

INTRODUCTION and OBJECTIVES

Many chemical reactions are mixing sensitive, their outcome depending upon the rate at which reactants are brought together. Examples include some azo-couplings, polymerisations and nitrations. Rapid mixing of reagents may be necessary to avoid by-product formation, thus increasing useful yield.

Rotor-stator mixers are widely used in the process industries, mainly for the blending of viscous mixtures or particle size reduction (e.g. emulsification). They incorporate a high speed rotor spinning close to a motionless stator and any liquid or solid/liquid mixture passing through is subject to high shear forces, chopping and turbulence.

Very little work on rotor-stator mixers has been published. However, some of the work that has(Bourne & Garcias-Rosas, 1985; Studer, 1990) reports that they show promise as chemical reactors because of the extremely intense turbulence that they produce. These references report work done on small scale laboratory rotor-stator mixers, there are no references on using other, larger, rotor-stator mixers as chemical reactors in the literature. However, rotor-stator mixers are used for this purpose in industry.

The effectiveness of a chemical reactor depends upon many things, for example the flow pattern, residence time and rate of mixing; when designing a reactor it is advantageous to have knowledge of these. It is also desirable to have other information, such as running costs and (in this case) how the mixer will contribute to pumping the process fluid. All of this information is sparse in the literature.

Since the availability of information required to design or select a rotor-stator mixer (and then choose operating conditions) is limited, this work aims to improve the state of the knowledge - through an experimental study. Turbulent energy dissipation information (to be estimated initially from overall energy balances), flow visualisation and residence time distribution data need to be produced to allow the design of a rotor-stator reactor. Once these data are available, then diazo-coupling experiments can be designed.

The research was specifically focused on the investigation of in-line rotor-stator mixers:

> *an in-line rotor-stator mixer is one that fits into a process pipeline, rather like a centrifugal pump, often contributing a pumping effect.*

The objectives of this work, therefore, were:

(a) To set up a suitably instrumented flow loop system incorporating an industrially sized rotor-stator mixer unit.

(b) to produce overall power balance (e.g. shaft power input and pumping output), flow visualisation and residence time distribution data for a range of rotor-stator geometries;

(c) to produce overall power balance and residence time distribution data for a mixer at half-scale;

(d) to design reactive mixing experiments using estimates derived from the data produced above and to conduct these reactive mixing experiments;

(e) to develop a general and quantitative description of the flow and mixing characteristics of rotor-stator mixers.

CHAPTER 2

LITERATURE REVIEW

Rotor-stator mixers have been in existence for about fifty years and have been used successfully in a number of applications, including emulsification (e.g. Pedrocchi & Widmer, 1988; Holley & Weisser, 1982) and viscous blending (e.g. Bouette, 1974). Their application to low viscosity reactive mixing applications is less frequent, but still significant (e.g. Bourne & Studer, 1992).

2.1 Rotor-stator mixer design

Rotor-stator mixers resemble centrifugal pumps and some designs have significant pumping capacities. The main differences between centrifugal pumps and rotor-stator mixers are as follows:

(i) In a rotor-stator mixer there is a narrow gap between the rotor and stator, known as the shear gap. This is usually thought to be the region of the mixer where high shear forces disperse and homogenise any fluid passing through it. In contrast, the impeller in a centrifugal pump rotates with a large clearance from the stationary volute wall.

(ii) The impeller in a rotor-stator mixer is not normally optimised for pumping. Pump impellers have swept blades to transmit momentum to the pumped fluid, while minimising separation and recirculation losses.

(iii) The volute (or impeller discharge collection region) in a rotor-stator mixer is not optimised. Pumps usually have a spiral volute to minimise head loss

through gradual pressure recovery.

These distinctions are shown in Figure 2.1 - a rotor-stator mixer - and Figure 2.2 - a centrifugal pump. The similarities between rotor-stator mixers and centrifugal pumps are examined in more detail in Section 2.4.

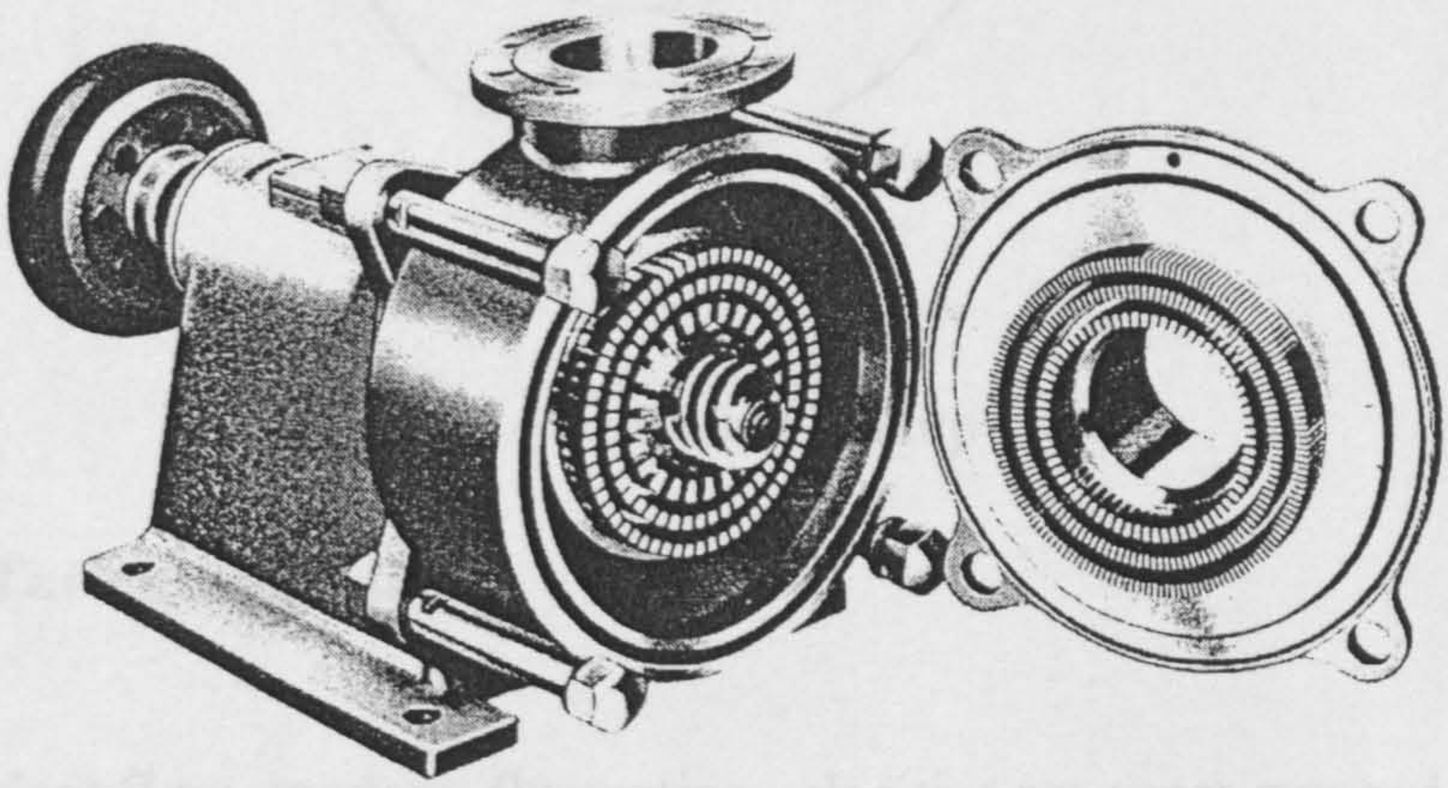

Figure 2.1 A rotor/stator mixer

2.2 Mixing processes

Mixing processes in turbulent flow will be discussed in this section to provide a basis for the literature on rotor-stator mixers.

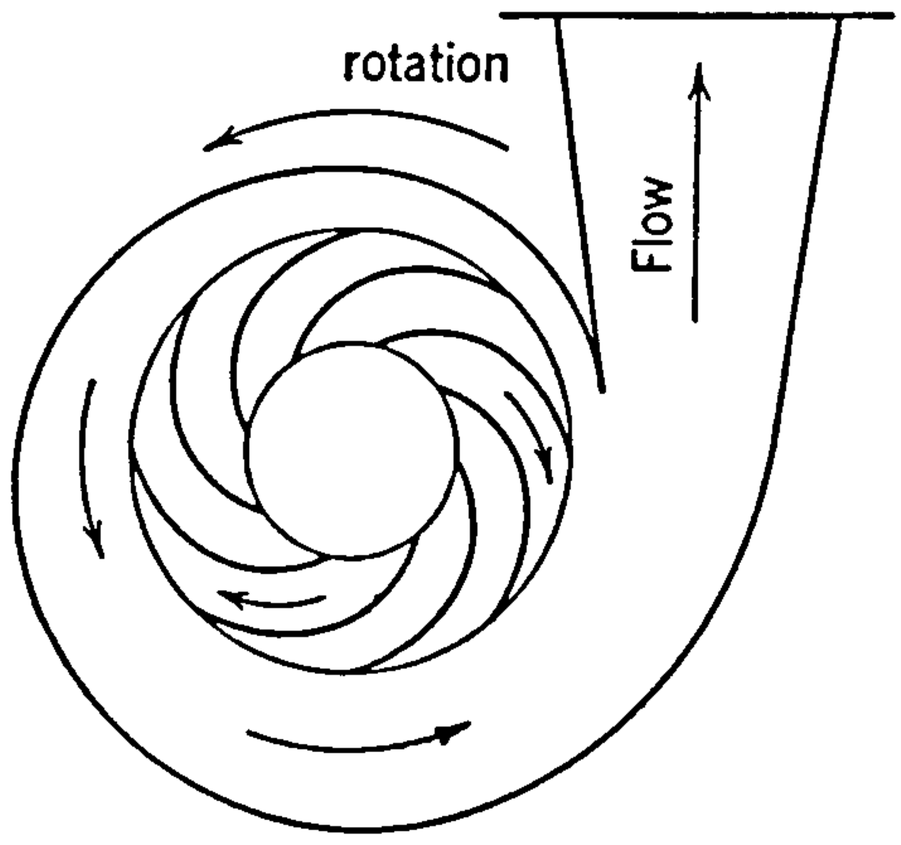

Figure 2.2 A centrifugal pump

2.2.1 Turbulent mixing

In turbulent flow, random, fluctuating velocities are superimposed upon the mean flow. Turbulence occurs as a result of the amplification of disturbances in the flow, when molecular viscosity no longer damps these disturbances and is consequently associated with high Reynolds numbers (a measure of the ratio of inertial to viscous forces). In turbulent flow the transport of concentration and momentum are orders of magnitude higher than in laminar flow, as illustrated by the rapid mixing of a dye tracer in turbulent flow.

Much of what follows in this section has been developed - principally by Baldyga and Bourne (e.g. Baldyga and Bourne, 1984; 1989) - from the Kolmogorov scenario for high Reynolds number turbulence (see Tennekes and Lumley, 1972). It is postulated that energy given to large eddies in the flow is passed on to ever smaller

eddies (down the 'energy cascade') until viscous dissipation to heat occurs within the smallest turbulent eddies. Below a certain eddy size (L), and at high enough Reynolds number, turbulent flow follows the 'universal' law shown in the energy spectrum curve (Figure 2.3) - a plot of the spectral density of kinetic energy at wave number k, which is proportional to the inverse of the eddy size. This curve shows energy supplied to turbulence through large scale eddies (the so-called energy containing eddies, in which the turbulent kinetic energy is highest) and energy dissipation within eddies below the Kolmogorov micro scale, λ_k, at which scale viscous forces become significant. In the range L to λ_k the spectrum follows the -3/5 law, and this is termed the inertial-convective sub-range.

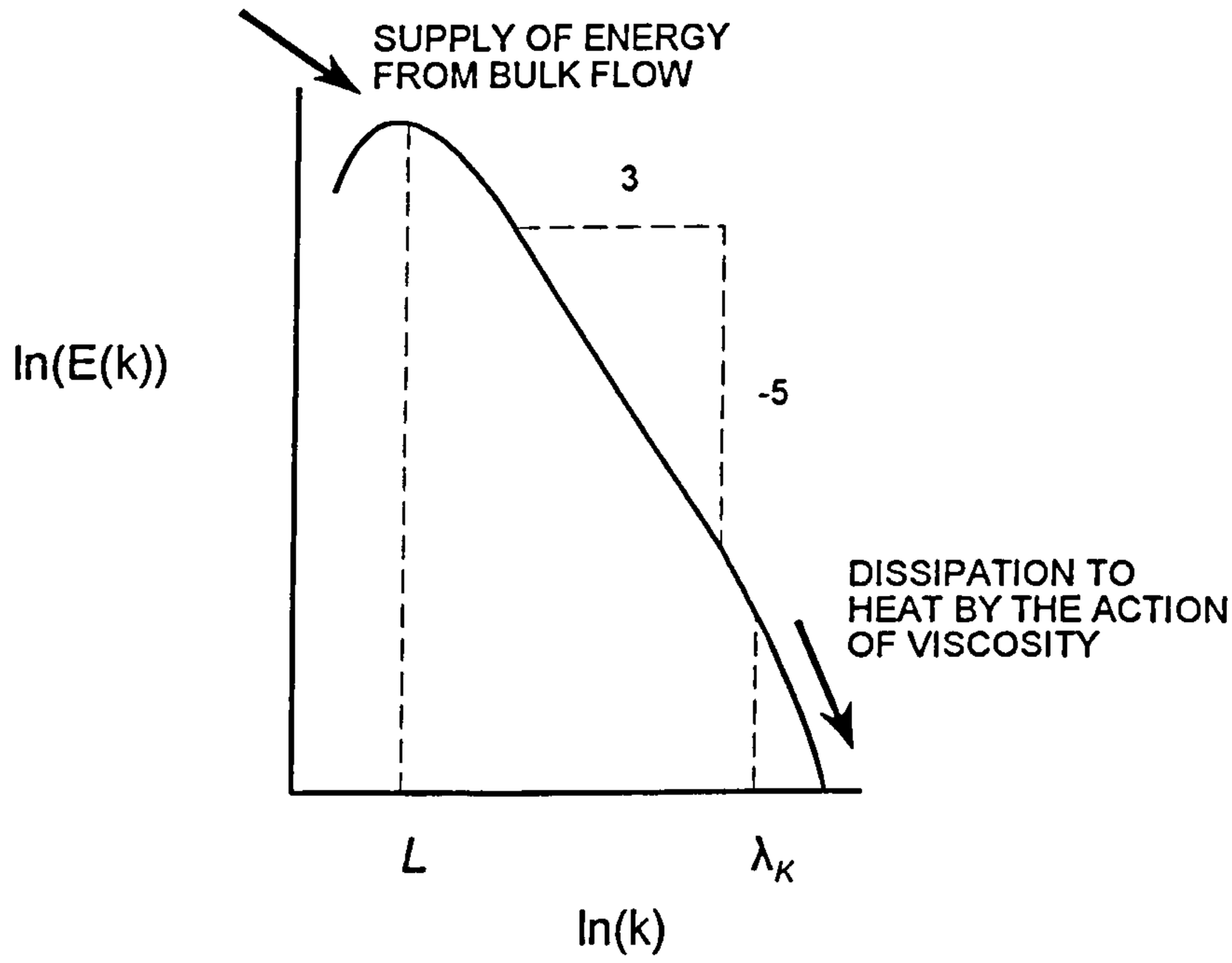

Figure 2.3 The energy spectrum. (Tennekes and Lumley, 1972)

The concentration spectrum for liquid mixtures is similar to the energy spectrum and characterises the concentration variance as and a function of eddy scale. Figure 2.4 (Baldyga and Bourne, 1984; Tennekes Lumley, 1972) shows the concentration spectrum for a liquid with large Schmidt number (where the kinematic viscosity is

much greater than molecular diffusivity, $\nu \gg D$). In Figure 2.4 the spectral density of concentration of wave number k at time t against k. In essence this plot shows that large concentration fluctuations are associated with small wave numbers (large eddies) and that large wave numbers (small eddies) contain small concentration fluctuations. Figure 2.4 shows how turbulence acts upon large scale fluctuations in concentration, ultimately reducing these fluctuations to the scale where molecular diffusion can act to bring about complete molecular mixing - allowing a chemical reaction to occur.

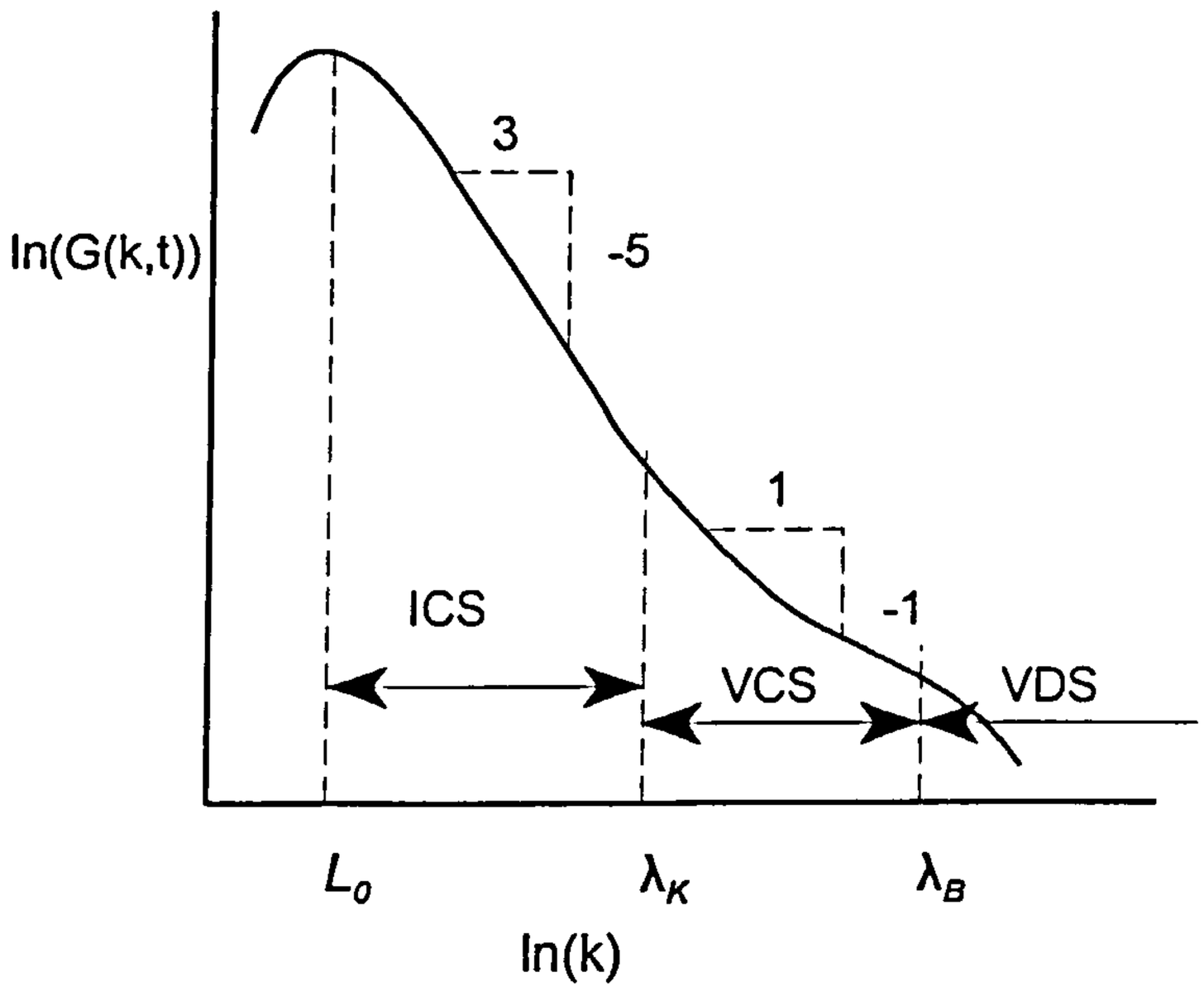

Figure 2.4 The concentration spectrum (Tennekes and Lumley, 1972)

The concentration spectrum is conventionally divided into three distinct regions: the inertial convective sub-range, ICS; the viscous convective sub-range, VCS; and the viscous diffusive sub-range, VDS (Tennekes and Lumley, 1972). The inertial convective sub-range extends from the largest eddy size, L_o, approximated by a

characteristic length of the equipment generating the flow (for example an impeller blade width in a stirred tank) to the Kolmogorov micro-scale, given by:

$$\lambda_K = \left(\frac{\mu^3}{\rho^3 \varepsilon} \right)^{1/4} \tag{2.1}$$

where μ is dynamic viscosity ($kg.m^{-1}.s^{-1}$), ρ is density ($kg.m^{-3}$) and ε is the turbulent energy dissipation rate per unit mass ($W.kg^{-1}$). Over this sub-range, mixing is independent of viscosity and molecular diffusion does not contribute to the reduction in variance (Bourne and Baldyga, 1984).

The viscous convective sub-range extends from the Kolmogorov micro-scale to the Batchelor micro-scale (Baldyga and Bourne, 1984):

$$\lambda_B = \left(\frac{\varepsilon \rho}{\mu D^2} \right)^{1/4} \tag{2.2}$$

where D is the molecular diffusivity ($m^2.s^{-1}$). In this part of the spectrum, molecular viscosity begins to affect eddy fluctuations and fluctuations are taken to the Batchelor micro-scale through laminar deformation. At the Batchelor micro-scale end of this sub-range, molecular diffusion becomes important.

Beyond this, in the viscous diffusive sub-range, molecular diffusion governs the rate at which concentration variance is dissipated. Full molecular mixing is completed in this sub-range.

Complete mixing results from the simultaneous occurrence of these mixing processes. The stages of mixing are categorised as (for example) 'macro'-mixing and 'micro'-mixing (Bourne and Baldyga, 1984a), and intermediate or 'meso'-mixing (Bourne and Baldyga, 1992).

2.2.2 Macro-mixing

The reduction in the variation of concentration or temperature on a coarse scale is termed macro-mixing and results from bulk flow patterns. It is often equipment dependent (i.e. to the left of the universal part of the concentration spectrum) and, if the flow is fully turbulent, macro-mixing is independent of viscosity.

Only the scale of segregation (or un-mixedness) is reduced by macro-mixing.

2.2.3 Meso-mixing

Meso-mixing is associated with the inertial convective sub-range and a time constant for meso-mixing in an isotropic turbulent mixer (given by Corrsin (1964) and used by Baldyga and Bourne (1992)) is given by:

$$t_{MESO} \sim \left(\frac{L_0^2}{\varepsilon}\right)^{1/3} \tag{2.3}$$

where L_0 is the initial scale of segregation. This gives the time required to reduce the scale of segregation from L to λ_K in a homogenous turbulence field with a dissipation rate of ε ($W.kg^{-1}$). It is also independent of viscosity.

2.2.4 Micro-mixing

A characteristic half-life for micro-mixing is the diffusive mixing time (Baldyga and Bourne, 1984), t_D, given by:

$$t_D \approx 2\left(\frac{\mu}{\rho\varepsilon}\right)^{1/2} arcsinh(0.05\,Sc) \tag{2.4}$$

Fluid engulfment (engulfment of reagents into eddies of other reagents) is often rate-determining (Baldyga and Bourne, 1989) and the appropriate characteristic half-life, t_E, is then given by:

$$t_E = 17\left(\frac{\mu}{\rho\varepsilon}\right)^{1/2} \tag{2.5}$$

2.2.5 Mixing and chemical reaction

The overall rate of a chemical reaction may depend upon both the intrinsic reaction kinetics and the rate of mixing. Chemical reactions can be classified as either slow, fast or instantaneous, with respect to the mixing rates. If the mixing time, t_M, is of the same order of magnitude as the reaction time, $t_{REACTION}$, then the reaction is labelled fast. Reactions where the mixing time is much less than the reaction time are termed slow and where the mixing time is much greater than the reaction time are termed instantaneous.

For many simple reactions, e.g. neutralisations, mixing rates will only affect the rate of productivity. However, with competing reactions the mixing rate can affect product selectivity or yield. Examples of these reactions include some azo-couplings, polymerisations and nitrations (Baldyga and Bourne, 1984).

Poor mixing can have undesirable economic, ecological and safety consequences, as illustrated by the following reaction scheme (Levenspiel, 1972):

$$A + B \rightarrow R \quad \text{(desired)} \tag{2.6}$$

$$R + B \rightarrow S \quad \text{(waste)} \tag{2.7}$$

The selectivity of products may be sensitive to mixing conditions. If the first (desirable) reaction is fast and the second (undesirable) is slow. Then, if *B* is fed slowly into *A* and then rapidly mixed, it reacts to form *R*, which is carried away.

However, if mixing is insufficiently rapid, when *R* is formed it will not be carried away from the reaction zone and some will combine again with *B* to form *S*. The selectivity of products is thus mixing-sensitive: it is a competitive chemical reaction. The product selectivity, *X*, for the reaction scheme given in Equations 2.6 and 2.7 is defined as:

$$X = \frac{2c_S}{(c_R + 2c_S)} \tag{2.8}$$

where c_S and c_R are the concentrations of *S* and *R* respectively.

If *R* is a high value product and *S* is a worthless or dangerous waste product, then it is necessary to maximise the yield of *R* (minimise *X*). This will improve the economics of the process, producing more *R* for given quantities of raw materials and reducing the need for the potentially expensive separation of *S* from the reaction products.

For a given set of chemical conditions (i.e. concentrations, stoichiometry), the best product selectivity can be obtained if micro-mixing is the rate limiting step (i.e slow compared to macro-mixing or meso-mixing). The probability of micro-mixing limiting a reaction increases when the reactor is run in semi-batch mode, the viscosity of the fluid is increased (Equation 2.5) or the number of feed tubes is increased (i.e. the macro-mixing is improved).

2.2.6 Feed rate and position

When conducting fast chemical reactions, the product selectivity can depend on the method by which reagents are introduced into the reactor, i.e. the feed tube arrangements (e.g. their position, size, and flow rates through them). Feeding high flow rates of the secondary reagent into a region of low mixing intensity can produce a dramatically different product selectivity from that obtained when feeding slowly into regions of high mixing intensity.

2.2.7 Flow pattern, residence time distribution

The other fluid dynamic consideration is the bulk flow pattern, i.e. what is occurring on the macro-scale. The reaction scheme given in Equations 2.6 and 2.7 would still produce some *S*, despite good micro-mixing close to a feed tube, if the flow patterns were such that the products of the first reaction were recirculated back into the reaction zone to combine with fresh reagents.

The bulk flow pattern throughout a mixer can be characterised by residence time distribution curves (Levenspiel, 1972). These are normally produced by measuring the outlet response to a pulse stimulus at the inlet. The two extreme flow patterns encountered in practice are dispersed plug flow and back mixed (Figure 2.5). When carrying out competitive chemical reactions, plug flow is normally desirable so that products are removed quickly from any fresh reagents.

Determination of the flow pattern, by using visualisation, analytical or computational techniques, is essential for the prediction of performance or diagnosis of the ills of reactors. Levenspiel (1972) gives a thorough background to this element of reactor design.

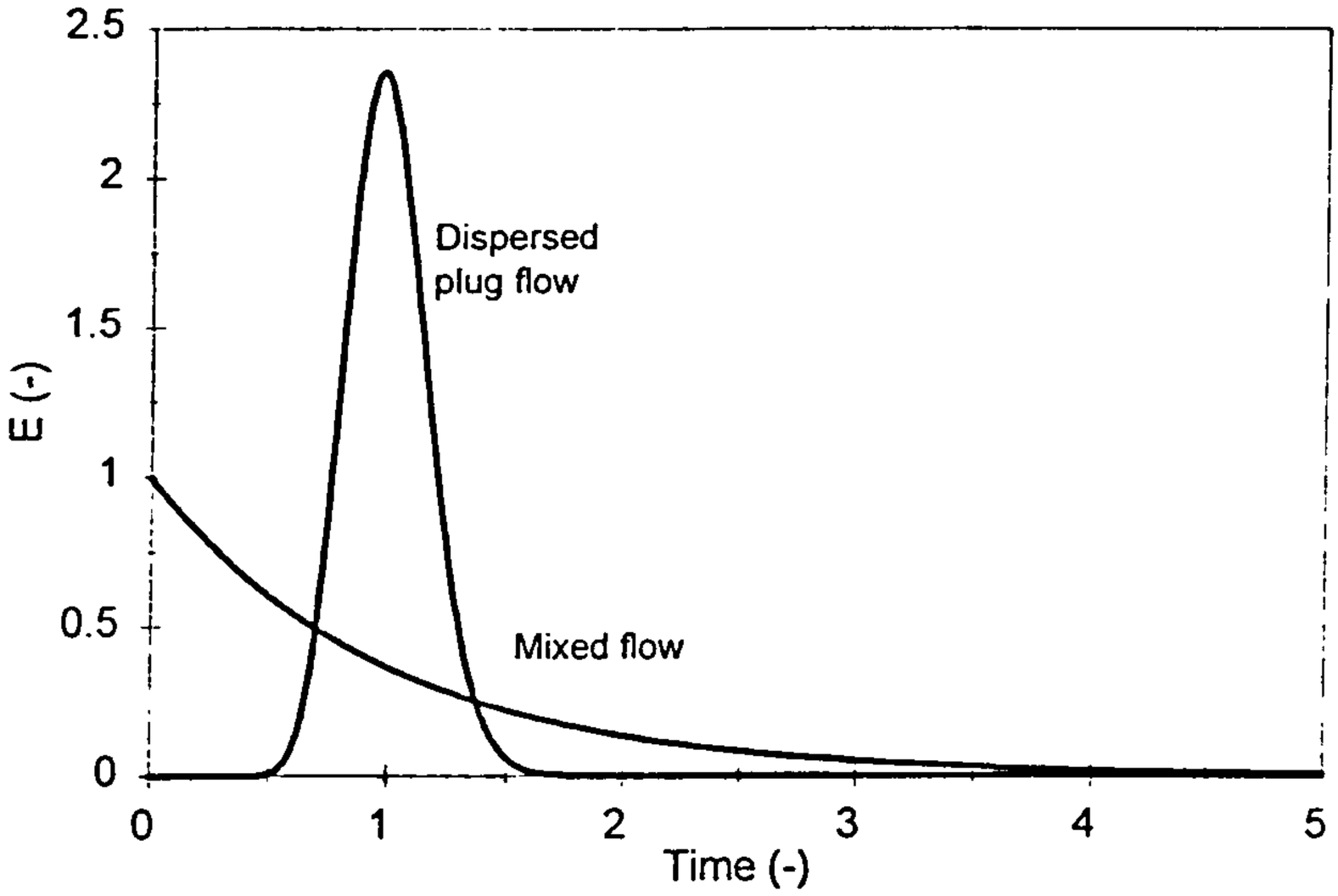

Figure 2.5 Residence time distribution curves for dispersed plug flow and mixed flow (Levenspiel, 1972)

2.2.8 Micro-mixing model

Baldyga and Bourne (1984) proposed a model for micro-mixing, the engulfment-deformation-diffusion model (EDD-model). Use of that model required the solution of a set of partial differential equations. Later, they simplified their model (Baldyga and Bourne, 1989), having identified the engulfment stage as rate determining under certain conditions; use of that model required the solution of a set of ordinary differential equations. This model is called the engulfment model (E-model)

When micro-mixing governs the overall mixing rate (i.e. when $t_{MICRO} \gg t_{MACRO/MESO}$) Baldyga and Bourne's micro-mixing model can be used to predict the outcome of a competitive chemical reaction (e.g Equations 2.6 and 2.7). The E-model will be

used in Chapter 5 to estimate turbulent energy dissipation rates using product selectivities from a competitive diazo-coupling reaction.

Here, the model is described with particular reference to the extended set of diazo-coupling reactions given in Equations 2.9 to 2.13:

$$A + B \rightarrow R \qquad k_{1\text{-}p} = 12238 \pm 446 \text{ m}^3 \text{ mol}^{-1} \text{ s}^{-1} \qquad (2.9)$$

$$A + B \rightarrow T \qquad k_{1\text{-}o} = 921 \pm 31 \text{ m}^3 \text{ mol}^{-1} \text{ s}^{-1} \qquad (2.10)$$

$$R + B \rightarrow S \qquad k_{2\text{-}o} = 1.835 \pm 0.018 \text{ m}^3 \text{ mol}^{-1} \text{ s}^{-1} \qquad (2.11)$$

$$T + B \rightarrow S \qquad k_{2\text{-}p} = 22.25 \pm 0.25 \text{ m}^3 \text{ mol}^{-1} \text{ s}^{-1} \qquad (2.12)$$

$$C + B \rightarrow Q \qquad k_3 = 124.5 \pm 1.0 \text{ m}^3 \text{ mol}^{-1} \text{ s}^{-1} \qquad (2.13)$$

It is assumed that a concentrated stream of a solution of B is fed into a stream carrying A and C in solution. The growth of X_B, the volume fraction of B in the local environment is modelled (Baldyga and Bourne, 1989) by:

$$X_B = Z_0 \frac{e^T}{1 - Z_0(1 - e^T)} \qquad (2.14)$$

where Z_0 is the initial value of X_B. T is a dimensionless time variable that is given as:

$$T = \alpha E \qquad (2.15)$$

where α is the age of a fluid element (the time since it entered the reactor in terms of the number of engulfments) and E is the engulfment rate. The engulfment rate depends upon the viscosity of the fluid, μ, and the turbulent energy dissipation rate per unit mass, ε:

$$E = \frac{1}{t_E} \propto \frac{1}{17}\left(\frac{\rho\varepsilon}{\mu}\right)^{1/2} \qquad (2.16)$$

The expression for the volume fraction of *B* given by in Equation 2.14 models the effect of self engulfment of *B*-rich regions by *B*-rich eddies. In a system where the initial volume fraction of *B* (Z_0) is small then the volume fraction of *B* (the reaction zone) grows almost exponentially. As the volume fraction increases, the growth is slowed by the self engulfment (Figure 2.6).

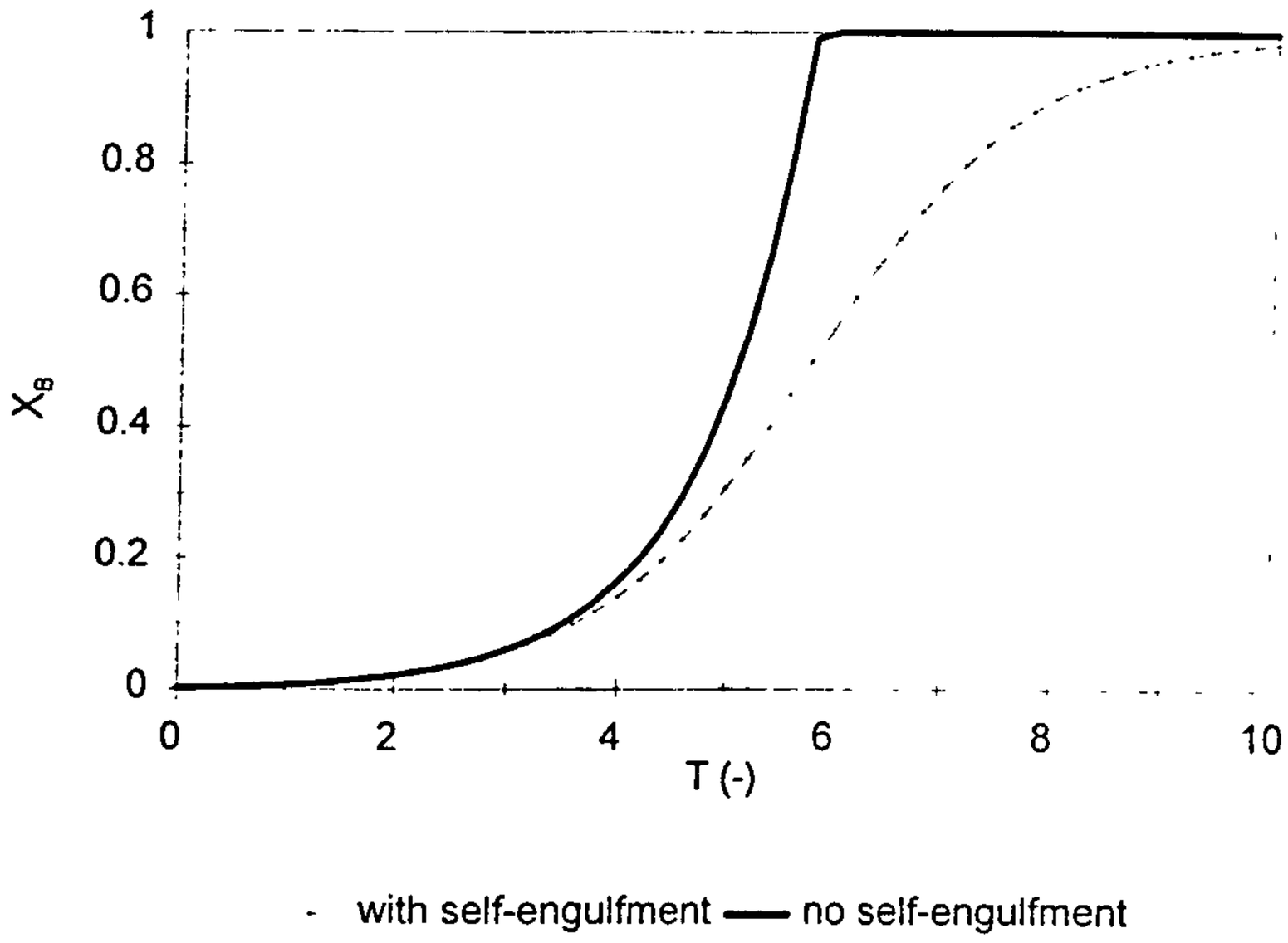

Figure 2.6 Effect of self-engulfment of *B*-rich eddies on growth of reaction zone

A mass balance on species *i* both inside and outside of the expanding reaction zone gives the E-model:

$$\frac{dC_i}{dT} = (1-X_B)(<C_i> - C_i) + Da\sum_j \beta_{ij} C_i C_j \qquad (2.17)$$

where $<C_i>$ is the mean dimensionless concentration of species *i* outside the reaction zone and C_i is the dimensionless concentration within the reaction zone:

$$C_i = \frac{c_i}{c_{B0}} \qquad (2.18)$$

The last term on the right hand side of Equation 2.17 is the rate of production (or consumption) of species *i*, taking into account the kinetic rates for the particular reactions involved. The summation is required because some species (i.e. *R* and *T*) are both produced and consumed during the reactions and other species (e.g. *A* and *B*) are consumed in more than one reaction. The Damkohler number, given in Equation 2.17, is a general one incorporating the kinetic constant for the slowest reaction (that between *R* and *B*) and this is multiplied by the factors β_{ij} where:

$$\beta_{ij} = \frac{k_{ij}}{k_{2-o}} \tag{2.19}$$

For example, for the reaction producing the mono azo dye *Q*, produced by combining *B* and *C* (Equation 2.13), the production term takes the form:

$$Da \sum_{j} \beta_{ij} C_i C_j = Da\ C_B\ C_C \tag{2.20}$$

where the Damkohler number, after multiplying by the appropriate β, is:

$$Da = \frac{k_3 c_{B0}}{E(1 + a)} \tag{2.21}$$

in which *a* is given by:

$$a = \frac{Q_A + Q_C}{Q_B} \tag{2.22}$$

where Q_i is the flow rate of substance *i*.

2.3 Rotor-stator mixers

Flow pattern, residence time distribution and the turbulent energy dissipation rate all affect the performance of a chemical reaction and the literature on rotor-stator mixers was reviewed with particular emphasis on these attributes.

2.3.1 Flow pattern

Because of the nature of rotor-stator mixers - with rotors spinning inside stators at 1000's of revolutions per minute - it is very difficult to observe flow patterns visually. Therefore, there is little in the literature, although some flow pattern information is deduced from other results.

Bourne and Garcias-Rosas (1986) used two model environments when modelling results from competitive diazo-coupling experiments conducted in an in-line rotor-stator. The first assuming plug flow through the reaction zone and the other fully back-mixed flow through the reaction zone. At low shaft speeds, the model results fitted the plug flow assumption and at high shaft speeds, they agreed with the back-mixed model. They concluded that residence time distribution measurements would confirm this.

They also obtained a better product selectivity when using Feed Position 2 (Figure 2.7) to introduce reagents than Feed Position 1 and it was reported that this was probably because of back mixing in the larger volume of Feed Position 1. They also used flow visualisation to estimate the volume of the reaction zone, but did not describe the flow pattern in detail.

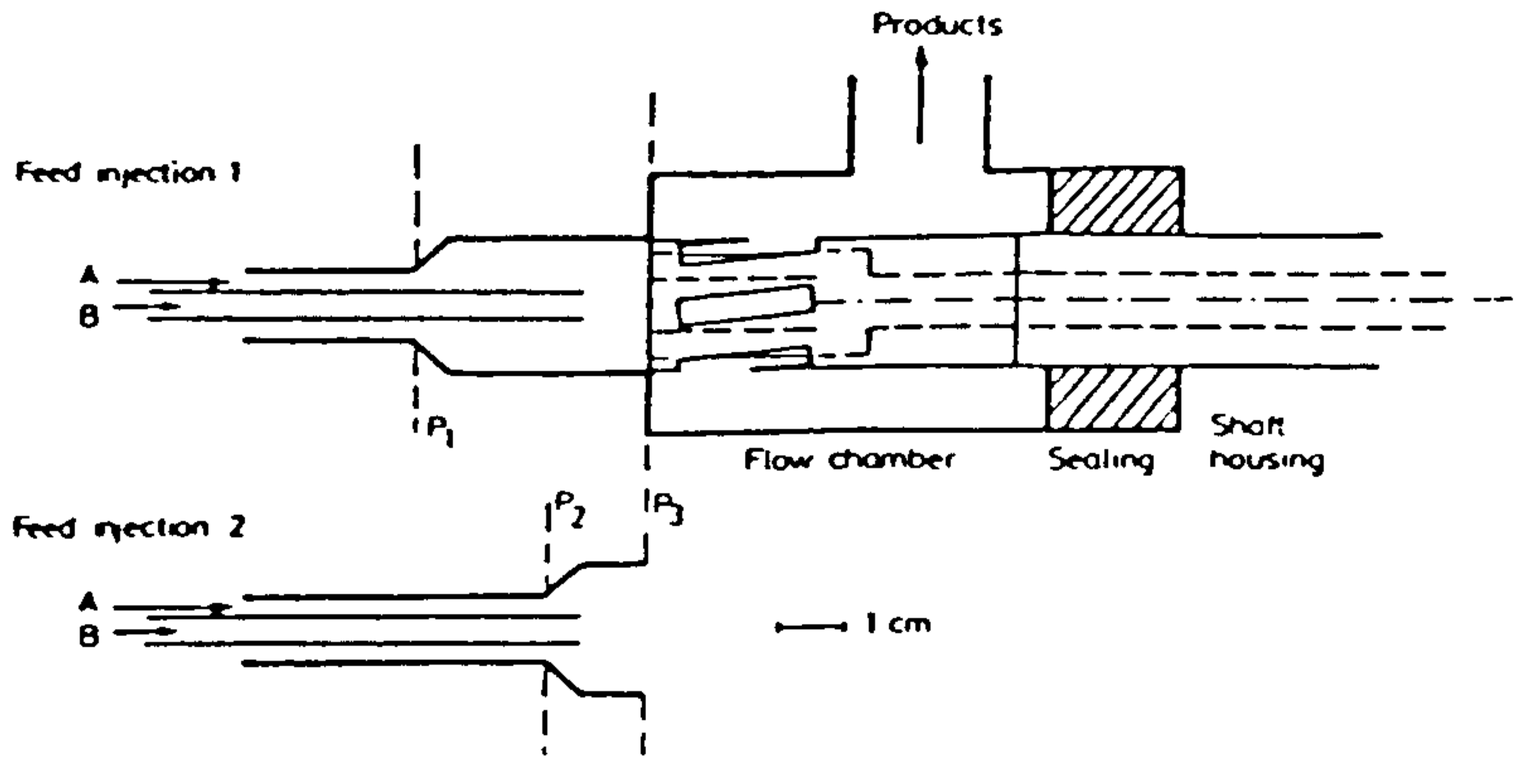

Figure 2.7 In-line rotor-stator unit investigated by Bourne and Garcias-Rosas(1986)

Studer (1990) also carried out some flow visualisation experiments, once again mainly to estimate the extent of the reaction zone for similar diazo-coupling experiments. It was also reported that, as the rotational speed was increased, the product selectivity became poorer (see Section 2.2.6); and it was reported that this increase was caused by back-mixing in the region of the reaction zone. He also suggested that as the mixer size is increased, when operating in the in-line mode, undesirable macro scale effects (for example back-mixing) may give poorer selectivity (shown by a deviation from E-model results assuming plug-flow). Increasing the excess of *A* in the reaction zone improved selectivity (and brought the plug flow model results closer to the experimental values). However, the industrial consequences of this may be overconsumption of reagents (Reagent *A* in this case) and this may not be permitted because of the cost of material *A* or its recycling cost. Nevertheless, from that work it was concluded that the flow pattern through the

reaction zone was approximately plug flow.

2.3.2 Residence time distribution

Studer (1990) presented residence time distribution curves for the whole mixer, for both step and pulse stimuli. Sodium chloride tracer was introduced into the centre of the rotor and the response was measured using an electrical conductivity probe in the outlet pipe. Results indicated that the machines that were tested exhibited back-mixed behaviour (indicated by a long tail in the residence time distribution) and that very little by-passing occurred (Figure 2.8). Significant tailing was also observed. He used a scheme comprising a plug flow reactor followed by a stirred tank reactor to model the RTDs. The experimental curves fell between the model curves for a stirred tank and for the combined plug flow and stirred tank reactor (Levenspiel, 1972). The residence time distribution for a stirred tank (mixed flow) is given by:

$$C = e^{-\left(\frac{t}{\tau}\right)} \tag{2.23}$$

where t is time and τ is the nominal residence time (= V/Q where V is the reactor volume and Q is the flow rate). The residence time distribution for a plug flow and mixed flow reactor in series is given by:

$$C = \left(\frac{V}{V_m}\right) e^{-\left(\frac{V}{V_m}\right)\left(t' - \frac{V_p}{V_m}\right)} \tag{2.24}$$

In Equation 2.24, V, V_P and V_M are the total volume and the volumes of the plug flow and back mixed regions. This scenario is physically realistic.

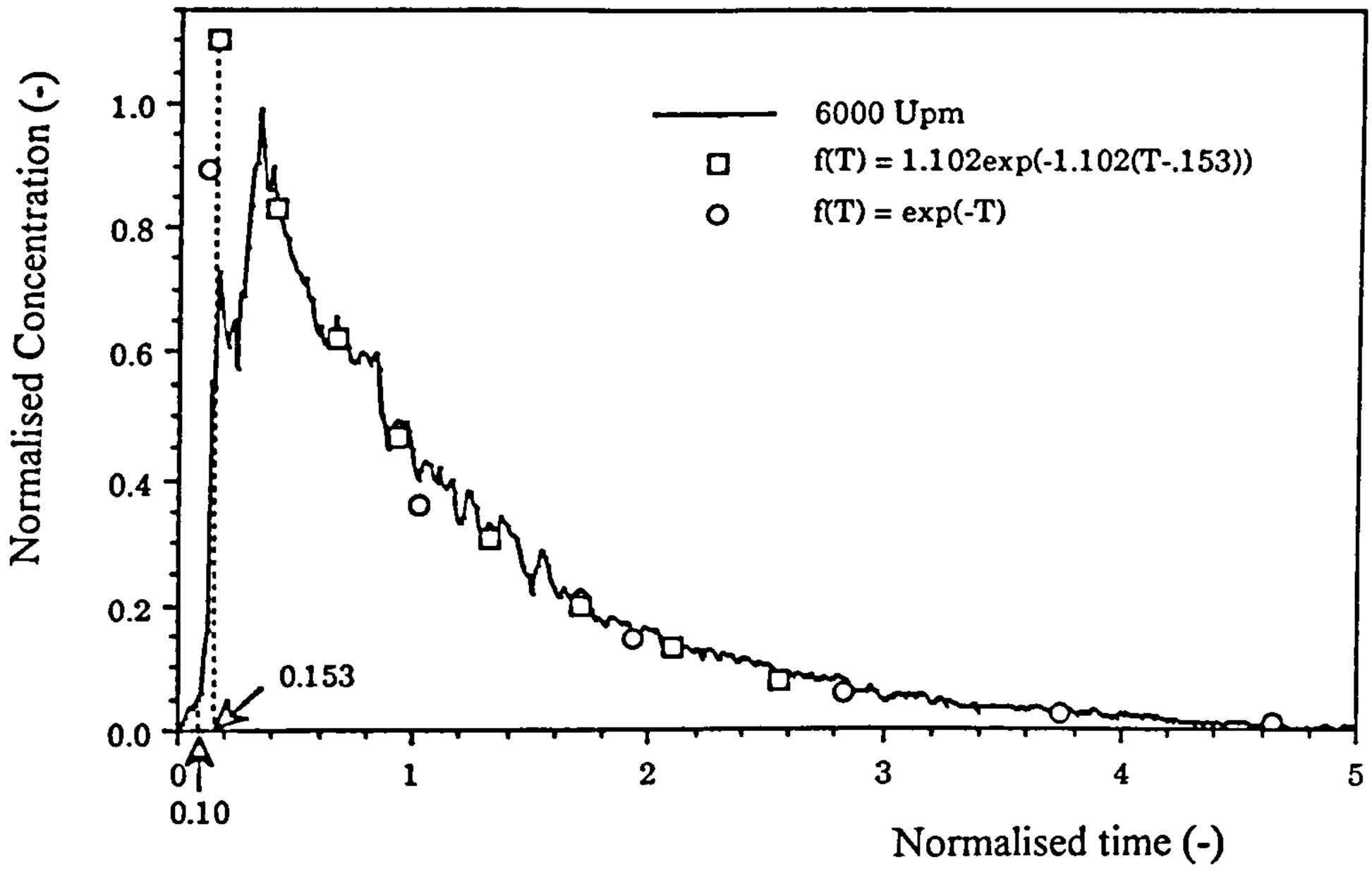

Figure 2.8 Residence time distribution curve produced by Studer (1990)

Sparks (1993) produced residence time distributions for a toothed ring rotor-stator mixer (measuring the response at the outlet to a pulse stimulus of salt tracer at the inlet). These showed severe tailing, and the author suggested reducing the size of the volute to reduce this effect. He found that Equation 2.24, the same outlet concentration expression as that used by Studer (1990), gave good agreement with his experimental results.

2.3.3 Turbulent energy dissipation rate, ε

Bourne and Garcias-Rosas (1986), using micro-mixing controlled diazo-coupling experiments, report that as the rotor speed was increased, the product selectivity (X) decreased, indicating an increase in turbulent energy dissipation rate. Using the EDD-model (Bourne and Baldyga, 1984) they estimated energy dissipation rates of

between 5 and 700 W kg^{-1} from the product selectivity data. This is close to the limit of applicability of the reaction scheme used (Bourne et al.,1992).

The energy dissipation data were correlated with:

$$\varepsilon = 4\times10^{-10}N^3 \qquad (2.25)$$

where ε is in $W.kg^{-1}$ and N in revolutions per minute.

They also estimated energy dissipation values using relationships for the drag on a rotating cylinder. This analysis was based upon the assumption that drag between the solid surfaces of the rotor and stator (if included) were responsible for the turbulent energy dissipation. This analysis gave very good agreement with values obtained using Equation 2.25 at low speeds but at higher speeds the agreement was poorer. They state that, for higher shaft speeds, the exponent 3 on N in Equation 2.25 is probably too high. Their theoretical drag analysis showed that 2.5 was more appropriate for the enclosed cylinder situation.

Studer (1990) reports values for ε (in $W.kg^{-1}$) in the mixer, given in terms of shaft speed (in rpm) for both mixers to be :

$$\varepsilon = 8.8\times10^{-7}N^{2.25} \quad \text{large mixer} \qquad (2.26)$$

$$\varepsilon = 1.8\times10^{-9}N^{2.75} \quad \text{small mixer} \qquad (2.27)$$

where N is in revolutions per minute. A potential error of up to 50% in the estimates of ε was quoted.

Pedrocchi and Widmer (1988), using rotor-stator mixers to produce emulsions, found that the drop size distribution (considered to be heavily dependent on ε) was

independent of shear gap size. This implies that the drop size determining region may not be the shear gap and that other effects are important. They reported that the design of the rotor-stator teeth was more important than shear gap thickness in determining the drop size distribution.

Sparks (1993) used an overall energy balance to estimate the magnitude of the losses in a toothed ring rotor-stator mixer (Figure 2.8). It was concluded that up to 70% of the shaft power input to a mixer is dissipated by hydraulic and leakage losses combined. No further breakdown of this energy dissipation was given. In the rotor-stator mixer that he studied (with a rotor diameter of 119.6 mm), 70% of the shaft power input at 3000 rpm and 3.0 $l.s^{-1}$ equates to around 1 kW. Since the overall mass of the water in the mixer was ~1 kg it was concluded that ε was of the order of 1 $kW.kg^{-1}$.

2.3.4 Mixing in rotor-stators

Bourne and Garcias-Rosas (1986) carried out work on a model X-20 Ystral mixer, a lab scale machine, in both in-line and semi-batch modes (Figures 2.7 and 2.10 respectively).

Figure 2.11 shows the rotors and stators investigated. The rotors were approximately 16 mm in diameter and the shear gap thickness was 0.25 mm. The rotor speed varied from 1000 to 13000 rpm and flow rates through the mixer, in the in-line mode, varied from 0.44 $dm^3.s^{-1}$ to 0.77 $dm^3.s^{-1}$.

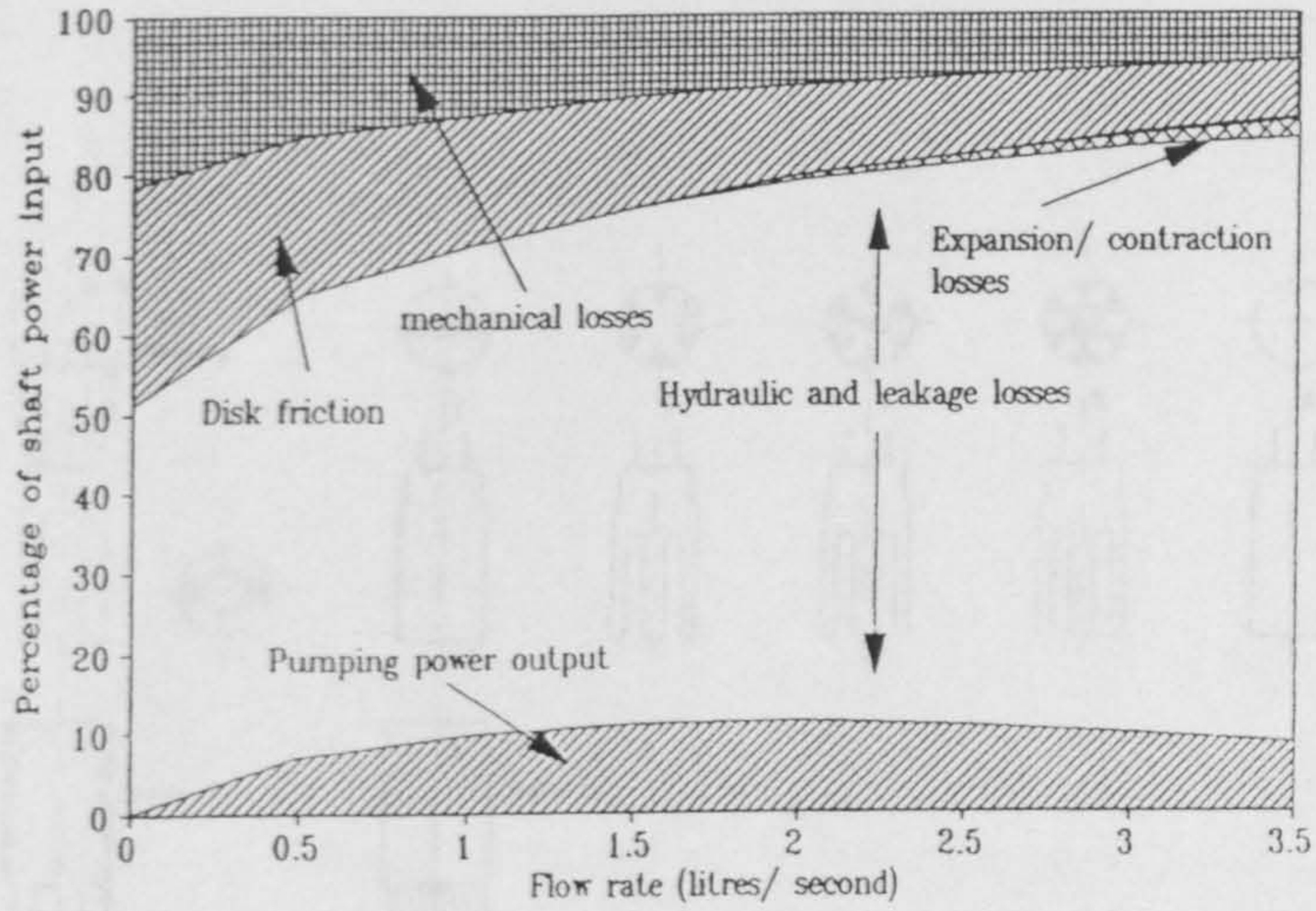

Figure 2.9 Energy balance plot for a rotor-stator mixer (Sparks, 1993)

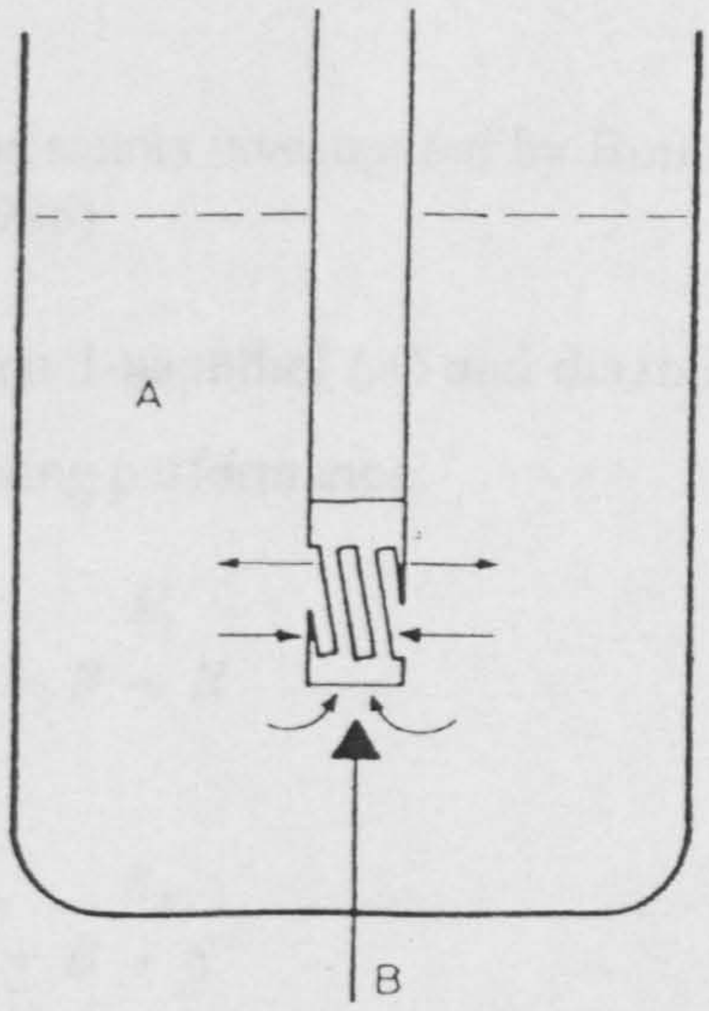

Figure 2.10 Rotor-stator mixer used for semi-batch experiments (Bourne and Garcias-Rosas, 1986)

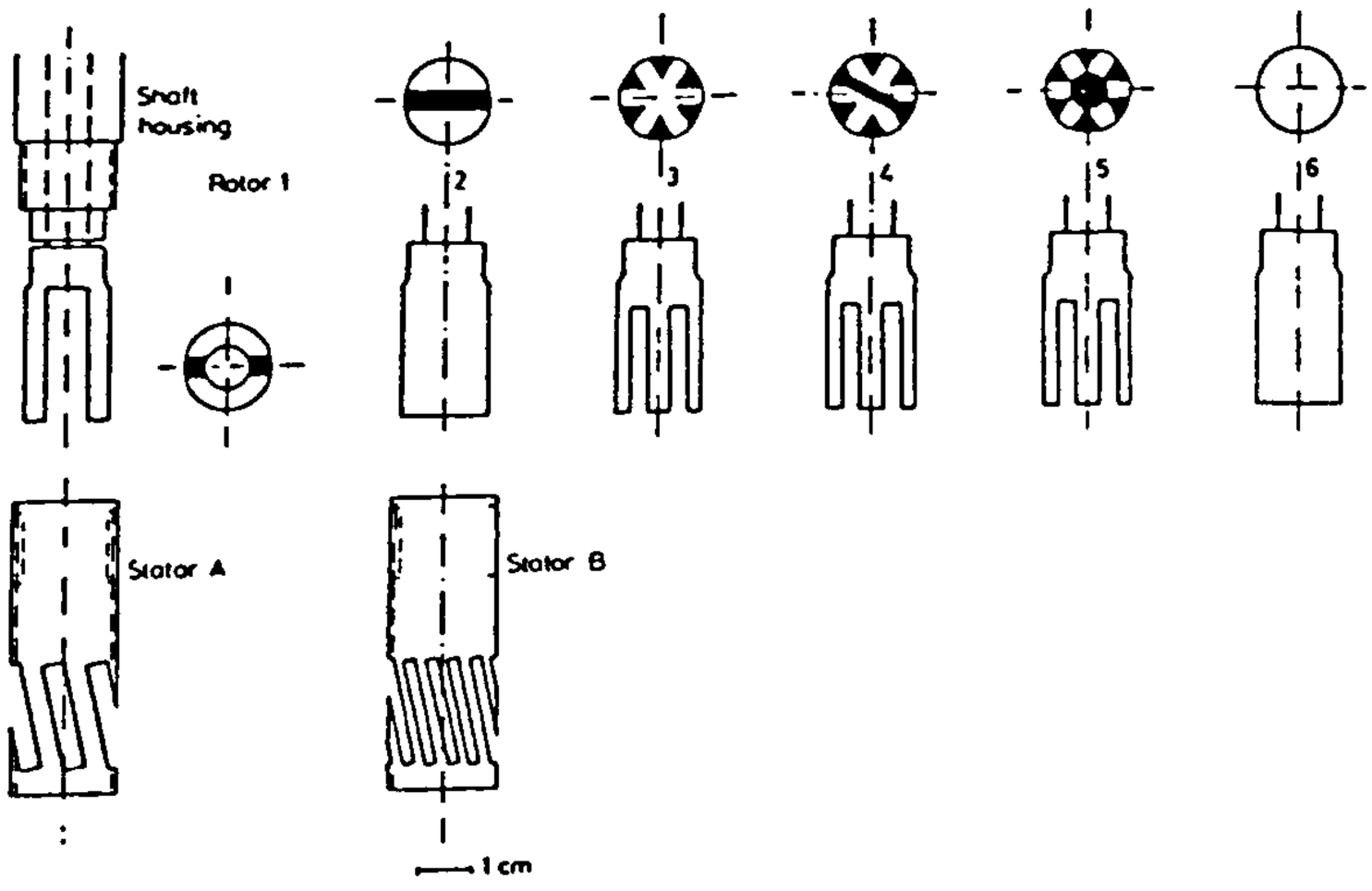

Figure 2.11 Rotors and stators investigated by Bourne and Garcias-Rosas (1986)

The mixing sensitive reaction between 1-naphthol (A) and diazotised sulphanilic acid (B), was used to characterise mixing performance:

$$A + B \xrightarrow{k_1} R \tag{2.28}$$

$$R + B \xrightarrow{k_2} S \tag{2.29}$$

where $k_1 \gg k_2$.

The same product selectivity, X, as given in Equation 2.8 was used:

$$X = \frac{2c_S}{(c_R + 2c_S)} \tag{2.8}$$

where c_S is the concentration of species S (bisazo dye) and c_R is the concentration of species R (monoazo dye). Improved micro-mixing (i.e. higher energy dissipation rate) will give less S and therefore a lower value for the product selectivity.

The following mass balance was used to check their results:

$$c_{B0} = c_R + 2c_S \tag{2.30}$$

where c_{B0} is the initial concentration of B. The concentrations of the products R and S, monoazo and bisazo dyes, were determined using a spectrophotometer. A balance within ±2% between the left hand and right hand sides of Equation (2.30) was obtained.

They conducted semi-batch and in-line experiments. The semi-batch experiments were conducted in glass beakers, with volumes from 0.001 to 0.005 m^3. In the in-line mixer they added Reagent B through two different arrangements (Figure 2.7). In semi-batch mode they introduced B into the beaker at a point 5 mm below the bottom of the mixer (Figure 2.10). The reagent flow rates were such that there was a slight excess of Reagent A ($n_{A0}/n_{B0} = 1.055 \pm 0.025$).

They found that the design of rotor and stator had a significant effect on product selectivity. Of the rotors and stators given in Figure 2.11, combination A-2 gave the lowest (best) product selectivity and the product selectivity was highest with rotor 6 (the solid cylinder).

Removal of the stator had little or no effect on the product selectivity, indicating that either the turbulent energy dissipation rates in the shear gap region and stator were not significantly higher than those in the rotor (or its discharge) or that the reaction was complete before the shear gap and stator were reached.

Studer (1990) worked on two differently sized rotor-stator mixers, using an extended azo-coupling reaction scheme to measure performance:

$$A + B \xrightarrow{k_{1\text{-}p}} R \tag{2.31}$$

$$A + B \xrightarrow{k_{1\text{-}o}} T \tag{2.32}$$

$$R + B \xrightarrow{k_{2\text{-}o}} S \tag{2.33}$$

$$T + B \xrightarrow{k_{2\text{-}p}} S \tag{2.34}$$

where A (1-naphthol) reacts with B (sulphanilic acid) to form either R (para-monoazo dye) or, to a lesser extent, T (ortho-monoazo dye). Both of these products can then react with B to give S (bisazo dye).

The product selectivity for this reaction scheme is given by:

$$X_S = \frac{2c_S}{(c_R + c_T + 2c_S)} \tag{2.35}$$

2.3.5 Feed position

Studer (1990) used a nozzle with a number of radial outlets, feeding inside the rotor, (Figure 2.12). This gave a good coarse scale distribution of Reagent B (i.e. improved macro-mixing) and gave much better selectivity than the value obtained with single tube feed nozzles.

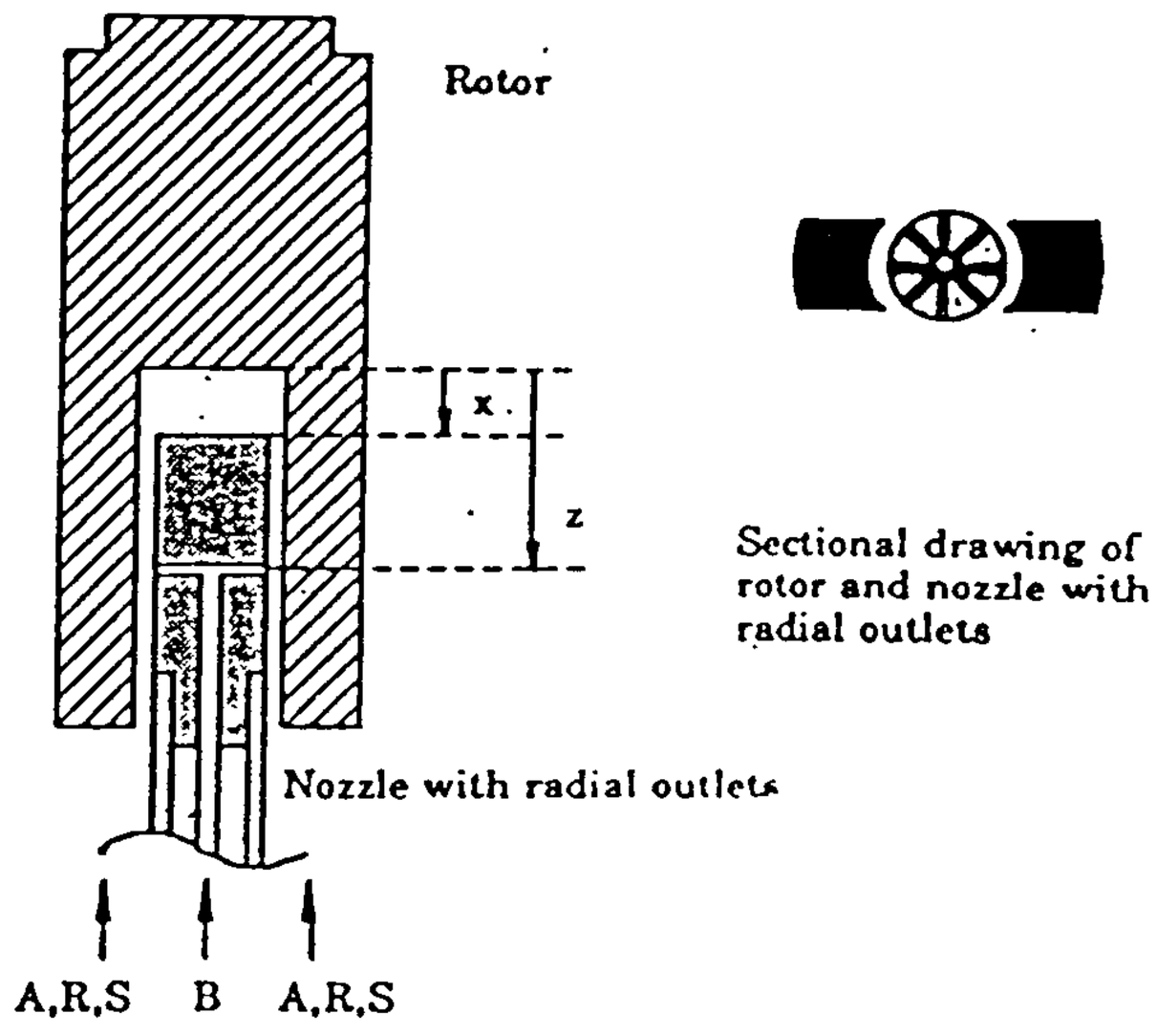

Sectional drawing of rotor and nozzle with radial outlets

Figure 2.12 Feed nozzle investigated by Studer (1990)

2.3.6 Scale-up

Two scale-up rules were considered by Studer (1990). The first ($N^{2.5}D^2$ = constant) was designed to give constant power per unit mass (the exponent of 2.5 was chosen as it is the average of the exponents given in Equations 2.26 and 2.27). The second scale-up rule was that of constant tip speed (ND = constant).

Constant tip speed gave better results and was selected, but the first rule gave satisfactory results (Figures 2.13 and 2.14)

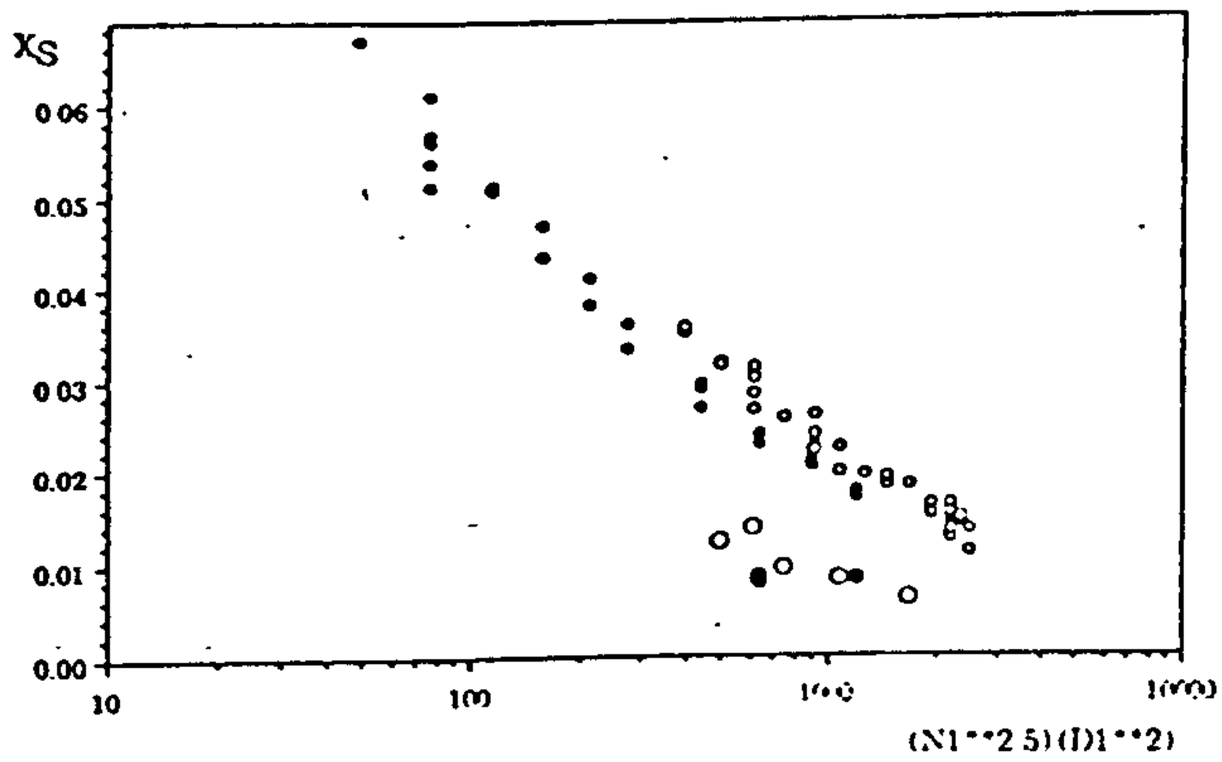

Fig. 14. Comparison of both mixers with the scale-up criterion $N^{2.5}d^2 = \text{const.}$ • Semi-batch, large mixer. ○ semi-batch, small mixer; ● in-line, large mixer; ○ in-line, small mixer.

Figure 2.13 Constant power per unit mass scale-up (Studer, 1990)

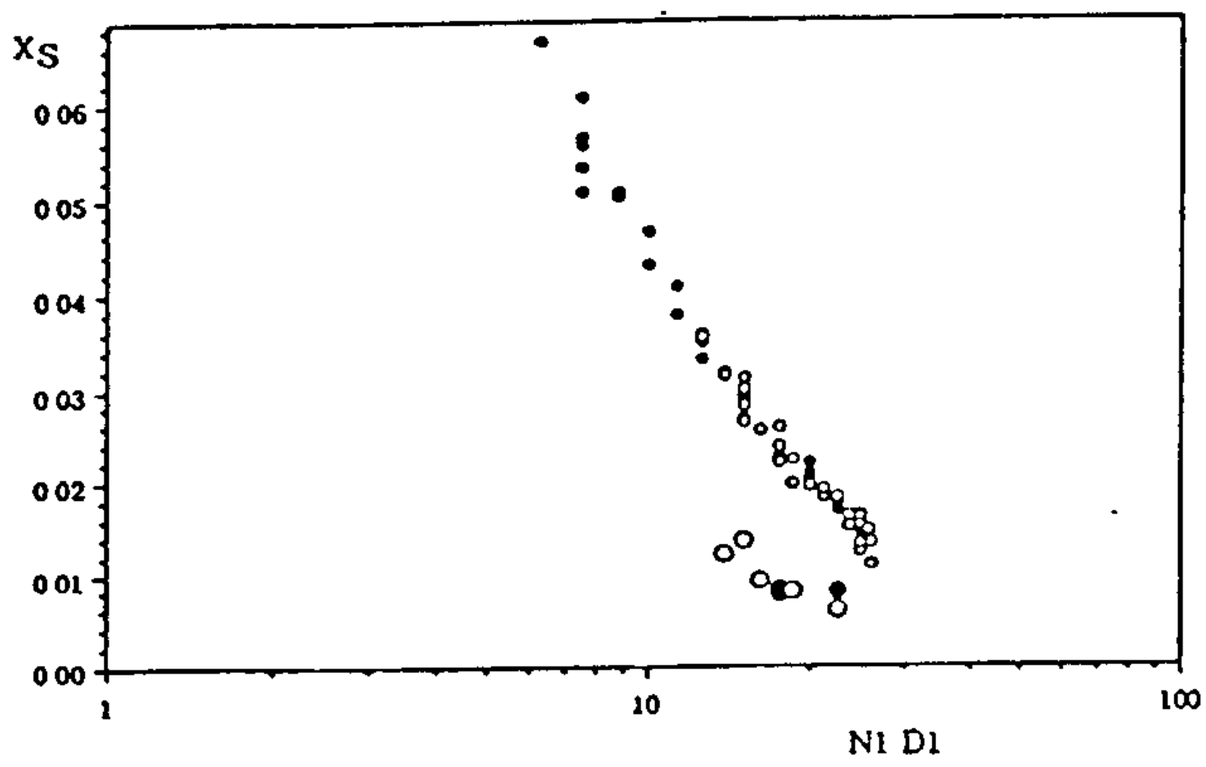

Fig. 15. Comparison of both mixers with the scale-up criterion of constant rotor tip speed. • Semi-batch, large mixer, ○ semi-batch, small mixer; ● in-line, large mixer; ○ in-line, small mixer.

Figure 2.14 Constant tip speed scale-up (Studer, 1990)

2.3.7 Power consumption

Various papers on rotor-stator equipment have been published. Those that contain correlations for shaft power (Bouette, 1974, Averbuhk, 1988) state that:

$$P_{SHAFT} \propto N^3 D^5 \tag{2.36}$$

Sparks (1993), when correlating power data with a flow rate supplied by another pump, found an exponent of between 1.99 and 2.2 on N. One worker (Summets, 1966) included the effect of flow rate in the correlation for power:

$$P_{SHAFT} = 0.931 N^3 D^5 \rho \mu^{-0.086} Q^{0.045} H_f^{-0.0787} d^{0.785} Z^{0.068} S^{0.46} \qquad (2.37)$$

where H_f is the distance between tooth centres, d is the tooth size, Z is the total number of teeth and S is the number of stages (number of rotors on the shaft). It is not clear from the paper, a translation from Russian, over what range the expression is valid, or what units the variables are in. However, it is particularly interesting that this expression (reported to fit experimental data to within 5%) shows a weak dependance upon the flow rate, Q, and that it includes the exponents on N and D given in Equation 2.36.

2.3.8 Pumping output

Rotor-stator mixers resemble centrifugal pumps, and they can contribute a significant pumping effect. Bourne and Garcias-Rosas (1986) report the pumping capacities of the various combinations of rotors and stators. They showed that Rotors 1 and 2 (Figure 2.11) had the best pumping capacity and that the other rotors (with the exception of the solid rotor) had similar pumping capacities. At high shaft speeds (over 3000 rpm) Q rose linearly with N.

Removal of the stator increased the pumping performance of the mixer, although in the semi-batch case it was reported that the stator was needed to reduce vortex formation in the beaker (the stator performing a similar role to the baffles in a stirred tank).

Sparks (1993) reported a pumping efficiency, η, of ~15% at the best efficiency point (BEP) for a rotor-stator mixer (rotor diameter ~0.12 m, rotational speed ~2000 to 3000 rpm).

2.4 Centrifugal pump literature

The literature on rotor-stator mixers is sparse, so literature on centrifugal pumps was reviewed. The similarities and differences between centrifugal pumps and rotor-stator mixers is discussed in Section 2.1.

2.4.1 Flow pattern

A large number of workers have investigated the flow patterns in centrifugal pumps. Those studies often focussed on one particular region within the pump, usually the inlet, impeller, impeller outlet or volute regions. The purpose of those studies was typically to improve the pumping efficiency, by understanding and then reducing the losses. Almost the opposite approach may be required for rotor-stator mixers, where the energy dissipation rates need to be maximised in order to improve mixing.

Recirculating flows exist, under certain operating conditions, throughout centrifugal pumps. Discharge and suction recirculation have been investigated by Karassik (1983) and Fraser (1982) who state that the amount of recirculation is dependent upon the throughput and rotational speed. At flow rates close to the best efficiency point (BEP), recirculation is minimal. Recirculating flows are shown in Figures 2.15 and 2.16.

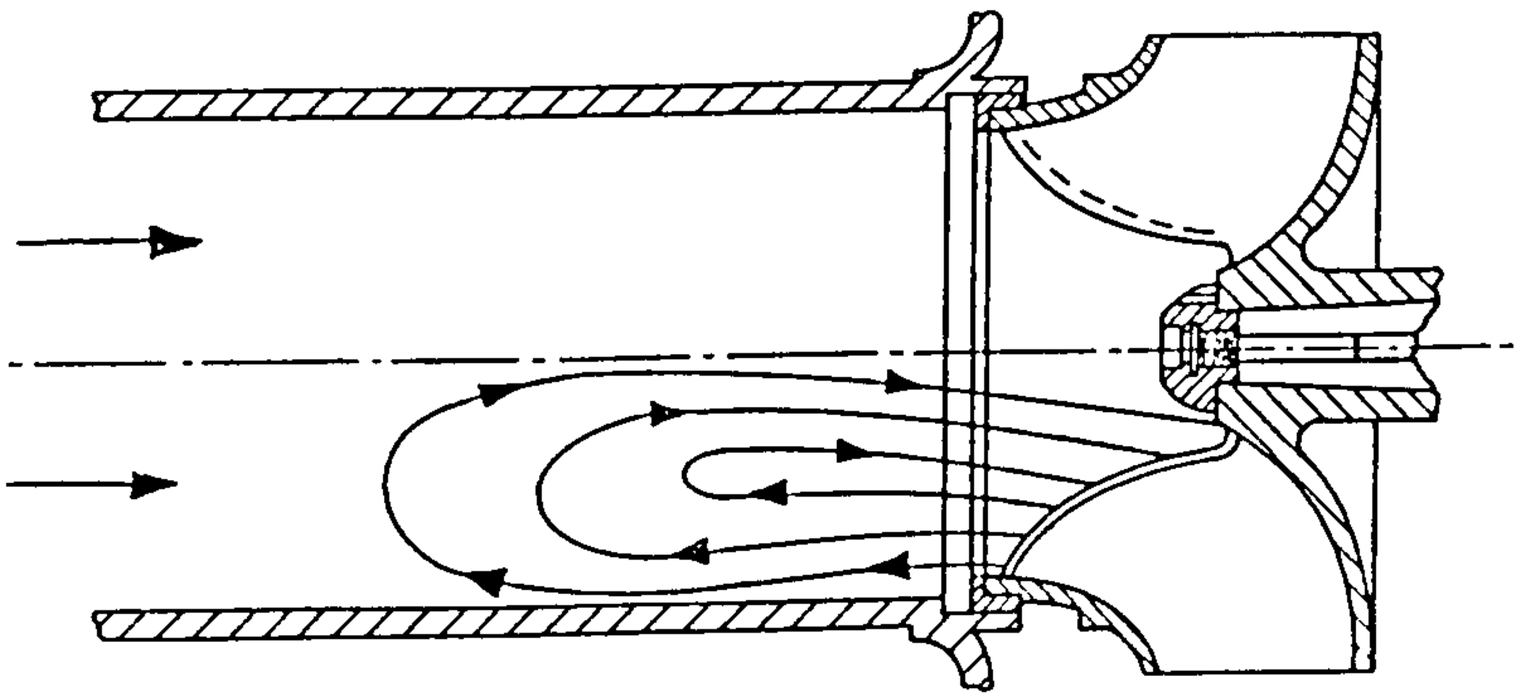

Figure 2.15 Recirculating flow in a pump inlet pipe (Yedidiah, 1985)

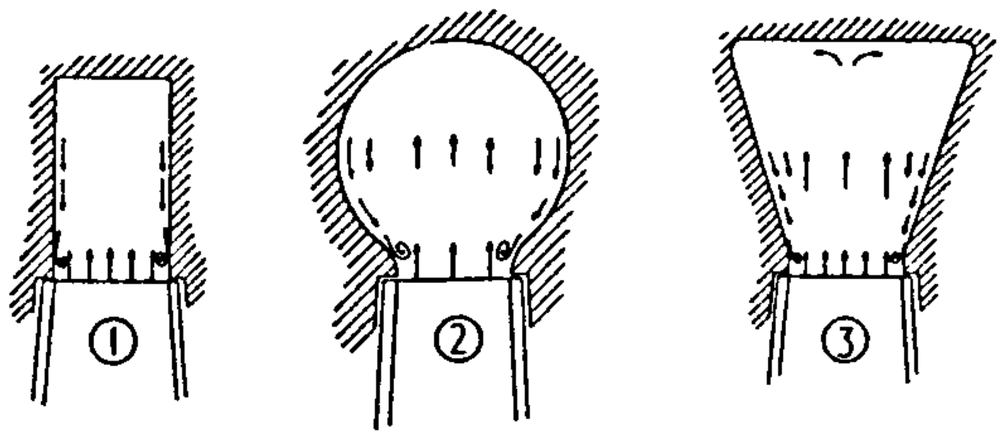

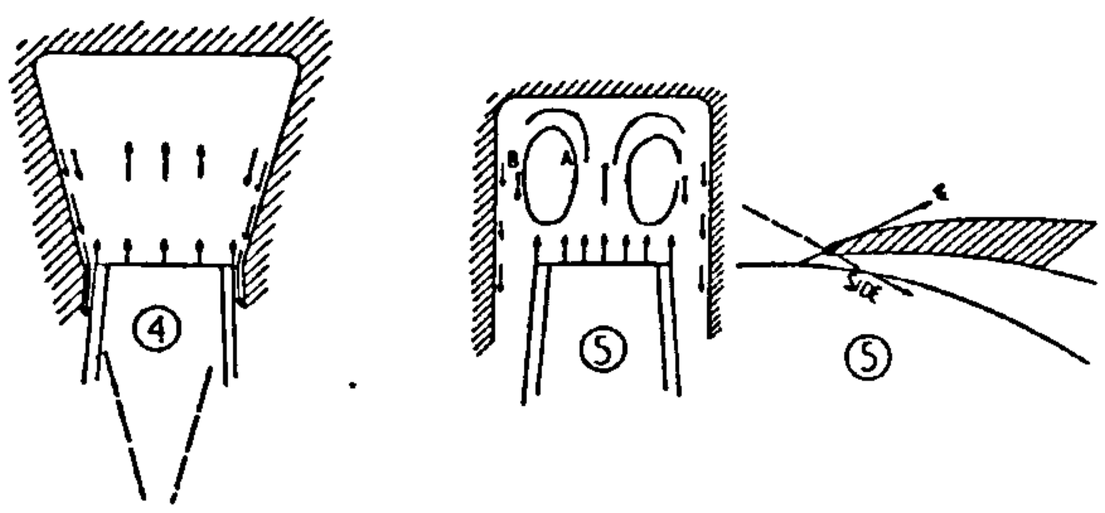

Figure 2.16 Recirculating flow in a pump volute (Copley et. Al., 1962)

Recirculating flow will cause tailing in the residence time distribution of a mixer. There is no information in the literature on recirculating flows in rotor-stator mixers.

Flow separation and re-attachment at the leading edge of pump impeller blades can affect pumping performance (Copley & Worster, 1961). These phenomena will

probably be more significant in rotor-stator mixers, as they are not generally designed to avoid them.

2.4.2 Residence time distribution

Residence time distributions have been produced for centrifugal pumps by Bolzern & Bourne (1985) using concentrated dye and a photocell. Figure 2.17 shows a typical experimental result from that work. The authors characterised their residence time distributions using the dispersion and stirred tanks in series models (Levenspiel, 1972). Under all operating conditions they report substantial back mixing in the pump. They reported that the RTD is insensitive to operating speed, flow rate and the viscosity of the fluid being pumped.

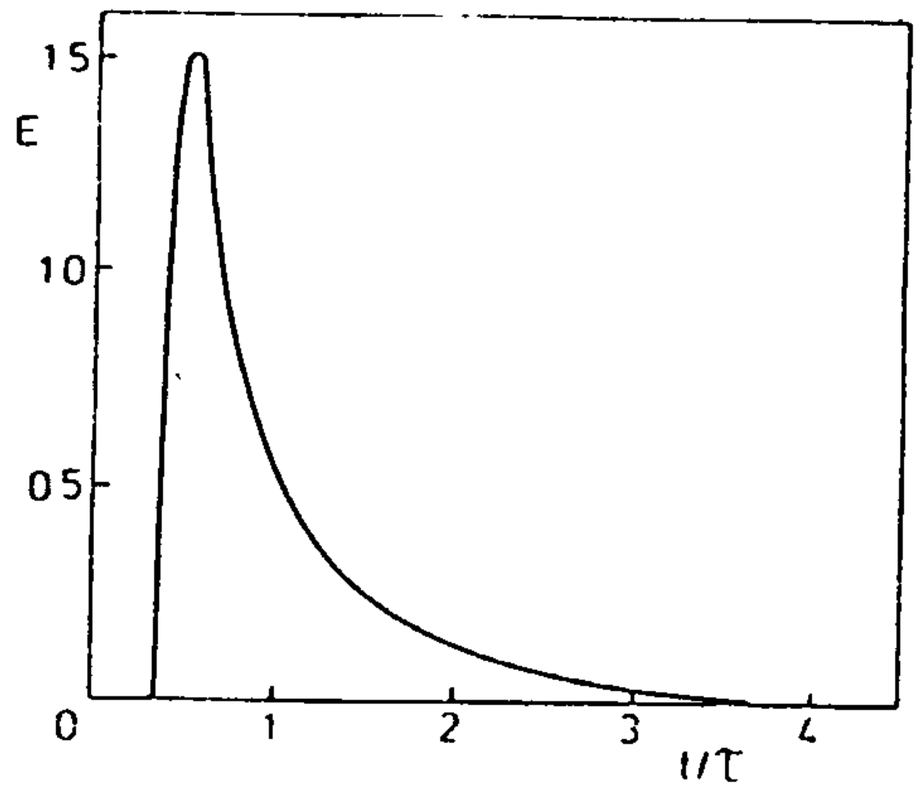

Figure 2.17 Residence time distribution curve for a centrifugal pump (Bolzern and Bourne, 1985)

Studer (1991) measured residence time distributions in a centrifugal pump. These

exhibited tailing and the author also used the axial dispersion and stirred tanks in series models to model the experimental RTD. The RTDs that were measured displayed pulsations after the peak concentration, indicating a circular motion that was much slower than the impeller tip speed. The tailing was reported to be due to dead zones within the pump.

Hearn (1992), measuring residence time distributions in a centrifugal pump with an open impeller, recommended the use of the model representing a plug flow region and a well mixed region (Equation 2.23). Equation 2.23 described the experimental RTDs well.

2.4.3 Energy dissipation

Books by Stepanoff (1957) and Anderson (1980) contain a power balance for pumps. In essence, this balance is given by:

$$P_{SHAFT} = P_{PUMP} + P_{MECH} + P_{DISC} + P_{LEAK} + P_{HYDRAULIC} \qquad (2.38)$$

The next Sections contain a discussion of the individual components.

(a) Shaft power - P_{SHAFT}

This is the shaft power input to the mixer and the designer of a rotor-stator mixer would need to know this so that the correct motor can be specified. This is directly analogous to the shaft power in a stirred tank and in a fully baffled stirred tank (Rushton et al, 1950) the shaft power is related to the rotational speed and diameter of the impeller by:

$$P_{SHAFT} = Po\,\rho N^3 D^5 \qquad (2.39)$$

where *Po* is the power number and depends upon impeller type. At high impeller Reynolds numbers (indicating fully turbulent conditions) the power number is constant for a given impeller design.

(b) Pumping power - P_{PUMP}

The pumping power output is defined as:

$$P_{PUMP} = Q\Delta p \tag{2.40}$$

The magnitude of the pumping power would be needed in order to assess whether an additional pump would be needed to move fluid through a process loop.

(c) Disc friction loss - P_{DISC}

Disc friction losses are caused by frictional drag on the solid surfaces of the rotor and are analogous to the skin friction losses in a motionless mixer. Disc friction losses are significant in pumps, so they will need to be accounted for when studying rotor-stator mixers.

(d) Mechanical losses - P_{MECH}

The mechanical losses, according to Stepanoff's definition, are the losses due to friction in the seals and bearings. Some definitions of mechanical loss include disc friction, not included here because the seal and bearing losses could be measured separately from the disc friction losses. Mechanical losses (and the disc friction loss) do not contribute to mixing (Bolzern and Bourne, 1985).

(e) Leakage (recirculation) losses - P_{LEAK}

The leakage loss can mean the loss due to leakage through seals or, as here, the loss due to fluid not passing through in the required direction. An example of this type of leakage (or recirculation) loss is when fluid passes back from the high pressure (downstream) side of the impeller to the low pressure (upstream) side. This is a macro-mixing mechanism (Bolzern and Bourne, 1985) and will influence the residence time distribution.

(f) Hydraulic losses - $P_{HYDRAULIC}$

Hydraulic losses (including turbulent losses) are the only losses that contribute to micro-mixing. A well designed centrifugal pump is a fairly poor mixer (Hearn, 1992) as the hydraulic losses are a fairly small part of its energy balance at or near to the best efficiency point (see below). Designers have been improving impeller designs for many years and pumps (centrifugal pumps in particular) are now very efficient.

Almost the opposite approach is needed when designing a rotor-stator mixer for use as a reactor for fast chemical reactions. A predictable region of high turbulent energy dissipation would be ideal.

Figure 2.18 shows a power balance for a double suction pump (in this balance disc friction is included in the mechanical loss and a recirculation loss is isolated from the leakage loss). Over a typical operating range, from 60% to 140% of the normal capacity, the percentage of power losses due to hydraulic losses increases from around 4% to more than 20%. Below the best efficiency point (BEP) recirculation losses dominate and above the BEP, hydraulic losses dominate.

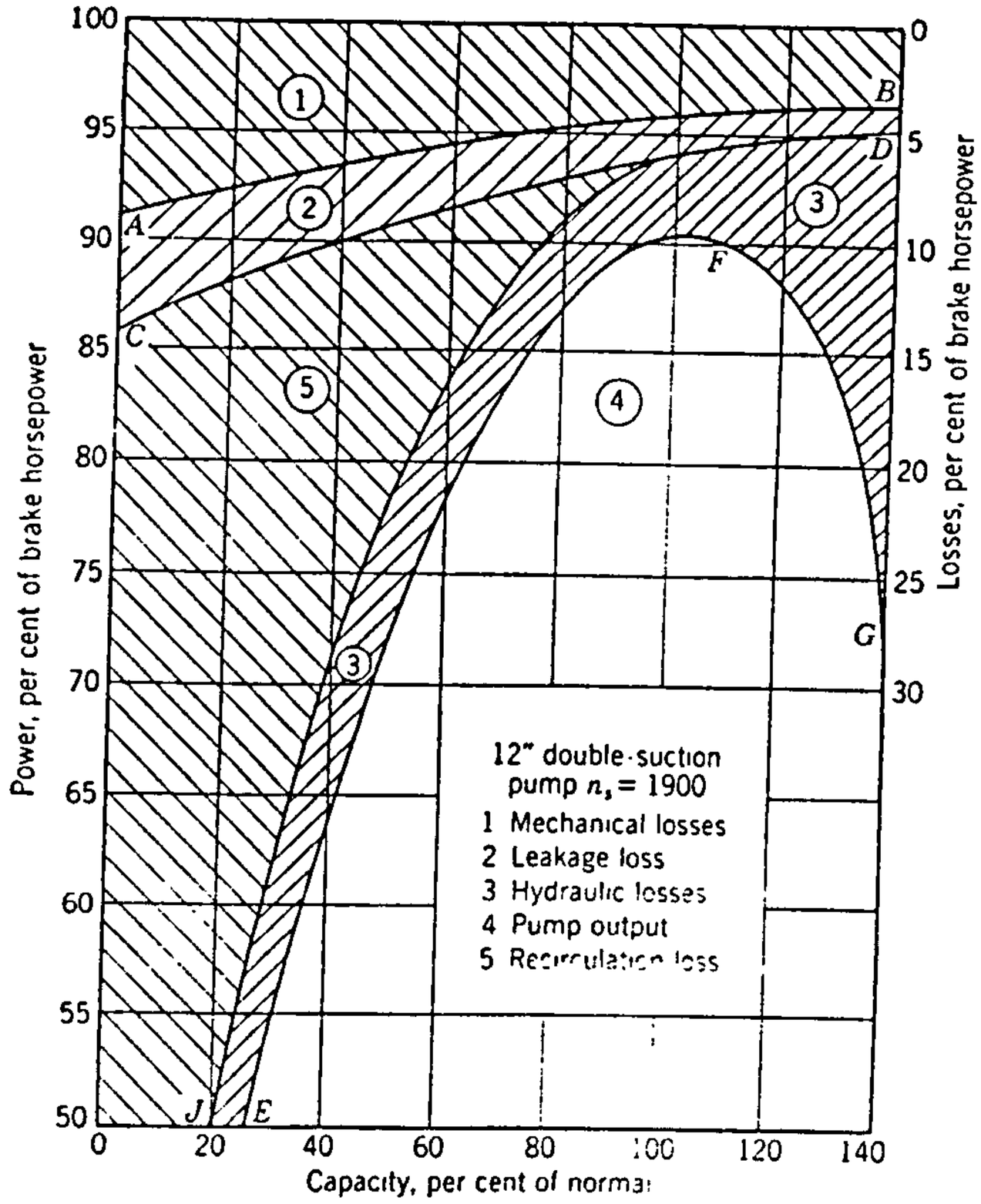

Figure 2.18 Overall power balance for a centrifugal pump (Stepanoff, 1957)

2.5 Conclusions

The review of literature showed that little work on rotor-stator mixers has been published. However, there is some work in the literature showing that they have attributes that make them suitable as chemical reactors. They exhibit high energy dissipation rates (100s $W.kg^{-1}$), combined with short residence times (~1 s). Also, the flow through the rotor approximates to plug flow under certain operating conditions.

There is little information on the cause and distribution of turbulent energy dissipation in rotor-stators, but it has been shown that there is significant turbulent energy dissipation in the rotor teeth. However, it is not clear how significant these dissipation rates are in the shear gap or the stator.

Significant improvement in performance, for competitive chemical reactions, is produced when using a multi-feed nozzle placed just upstream of the rotor teeth rather than a single-feed nozzle. The multi-feed nozzle provides a good initial macro-scale distribution of reagents.

The literature is mainly concerned with small, laboratory scale, devices. Little work has been done on industrially sized units. The only information in the literature on scale-up states that the rule of constant tip speed should be used for micro-mixing controlled reactions.

CHAPTER 3

EXPERIMENTAL EQUIPMENT, MATERIALS AND METHODS

A custom built test mixer was acquired and fitted into a test loop for the performance of power balance, flow visualisation, residence time distribution and diazo-coupling experiments.

Power balance and residence time distribution experiments, were used to give data on the overall performance of rotor-stator mixers, for example how shaft power or pumping efficiency is affected by rotor-stator design, size or operating conditions. Global experiments were also used to give data from which to deduce local effects, for example how changes in the overall residence time distribution or shaft power could be attributed to local flow features.

Local experiments, flow visualisation and reactive mixing tests, were used to provide direct input into the description of flow and mixing. Dye tracer and an acid-base decolourisation scheme were used to visualise local flow patterns throughout the mixer.

Reactive mixing experiments, using the extended diazo-coupling reaction scheme (Bourne et. al., 1992), were used to provide qualitative data (best feed position, trends associated with changing shaft speed, flow rate etc.) and quantitative data - for example local energy dissipation rates.

Addresses of the equipment and instrumentation suppliers are given in Appendix 1, instrumentation calibration details are given in Appendix 2 and the procedures used

to prepare chemicals for the reactive mixing experiments are given in Appendix 3.

3.1 Test loop and instrumentation

The test mixer (based on a Silverson 425 LSM machine) was fitted into a flow loop between two tanks of 2.5 m^3 capacity, shown in Figure 3.1 and Plate 3.1. Flows of water through the test loop were generated by a Flygt pump BS 20066.171 submersible pump (2.2 kW), connected to a frequency inverter so that pump speeds and therefore flow rates could be controlled. Flow rates were measured with an Altometer SC80 AS magnetic flow meter.

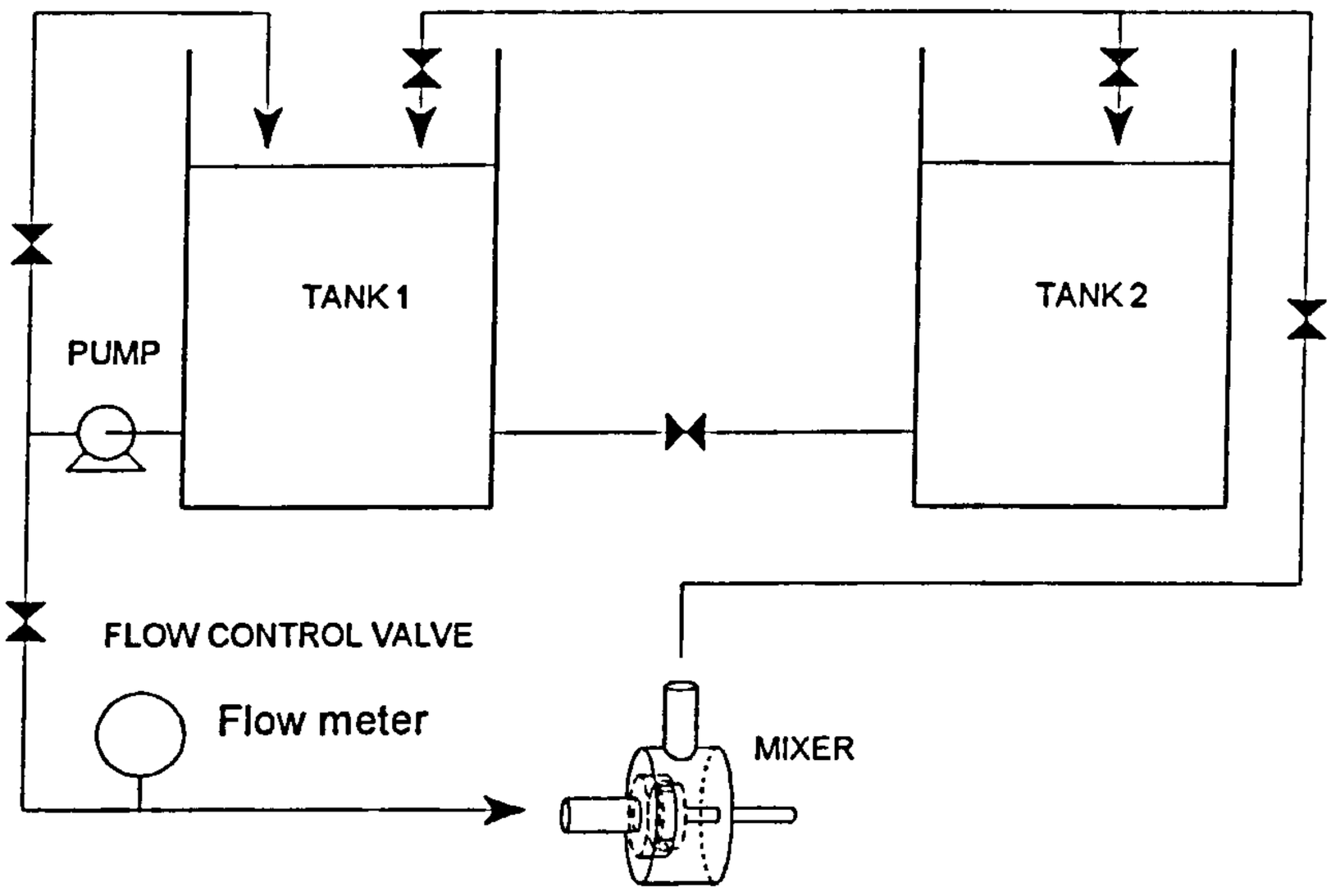

Figure 3.1 Flow loop

A variety of tests were performed on the rig, so the flow loop was designed to be able to operate in different modes, returning the flow into either Tank 1 or Tank 2. The rotor shaft was split and a T 30 FD torque transducer connected to a KMN 902.D signal amplifier, both from Hottinger Baldwin Messtechnik, was fitted between flexible couplings.

Water flow rates up to approximately 5 $l.s^{-1}$ were possible. The maximum shaft speed used in the rotor-stator mixer was 4000 revolutions per minute (66.67 revolutions per second). At high speeds and low flow rates there was sometimes audible cavitation; this was partially alleviated by applying back pressure (half closing a downstream valve).

The mixer volume was measured by blanking off the inlet flange and filling the mixer with a measured volume of water. The volute was a cylinder with diameter 172 mm and length 110 mm. The inlet and outlet pipe diameters were 50.8 mm (2"). The outer casing was reproduced in clear acrylic so that the flow could be seen. A half-scale unit was also made, in clear acrylic, for scale tests.

3.2 Rotor-stator mixer designs

The same basic drive unit was used for all heads (a Silverson 425 LSM machine, Plate 3.1). However, three basic rotor-stator designs were fitted into the machine: 'Toothed', 'Half-scale toothed' and 'Silverson'. In all cases the rotor was held on the shaft by a bullet-shaped nut. The standard Silverson 425 LSM casing was used for most of the experiments, except for the half-scale tests when a scaled casing was used.

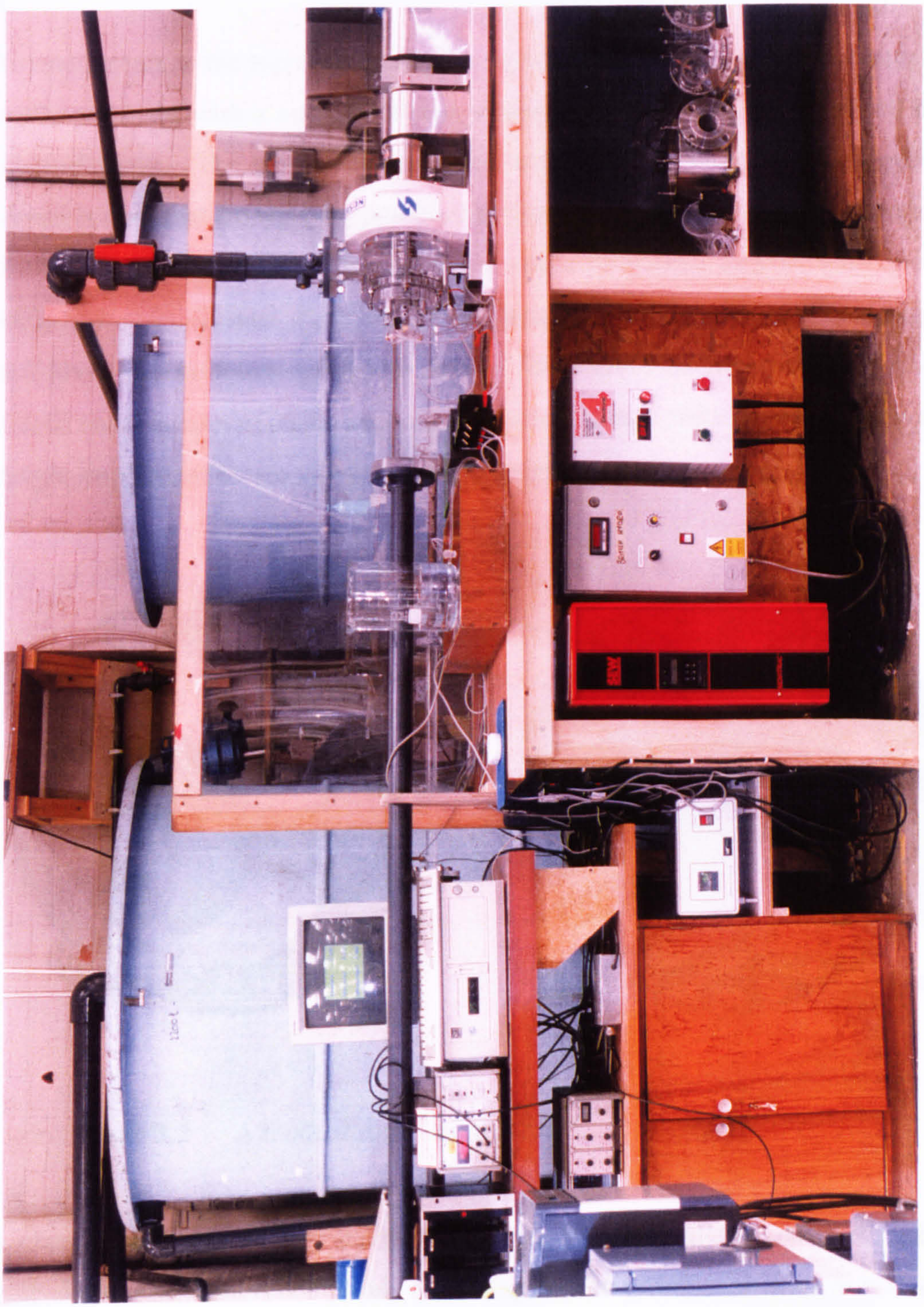

Plate 3.1 Photograph of test rig

3.2.1 Toothed

Toothed refers to the type of rotor-stator shown in Figure 3.2, where the rotor and stator are discs with a number of (approximately) trapezoidal teeth around their circumference. The toothed rotor-stators used in this project were designed to resemble units that are typically produced by German and Swiss manufacturers (e.g. Ystral, IKA, Kinematica). The units were made from clear acrylic, with one set made from stainless steel. Four different designs of rotors and stators were designed and made (by in-house workshops and by Silverson Machines Limited), giving sixteen combinations of toothed rotors and stators. These were designed to give an insight into the processes occurring in the shear gap region.

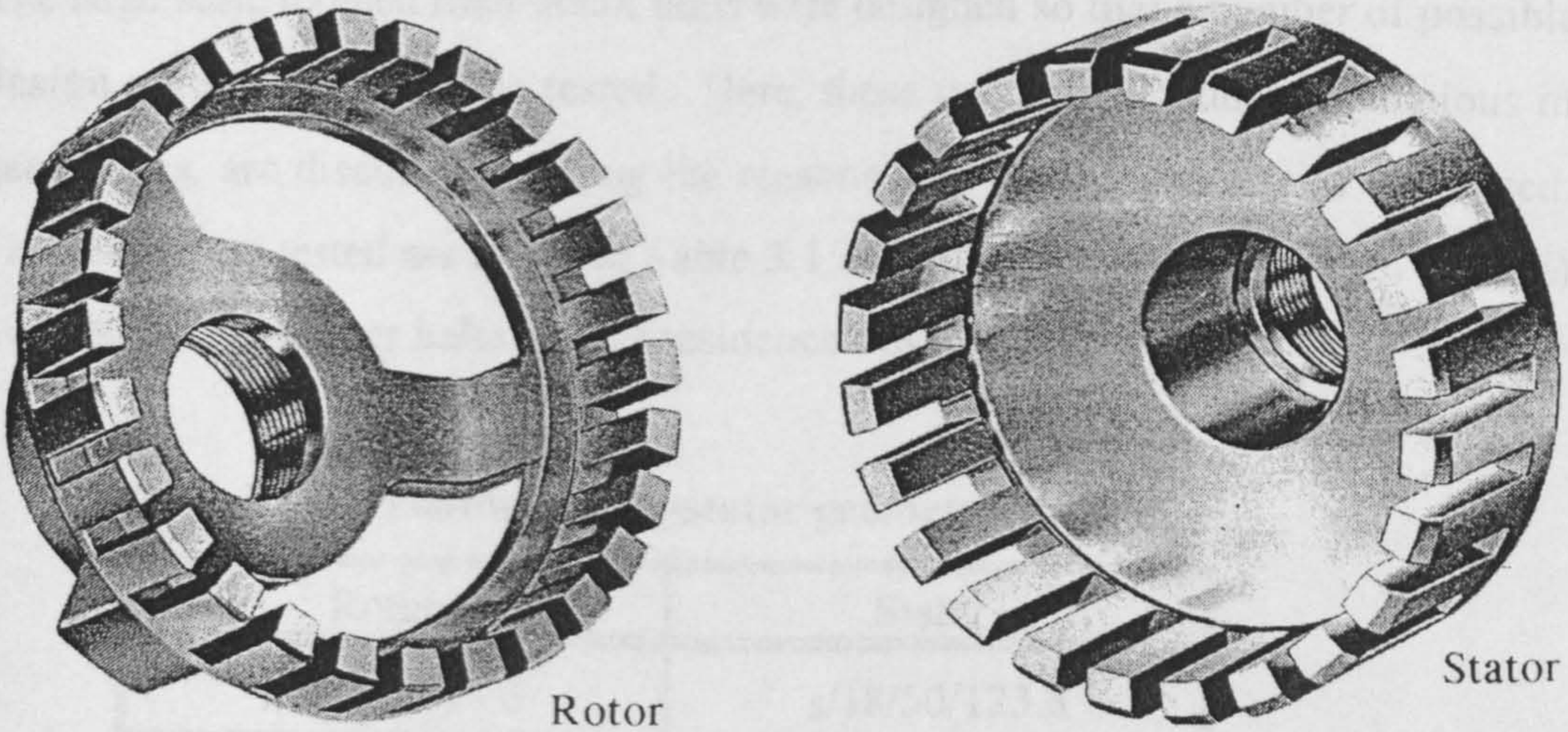

Figure 3.2 A toothed rotor-stator mixer

A classification system was developed which, although cumbersome, describes toothed rotors and stators completely (assuming that the distribution of teeth is even) and is used throughout this work. The following is an example classification for a

rotor:

r/18/50/119.6

where **r** denotes rotor, **18** is the number of teeth, **50** is the percentage open area and **119.6** is the outer diameter of the rotor in mm.

The stator classification is very similar:

s/19/50/123.8

where **s** denotes stator, **19** is the number of teeth, **50** is the percentage open area and **123.8** is the inner diameter of the stator. This system allows the shear gap size to be found easily, by subtracting the rotor outer diameter from the stator inner diameter and dividing by two. In this example the shear gap thickness is 2.1 mm.

The large scale toothed rotor-stator units were designed so that a number of possible design parameters could be tested. Here, these geometries, and combinations of geometries, are discussed - giving the reasons why certain geometries were used. The geometries tested are listed in Table 3.1 and all combinations (sixteen in total) were tested for power balance and residence time distribution data.

Table 3.1 Toothed rotor-stator geometries tested

Rotors	Stators
r/18/50/119.6	s/18/50/123.8
r/18/50/121.45	s/18/33/123.8
r/18/50/123.34	s/19/50/123.8
r/12/67/121.45	s/36/50/123.8

The aim of this work was to improve the understanding of the flow and mixing in a rotor-stator mixer. The most important mixing zone in a rotor-stator mixer is the immediate vicinity of the rotor teeth/blades, the shear gap and the stator teeth/slots.

In the work reported here, global measurements were used to establish:

- flow pattern and mixing information
- energy dissipation characteristics.

For example, changing the shear gap thickness, keeping everything else the same (numbers of teeth, open areas of both rotor and stator) and measuring shaft power can give information about the energy dissipation mechanisms in the shear gap vicinity. This knowledge can then be used to estimate the turbulent energy dissipation rates and hence mixing performance. The findings from these experiments might then be checked using experiments that investigate localised effects, for example azo-coupling tests.

The first three rotors in the list all had 18 teeth and 50% open area; the only difference was the outer diameter. This gave three shear gap thicknesses: 2.10 mm, 1.18 mm and 0.23 mm (the thinnest gap was close to the standard shear gap thickness for a Silverson). A fourth rotor had 12 teeth, 66% open area, with a shear gap thickness of 1.18 mm.

A difference in mixing (and pumping) performance might be expected if the stator open area (and tooth/slot shape) was changed, as this would change the flow pattern. The flow through **s/36/50/123.8** might be very different from the flow through **s/18/50/123.8** even though they have the same open area.

Rotor-stator interaction could also be varied. With an 18 toothed rotor (e.g **r/18/50/123.34**) and an 18 toothed stator (**s/18/50/123.8**) the effective open area varies from fully closed to fully open, when the rotor and stator teeth are in alignment (Figures 3.3 and 3.4). A pulsating flow might be expected, especially

with the thinnest shear gap, where the fully closed condition might provide a more effective barrier to the flow than for the larger shear gap. However, when using the same rotor (**r/18/50/123.34**) with stator **s/19/50/123.8** (or **s/36/50/123.8**) the effective open area remained constant (at 50%). With **s/19/50/123.8** the open part of the ring will rotate at the blade passing frequency (Figure 3.5) and with **s/36/50/123.8**, adjacent teeth will be alternatively opened and closed (Figure 3.6).

The 12 toothed rotor (**r/12/67/121.45**) was designed to investigate the effect of the number of teeth and, therefore, rotor-stator interaction (Figure 3.7).

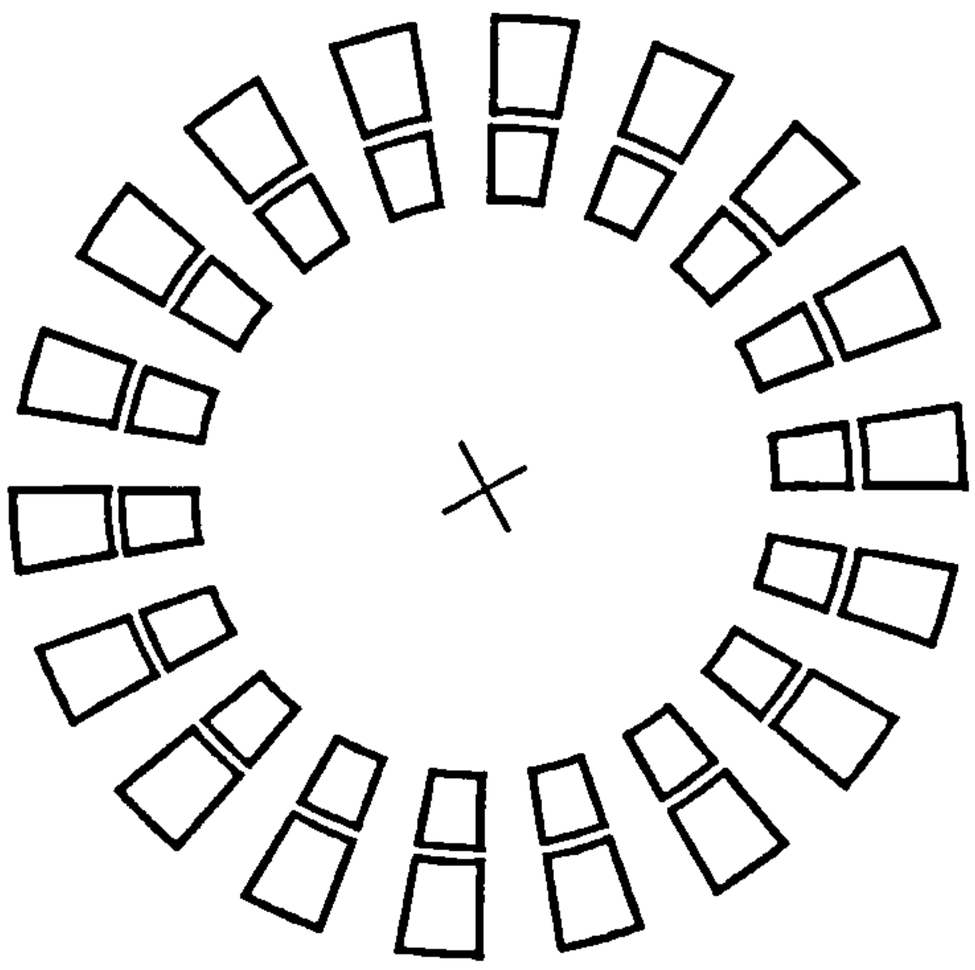

Figure 3.3 18 toothed rotor-18 toothed stator (fully open condition)

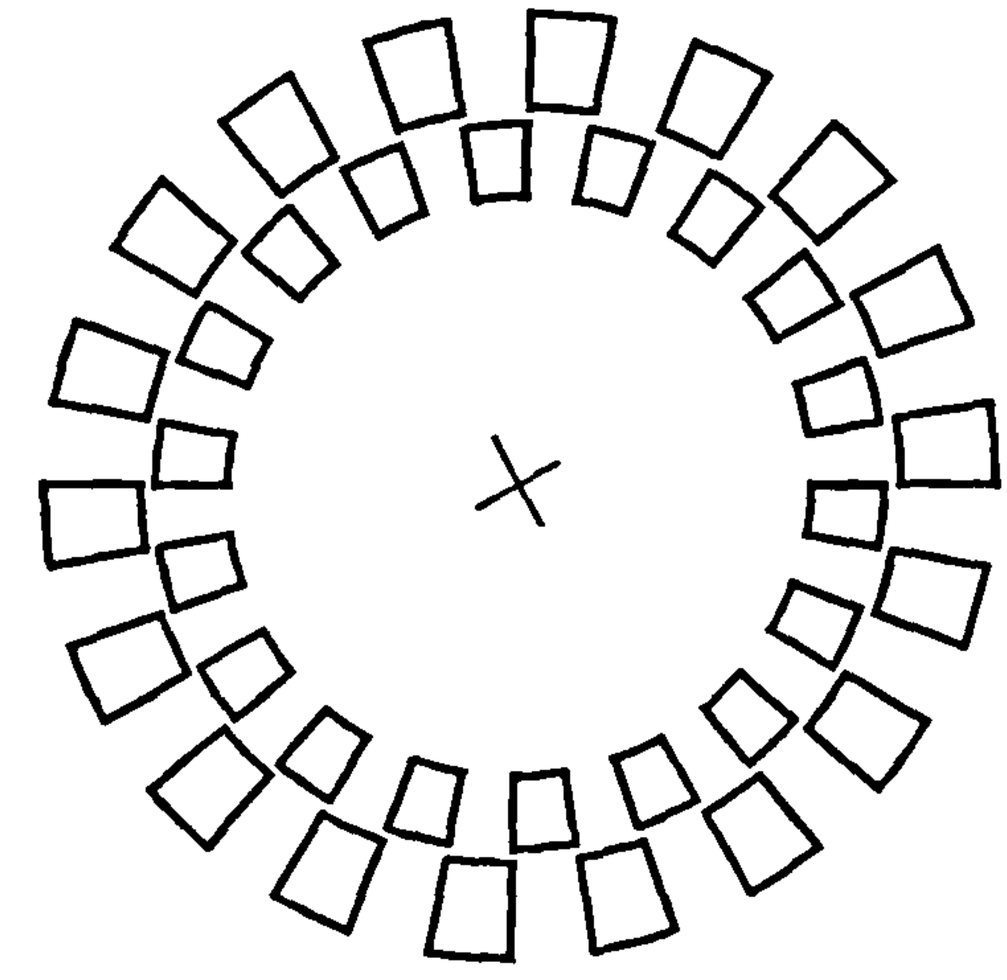

Figure 3.4 18 toothed rotor-18 toothed stator (fully closed condition)

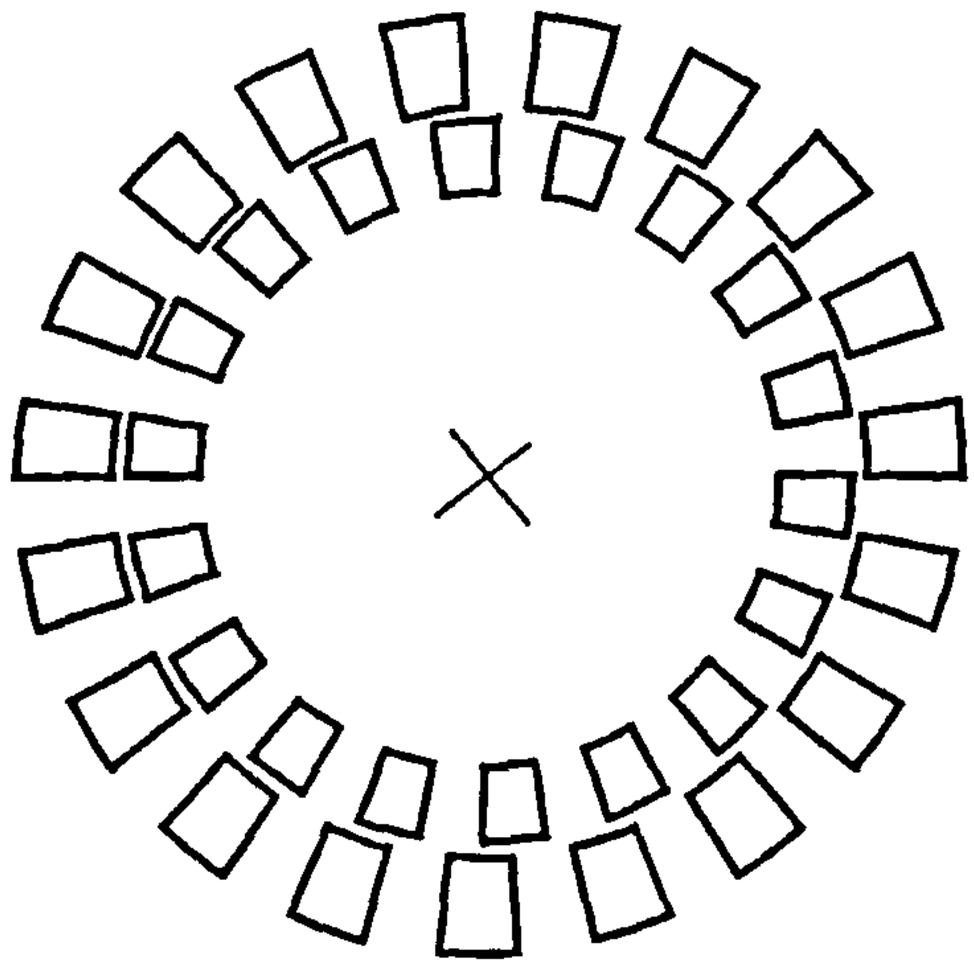

Figure 3.5 19 toothed stator with 18 toothed rotor

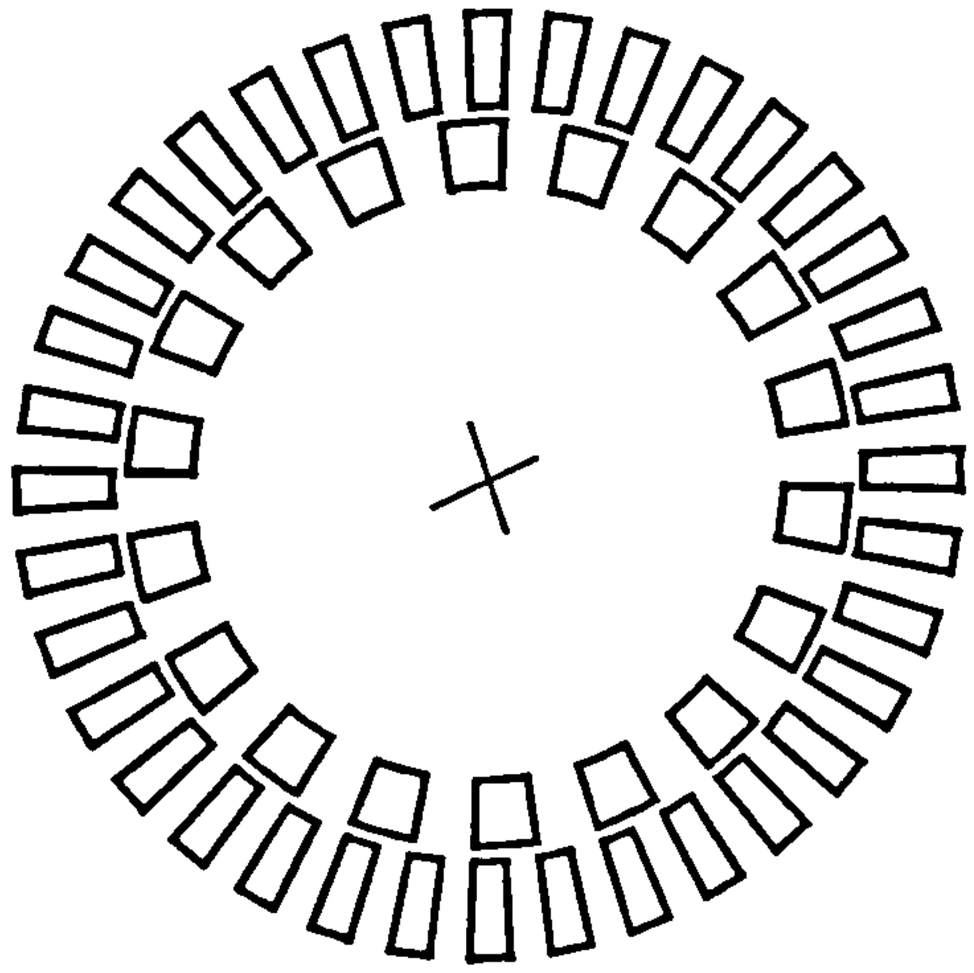

Figure 3.6 36 toothed stator with 18 toothed rotor

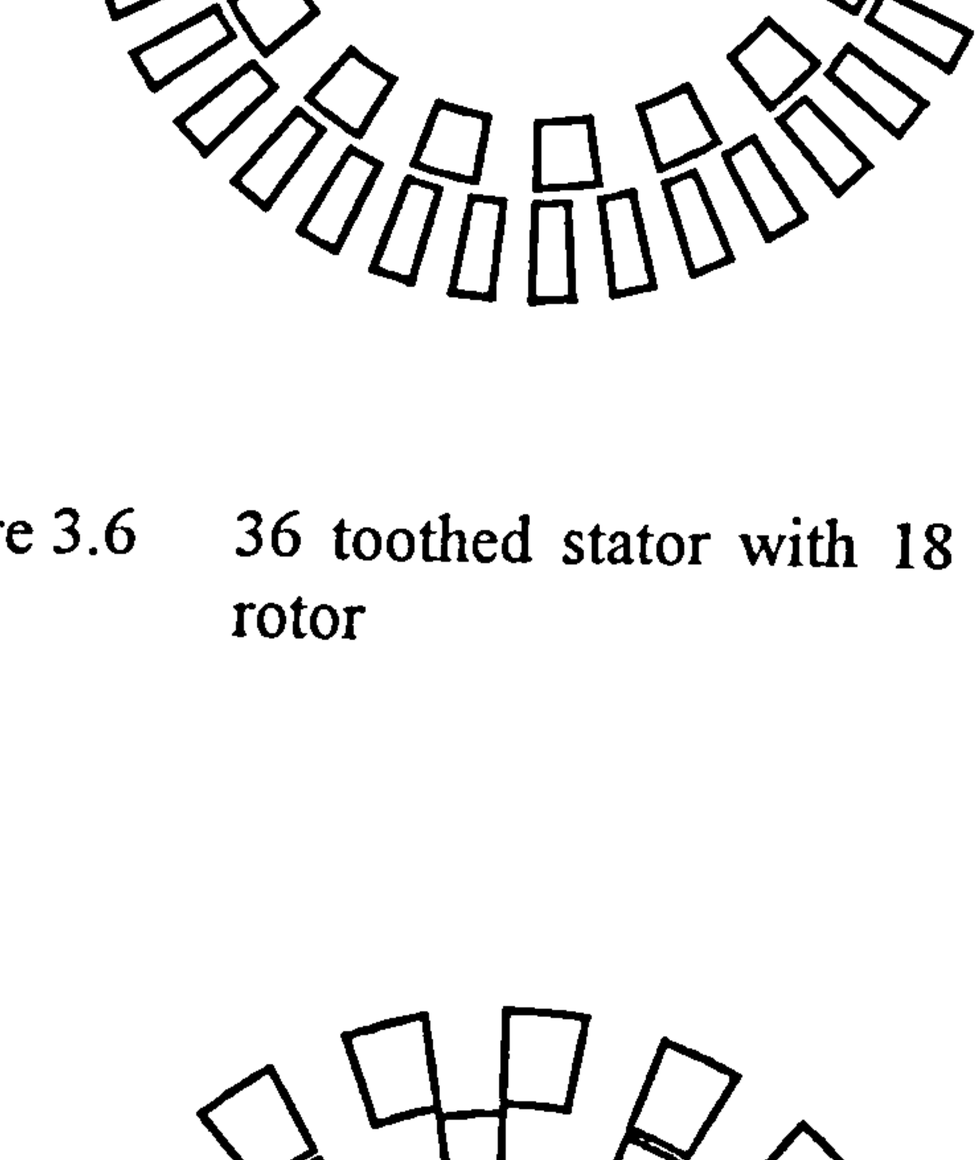

Figure 3.7 12 toothed rotor with 18 toothed stator

3.2.2 Half-scale toothed

In order to investigate the effects of scale, a rotor-stator set was made to half-scale. The shear gap thickness was kept at 0.23 mm - the thinnest used with the large scale units - with 18 teeth on both the rotor and stator. Therefore the classification of these units is **r/18/50/61.44** and **s/18/50/61.9** (copies of **r/18/50/123.34** and **s/18/50/123.8**). This was fitted into a half scale version of the rotor-stator casing. It was fitted onto the existing drive unit and used the same tanks and delivery pump as the large scale mixer (Plate 3.2).

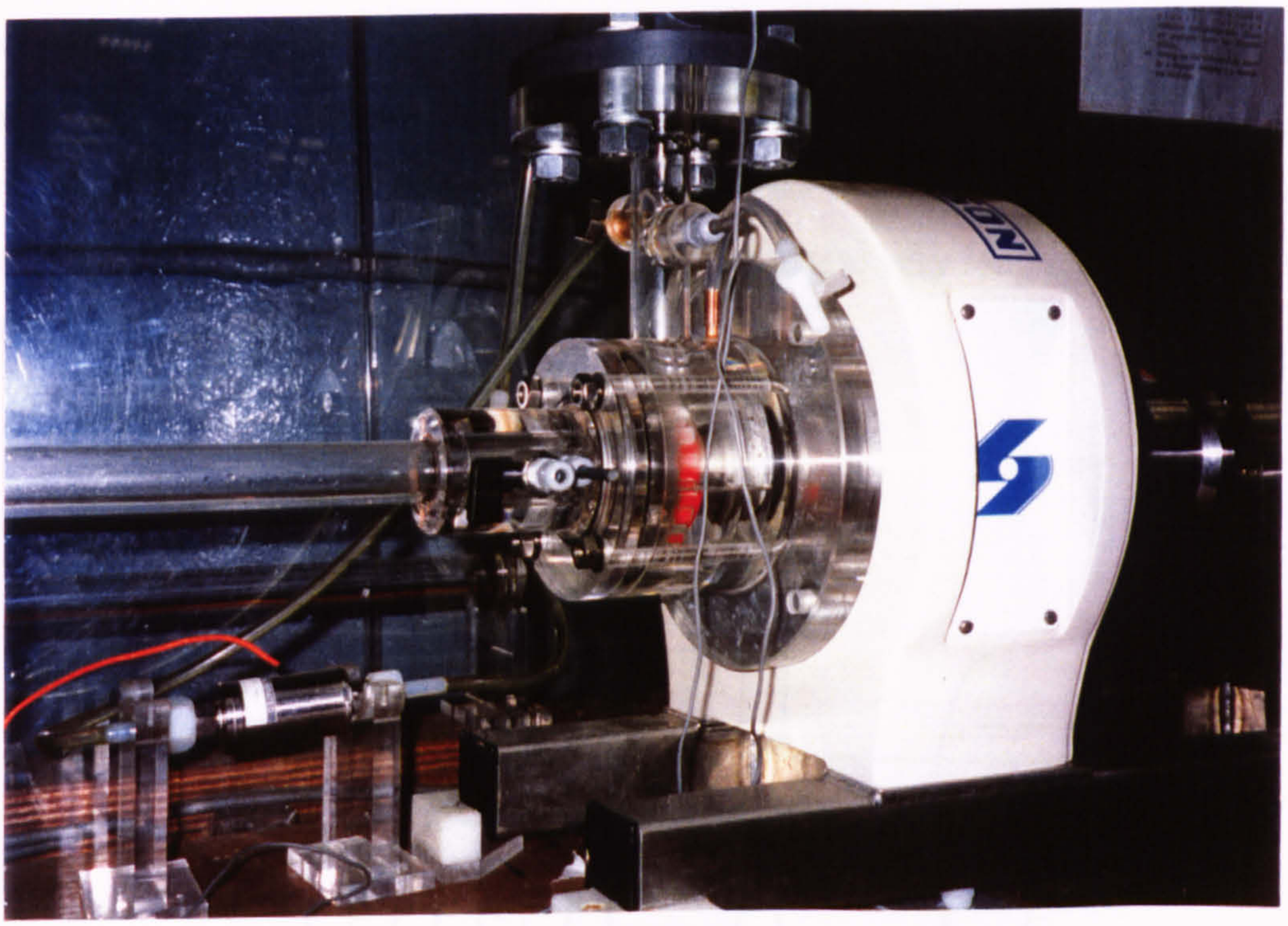

Plate 3.2 Half-scale rotor-stator unit

In order that the scaled down mixer could be fitted onto the existing drive unit, some scaling compromises were unavoidable:

(i) the existing shaft (complete with seal spring) was retained;

(ii) the existing seal and bearings were retained. Mechanical losses therefore remained un-changed between the scales;

(iii) a chamber was machined into the mixer to allow fluid to cool the seal;

(iv) the bullet-shaped nut holding the rotor in place was slightly larger relative to the rotor than at full scale.

These scaling compromises are shown in Figure 3.8. The major effect was that the liquid volume in the volute was slightly smaller relative to the overall volume (when compared to the full-scale unit). It was also possible that a small amount of liquid could pass into the chamber containing the seal, leading to very long residence times as the liquid was slowly flushed out.

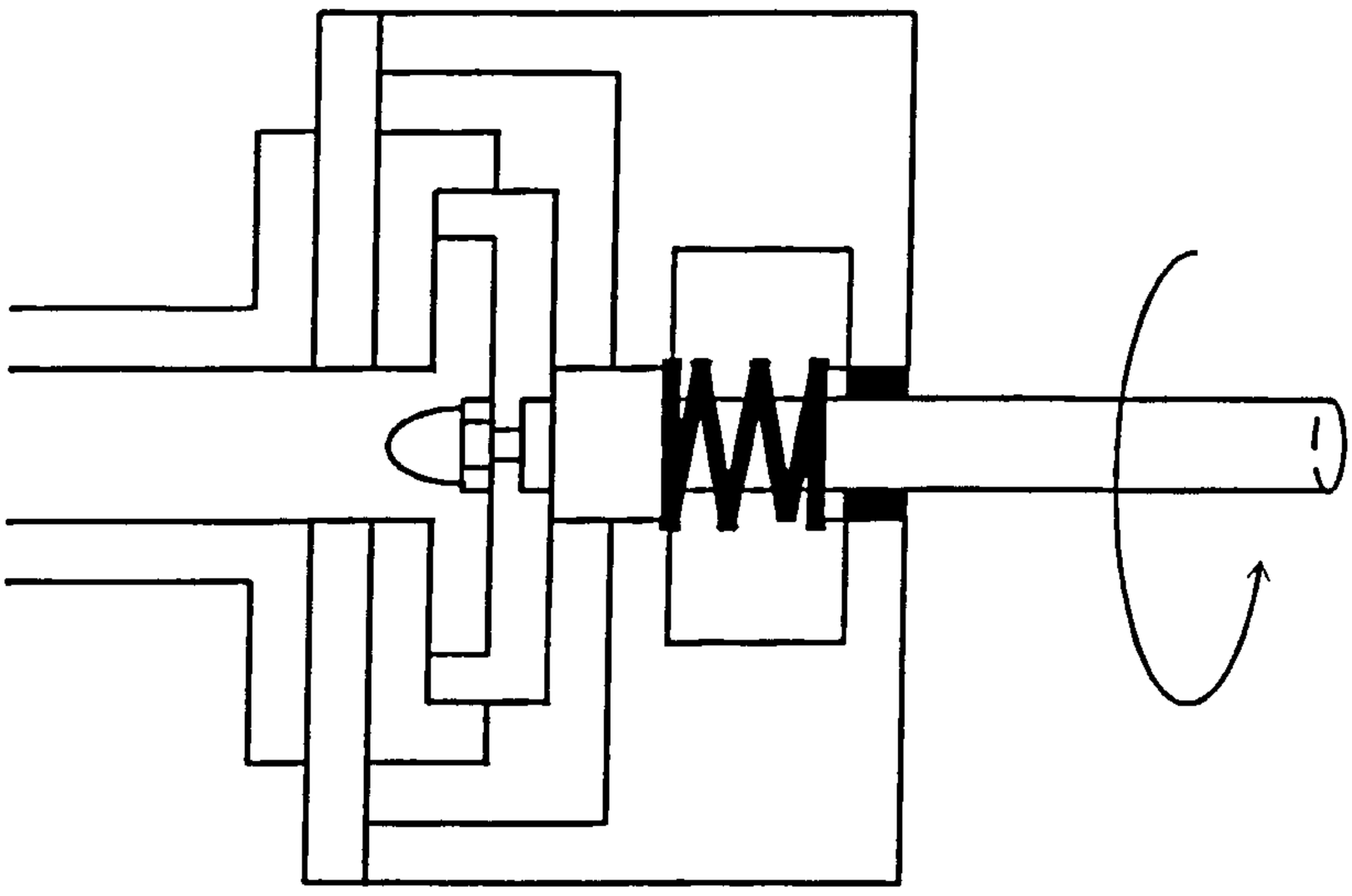

Figure 3.8 Half-scale rotor-stator unit

Much lower shaft torques were expected at this scale, compared to those at the large scale, and so the shaft torque transducer was re-calibrated over a lower range to ensure that reliable results were taken. However, it was recognised that the potential experimental errors would be greater at this scale.

3.2.3 Silverson

This unit was a standard unit produced and supplied by Silverson Limited. The main difference between the Silverson and toothed units was that the rotor resembled more closely the impeller of a centrifugal pump, with swept blades. The shear gap thickness was 0.23 mm. This unit is shown schematically in Figure 3.9, and is compared with the toothed type in Plate 3.3.

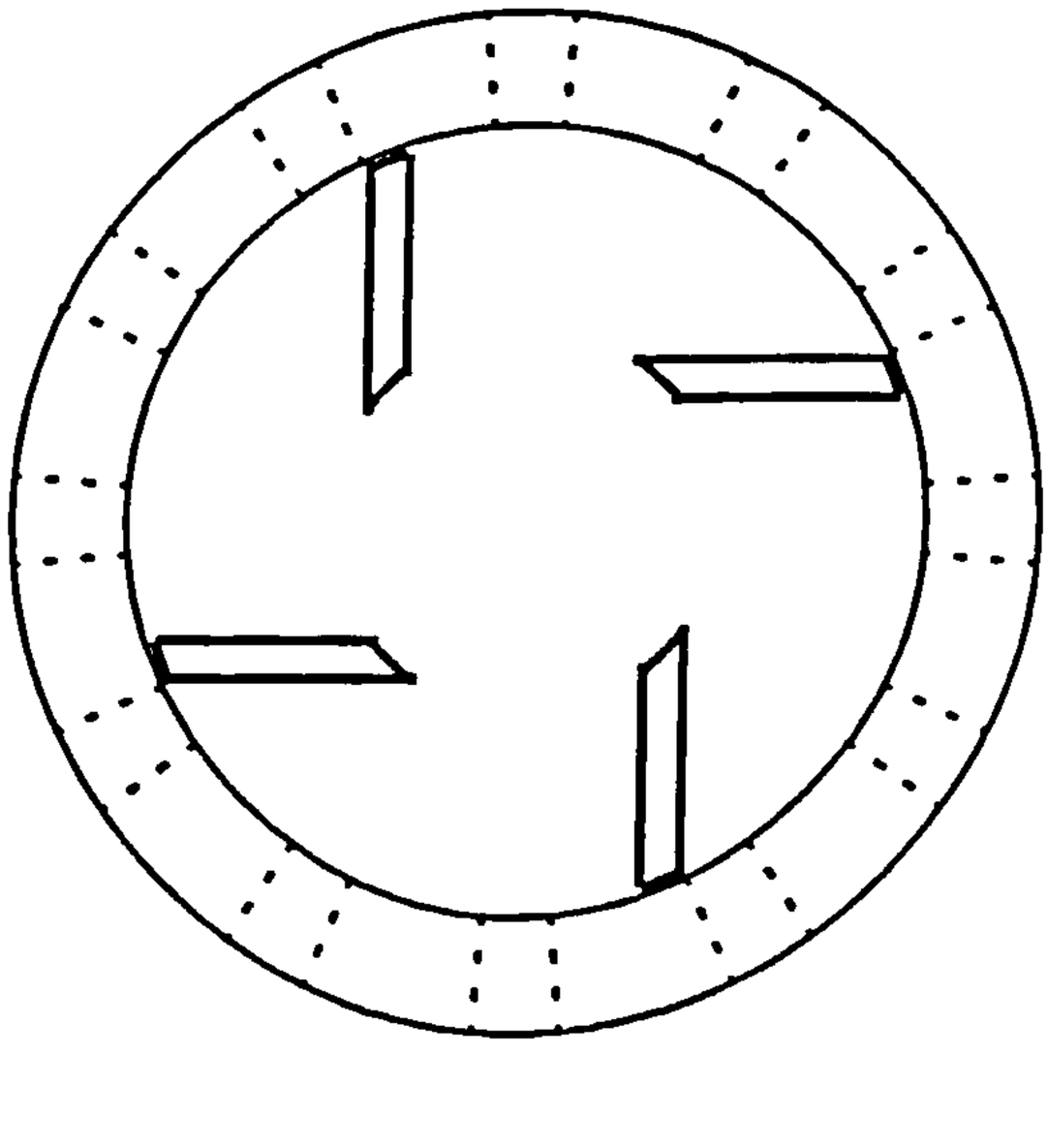

Figure 3.9 The Silverson unit

Plate 3.3 The Silverson unit compared to a toothed unit

3.3 Experimental materials

Mains tap water at room temperature was used for the power balance, flow visualisation and residence time distribution experiments.

For the diazo-coupling experiments, the following compounds were used: sulphanilic acid, sodium nitrite, sodium hydrogen carbonate, sodium carbonate, hydrochloric acid, urea, 1-naphthol, 2-naphthol. These experiments were conducted in de-ionised water at 25°C.

For some of the diazo-coupling experiments the viscosity of the solutions were increased by the addition of Natrosol 250 GR powder. The viscosity of the solution was then checked using a Contraves rheomat 115 rheometer.

3.4 Operation of Rig

The rig was operated as follows:

(i) the submersible pump was switched on and the valves feeding the mixer were opened.

(ii) A high water flow rate (>2 $l.s^{-1}$) was passed through the mixer to remove any air that had accumulated.

(iii) The rotor-stator mixer was then switched on and the rotational speed set using a frequency inverter.

(iv) The flow rate through the mixer was set using the frequency inverter that controlled the submersible pump and control valves.

Once the mixer was running, the flow rate or rotor speed could be varied using the frequency inverters and the control valve.

3.5 Experimental methods

3.5.1 Energy balance

The overall energy balance was shown in Section 2.4.3 to be given by:

$$P_{SHAFT} = P_{PUMP} + P_{MECH} + P_{DISC} + P_{LEAK} + P_{HYDRAULIC} \qquad (2.38)$$

where P_{SHAFT} is the shaft power input, P_{PUMP} is the pumping power output, P_{DISC} is the power loss to disc friction, P_{MECH} is the power lost to seal and bearing losses and $P_{HYDRAULIC}$ and P_{LEAK} are the power due to hydraulic (useful to mixing) and leakage losses.

Not all of the components of the overall energy balance could be determined, for example the distinction between leakage and hydraulic losses is not clear (Sparks, 1993). This section will look at each of the components individually, describing the experimental method used to measure them, or the assumptions made in estimating them.

(a) P_{SHAFT}

P_{SHAFT} was found by measuring shaft torque, Λ, and rotational speed, N:

$$P_{SHAFT} = 2\pi N\Lambda \tag{3.1}$$

N, the rotational speed was measured with a hand-held optical tachometer.

The transducer was calibrated by locking the shaft at one end and adding water to a beaker suspended from a bar fixed horizontally onto the shaft. The incremental volumes of water, the moment arm length and the meter readings were recorded and a regression was performed to determine the calibration constant, see Appendix 2.

(b) P_{PUMP}

Pumping power output was determined by measuring the flow rate through and the pressure rise across the mixer:

$$P_{PUMP} = Q\Delta p \tag{3.2}$$

A 1 bar Druck differential pressure transducer was connected to wall tappings located 1.5 pipe diameters upstream and 3.0 pipe diameters downstream of the mixer. The transducer was calibrated against a Druck DPI 600 digital pressure

indicator. A typical calibration is given in Appendix 2. Since a differential pressure transducer was used (and this was mounted horizontally on the work bench), there was no need to adjust for static head - i.e. at rest the differential pressure transducer read zero bar. Also, the inlet and outlet pipe were of the same diameter, so no adjustment for velocity head was made

(c) P_{MECH}

The rotor was removed and the shaft rotated in the mixer alone. It was assumed that power consumed due to drag on the shaft was small compared to the seal and bearing losses. Equation 3.1 was then used to calculate the mechanical losses.

(d) P_{DISC}

The rotational speed of the rotor, N, was measured and the theoretical power loss to disc friction calculated using two expressions. The first (Equation 3.3, Stepanoff, 1957) assumes that the rotor is a thin disc and the second (Equation 3.4, Jekat, 1986) includes the effect of rotor thickness:

$$P_{DISC} = KN^3D^5 \tag{3.3}$$

$$P_{DISC} = KN^3D^4(D + 5E) \tag{3.4}$$

where K is a constant (=24.8) and E is the rotor thickness at the circumference.

(e) P_{LEAK} **and** $P_{HYDRAULIC}$

These losses were not directly measured, but it was assumed that together they accounted for the difference between the shaft power input and the sum of the losses

above:

$$P_{HYDRAULIC} + P_{LEAK} = P_{SHAFT} - (P_{PUMP} + P_{MECH} + P_{DISK}) \qquad (3.5)$$

3.5.2 Residence time distribution

Residence time distribution curves were produced using a pulse stimulus-response technique with a sodium chloride solution as a tracer. The pulse was injected 1.5 pipe diameters upstream of the mixer and sampled 3.0 diameters downstream of the outlet.

The tracer injector was made in the workshops at the Eidgenössiche Technische Hochschule, Zürich. The injector is shown schematically in Figure 3.10. The small chamber in the end of the injector was filled with a sodium chloride solution (concentration approx. 200 g dm^{-3}). This was released by pulling a small trigger, causing a spring to push the chamber out of the tube. A conductivity probe close to the injector was used to sample the inlet pulse and therefore a measure of the opening time.

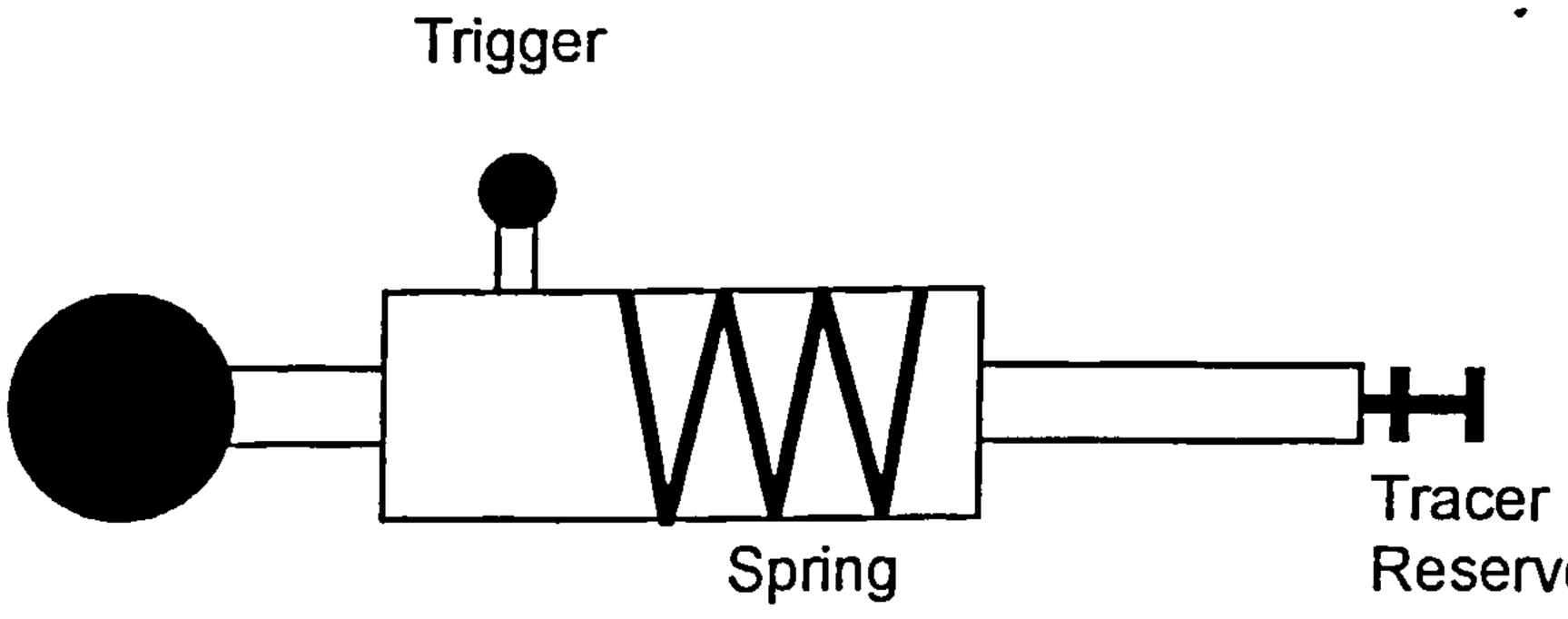

Figure 3.10 The tracer injector

The conductivity probes (Figure 3.11) were made of two platinum wires coated in black, amorphous platinum which were set into a resin shaft (Ruszkowski, 1985).

These probes gave a linear response to concentration change. The probe output was amplified by a standard signal amplifier (produced by in-house workshops) and recorded using a bespoke data acquisition program that stored the signal from the amplifier (via an analogue to digital board) as a temporary text file on the computer hard disk. In the residence time distribution tests, conductivity probe values were sampled for between 2 and 20 seconds during each test (depending upon the flow rate and, hence, nominal residence time) with 5000 values taken per second. The temporary text file was then imported to a spreadsheet package for analysis.

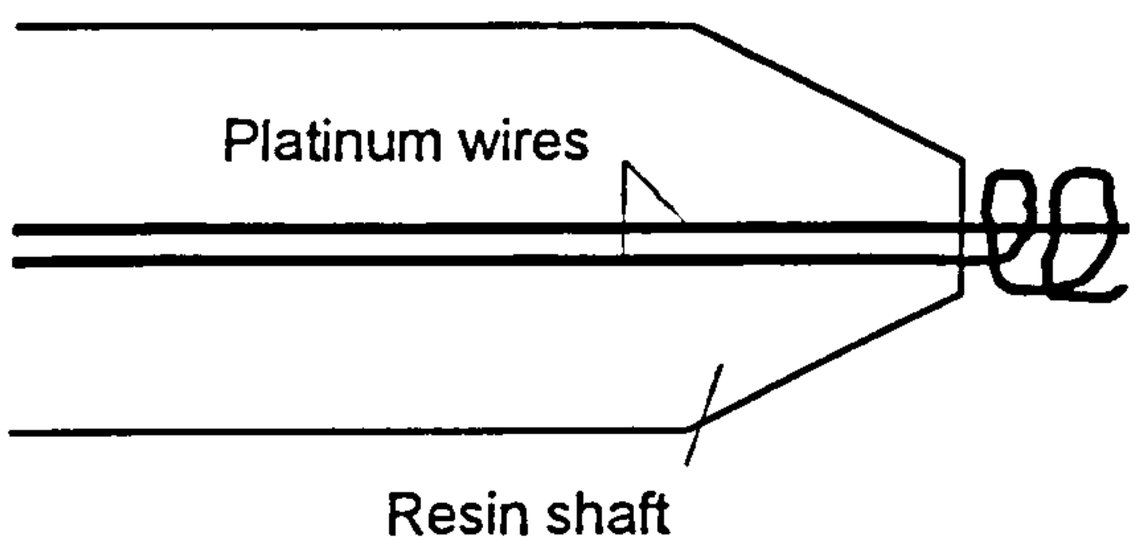

Figure 3.11 The conductivity probe

So that the residence time distributions could be compared with theoretical models and each other on equal terms, they were normalised. The time axis was made dimensionless by dividing by the nominal residence time. All RTD curves were normalised by making the area under the curve equal to one (Levenspiel, 1972):

$$\int_0^\infty C_\theta \, d\theta = 1 \qquad (3.6)$$

A comparison of the inlet and outlet tracer distributions is given in Section 5.3.

3.5.3 Flow visualisation

Three tracers were used for flow visualisation: air bubbles, dye and an acid-base decolourisation scheme. The first two methods did not give a clear view of the flows because they were rapidly dispersed throughout the mixer. The air tracer also tended to collect as a large void on the rotor shaft.

(a) Acid-base decolourisation

The best visualisation was obtained using the acid-base decolourisation scheme - hydrochloric acid and sodium hydroxide with bromo thymol blue tracer. Figure 3.12 shows a schematic diagram of the experimental method. Base solution (coloured with indicator) was injected into the mixer, using a peristaltic pump, to mix with dilute acid that was pumped through the mixer. This produced a flame of blue that decolourised as the base was neutralised by the acid.

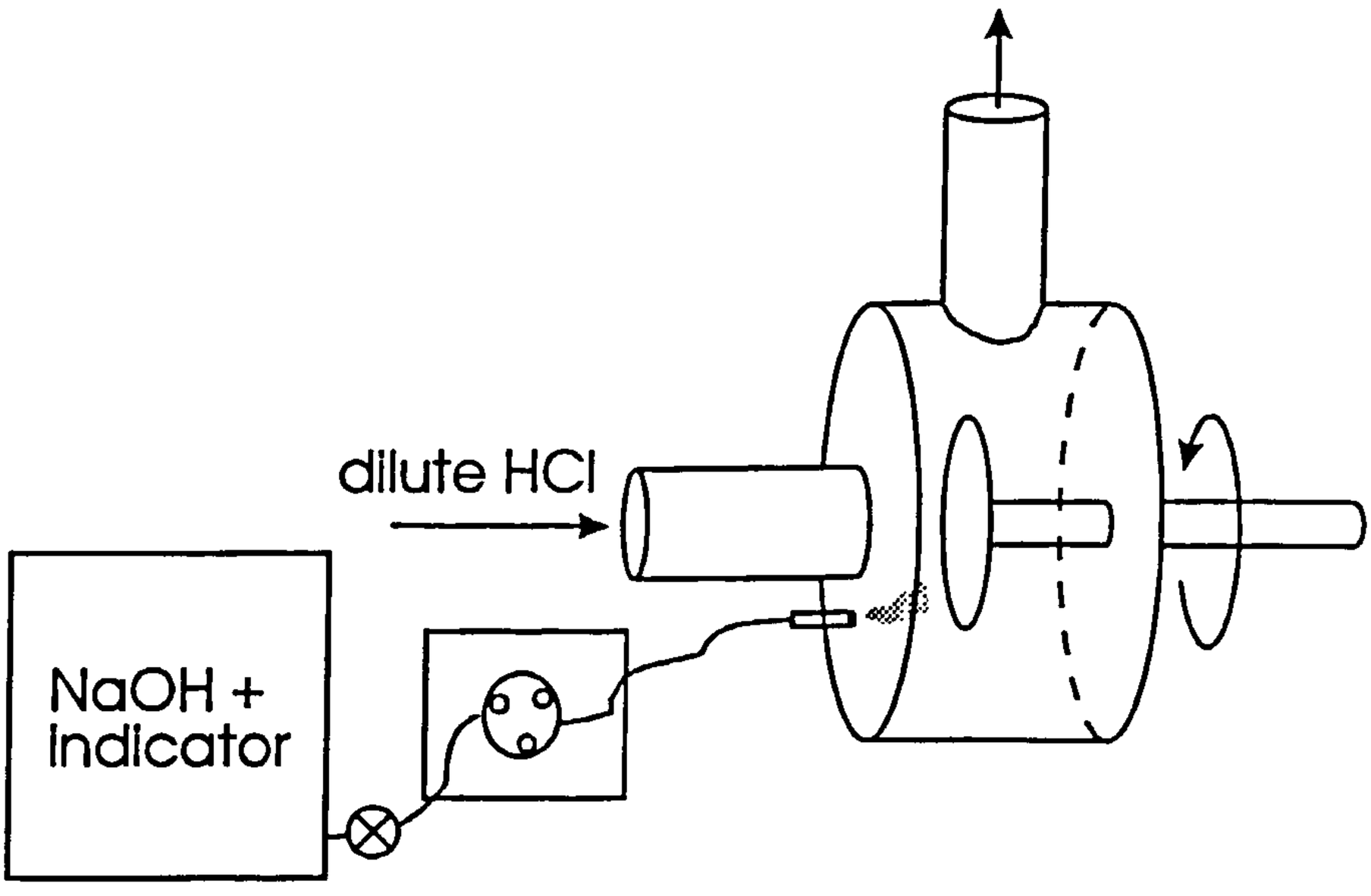

Figure 3.12 Experimental setup for the acid-base visualisation

This experiment was run in semi-batch mode, the effluent from the mixer being returned to Tank 1. The pH of the incoming stream therefore increased slowly during an experiment. When necessary, the pH could be lowered by adding more concentrated hydrochloric acid to Tank 1.

Acid-base decolourisation can be used to quantify mixing performance, by measuring the size of the reaction zone (knowing the local fluid velocities) and using a mixing model (Tovstiga, 1986). However, Tovstiga's studies were done in a pipe, where estimation of the reaction time was possible. In the rotor-stator mixer, given the nature of the device, it was too difficult to follow the flow in sufficient detail to make a quantitative judgement of the turbulent energy dissipation rates.

(b) Feed tube location

In order to investigate the effect of feed tube location and number, a method of feeding for the visualisation (and diazo-coupling) experiments was developed. This involved passing feed tubes through the stator. The feed tubes were held in threaded sleeves that were screwed into tapped holes on the stator, passing through the inlet pipe flange.

Four feed tube locations were used (Figure 3.13):

I through the stator backplate to a point just upstream of the rotor teeth;

II through the stator backplate into the centre of the rotor teeth;

III through the stator backplate into the shear gap;

IV through a stator tooth into the shear gap.

A stator was made, in clear acrylic, that had a feed of type IV in all 18 of the teeth. This was made in two pieces, with a groove machined to connect the feeds that went to each tooth (Figure 3.14)

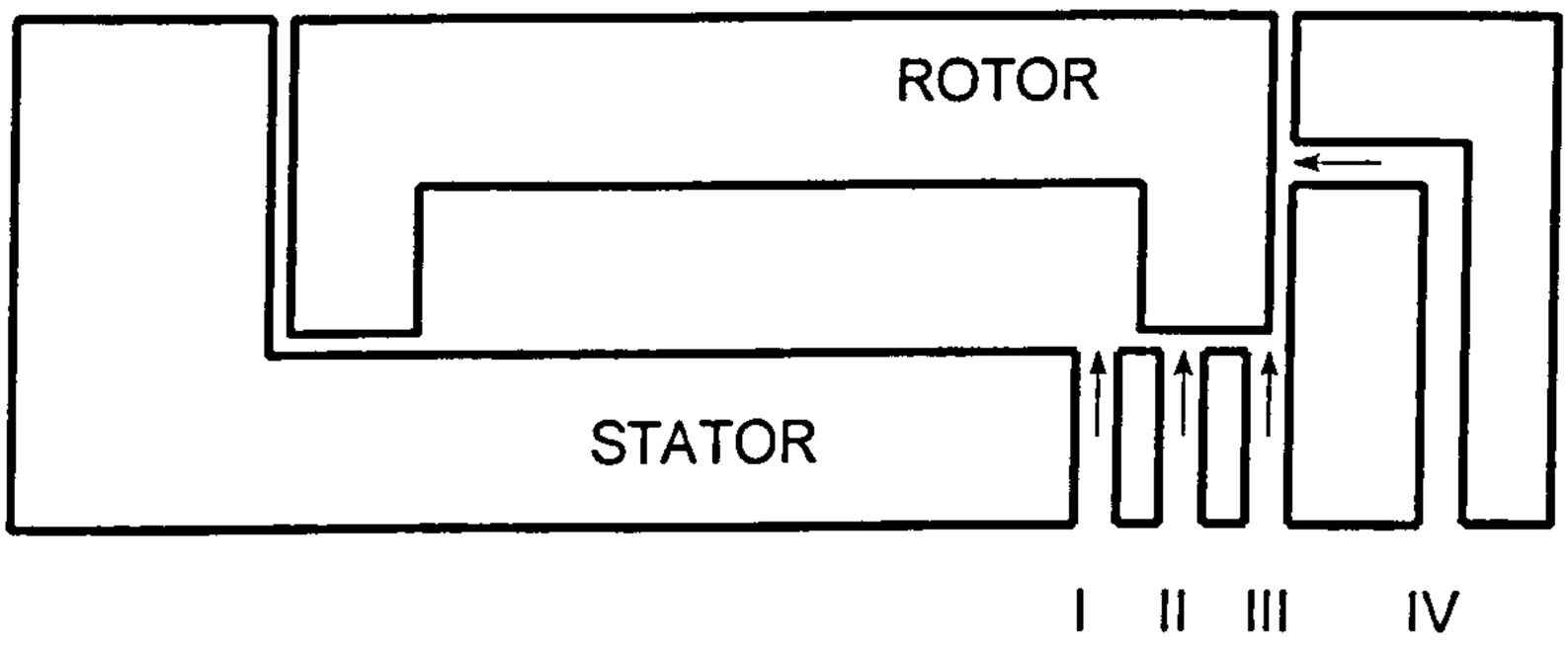

Figure 3.13 Feed positions for flow visualisation and diazo-coupling experiments

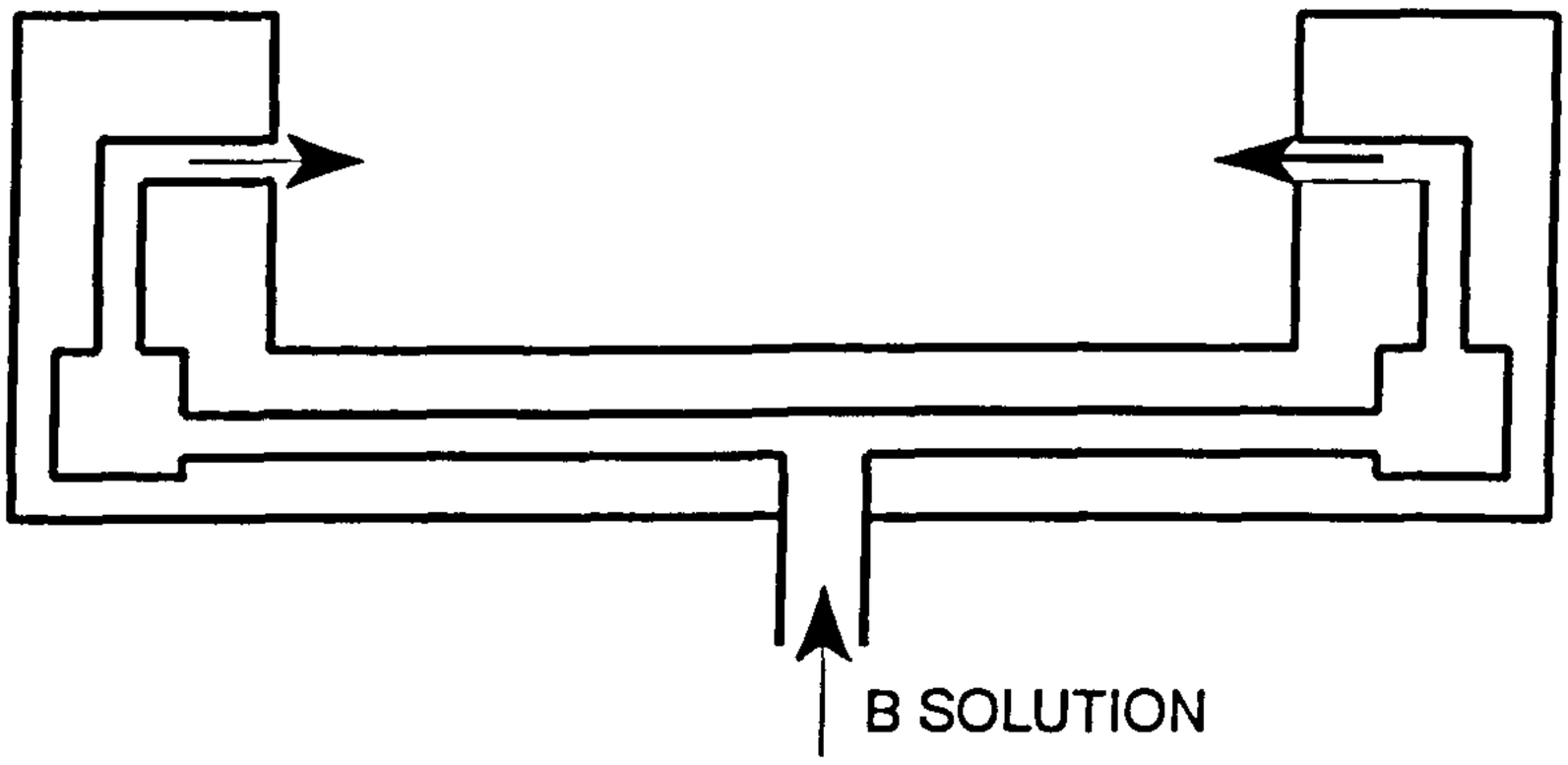

Figure 3.14 Feeding through all 18 stator teeth using a manifold

(c) Computational fluid dynamics

A computational fluid dynamics (CFD) study was used to model the flow in a rotor-stator mixer, predominantly for comparison with flow visualisation data. This was done using Harwell Flow3D version 3.1 running on a Silicon Graphics Indigo workstation with 64 Mbytes of RAM with the IRIX 5.3 operating system.

This study also produced values for ε, the turbulent energy dissipation rate, for comparison with the values estimated using the diazo-coupling experiments.

3.5.4 Competitive chemical reaction

This work used the set of fast, competing chemical reactions known as the extended Bourne reaction scheme (Bourne et. al. 1990, 1992). This was used in Section 2.2.8 when describing the E-model :

$$A + B \rightarrow R \qquad k_{1\text{-}p} = 12238 \quad \pm 446 \text{ m}^3 \text{ mol}^{-1} \text{ s}^{-1} \qquad (2.9)$$

$$A + B \rightarrow T \qquad k_{1\text{-}o} = 921 \quad \pm 31 \text{ m}^3 \text{ mol}^{-1} \text{ s}^{-1} \qquad (2.10)$$

$$R + B \rightarrow S \qquad k_{2\text{-}o} = 1.835 \quad \pm 0.018 \text{ m}^3 \text{ mol}^{-1} \text{ s}^{-1} \qquad (2.11)$$

$$T + B \rightarrow S \qquad k_{2\text{-}p} = 22.25 \quad \pm 0.25 \text{ m}^3 \text{ mol}^{-1} \text{ s}^{-1} \qquad (2.12)$$

$$C + B \rightarrow Q \qquad k_3 = 124.5 \quad \pm 1.0 \text{ m}^3 \text{ mol}^{-1} \text{ s}^{-1} \qquad (2.13)$$

This contains consecutive-competitive reactions (Equations 2.9 to 2.12) and parallel-competitive reactions (Equations 2.9 and 2.13).

All of these reactions compete for diazotized sulphanilic acid, *B*. *A* (1-naphthol) goes to two <u>different</u> monoazo isomers (para and ortho), *R* and *T*, which can both couple to <u>the same</u> bisazo dye, *S*. *C* (2-naphthol) couples with *B* to form a single mono azo dye, *Q*.

The product distribution from these reactions can be mixing dependent under certain circumstances and may be characterised by the product distribution with respect to *Q*, X_Q, defined as:

$$X_Q = \frac{c_Q}{c_R + c_T + 2c_S + c_Q} \qquad (3.7)$$

where c_i = concentration of species *i*.

The chemical concentrations used are given with the results (Section 4.4). This section gives the method used and the recipe for the chemical preparation is given in Appendix 3.

Tank 1 was filled with 2.2 m^3 of a solution of 1- and 2-naphthol (*A* + *C*) dissolved in de-ionised water, the solution was buffered using equimolar amounts of $NaHCO_3$ and Na_2CO_3 to ensure that there would be no pH gradients in the reaction zones. A volume of 0.002 m^3 of diazotized sulphanilic acid (B) was made up in a beaker. During the experiments, Reagents *A* and *C* were pumped from Tank 1 through the mixer to Tank 2 and Reagent *B* was fed into the mixer from the beaker using a peristaltic pump (Watson Marlow 505s with 303 pump heads). The flow rate of the naphthol solution was measured using a magnetic flow meter and the flow rate of *B* was calibrated by placing the beaker on a laboratory scale and monitoring the rate of change of weight (i.e. the mass flow rate). During each run, the flow rate of *B* was set using pre-calibrated speeds on the peristaltic pump. The experiments were conducted in continuous mode, with the reacted chemicals kept in Tank 2 prior to disposal. Samples were taken from a small tap on the outlet pipe (well downstream of the mixer), and then buffered further to give an ionic strength of 444.4 mol m^{-3} (required for the spectrophotometry).

A Hewlett Packard 8452A diode array spectrophotometer was used for the analysis of the samples to determine the concentrations of the dyes produced by the reaction. This was controlled by software on a personal computer (Vale 486 DX33) and ASCII text files were produced giving the absorption over a range of wavelengths, at 2 nm intervals. In order to analyse the data further it was necessary to convert these files so that they gave the spectra over 10 nm intervals. This was done using

a simple FORTRAN program. A sample absorption spectrum, with 10 nm intervals,

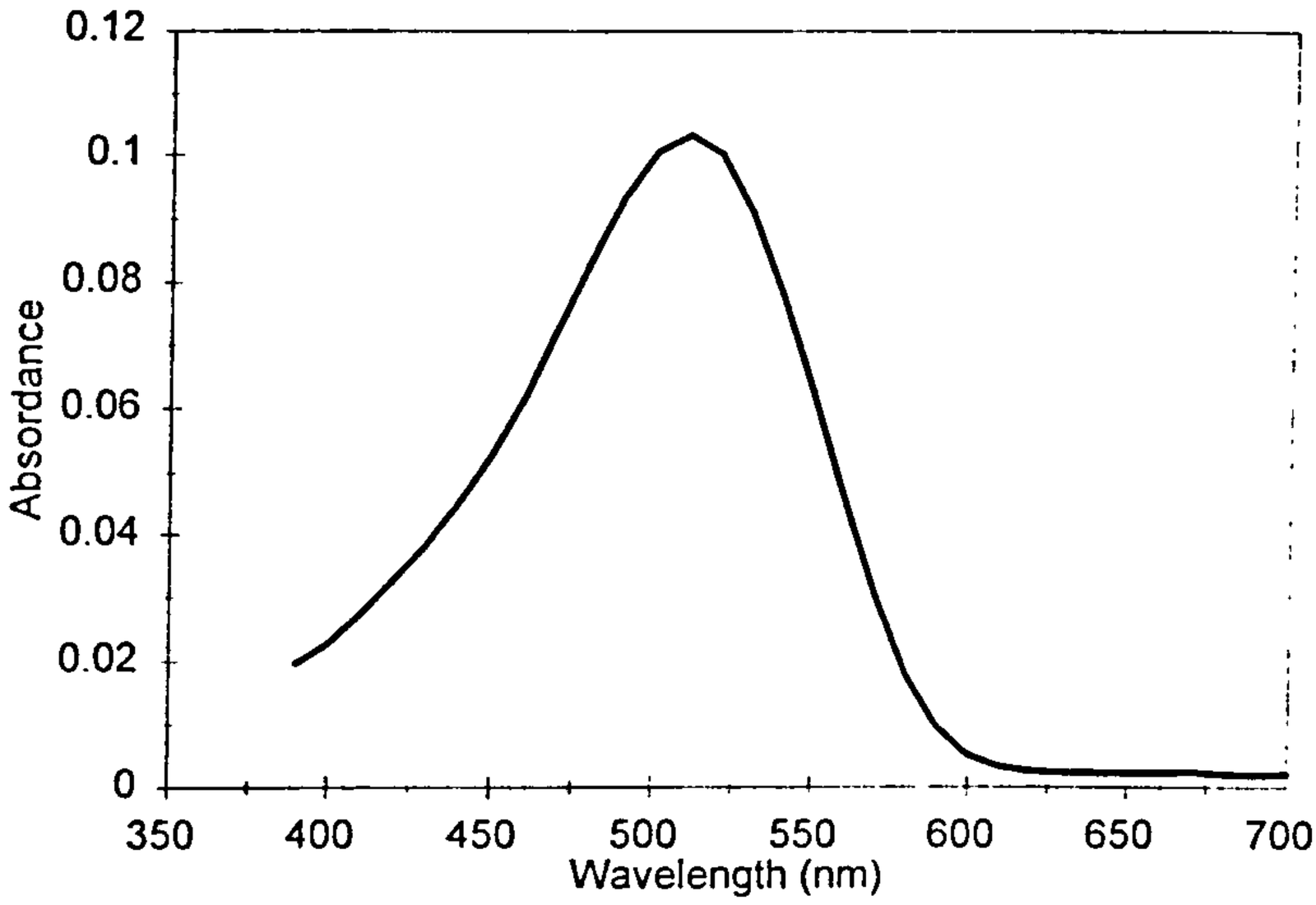

Figure 3.15 An example of an absorption spectrum produced using the spectrophotometer

is given in Figure 3.15.

The spectrophotometry produced a series of absorption spectra, saved as ASCII files with 10 nm intervals. These were analysed with a four parameter regression over the range 390 to 700 nm (using STATGRAPHICS v2.1) given by:

$$A(\lambda) = d\epsilon_R(\lambda)c_R + d\epsilon_T(\lambda)c_T + d\epsilon_S(\lambda)c_S + d\epsilon_Q(\lambda)c_Q \qquad (3.8)$$

where A is the absorbance, d is the light path (the width of the cuvette used in the spectrophotometer, always 0.01 m), and ϵ_i is the molar absorbance coefficient of species i, given by Bourne et al (1990 & 1992).

This yielded concentrations of the reaction products, c_i. X_Q was then determined

using Equation 3.7. The mass balance was checked using:

$$c_{B0} = c_R + c_T + 2c_S + c_Q \qquad (3.9)$$

Bourne et al (1992) report that the experimental error on X_Q, using these apparatus and techniques is ±0.005. The accuracy of the spectrophotometer was checked using a sample provided by Prof. Bourne's workers which gave identical results to those obtained by them (Hearn, 1994). In addition, diagnostic checks made on the spectrophotometer with each test showed that the unit was working correctly. These checks included scanning a sample of de-ionised water, which gave a 'zero reading'. Further confidence in the result produced by the spectrophotometer was obtained from the mass balance check (Equation 3.9).

Therefore, for this work, it was assumed that the possible error on X_Q was ±0.005. The implications of this possible error on the analysis of the results are discussed in Section 5.5.2.

3.6 Discussion of the experimental approach

The diazo-coupling technique described above was used to investigate the performance of the rotor-stator unit as a chemical reactor. This technique was used because it is well documented and has been used to investigate other types of reactor (e.g. motionless mixers, stirred tank mixers).

The diazo-coupling experimental work was done for two main reasons. Firstly, to produce qualitative information, for example the effect of feed tube location or operating condition on product yield. Information like this is useful in it own right, since it may allow a design engineer to make informed decisions on how to improve the yield from a particular process. Secondly, the diazo-coupling data are useful for

examining the characteristics of the flow and mixing in a reactor. Since a robust model for micro-mixing (that uses ε as an input) exists (Section 2.2), then the data taken under micro-mixing limited conditions can be analysed to estimate a value for ε. ε is a parameter that may also be used in other models, e.g. models predicting drop size in inviscid liquid-liquid mixtures. For this reason, the diazo-coupling experiments were designed with the aim of ensuring that micro-mixing controlled the mixing rate.

In order to select chemical and operating conditions that give micro-mixing-controlled results, knowledge of the turbulent energy dissipation rate and flow pattern through the mixer is required. However, there is very little information on these in the literature on rotor-stator mixers and none on mixers of the geometry and scale investigated here. Nonetheless, estimates of the turbulent energy dissipation rate could be made from overall energy balances and the flow pattern could be visualised. Therefore the progression of the experimental work was: (I) measure the overall energy balance. (ii) Determine flow patterns through the mixer.(iii) Use the above data to design and execute diazo-coupling runs.

This approach also provided useful data at each stage, for example the performance of rotor-stator mixers as pumps and the effect of tooth design or shear gap thickness on shaft power draw.

Throughout this work, the conditions for the use of Baldyga and Bourne's (1989) E-model for micro-mixing were satisfied ($c_{B0} \gg c_{A0}$ and $Sc < 4000$). Therefore, when micro-mixing was shown to limit the mixing rate, the E-model was used to estimate ε. The E-model was also used when designing the diazo-coupling experiments, using estimates for ε produced from the overall power balance work to ensure that, if micro-mixing controlled the mixing rate, the product distribution would be

sensitive (i.e. would change significantly) over the range of the experimental conditions. A listing of the computer program used to solve the E-model equations, using a modified mid-point Euler method, is given in Appendix 5. The model is discussed in Section 2.2.8.

The product distribution for the extended Bourne reaction scheme used to characterise the mixing performance, X_Q, depends upon several factors for example: the stoichiometric ratios of the reagents, given by:

$$\sigma = \frac{n_{A0}}{n_{B0}} \tag{3.10}$$

$$\xi = \frac{n_{C0}}{n_{B0}} \tag{3.11}$$

where n_{A0} is the initial number of moles of substance A etc; the ratio of reagent flow rates, a (Equation 2.22); the scale of the rate limiting mixing step (macro/meso/micro-mixing) and Damkohler number (e.g. Equation 2.21) which is a measure of mixing rate that includes ε.

X_Q will also depend on the flow through the reaction zone. Plug flow will ensure that reaction products are not re-engulfed into the reaction zone to react with fresh B. In a back-mixed reactor this will occur and therefore reaction by-products may be formed. It was assumed for the analysis in this work that the rotor-stator behaved as a plug-flow reactor.

The reaction scheme, then, is sensitive to mixing conditions, but these mixing conditions must be chosen carefully: if mixing is too rapid then the product

selectivity approaches a kinetic limit (which can be calculated to be $X_Q = 0.067$, Bourne et al 1992). This limit exists as the reaction scheme is competitive parallel, if it were competitive consecutive (as the scheme given in Equations 2.28 and 2,29 is) then product selectivity can approach zero. The most valuable mixing conditions from the point of view of determining the turbulent energy dissipation rate, ε, and therefore the conditions sought here are those where micro-mixing limits the overall rate of mixing (i.e. it is the slowest step, see Section 2.2). Further, it is also desirable to find mixing conditions to which the product selectivity is sensitive (i.e. a small change in mixing condition gives a large change in product selectivity) since this will reduce the importance of the experimental error on X_Q.

In general terms, the faster the mixing, the lower X_Q was. If Q were a waste product (and S, R & T were the desired products) then a greater yield is given by faster mixing.

Broadly, the design of diazo-coupling experiments proceeded as follows (Figure 3.16). A set of operating conditions (N and Q) were selected. Then, using data from the overall energy balance work, values for ε were calculated (Sections 2.33, 5.1.6 and 5.1.7). Chemical conditions (concentrations and addition rates) were then selected. The E-model was then used to predict product selectivities (X_Q) for each value of ε (for fixed chemical conditions, ε is the only variable that is changed in the input to the E-model and it depends on N and Q).

X_Q values were then plotted against operating condition (represented solely by ε) and they were checked for sensitivity. Once conditions where X_Q varied significantly with ε were established, these conditions were adopted. The process was labourious and time-consuming. It should be possible to produce "batch files" for any future work which could be set-up easily and left to run for many hours.

In addition, checks to ensure that micro-mixing limited the overall mixing rate were made (developed in Section 5.4.1).

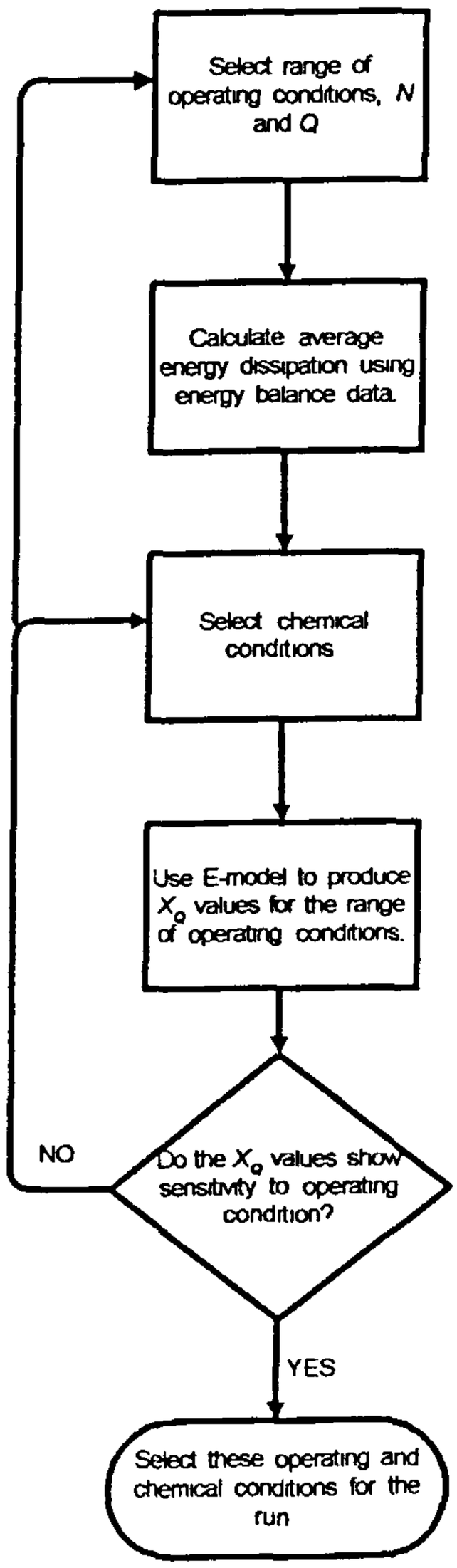

Figure 3.16 Flow-chart showing procedure for designing diazo-coupling tests.

CHAPTER 4

RESULTS

A range of experiments were carried out, covering the areas of the power balance, flow visualisation studies, residence time distribution measurements and diazo-coupling reactions. The details of the experiments and the locations of the data produced are identified below and discussed in Chapter 5.

4.1 Power balance

Power balance data (shaft torque and differential pressure at given shaft speeds and flow rates) over the range 0 to 3000 revolutions per minute in 500 rpm intervals and 0 to 5 $l.s^{-1}$ in 0.5 $l.s^{-1}$ intervals, were collected for each of the toothed designs and the Silverson design. Similar data were collected for the half-scale toothed mixer, over the range 0 to 4000 rpm (500 rpm intervals) and 0.0 to 3.2 $l.s^{-1}$ (in 0.1 or 0.2 $l.s^{-1}$ intervals). These raw data are presented in Appendix 4. The analysis of the raw data for the power balance (e.g. shaft power, pumping efficiency) is presented in Section 5.1.

4.2 Flow visualisation

Flow visualisation was undertaken throughout the experimental phase of this work. The visualisation was performed using a variety of tracers: air bubbles, dye, dust particles and acid-base decolourisation. Many of the flow visualisation tests were videotaped, using a camera with a magnifying lens and the resulting footage was replayed to determine flow features in the mixer (the shutter speed on the camera was adjustable, allowing the rotor to be frozen on the screen). The findings of the

flow visualisation work are presented in Section 5.2.

4.3 Residence time distribution

Residence time distribution measurements were taken for all of the rotor-stator designs, over the complete range of operating conditions. Results are given in Section 5.3.

4.4 Diazo-coupling

The diazo-coupling experiments were conducted as groups of experiments, termed runs. During each run, a number of samples were taken for analysis.

Preliminary runs were used to develop experimental procedures. The main finding of the early runs was that X_Q was much lower when feeding through a feed directly onto the rotor hub than when feeding into the inlet pipe upstream of the mixer. This confirmed that it is unwise to feed into the inlet pipe of a rotor-stator mixer when conducting fast, mixing controlled reactions.

Unfortunately, the results from one of the later runs could not be used because of an unidentified contaminant that interfered with the spectrophotometric analysis.

The runs presented in this thesis are detailed in the following sections. For all runs reported here, the concentration of A was 0.03 mol.m^{-3}, the concentration of C was 0.17 mol.m^{-3} and the concentration of B was 50 mol.m^{-3}.

4.4.1 Run 1 - r/18/50/119.6 & s/18/50/123.8, viscosity = 0.89 cP

For this run the method of feeding through the stator was developed and the four feed tube positions shown in Figure 3.13 were used. Four samples were taken and the results are presented in Table 5.5.

4.4.2 Run 2 - r/18/50/123.34 & s/18/50/123.8, viscosity = 5.9 cP

For this experiment, the viscosity of the reactants was changed by the addition of Natrasol GR, giving a Newtonian solution. This higher viscosity was used to slow the micro-mixing step, attempting to make it limit the overall mixing rate (macro-mixing and meso-mixing rates are unaffected by viscosity). The four feeds upstream of the rotor teeth (Position II) and two tooth feeds (Position IV) on adjacent teeth were used. 14 samples were taken and they are presented in Table 5.6.

4.4.3 Run 3 - r/18/50/121.45 & s/18/50/123.8, viscosity = 4.0 cP

Similar feeding arrangements to those in Run 4 were used. 15 samples were taken and they are presented in Table 5.7.

4.4.4 Run 4 - r/18/50/123.34 & s/18/50/123.8, viscosity = 6.6 cP

Reagents *B* was fed using the 18 feed tube manifold stator (Figure 3.14). 19 samples were taken and they are presented in Table 5.9.

CHAPTER 5
DISCUSSION

The power balance, residence time distribution and flow visualisation data and findings will be analysed and discussed in the following sections. The design of diazo-coupling experiments will be discussed in the light of the findings from the above and diazo-coupling data will be presented and analysed to estimate local turbulent energy dissipation rates. Finally, the flow and mixing in rotor-stator mixers will be discussed.

5.1 Power balance

The individual components of the power balance are given in Equation 2.38:

$$P_{SHAFT} = P_{PUMP} + P_{MECH} + P_{DISC} + P_{LEAK} + P_{HYDRAULIC} \qquad (2.38)$$

5.1.1 Shaft power, P_{SHAFT}

Examples of shaft power results - for two of the toothed designs (**r/18/50/123.34** & **s/18/50/123.8** and **r/18/50/121.45** & **s/36/50/123.8**), the Silverson and the half-scale toothed, are shown plotted versus flow rate for a range of shaft speeds in Figures 5.1 to 5.4 respectively.

General observation of these data show that, with the same operating conditions, the toothed rotor-stator with the thinnest gap (Figure 5.1) draws more power than the rotor-stator with the medium shear gap (Figure 5.2). The Silverson draws slightly less shaft power than the toothed designs and the half-scale mixer draws

significantly less shaft power. In all cases, shaft power increases with both shaft speed and flow rate.

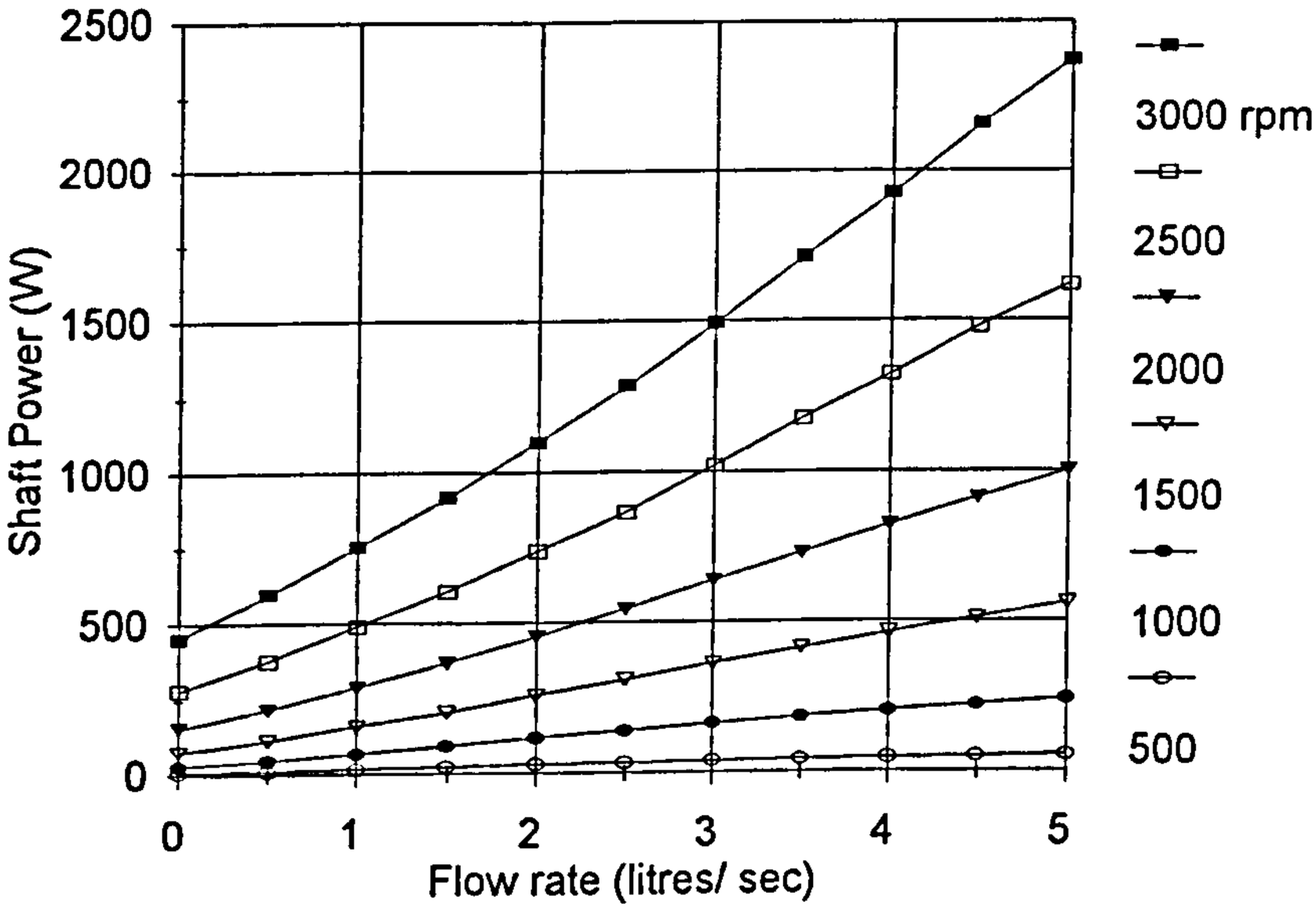

Figure 5.1 Shaft power versus flow rate for a range of shaft speeds **(r/18/50/123.34 & s/18/50/123.8)**

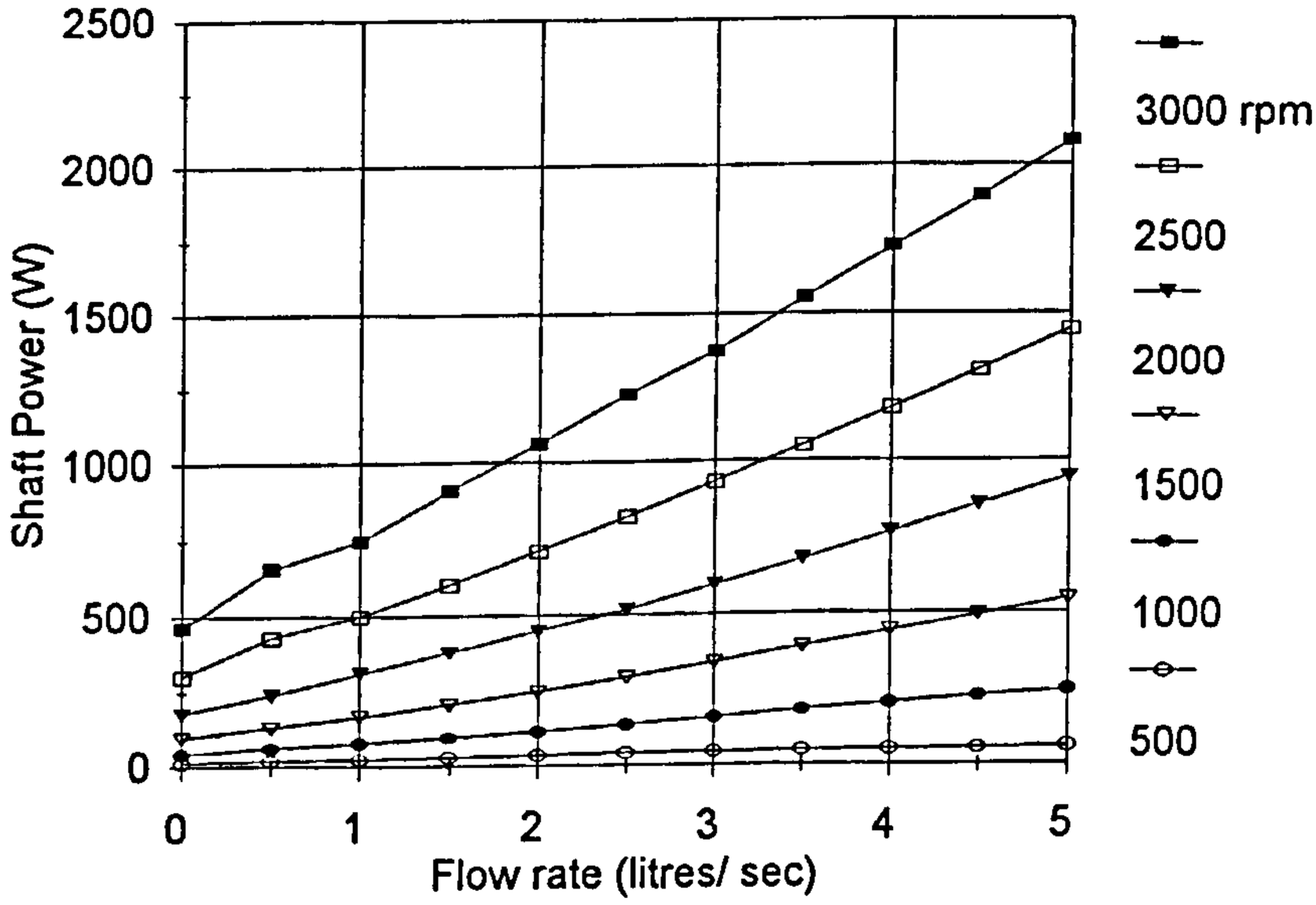

Figure 5.2 Shaft power versus flow rate for a range of shaft speeds **(r/18/50/121.45 & s/36/50/123.8)**

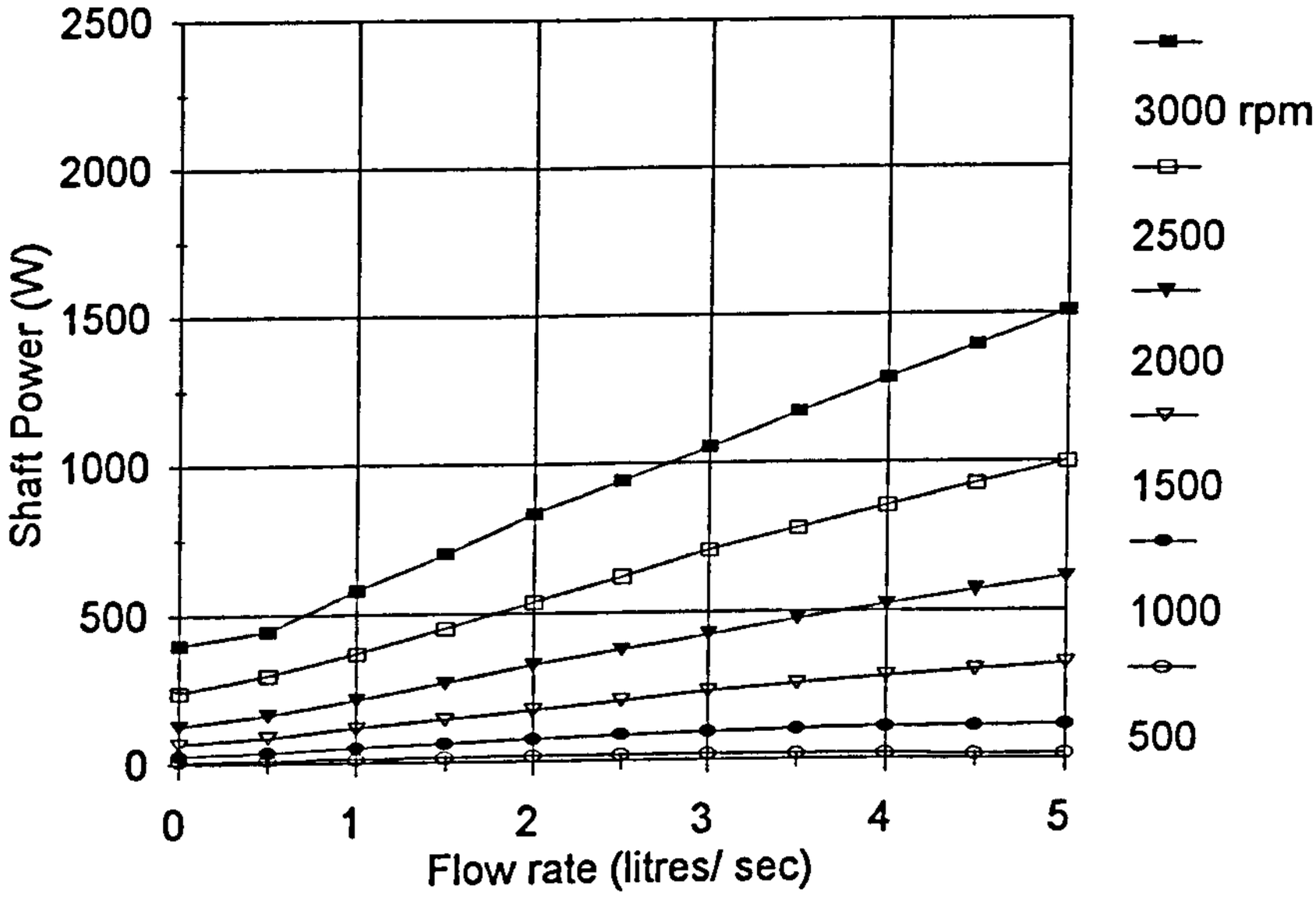

Figure 5.3 Shaft power versus flow rate for a range of shaft speeds (Silverson)

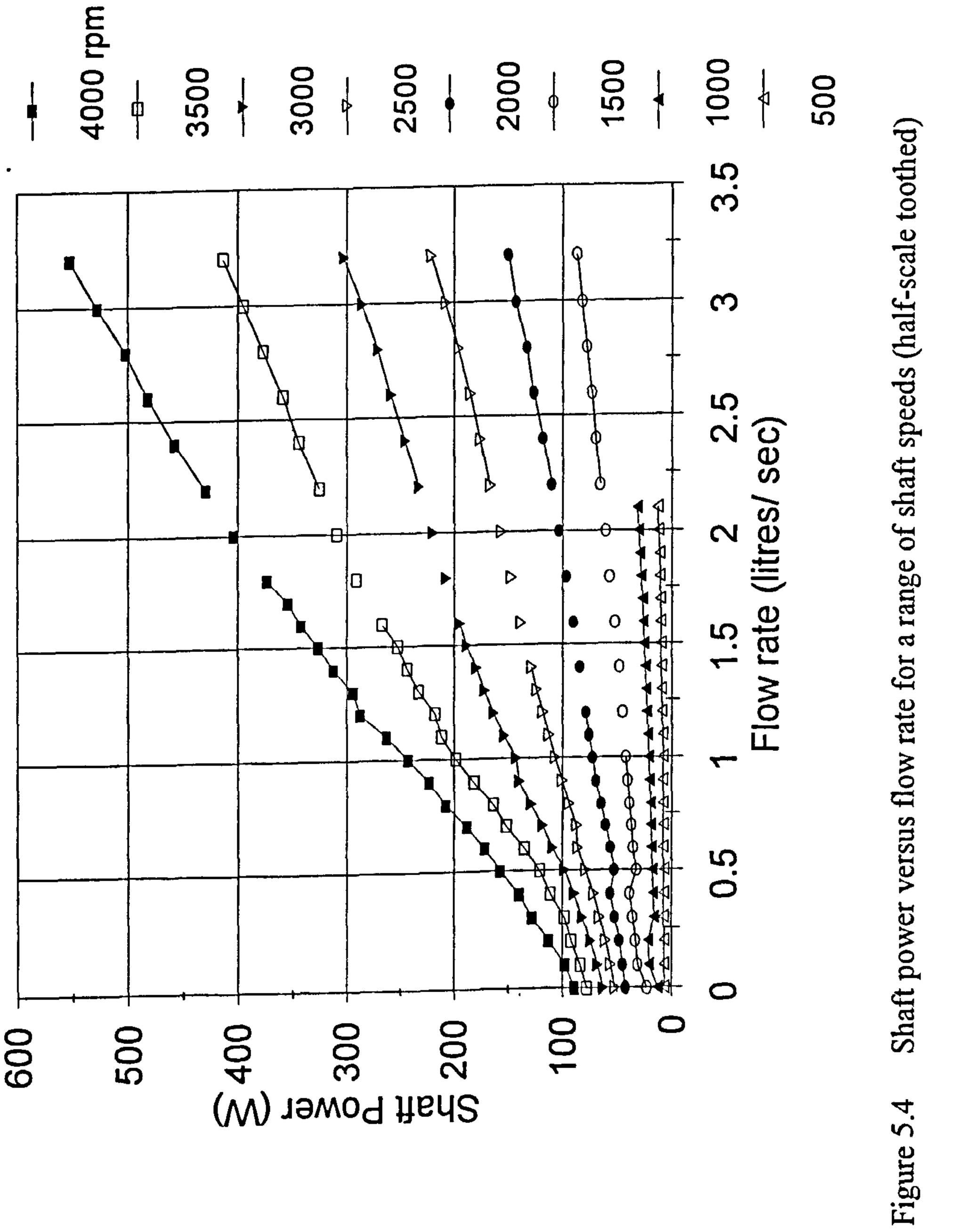

Figure 5.4 Shaft power versus flow rate for a range of shaft speeds (half-scale toothed)

(a) Effect of rotor-stator design

The toothed rotor-stator units designed for this work allowed the shear gap thickness, the number of teeth (on both rotor and stator), the open area (of both rotor and stator) and rotor-stator interaction (how the rotor and stator teeth align) to be varied. The effect of changing these parameters is discussed below

Figure 5.5 shows shaft power versus shear gap thickness, at 3000 rpm and 3.0 $l.s^{-1}$, for all toothed rotor-stator combinations. This shows that shaft power is significantly higher with the thinnest shear gap, but is approximately the same for the medium and thickest shear gaps. Furthermore, for all rotors the shaft power is significantly lower with **s/18/33/123.8**. The spread of shaft power data is not affected by shear gap thickness significantly, being of the order of 100 W for each grouping of points. The increase in shaft power at the smallest shear gap could be due to a direct loss (due to mean velocity gradients in the shear gap between rotor and stator teeth). However, **s/18/33/123.8** (the stator with the smallest open area - and therefore the 'longest' shear gap) has the lowest shaft power. If losses due to mean velocity gradients in the shear gap are at all significant with the thinnest shear gap, then they will be insignificant for the medium and thick shear gaps (since there is little difference in shaft power between these two shear gap thicknesses).

Figure 5.6 shows shaft power versus flow rate for a range of shear gap thicknesses, also showing that the shaft power increases with flow rate. As was shown in Figure 5.5, the shaft power is highest with the thinnest shear gap and is similar with the medium and thickest shear gaps.

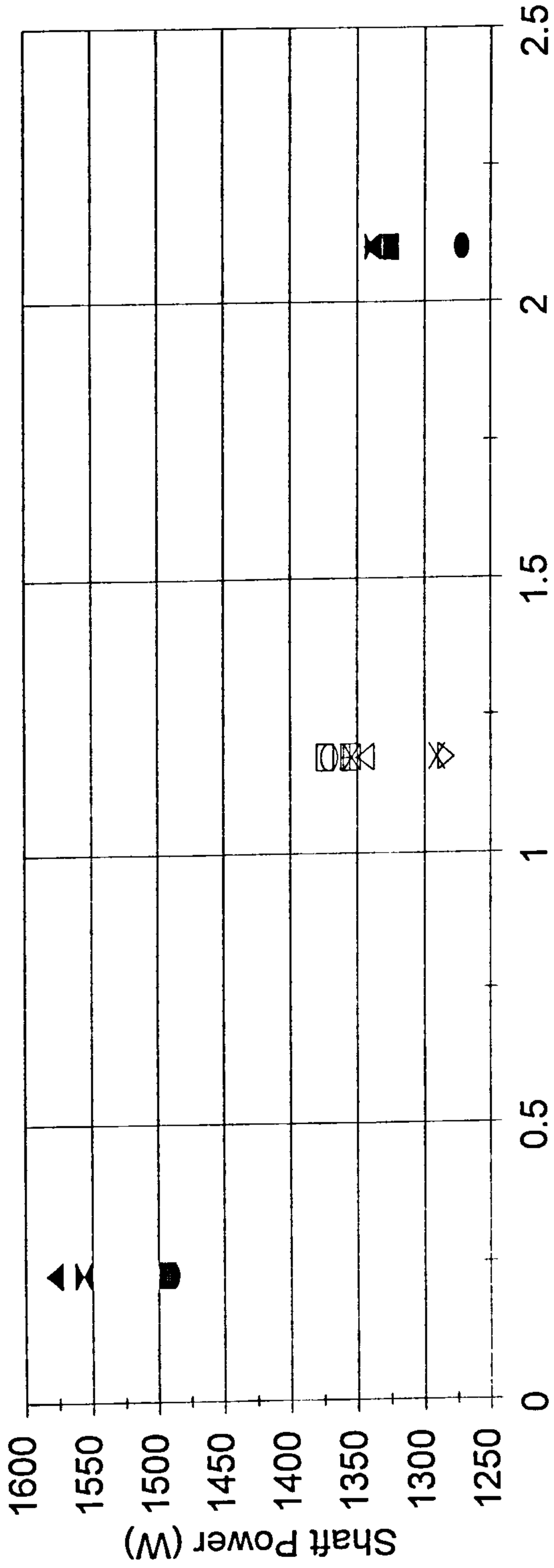

Figure 5.5 Shaft power for all toothed combinations at 3000 rpm and 3.0 $l.s^{-1}$.

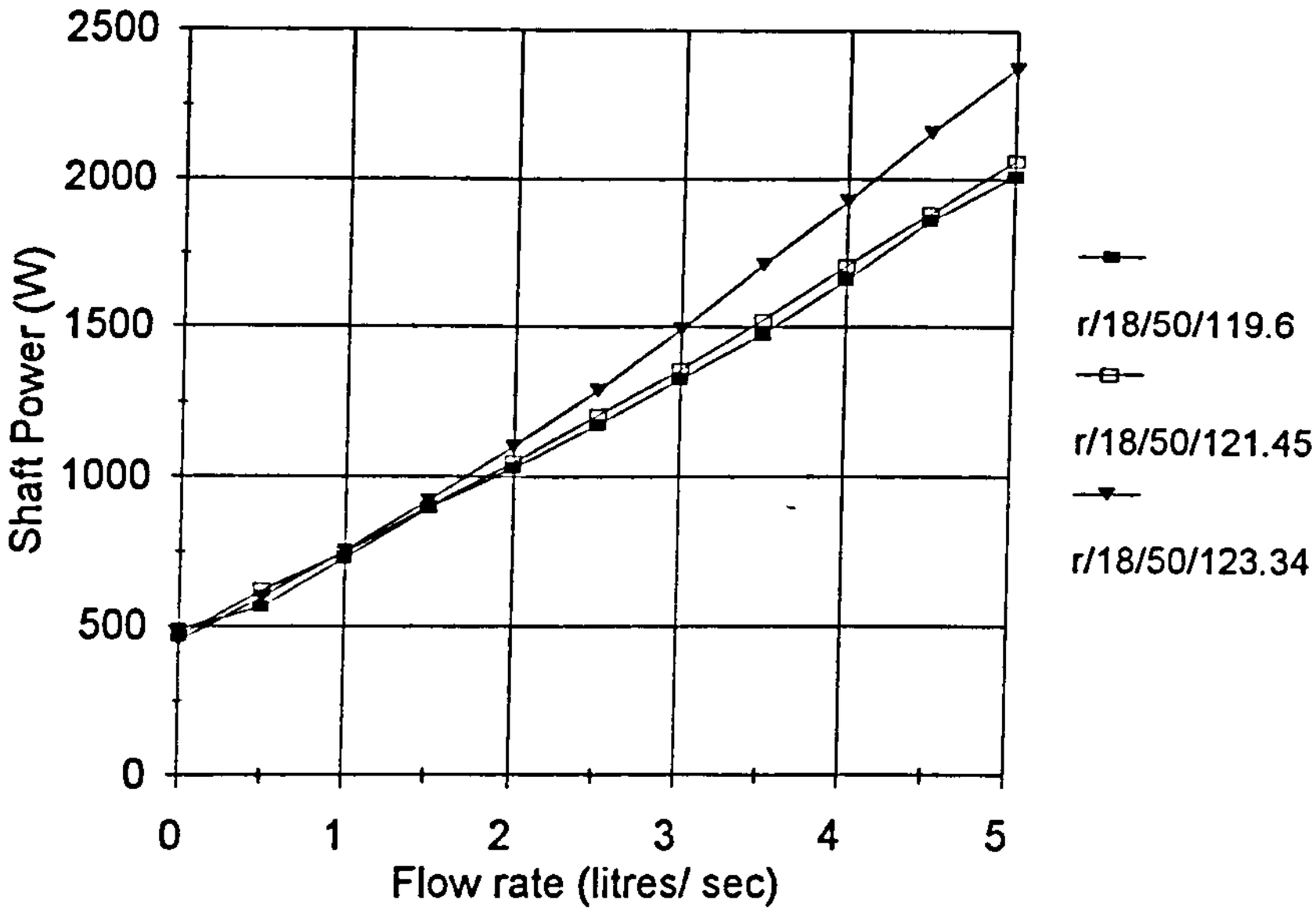

Figure 5.6 Shaft power versus flow rate for a range of shear gap thicknesses with **s/18/50/123.8** (at 3000 rpm)

There is little change in shaft power as the number of teeth on the rotor is changed. Figure 5.7 shows shaft power data for the 12 and 18 toothed rotors (both with **s/18/33/123.8**). For both of the shaft speeds shown in this figure (2000 and 3000 rpm), there is little difference in shaft power. This supports the finding above that losses in mean velocity gradients in the shear gap are small with the medium shear gap thickness, as the contact length (the length within which these losses would occur) between the rotor and stator is changed by changing the number of teeth yet there is little difference in shaft power. If there were a significant increase in shaft power then one possible explanation would be increased losses in the shear gap.

The effect of stator design is shown in Figure 5.8 in which shaft power is given versus flow rate for **r/18/50/121.45** with each of the stators (at 3000 rpm). Shaft power is lowest with **s/18/33/123.8**, as above. Stator design has little effect on shaft

power in the cases of the other stator designs. The possible effect of pulsation through the rotor-stator as stator slots are blocked by the rotor teeth, as discussed in Section 3.2.1, is not detected using these measurements. The effective open area of the 18 toothed rotor with 18 toothed stator arrangement goes from fully open to fully closed, whereas for the 19 and 36 toothed stators with the 18 toothed rotor the open area remains constant (at 50%) i.e. there is little difference between **s/18/50/123.8** and the **s/19/50/123.8** and **s/36/50/123.8** toothed stators.

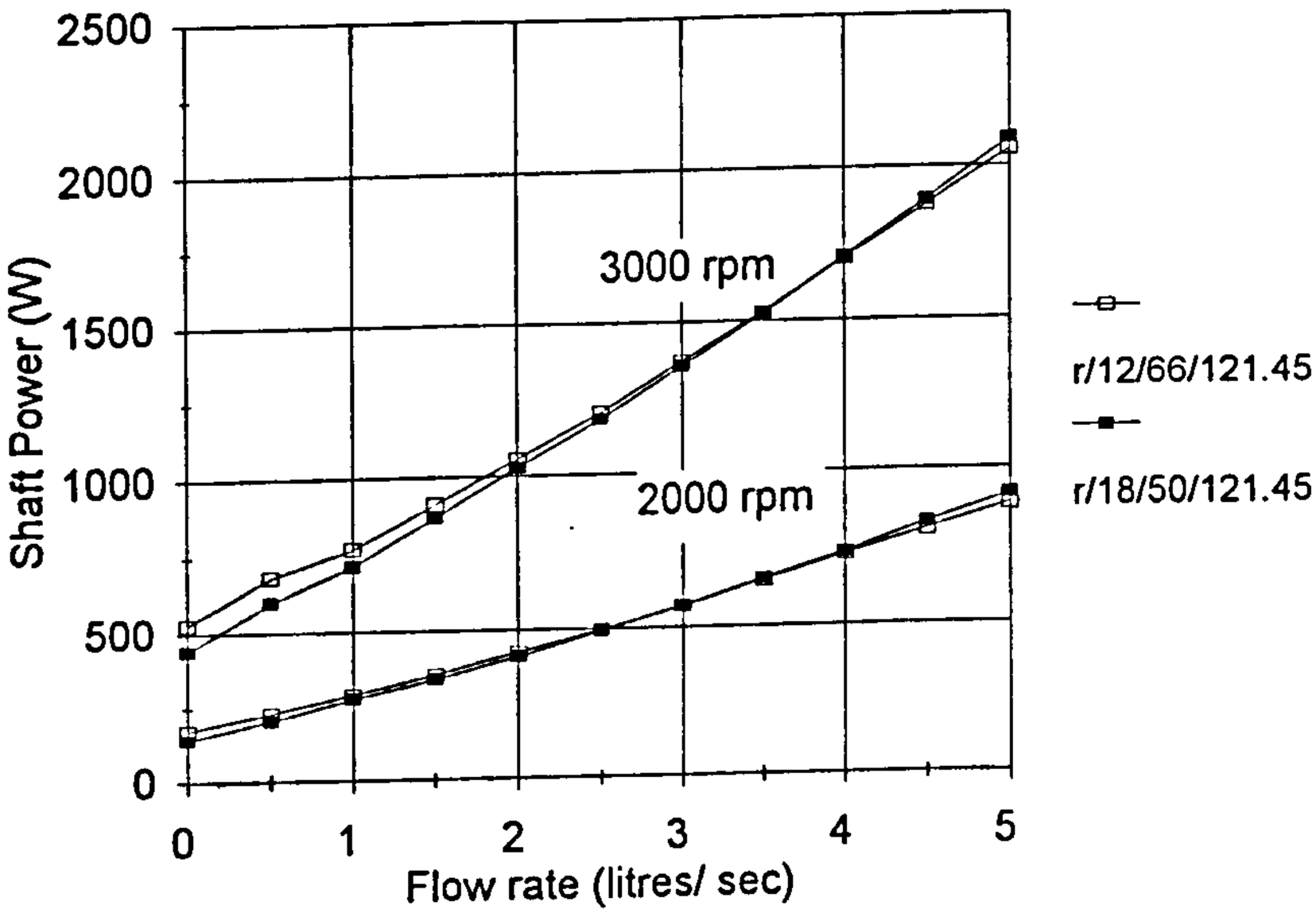

Figure 5.7 Effect of changing number of teeth on rotor (**s/19/50/123.8**)

Shaft power for the Silverson unit (Figure 5.3) is lower than that of the combination **r/18/50/123.34** and **s/18/50/123.8** (the toothed unit with the same shear gap thickness), shown in Figure 5.1. The rotor diameter of the Silverson (107.95 mm) is slightly less than the toothed rotor used here and this might account for some of the difference in shaft power (see Equation 3.38). It is also likely that hydraulic losses were lower within the blades on the Silverson rotor (producing lower hydraulic losses in the region upstream of the shear gap - where the water is accelerated tangentially).

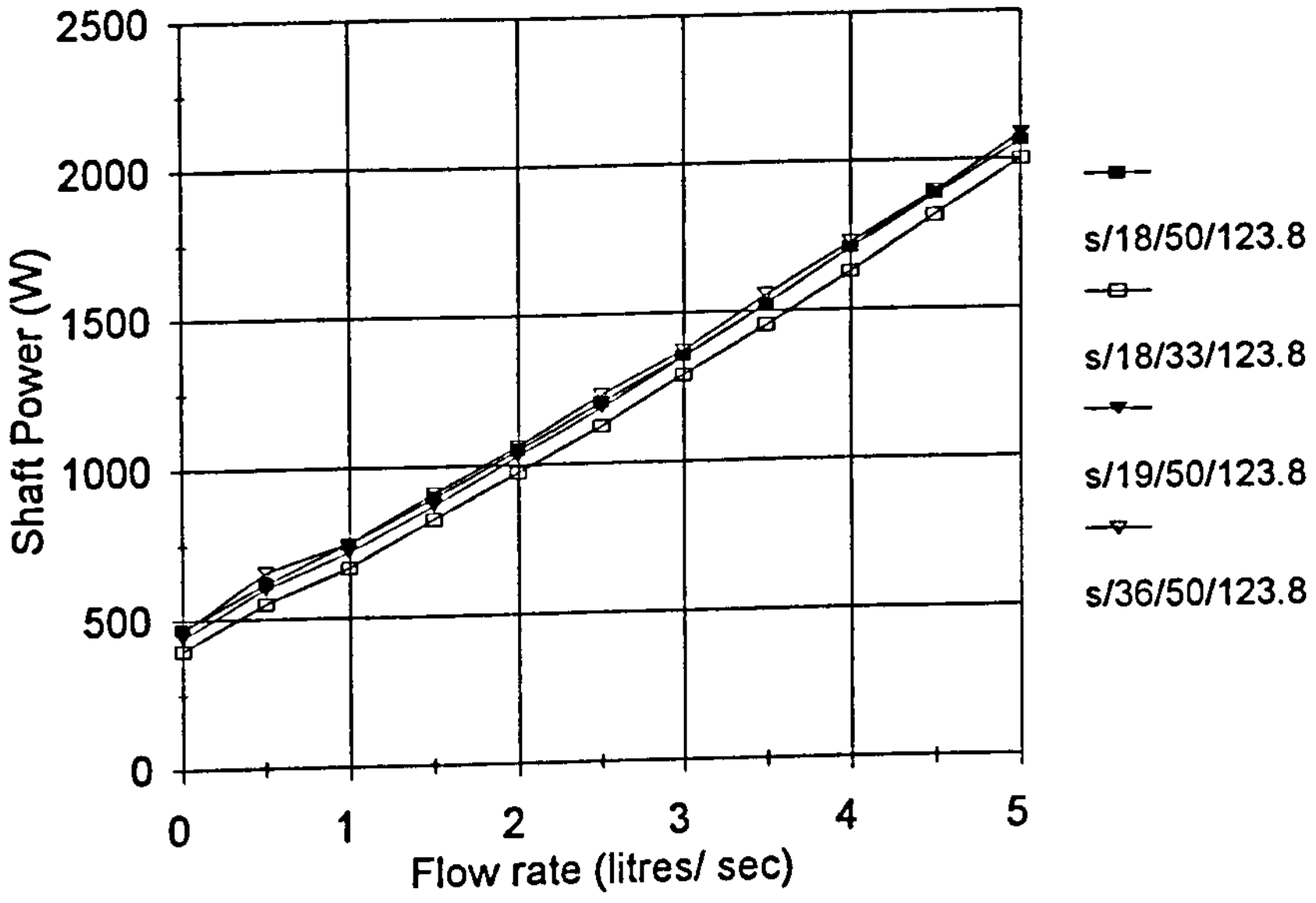

Figure 5.8 Effect of stator design on shaft power (**r/18/50/121.45**) at 3000 rpm

(b) Effect of scale

The half-scale toothed unit can be compared with **r/18/50/123.34** & **s/18/50/123.8.** Both of these have 18 teeth on the rotor and stator and a shear gap thickness of 0.23 mm. Figures 5.1 and 5.4 show shaft power for these units versus flow rate and shaft speed. At the same operating condition (for example 3000 and 1.0 l s^{-1}) the shaft power for the large and small units are 1493 W and 286 W respectively. This is a factor of 5.2 change with scale, or (scale ratio)$^{2.3}$. The effect of scale change is considered further in Section 5.1.6.

At 4000 rpm (the same tip speed as 2000 rpm at the large scale) and zero flow rate, the shaft power is 89 W (compared to approximately 380 W at the large scale). These figures also show that, even at zero flow rate, the shaft power can be significant. This is because of a combination of the mechanical, disc friction and

rotor-stator interaction losses. The mechanical (seal and bearing) and disc friction losses will be subtracted from the energy balance to leave the pumping power output and hydraulic and leakage losses, considered later (Section 5.1.6). This will be done because these losses are significant when considering motor power requirements but they do not do useful work on the fluid (contributing to pumping or mixing).

(c) Effect of operating condition

The data obtained for the toothed geometries were analysed, assuming that the shaft power depends on the shaft speed and flow rate, according to:

$$P_{SHAFT} = PnN^{f}Q^{g} \qquad (5.1)$$

where Pn is similar to a power number, although this equation is not dimensionless. The results of a regression performed on this data are given in Table 5.1.

The exponents on N and Q are ~2 to 2.5 and ~0.8 to 1 respectively. Studer (1990) found an exponent of 2.25 on N in an expression for the energy dissipation rate in a rotor-stator mixer, which could be proportional to the overall shaft power. In addition the Pn values are scattered, ranging from 14.6 to 62.5. There are no obvious trends in the exponents and Pn values in this table, apart from an increase in Pn with the thinnest shear gap.

Table 5.1 Regression results (Equation 5.1)

Geometry	*Pn*	*f*	*g*	R^2
r/18/50/119.6 & s/18/50/123.8	23.87	2.23	0.821	0.993
r/18/50/119.6 & s/18/33/123.8	23.30	2.31	0.876	0.985
r/18/50/119.6 & s/19/50/123.8	14.58	2.56	0.934	0.961
r/18/50/119.6 & s/36/50/123.8	19.37	2.46	0.918	0.953
r/12/67/121.45 & s/18/50/123.8	22.74	2.29	0.846	0.986
r/12/67/121.45 & s/18/33/123.8	55.46	2.25	0.976	0.978
r/12/67/121.45 & s/19/50/123.8	27.46	2.26	0.853	0.984
r/12/67/121.45 & s/36/50/123.8	31.35	2.19	0.835	0.989
r/18/50/121.45 & s/18/50/123.8	46.28	2.38	1.02	0.951
r/18/50/121.45 & s/18/33/123.8	46.59	2.25	0.947	0.990
r/18/50/121.45 & s/19/50/123.8	34.03	2.31	0.924	0.985
r/18/50/121.45 & s/36/50/123.8	33.07	2.01	0.729	0.996
r/18/50/123.34 & s/18/50/123.8	47.60	2.25	0.925	0.990
r/18/50/123.34 & s/18/33/123.8	62.51	2.09	0.871	0.997
r/18/50/123.34 & s/19/50/123.8	32.13	2.29	0.914	0.992
r/18/50/123.34 & s/36/50/123.8	37.99	2.16	0.829	0.998

However, when values determined using Equation 5.1 and the *Pn* numbers from Table 5.1 are plotted versus measured data (Figure 5.9 for **r/18/50/121.45 & s/18/50/123.8**) it is clear that, while the measured data approximately follow the correlation, it is made up of individual sets of curves (a curve for each shaft speed). This shows that the shaft power either depends upon other variables or another function of the same variables (for example, at this stage the effect of rotor size has not been considered). Analysis of these results is developed further in Section 5.1.6.

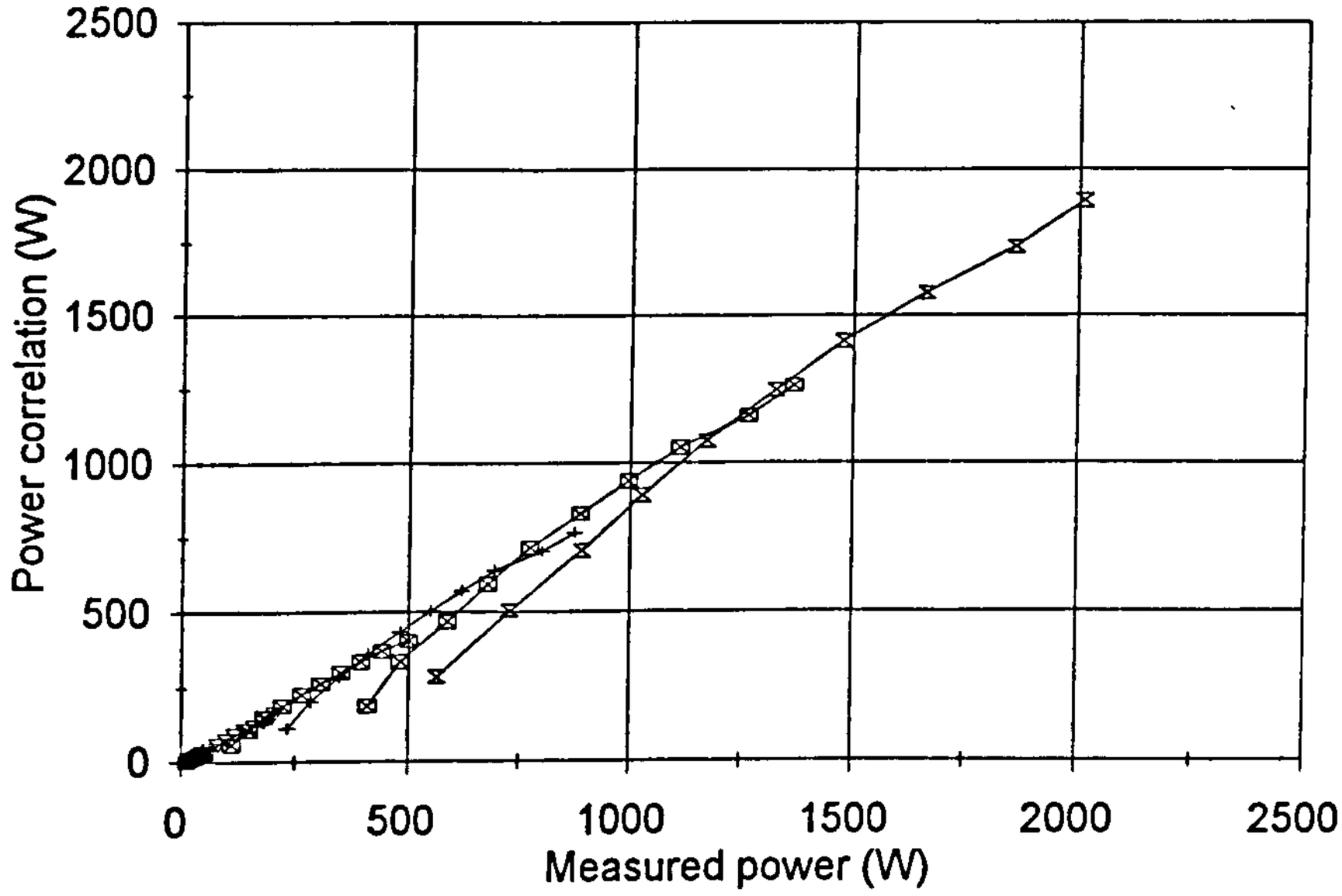

Figure 5.9 Measured power data versus power correlation (Equation 5.1)

5.1.2 Pumping power, P_{PUMP} and pumping efficiency, η

Figures 5.10 to 5.13 show pumping power data versus flow rate for two selected toothed rotor-stator combinations (**r/18/50/123.34 & s/18/50/123.8, r/18/50/121.45 & s/36/50/123.8**) and for the Silverson and half-scale toothed units.

These data show that, at the same operating condition (i.e the same shaft speed and flow rate), the Silverson produces a higher pumping power than the toothed type. This might be expected since the Silverson's blades more closely resemble centrifugal pump impeller blades. The pumping efficiency is defined by:

$$\eta = \frac{P_{PUMP}}{P_{SHAFT}} \tag{5.2}$$

and the pumping efficiency is therefore greater for the Silverson than the toothed design.

However, the pumping efficiencies measured here (~10% for the toothed designs and ~20% for the Silverson) are low compared to centrifugal pumps, for which pumping efficiencies approaching 100% are possible. In centrifugal pump design, the pressure recovery process - transforming the kinetic energy of fluid discharged by the impeller into pumping output- has been optimised over many years of development. Therefore, the actual pumping performance approaches the theoretical performance - predicted using standard equations (Cherhassky, 1980; Stepanoff, 1957). However, in the case of a rotor-stator mixer, the pressure recovery step is far from optimised, accounting for the poor pumping efficiency of these machines. In rotor-stator mixers the flow straightening effect of the stator produces some pressure recovery. Unfortunately, if significant pumping is required, this process does not occur without large losses (principally to turbulence and direct friction losses). This is because tangentially-moving fluid with high kinetic energy impacts onto the stator and then exits the stator in a predominantly radial direction (Section 5.2). Guide vanes (analogous to the stator) are sometimes used in a centrifugal pump; however, these are optimised with respect to the angle at which fluid is discharged from the impeller. The teeth in the stators used for these tests were not optimised with respect to pumping performance and are probably not optimised for pumping on any industrial units.

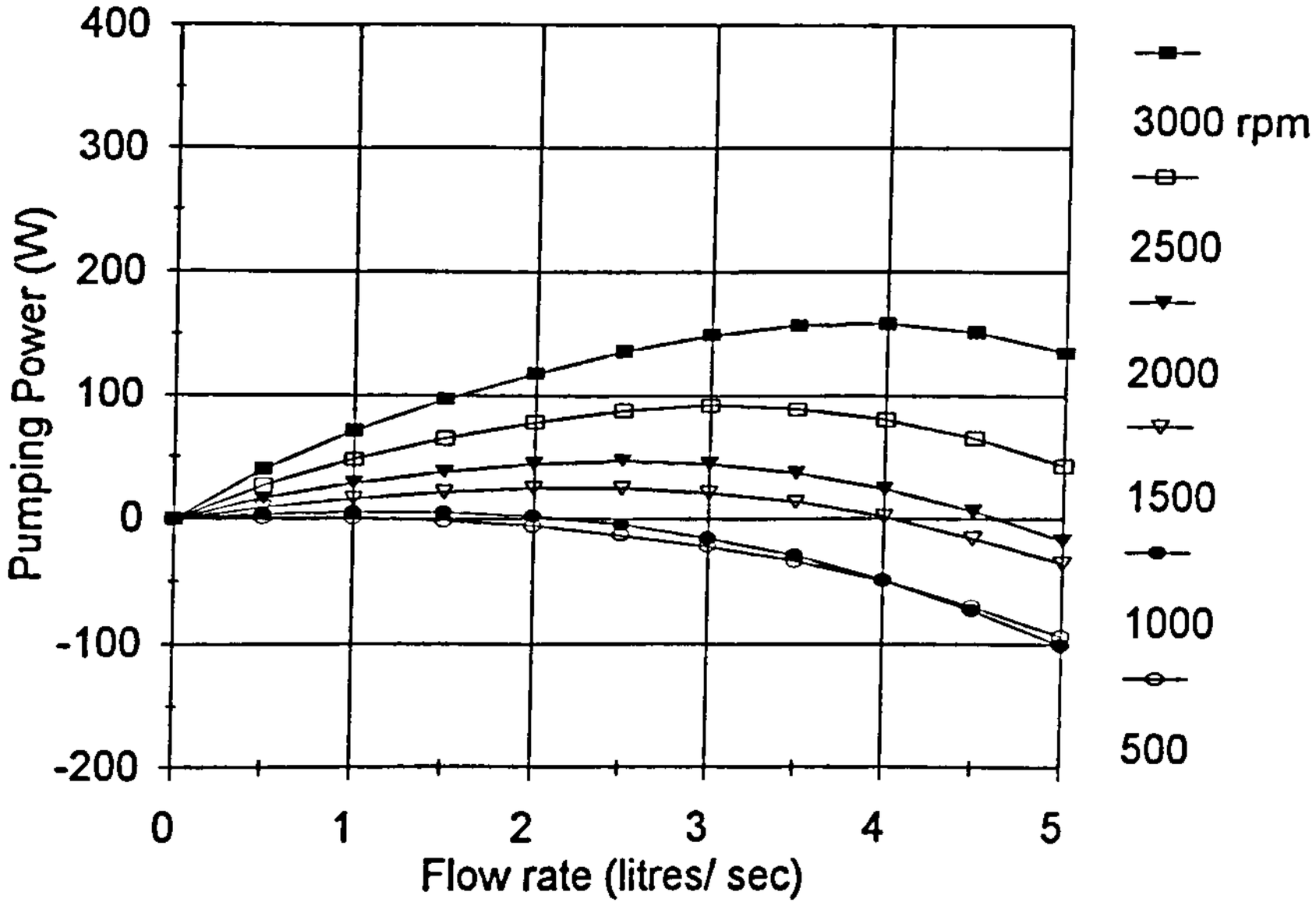

Figure 5.10 Pumping power versus flow rate for a range of shaft speeds **(r/18/50/123.34 & s/18/50/123.8)**

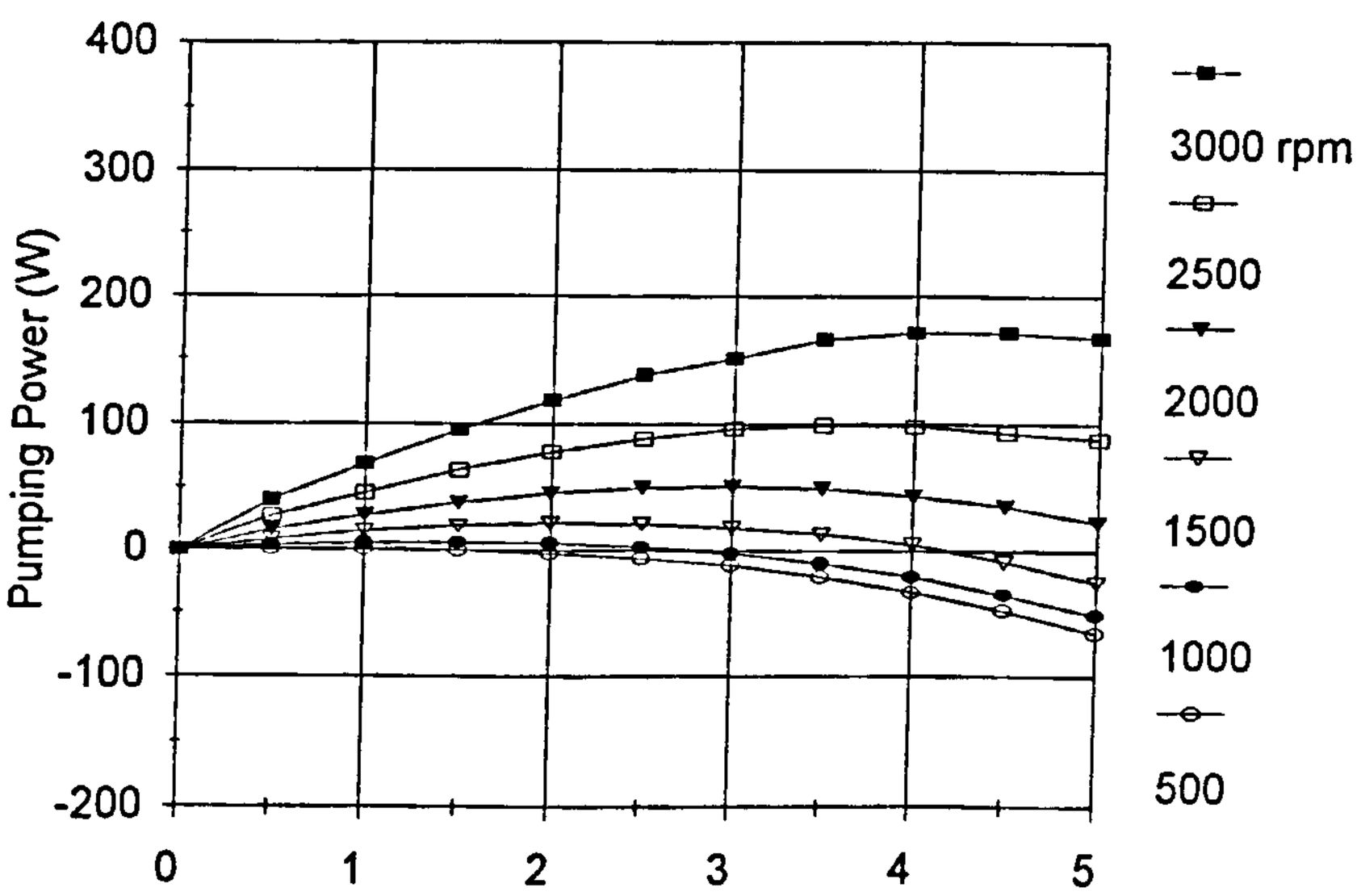

Figure 5.11 Pumping power versus flow rate for a range of shaft speeds **(r/18/50/121.45 & s/18/50/123.8)**

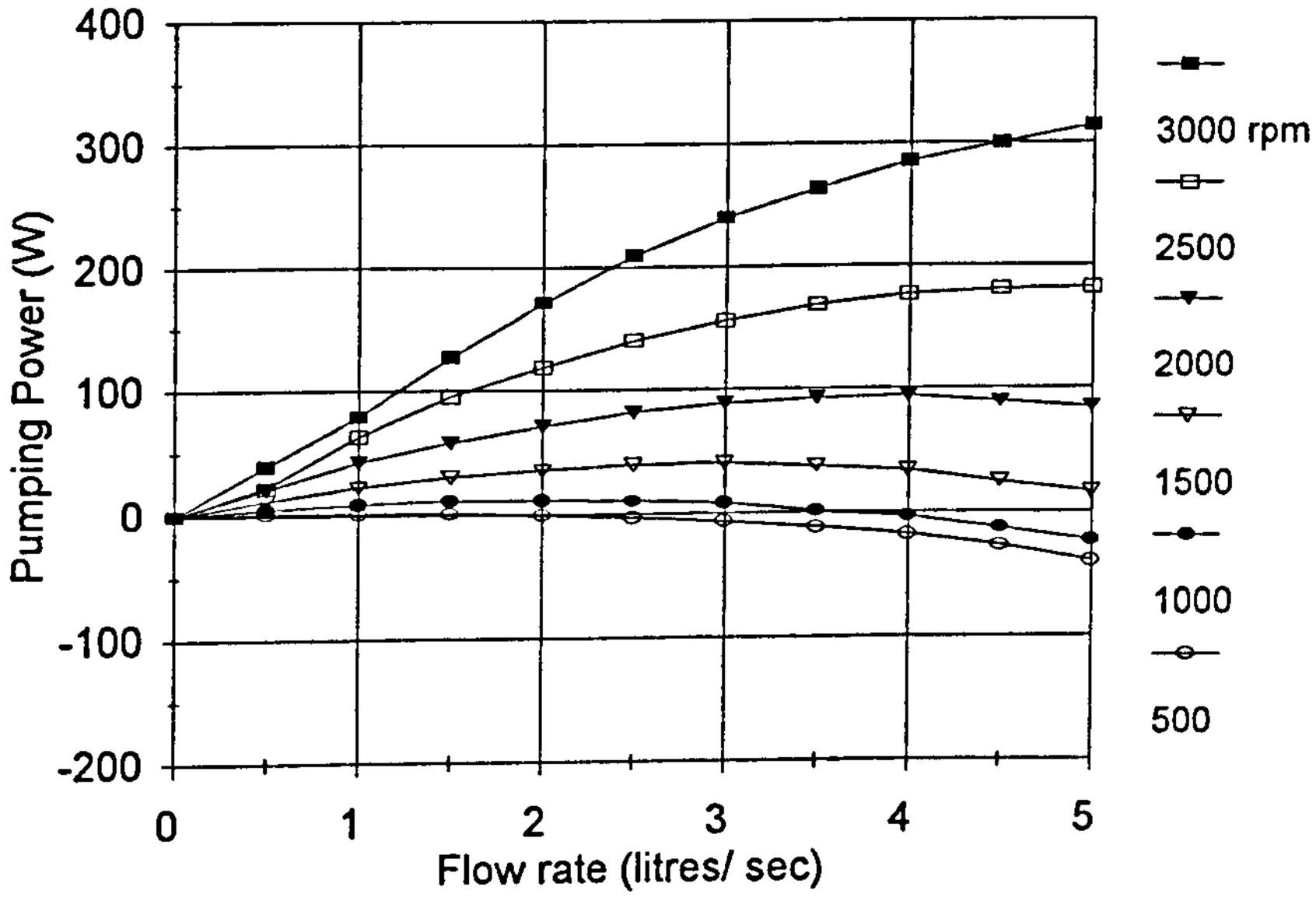

Figure 5.12 Pumping power versus flow rate for a range of shaft speeds (Silverson)

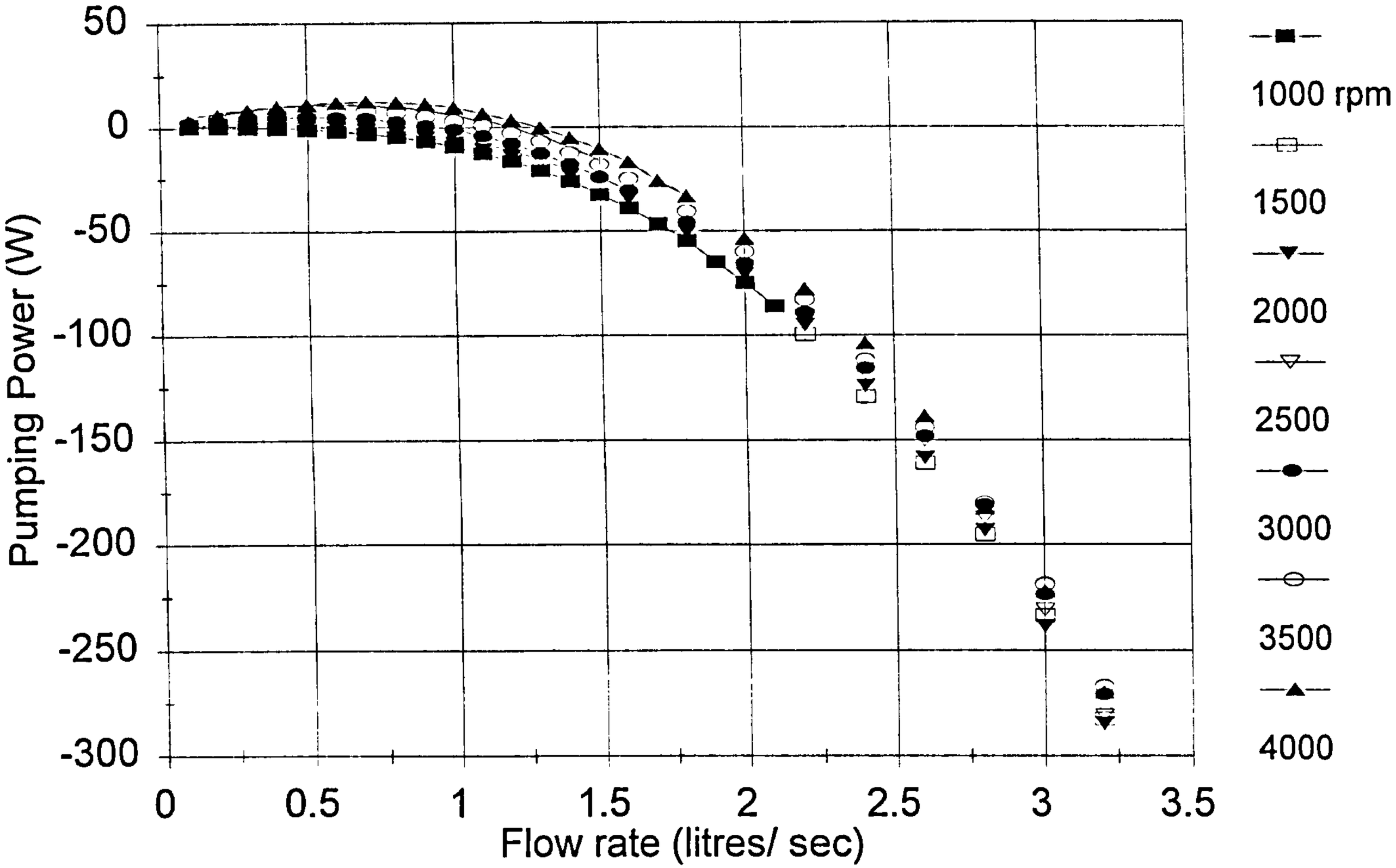

Figure 5.13 Pumping power versus flow rate for a range of shaft speeds (half-scale toothed)

At low flow rates and high shaft speeds the curves for the Silverson appear to drop sharply (Figure 5.12 and Appendix A4.17). Investigation of these results showed that the differential pressure values at these conditions were not reproducible. Visualisation, using the clear acrylic mixer, revealed that gas formation (probably a liberation of dissolved air) causing partial de-priming of the rotor, may be responsible for this.

(a) Effect of rotor-stator design

Figure 5.14 shows pumping power results for all of the toothed designs, at 3000 rpm and 3.0 $l.s^{-1}$. The spread of these data increases as the shear gap thickness was reduced, from a spread of approximately 20 W with the thickest shear gap, to 100 W for the thinnest shear gap. The implication here is that the pressure recovery process, discussed above, is insensitive to rotor-stator interaction when the rotor and stator are separated by a thick shear gap and rotor-stator interaction becomes increasingly important as the shear gap thickness reduces. If the pressure recovery step is sensitive to rotor-stator interaction, then the turbulence generating process will also be sensitive to rotor-stator interaction.

In Figure 5.14, the medium shear gap thickness pumping power data are generally slightly higher than those data taken for the thick and thin shear gaps, suggesting that there may be an optimum shear gap thickness for pumping. Figures 5.15 and 5.16 show pumping power data for stators **s/18/50/123.8** and **s/19/50/123.8** with the three shear gap thicknesses. With the 18 toothed stator, the highest pumping power is obtained with the thickest shear gap and with the 19 toothed stator the highest pumping power is obtained with the medium shear gap. These results also show that the pumping power (and therefore turbulence generation) depends upon rotor-stator interaction.

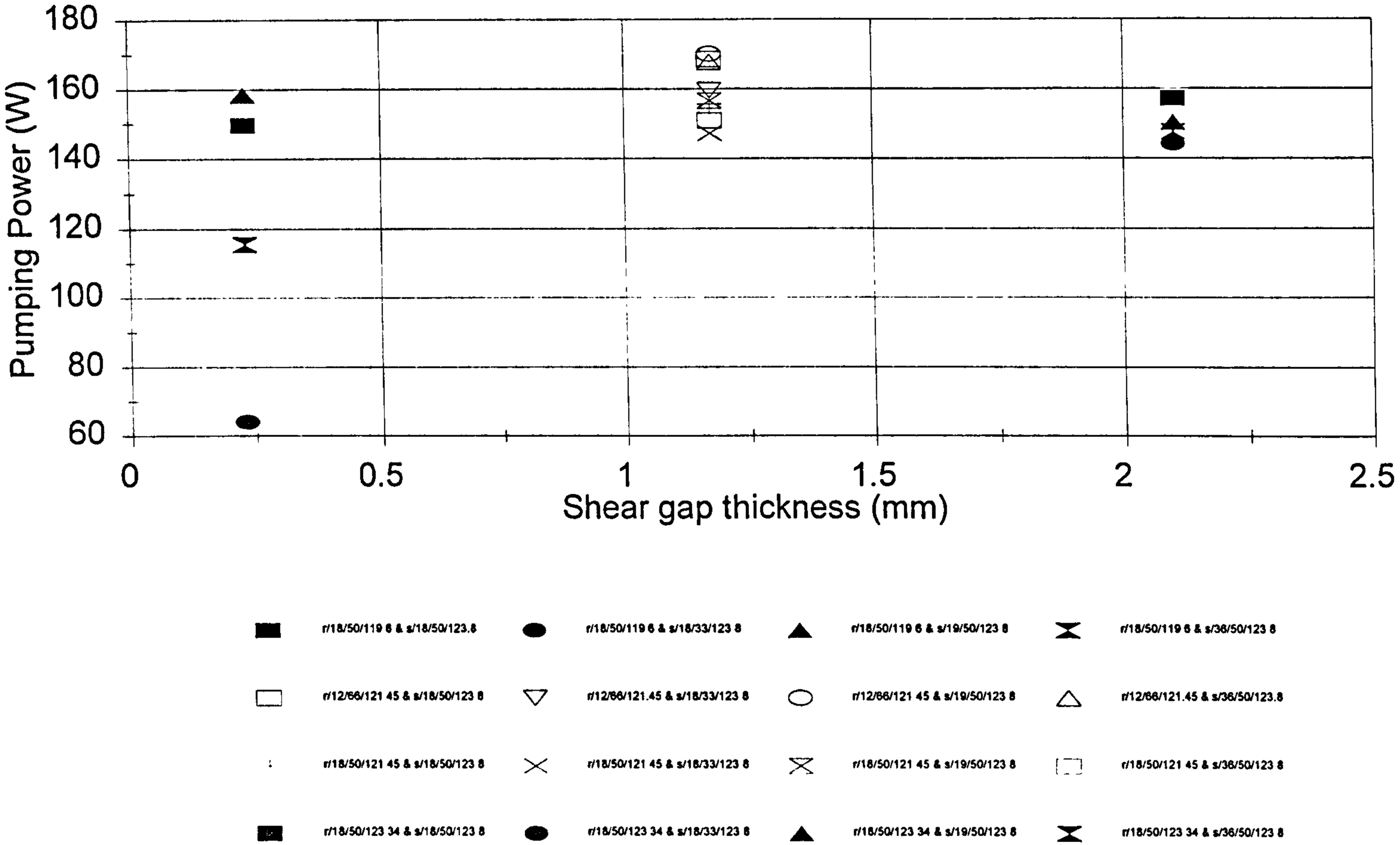

Figure 5.14 Pumping power for all toothed combinations at 3000 rpm and 3.0 $l.s^{-1}$.

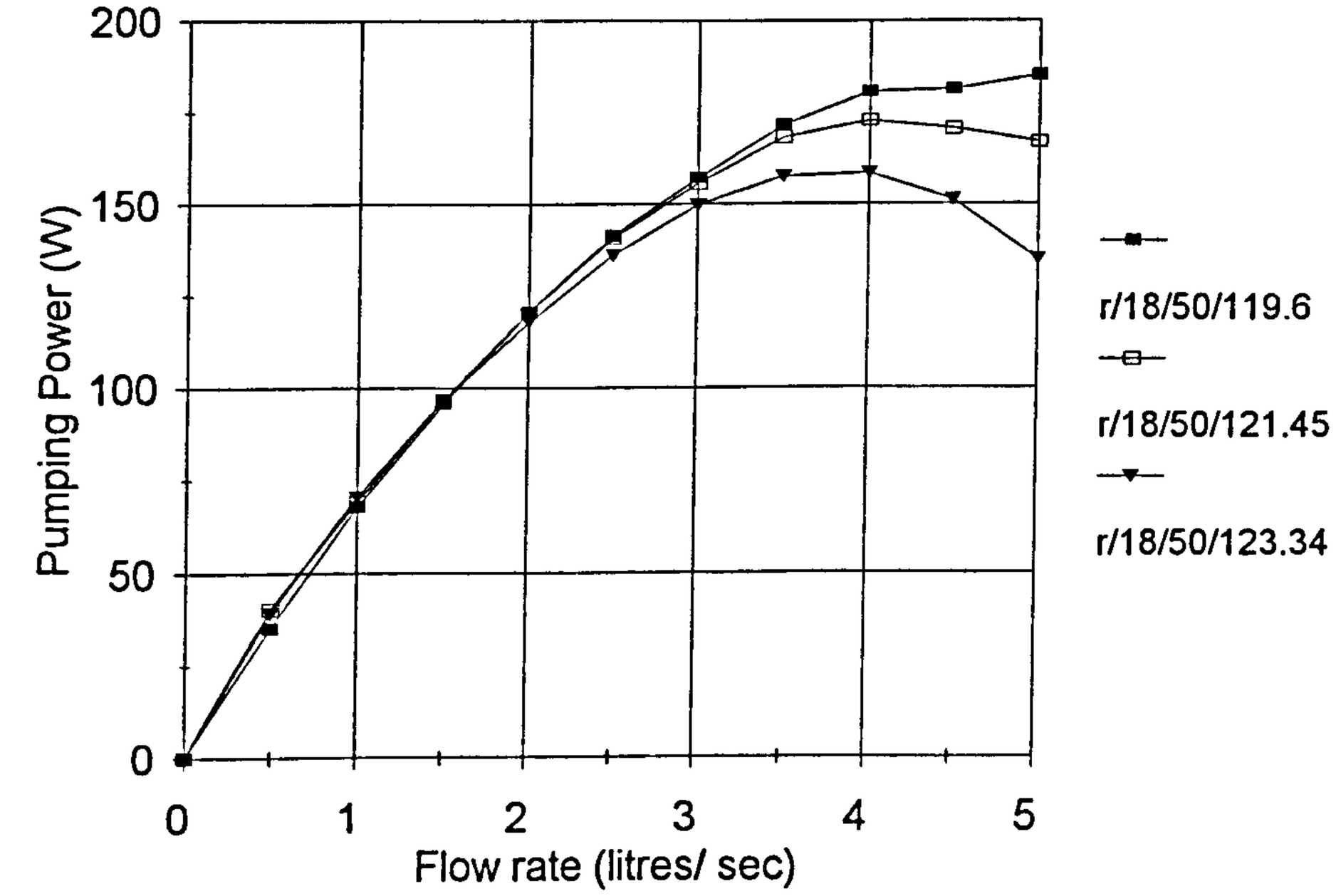

Figure 5.15 Pumping power versus flow rate for a range of rotors with **s/18/50/123.8** at 3000 rpm

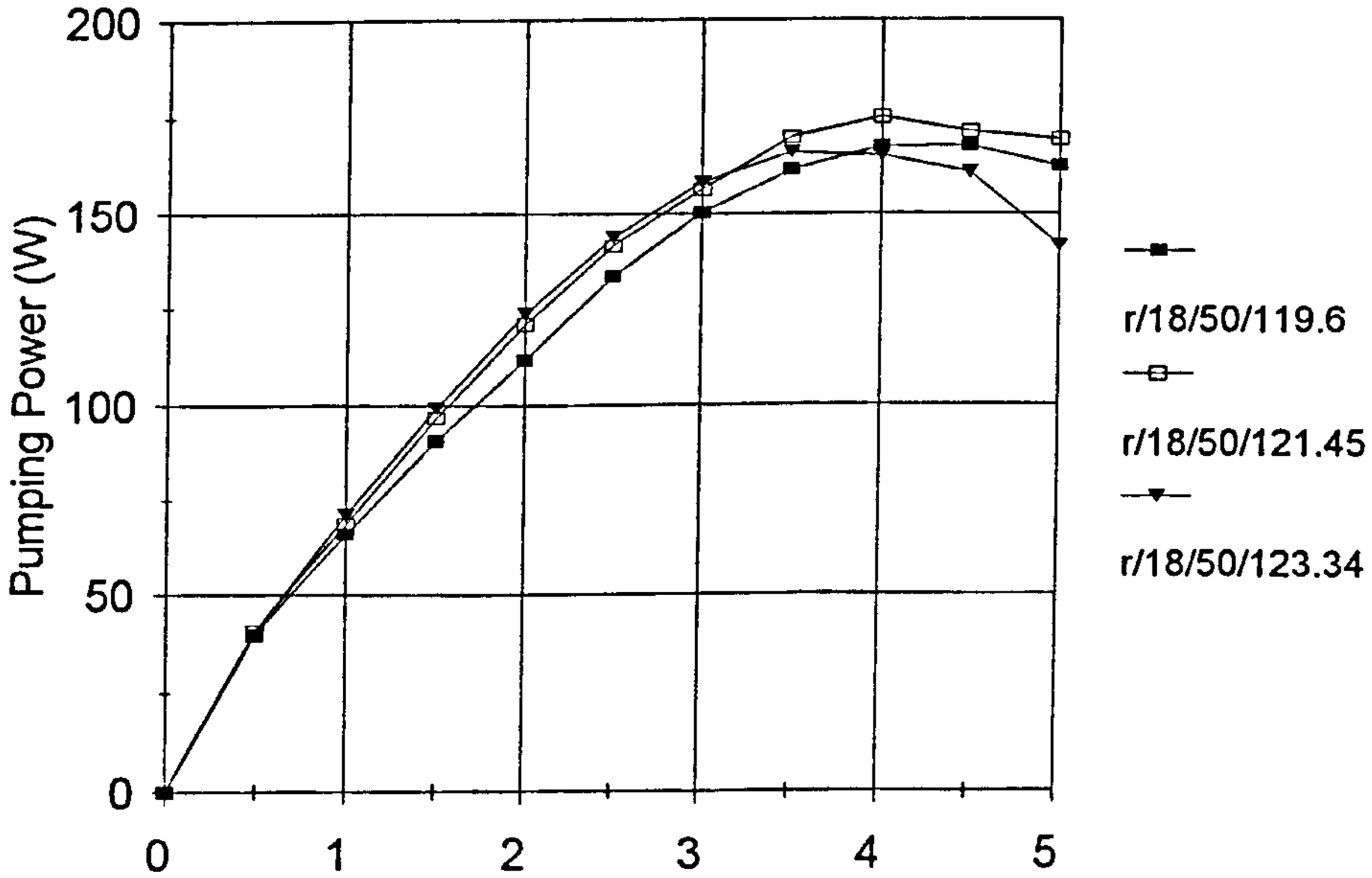

Figure 5.16 Pumping power versus flow rate for a range of rotors with **s/19/50/123.8** at 3000 rpm

Table 5.2 gives the peak pumping efficiencies measured. With the exception of the data taken with **r/18/50/123.34** (the thinnest shear gap) the highest pumping efficiency is obtained with stator **s/18/33/123.8**.

Table 5.2 Peak pumping efficiencies of rotor-stator designs

Rotor-stator design	η
r/18/50/119.6 & s/18/50/123.8	12.05
r/18/50/119.6 & s/18/33/123.8	12.21
r/18/50/119.6 & s/19/50/123.8	11.22
r/18/50/119.6 & s/36/50/123.8	11.03
r/12/66/121.45 & s/18/50/123.8	12.44
r/12/66/121.45 & s/18/33/123.8	12.92
r/12/66/121.45 & s/19/50/123.8	12.40
r/12/66/121.45 & s/36/50/123.8	12.48
r/18/50/121.45 & s/18/50/123.8	11.70
r/18/50/121.45 & s/18/33/123.8	12.01
r/18/50/121.45 & s/19/50/123.8	11.95
r/18/50/121.45 & s/36/50/123.8	11.24
r/18/50/123.34 & s/18/50/123.8	10.73
r/18/50/123.34 & s/18/33/123.8	8.94
r/18/50/123.34 & s/19/50/123.8	10.70
r/18/50/123.34 & s/36/50/123.8	9.44
Silverson	22.85
half-scale toothed	7.40

This result is examined further by plotting pumping efficiency versus flow rate for rotor **r/12/66/121.45** and each of the stators (Figure 5.17). This graph shows that, for this rotor, the pumping efficiency does not depend on the stator design for the three stators with an open area of 50%. The curve for **s/18/33/123.8**, however, has a different shape from the other curves, with a higher maximum, which occurs at a lower flow rate. The pumping efficiency drops below those of the other stator designs for flow rates above the best efficiency. This result suggests that pumping

efficiency depends more upon stator open area than rotor-stator interaction. The open area of the Silverson unit is ≈35% (i.e. lower than 50%), and this may also contribute to the improved pumping of the Silverson design.

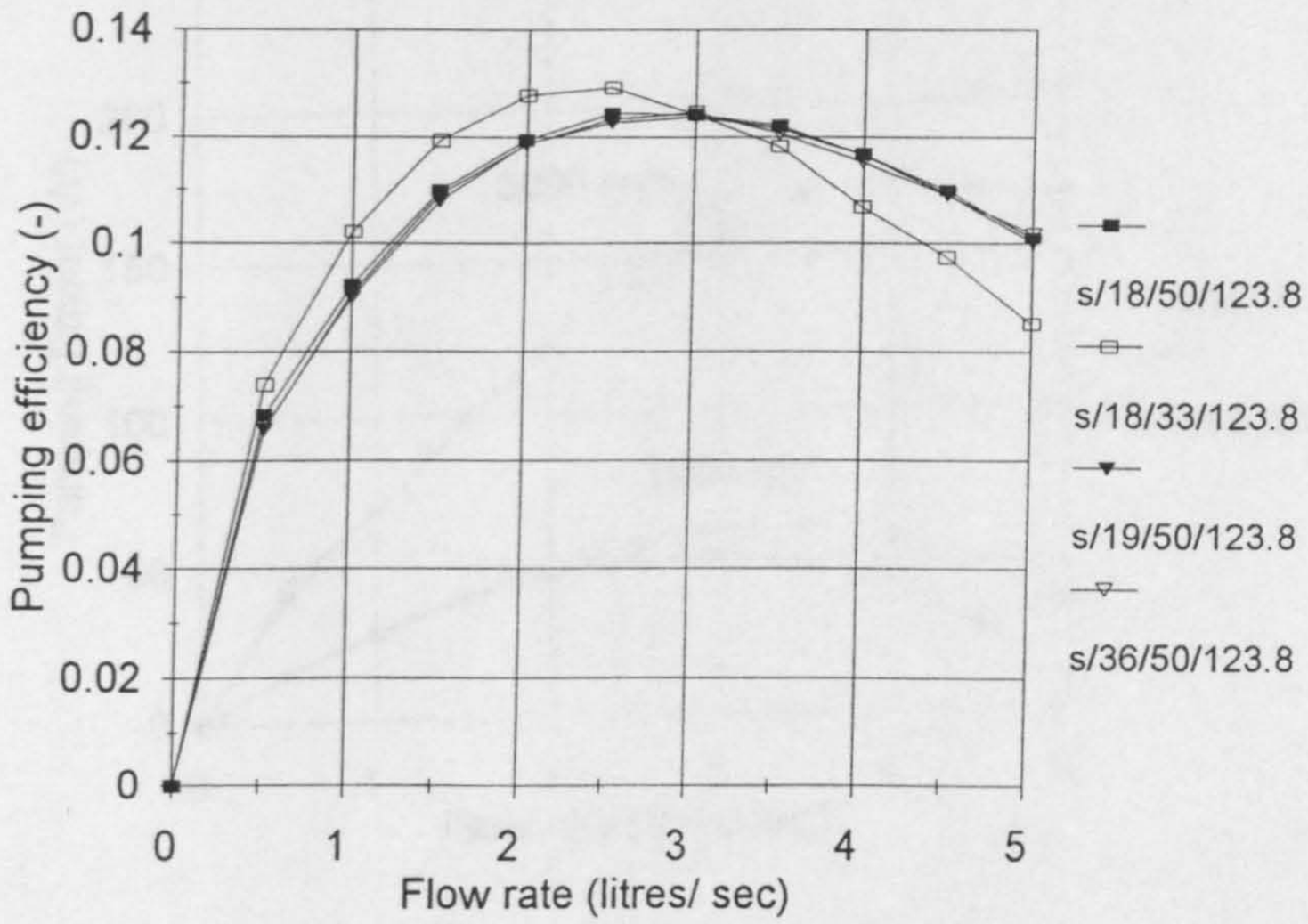

Figure 5.17 Pumping power versus flow rate for a range of stators with **r/12/66/121.45** at 3000 rpm

Figure 5.18 shows pumping efficiency versus flow rate for the two rotors with the medium shear gap (**r/12/66/121.45** & **r/18/50/121.45**), showing that the 12-toothed rotor is a more efficient pump, producing a higher pumping power for the same shaft power (Figure 5.7). Bourne and Garcias-Rosas (1986) also found that reducing the number of teeth on the rotor improved the performance of their unit as a pump.

It was shown in Section 5.1 that rotor-stator interaction does not affect shaft torque significantly. However, here it is shown that rotor-stator interaction can affect pressure recovery (which occurs in the immediate vicinity of the shear gap) significantly. If the pressure recovery process depends on how rotor and stator interact, then this implies that the turbulence and skin friction losses in this small

region must be affected as well. This in-turn suggests that stators might be designed to optimise for turbulence production.

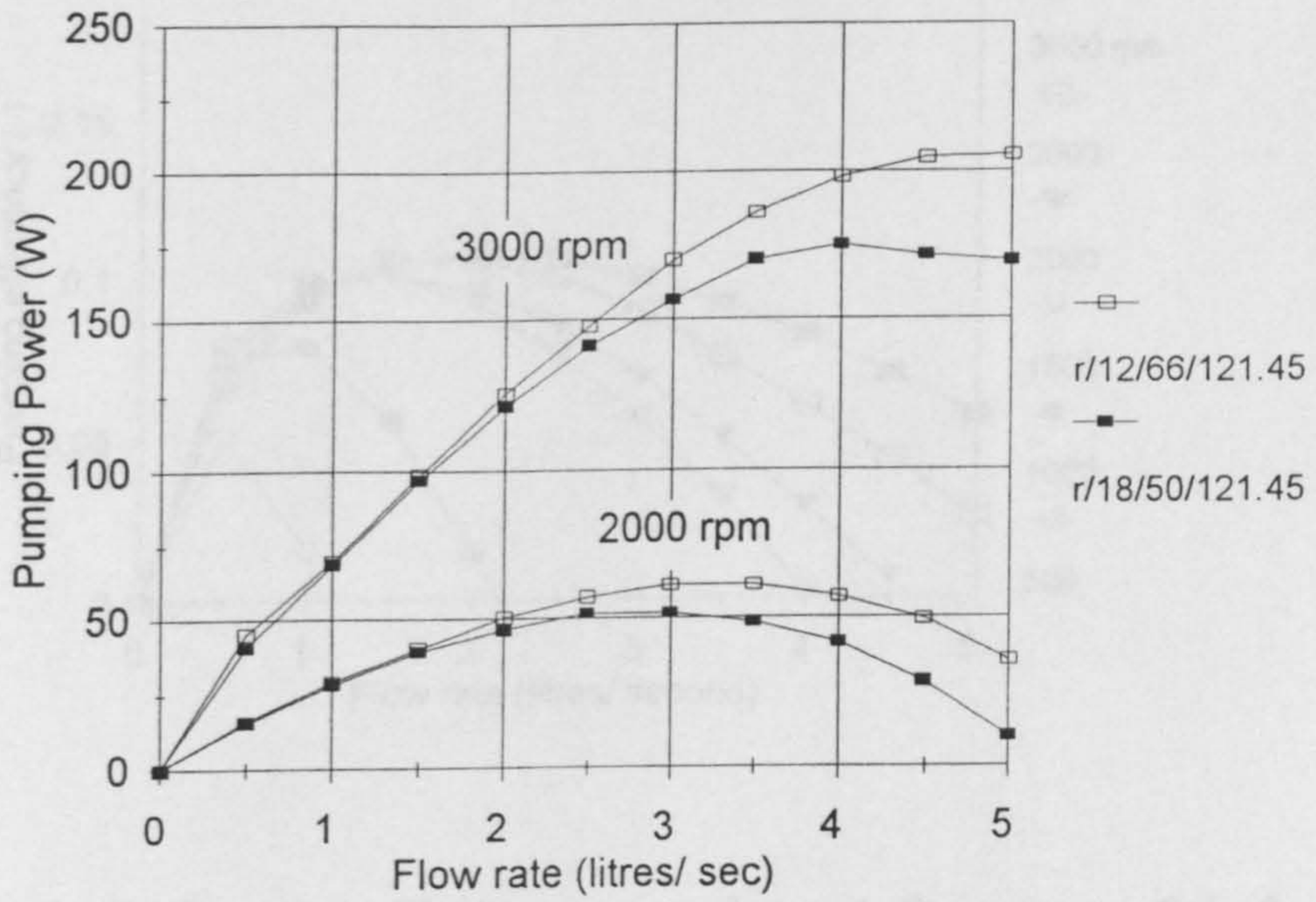

Figure 5.18 Effect on pumping efficiency of changing the number of teeth on the rotor (with **s/19/50/123.8**)

(b) Effect of scale

Figures 5.19 and 5.20 show pumping efficiency curves for a toothed (**r/18/50/123.34 & s/18/50/123.8**) and half-scale toothed mixers. These curves show that the large scale mixer is more efficient at pumping than the half-scale unit. However, at the half-scale, the mechanical losses are larger relative to the total shaft power. Figures 5.21 and 5.22 show the pumping efficiency at both scales expressed as the pumping power output over the shaft power with the estimates of disc friction and mechanical losses removed. Here the comparison between the half-scale and large-scale toothed units is more favourable, with the best efficiency of the small scale mixer being very close to the best efficiency of the large scale unit. Smaller scale industrial units will also have smaller seals and bearings and therefore lower mechanical losses, unlike

the results given here, where they are essentially the same at both scales.

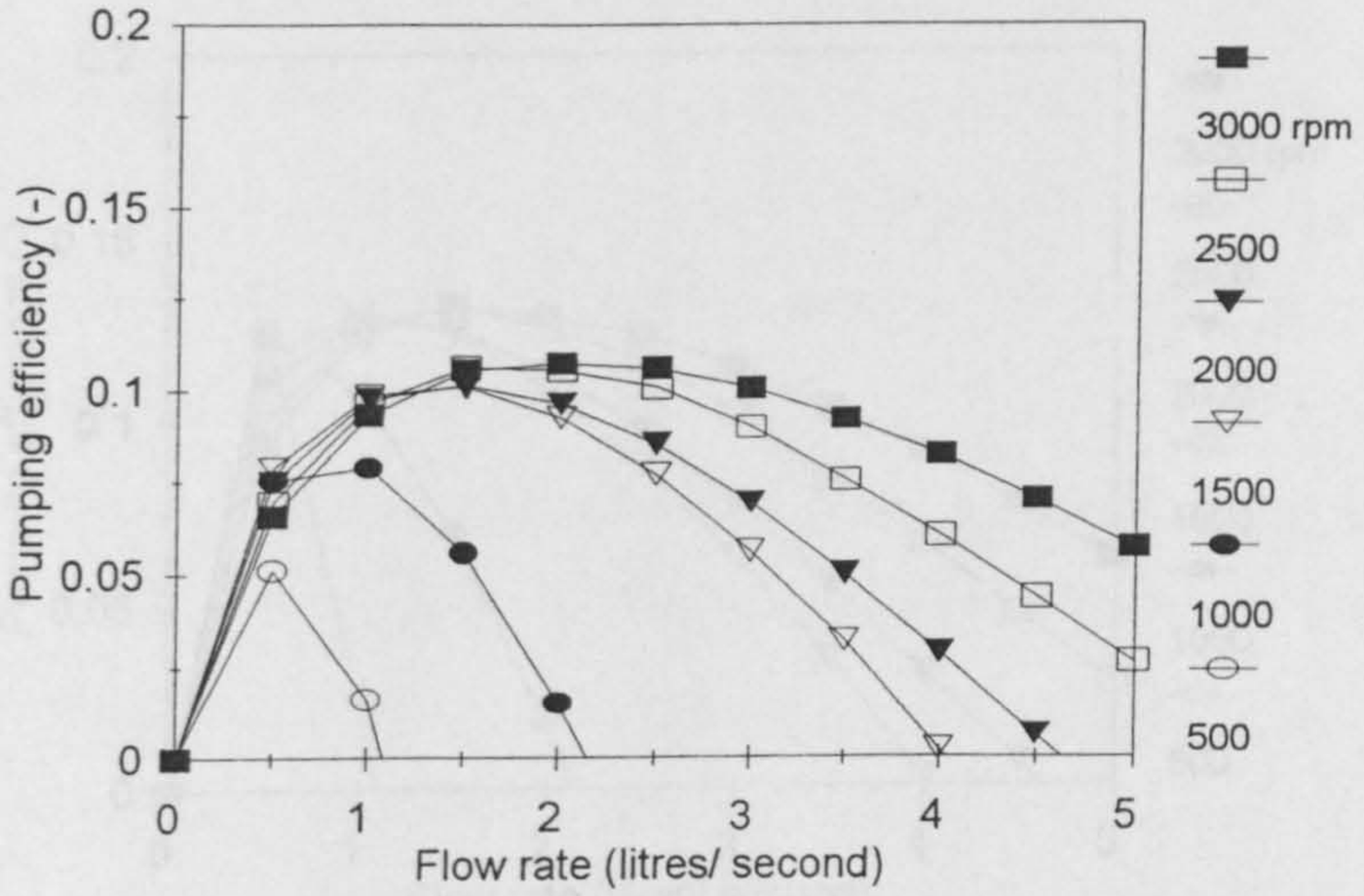

Figure 5.19 Pumping efficiency versus flow rate for a range of shaft speeds (**r/18/50/123.34 & s/18/50/123.8**)

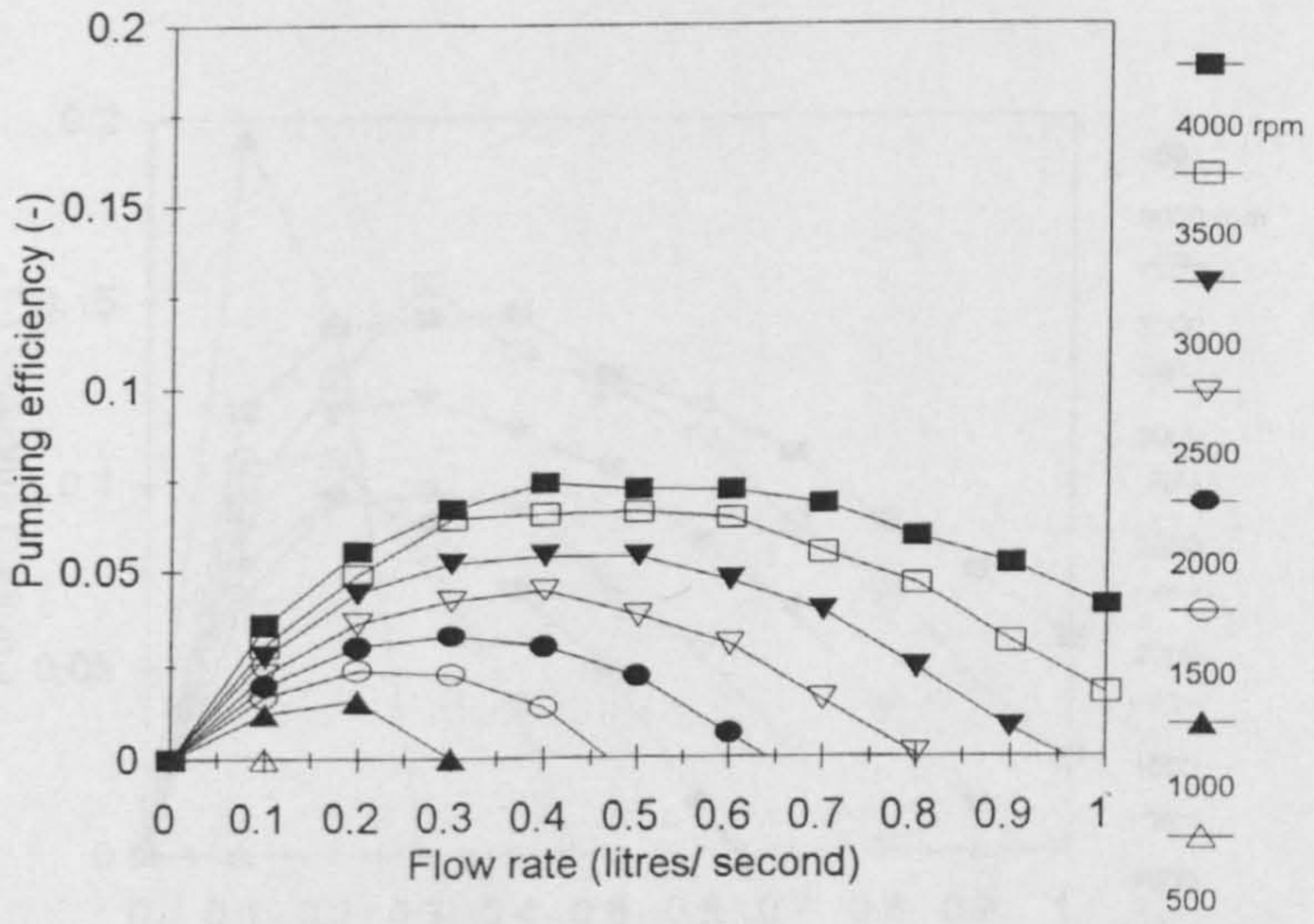

Figure 5.20 Pumping efficiency versus flow rate for a range of shaft speeds (half-scale toothed)

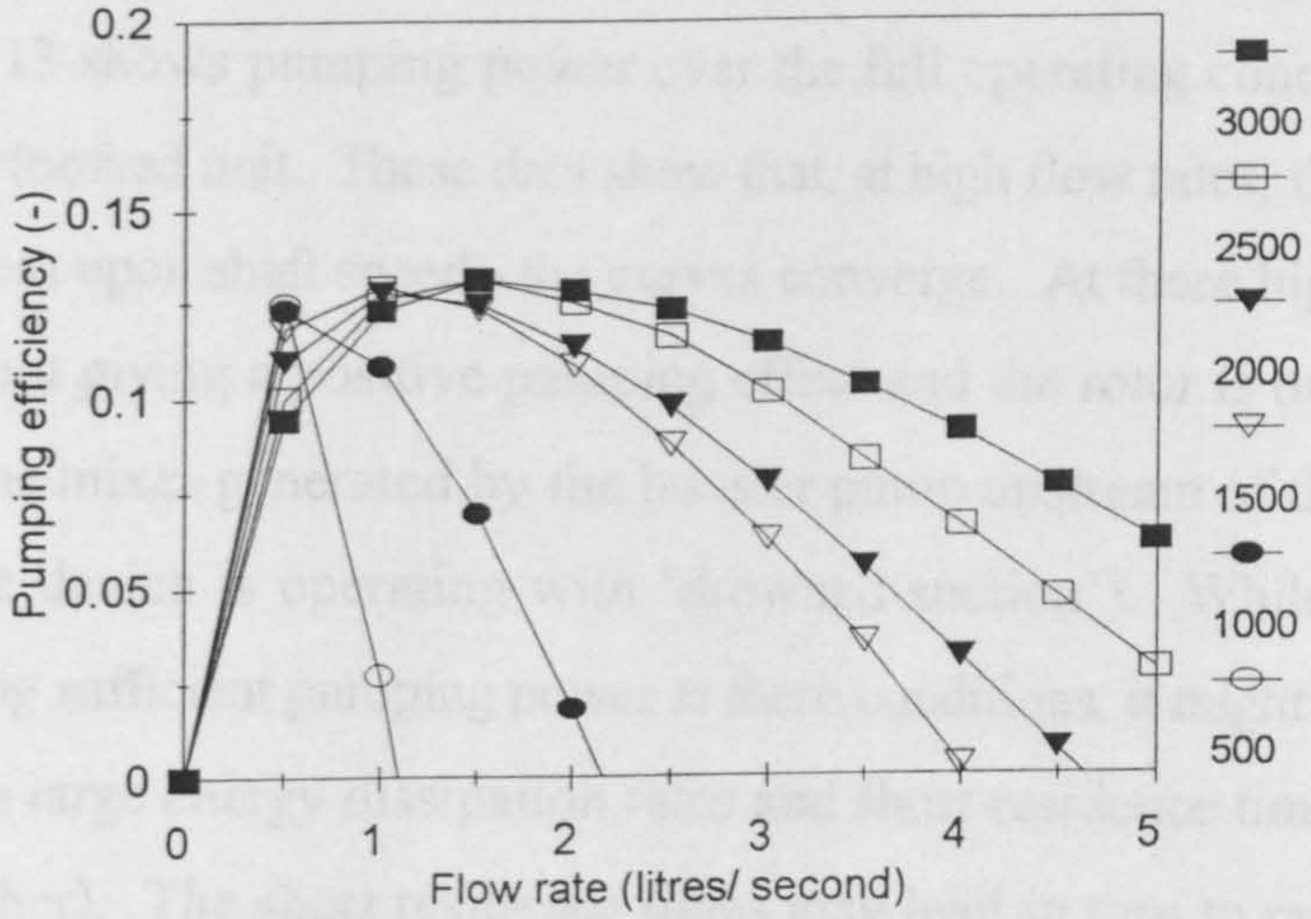

Figure 5.21 Adjusted pumping efficiency versus flow rate for a range of shaft speeds (**r/18/50/123.34** & **s/18/50/123.8**)

Figure 5.22 Adjusted pumping efficiency versus flow rate for a range of shaft speeds (half-scale toothed)

(c) Effect of operating condition

Figure 5.13 shows pumping power over the full operating condition range for the half-scale toothed unit. These data show that, at high flow rates, the pumping power depends less upon shaft speed - the curves converge. At these higher flow rates the mixer is not giving a positive pumping effect and the rotor is overrun by the flow through the mixer generated by the booster pump upstream of the mixer (in pump jargon the device is operating with 'drowned suction'). While the mixer is not contributing sufficient pumping power at these conditions, it might still act as a good mixer with large energy dissipation rates and short residence times (since the flow rate is higher). The short residence times may lead in turn to reduced by-product formation in certain competitive chemical reaction mixing applications.

At 500 rpm (on the half-scale unit) the pumping effect of the rotor is negligible, but the rotation ensures that the pressure drop across the mixer is averaged between the fully open and fully closed positions (Section 3.2.1). Using the inlet pipe velocity, u, a regression was performed on the data and it was found that:

$$\Delta p = 4.64\ \rho u^{2.01} \qquad (5.3)$$

where Δp is in Pa. This is the type of expression that should be obtained for static components in pipe-lines, for example pipe bends or valves, albeit with an exponent on u of precisely 2.0 (Miller, 1990). The loss coefficient (4.64) is high, accounting for the pipe inlet/ outlet losses as well as the losses through the rotor-stator shear gap region, as though the rotor were not moving. If the unit is considered to comprise an expansion followed by a contraction, then loss coefficients can be looked up in standard references. The accepted loss coefficient for a sudden expansion is close to 1.0 (where the change in the open area of the flow is great) and close to 0.5 for a sudden contraction (Massey, 1983; Miller, 1990), giving a total loss coefficient of

approximately 1.5. That the loss coefficient measured greatly exceeds this value indicates that the losses through the rotor-stator teeth are significant. This loss will be called the static loss and will contribute to mixing in the same way as losses in a motionless mixer in a pipe.

At 3.0 l s^{-1}, the static loss component (for the large scale unit, assuming that the loss coefficient remained constant on scale-up and using Equation 5.3) is:

$$P_{STATIC} = Q\Delta P \simeq 30\ W \tag{5.4}$$

This value is small compared to P_{SHAFT} (<5%) when the shaft speed is above (say) 1500 rpm. Only two diazo-coupling tests were done in this work above 3.0 l.s^{-1}, so the static losses were disregarded throughout the rest of this thesis when considering energy dissipation.

However, when a rotor-stator mixer is operating drowned, there will be little likelihood of cavitation and energy dissipation (and mixing) will result from both the static loss as well as the losses associated with the energy of the rotor. This may prove to be a good use of a rotor-stator mixer (although it does rely upon providing a significant upstream head) and warrants some investigation,.

The static loss will be considered together with the power supplied to the fluid by the rotor in Section 5.1.7.

The effect of forcing water through the mixer on the residence time distribution is discussed further in Section 5.3.

For the thinnest shear gap (i.e. the rotor-stator combinations using rotor **r/18/50/123.34**), the differential pressure across the mixer was lower when the mixer

was stationary than when the rotor was moving slowly (Figures A4.13 to A4.14). For stators **s/18/50/123.8 & s/18/33/123.8** this was because the rotor was held in the fully open position (Figure 3.3) when stationary and therefore gave a lower resistance to flow than when the rotor was moving. However, for the 19 and 36 toothed stators there are no open or closed positions. The open area of the rotor-stator combination remains constant at 50%. Therefore, the lower pressure drop when the rotor is stationary was probably due to the angle at which the water impinged onto the stator. When the rotor was stationary, the water would flow radially through the stator; but when the rotor was moving, the water would impinge onto the stator with a tangential component and the stator would offer an increased resistance.

5.1.3 Mechanical loss

The mechanical loss was measured by spinning the rotor shaft in water with the rotor removed. The shaft torque is therefore due to friction within the seal and bearing and drag on the shaft and spring in the water (which is assumed to be small).

Table 5.3 gives the shaft torque measured and compares these results with values obtained previously on the same rig (Sparks, 1993). This shows that the mechanical losses have reduced slightly over the three years of operation, possibly indicating that components have become worn in. The shaft torque remains approximately constant over the range of shaft speeds.

A value for the torque, due to the mechanical components, of 0.13 N.m is used in the subsequent analysis (this is the average of the values given in the left hand column of Table 5.3). The corresponding value for the mechanical loss (using Equation 3.1) at 3000 rpm is 41 W, compared to measured shaft powers for the

rotor-stator units of (typically) 1.5 to 2 kW. Therefore at high shaft speeds, which are of greatest interest in this work, the mechanical losses account for only ~2.5% of the shaft power. Any variability in the mechanical loss will therefore have little effect on the overall power balance. The measured shaft torque does, however, vary between runs and torques due to mechanical losses of up to 0.23 N.m have been measured. The potential error is therefore 0.1 N.m, or 31 W at 3000 rpm.

Table 5.3 Shaft torque measured due to mechanical losses

N (rpm)	Λ (N.m)	Λ (N.m) (Sparks, 1993)
500	0.125	0.141
1000	0.127	0.144
1500	0.133	0.136
2000	0.131	0.150
2500	0.128	0.152
3000	0.133	0.156

5.1.4 Disc friction, P_{DISC}

A measure of disc friction was obtained by spinning a smooth disc with the same dimensions as **r/18/50/119.6** and measuring the shaft torque (the shaft torque due to mechanical losses was subtracted). This measured disc friction is shown in Figure 5.23 along with the disc friction loss predicted by Equation 3.4:

$$P_{DISC} = 24.8 \times N^3 D^4 (D + 5E) \qquad (3.4)$$

This measured disc friction is higher than the calculated disc friction, but is of the correct order of magnitude. For the rest of this work, measured values of P_{DISC} were be used. For the half-scale unit, measured disc friction values were not available. Therefore, for the half-scale energy balance (Figure 5.2.6), disc friction was taken

to be that for the full scale multiplied by the scaling factor raised to the power 5.

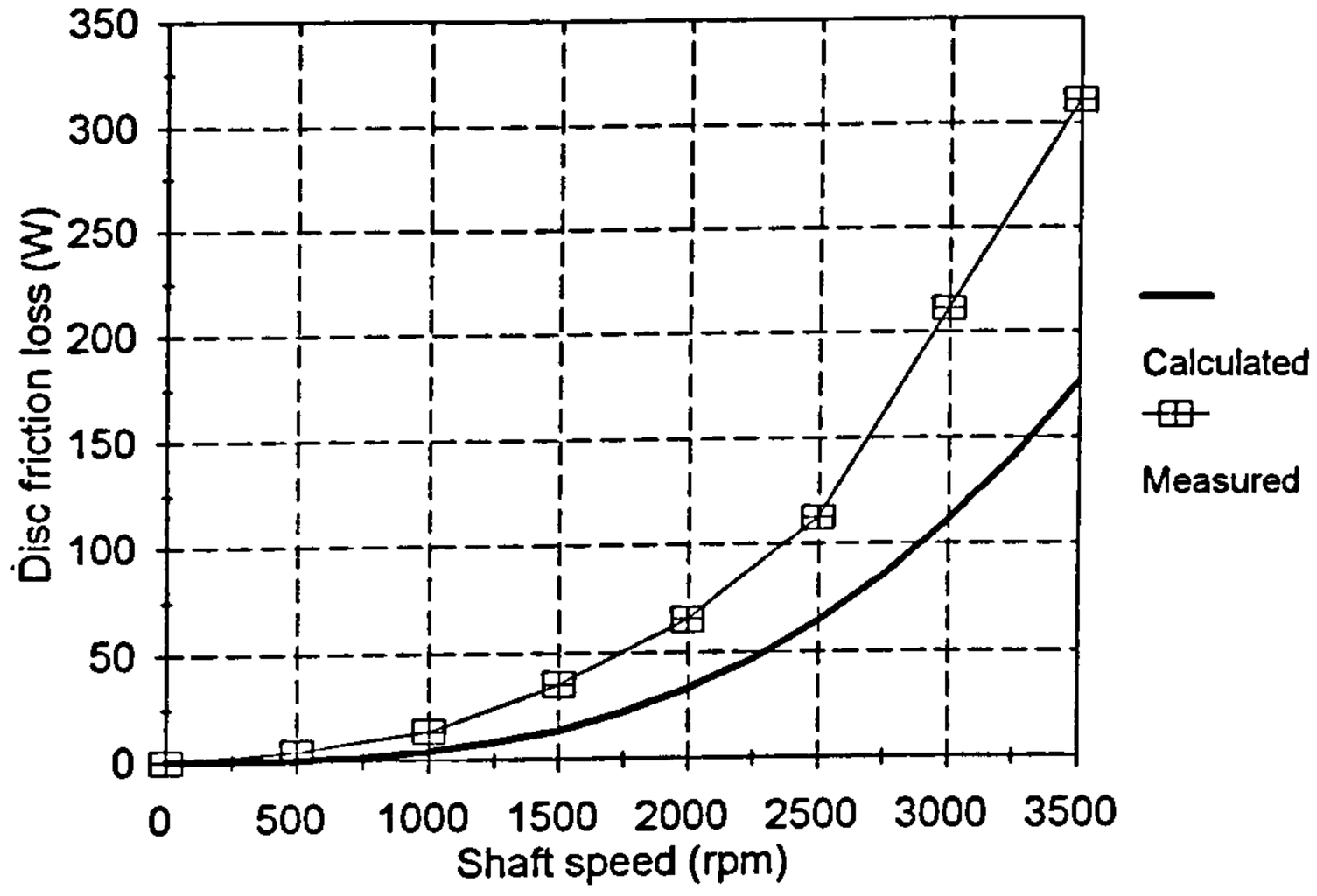

Figure 5.23 Disc friction loss - measured and calculated using Equation 3.4

5.1.5 Overall power balances - leakage and hydraulic losses

Overall power balances for one toothed unit (**r/18/50/123.34** & **s/18/50/123.8**), the Silverson and the half-scale toothed mixers are given in Figures 5.24 to 5.26.

The power balance curves for each of the units are similar, and a number of general observations can be made. Firstly, the pumping efficiency is lower than that for a centrifugal pump (as in Section 5.1.2), the pumping component of the balance is also flatter than that for a centrifugal pump (Figure 2.18). In a centrifugal pump, the best pumping efficiency occurs when the tip speed of the rotor matches the speed of the fluid in the volute. Therefore, in a centrifugal pump, the hydraulic and leakage losses increase slightly at flow rates above and below the best efficiency point, as separation and recirculation increase. In rotor-stator mixers the rotor discharge is separated from the volute by the stator, so it is not possible for the speed of the

water in the volute to match the tip speed of the rotor. The losses in a rotor-stator mixer

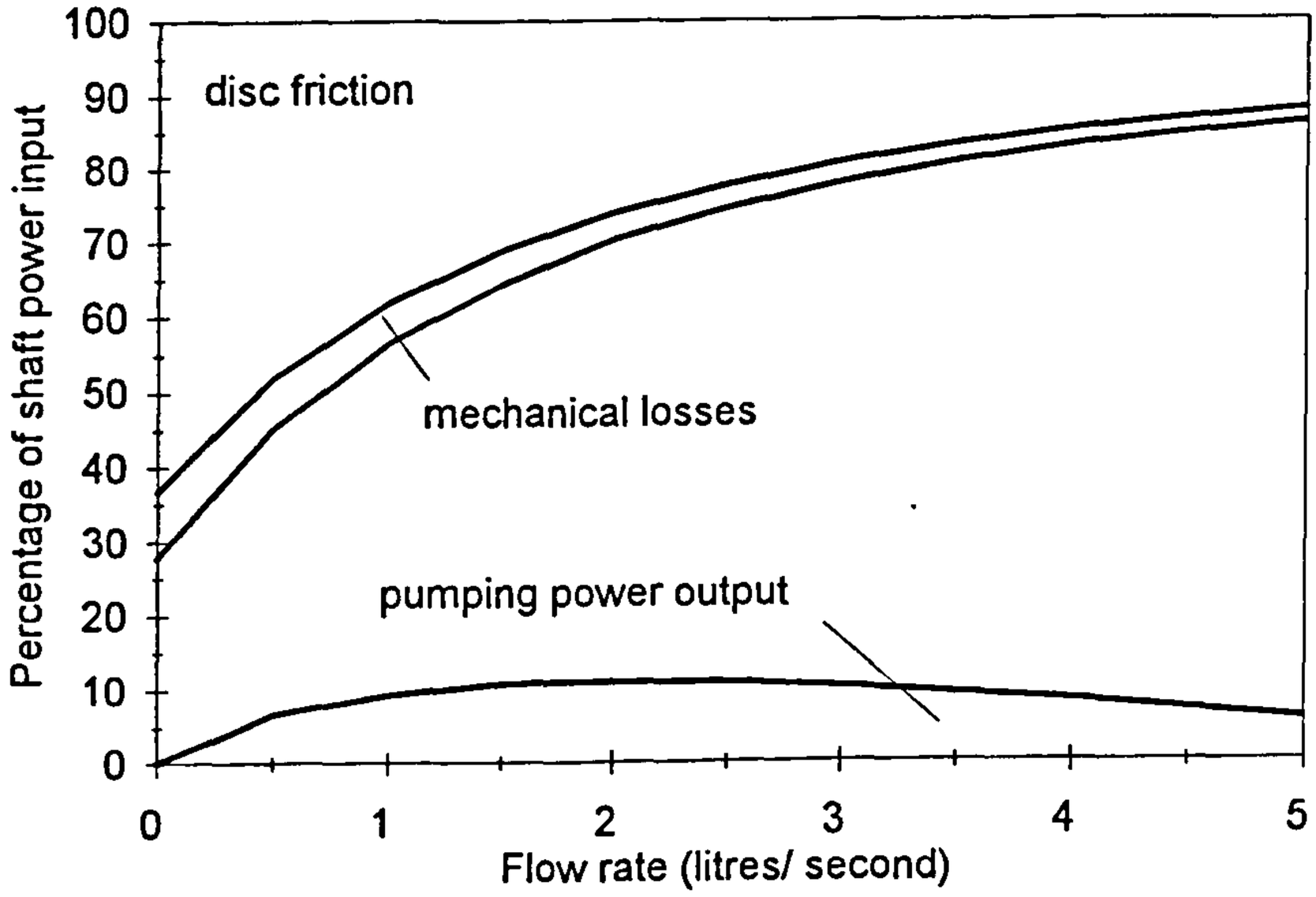

Figure 5.24 Overall power balance for **r/18/50/123.34 & s/18/50/123.8**) at 3000 rpm

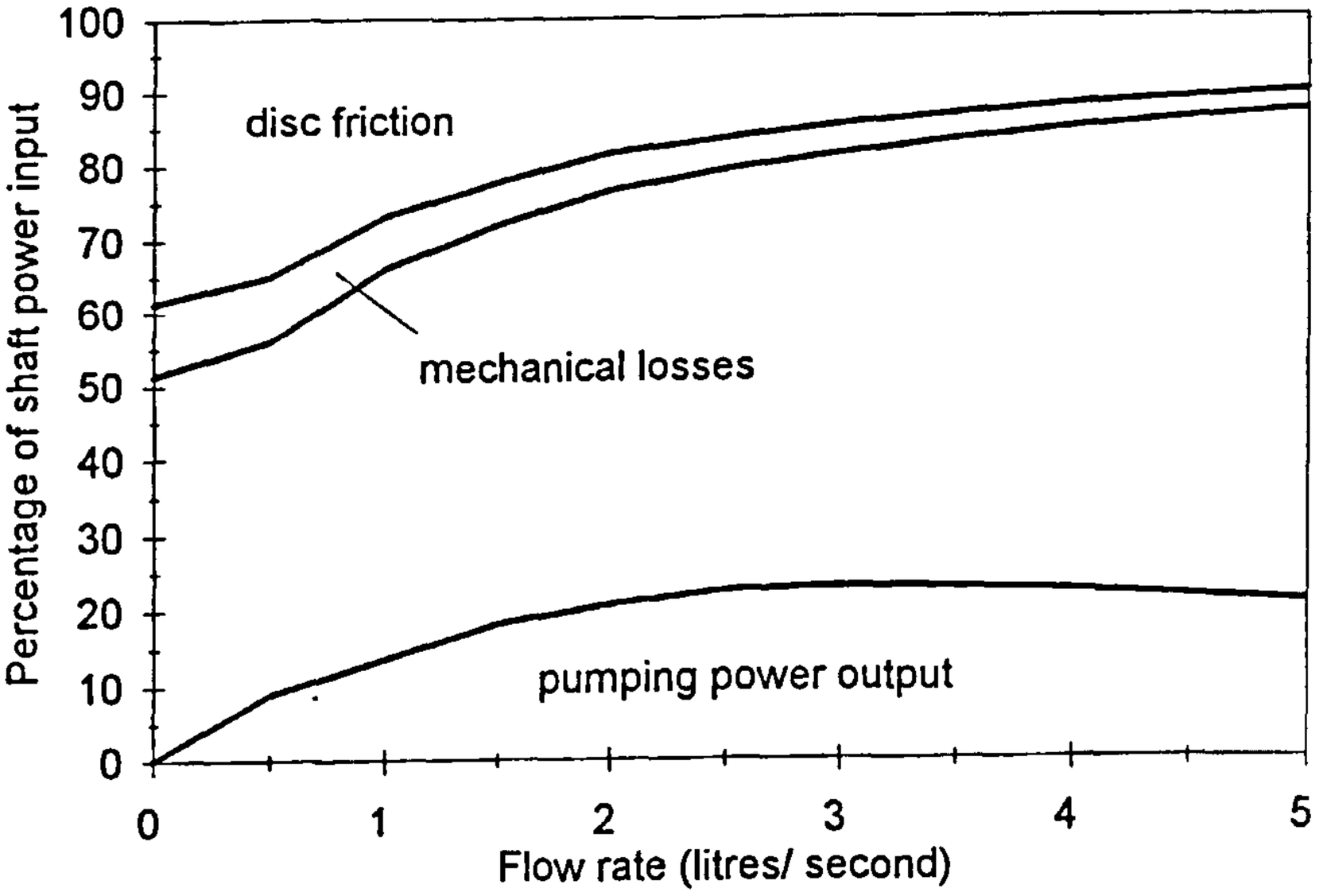

Figure 5.25 Overall power balance for the Silverson unit at 3000 rpm

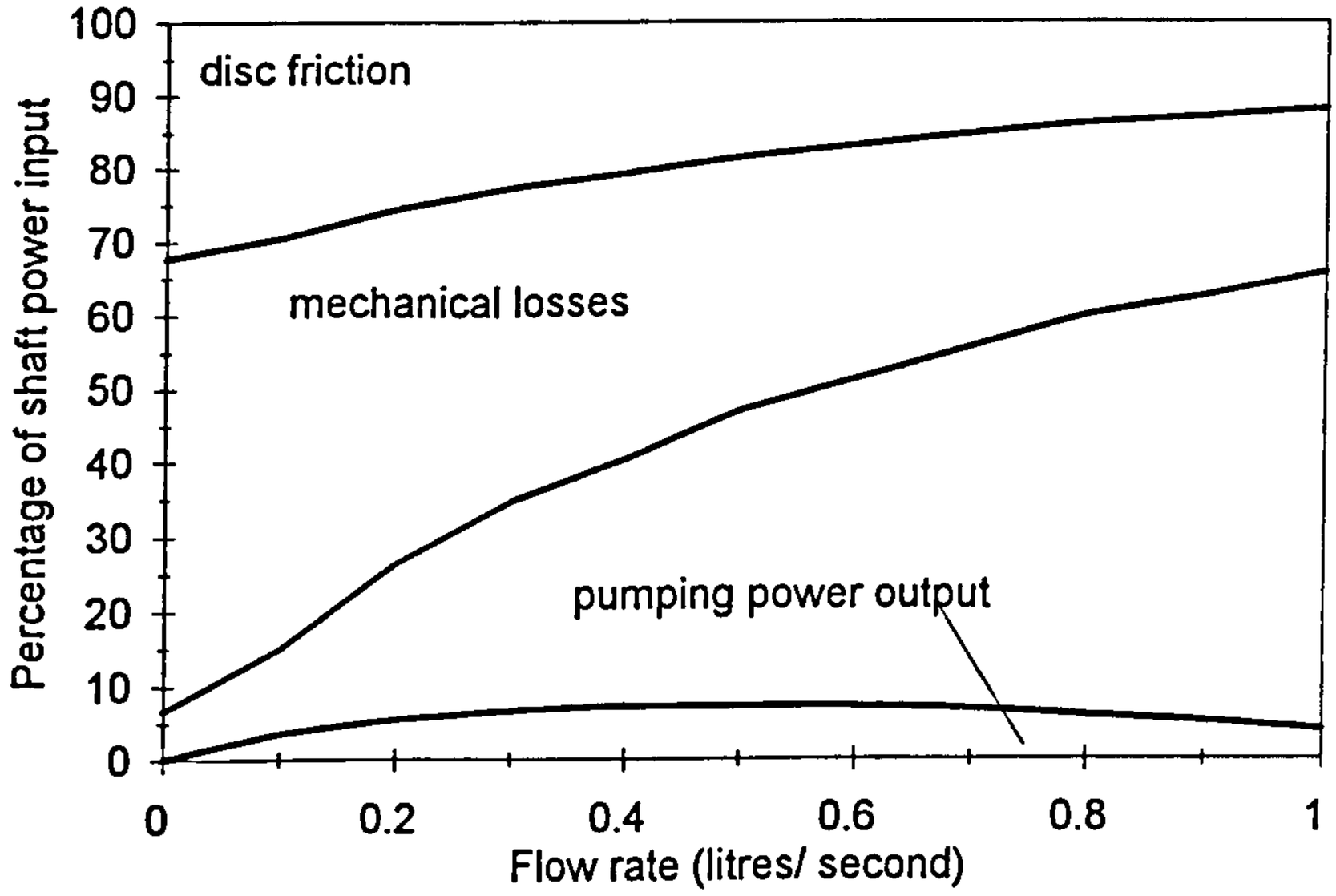

Figure 5.26 Overall power balance for the half-scale unit at 4000 rpm

are probably due to the acceleration of the fluid in the rotor and the abrupt deceleration of the fluid in the stator (Section 5.2), so the magnitude of the recirculation and hydraulic losses will be significant over the full range of operation.

A much greater proportion of the shaft power is dissipated through hydraulic and leakage losses (which contribute to mixing) than for a centrifugal pump. Up to 70% of the shaft power is not accounted for by pumping power or disc or mechanical losses. It is therefore concluded that this power is dissipated in the mixer through hydraulic and leakage losses combined. No further breakdown of these losses is possible using the overall power balance work presented here.

These general observations were reported previously for **r/18/50/119.6** & **s/18/50/123.8** (Sparks, 1993) but apply equally to the other designs.

5.1.6 Power supplied to the fluid by the rotor

The mechanical and disc friction losses contribute negligibly to the mixing and pumping in a rotor-stator mixer. It is also known that the disc friction component is proportional to N^3 (Section 5.1.4). Therefore, subtracting estimates for the mechanical and disc friction losses from the measured shaft power leaves P_{PUMP} + P_{LEAK} + $P_{HYDRAULIC}$ for a range of flow rates and shaft speeds. The sum of these components will be called the power supplied to the fluid by the rotor, P_{FLUID}.

Assuming a relationship for P_{FLUID} of the form:

$$P_{FLUID} = (P_{PUMP} + P_{LEAK} + P_{HYDRAULIC}) = PnQ^{f}N^{g}D^{h} \qquad (5.5)$$

and performing a multiple regression using all of the power data (including those with a net pressure drop) leads to the following result:

$$P_{FLUID} = 3.01\ Q^{0.75}N^{2.17}D^{2.4} \qquad (5.6)$$

The R^2 value for this correlation is 0.984, indicating a good correlation. The exponents on Q, N and D in Equation 5.6 are close to 1, 2 and 2 respectively and the following analysis examines the value of these exponents in detail.

Flow visualisation results (Section 5.2) showed that fluid in the rotor region of the mixer follows the rotor teeth, moving at speed v_{TIP}. Therefore, the kinetic energy of a fluid element at the rotor tip, of mass m, is given by:

$$\text{K.E} = \frac{1}{2}m v_{TIP}^2 \qquad (5.7)$$

the equivalent power is given by:

$$P = \frac{1}{2}\rho Q v_{TIP}^2 \tag{5.8}$$

so, as $v_{TIP} = \pi ND$ (Equation 5.16):

$$P_{FLUID} = \frac{1}{2}\pi^2 N^2 D^2 Q \tag{5.9}$$

In the analysis leading to Equation 5.9 the radial component of the fluid velocity vector (v_{RADIAL}) is omitted, as v_{RADIAL} through the rotor and stator, when they have the same open area, will be similar and for most of the data presented here, $v_{TIP} \gg v_{RADIAL}$ (Section 5.2). A more elaborate analysis that considers the exit velocity vector for fluid leaving the rotor could allow optimisation for pumping (by aligning stator blades with the flow, minimising losses) or mixing (maximising losses by designing for an exit velocity that impinges onto the stator).

Equation 5.9 is similar to 5.6 and it was assumed that the power given to the fluid by the rotor, P_{FLUID}, was given by (as for an impeller in a stirred tank):

$$P_{FLUID} = Po\rho N^2 D^2 Q \tag{5.10}$$

A simple regression was performed on the measured data to produce values for *Po* (Table 5.4). The values of *Po* are all ~10, with the values for the thinnest shear gap rising to ~11.5 and the value for the half-scale unit dropping to 9.2. In addition, the values for stator **s/18/33/123.8** are significantly lower for the thick and two medium shear gap thicknesses, which consistent with the findings from Section 5.1.1.

The constant, *Po*, is directly analogous to the power number of an impeller in a stirred tank and the correlation given in Equation 5.10 is dimensionally correct. Equation 5.10 was used for the subsequent analysis of energy dissipation rates.

Figure 5.27 shows values calculated using Equation 5.10 for the half-scale unit and the corresponding large-scale unit (**r/18/50/123.34 & s/18/50/123.8**) versus measured data. Equation 5.10 gives a good fit to the measured data. However, Equation 5.10 predicts zero shaft power when the flow rate is zero when the rotor still supplies power to the fluid (these values are omitted from Figure 5.27). In addition, the fit to the measured data is poorer at low flow rates than for high flow rates, shown by the values that fall below the main grouping.

Table 5.4 Results of a regression performed using Equation 5.9

Rotor-stator	***Po***	**R^2**
r/18/50/119.6 & s/18/50/123.8	10.32	0.985
r/18/50/119.6 & s/18/33/123.8	9.80	0.986
r/18/50/119.6 & s/19/50/123.8	10.34	0.978
r/18/50/119.6 & s/36/50/123.8	10.31	0.968
r/12/66/121.45 & s/18/50/123.8	10.04	0.982
r/12/66/121.45 & s/18/33/123.8	9.84	0.992
r/12/66/121.45 & s/19/50/4.784	10.16	0.980
r/12/66/121.45 & s/36/50/123.8	10.06	0.984
r/18/50/121.45 & s/18/50/123.8	10.27	0.988
r/18/50/121.45 & s/18/33/123.8	9.91	0.994
r/18/50/121.45 & s/19/50/123.8	10.33	0.990
r/18/50/121.45 & s/36/50/123.8	10.31	0.986
r/18/50/123.34 & s/18/50/123.8	11.39	0.995
r/18/50/123.34 & s/18/33/123.8	11.49	0.997
r/18/50/123.34 & s/19/50/123.8	11.95	0.994
r/18/50/123.34 & s/36/50/123.8	11.62	0.994
Silverson	9.78	0.973
half-scale toothed	9.19	0.991

The lowest R^2 (and therefore poorest fit) was obtained for the Silverson. However, this still provides a useful way of estimating the power supplied to the fluid by the rotor for given operating conditions and scale.

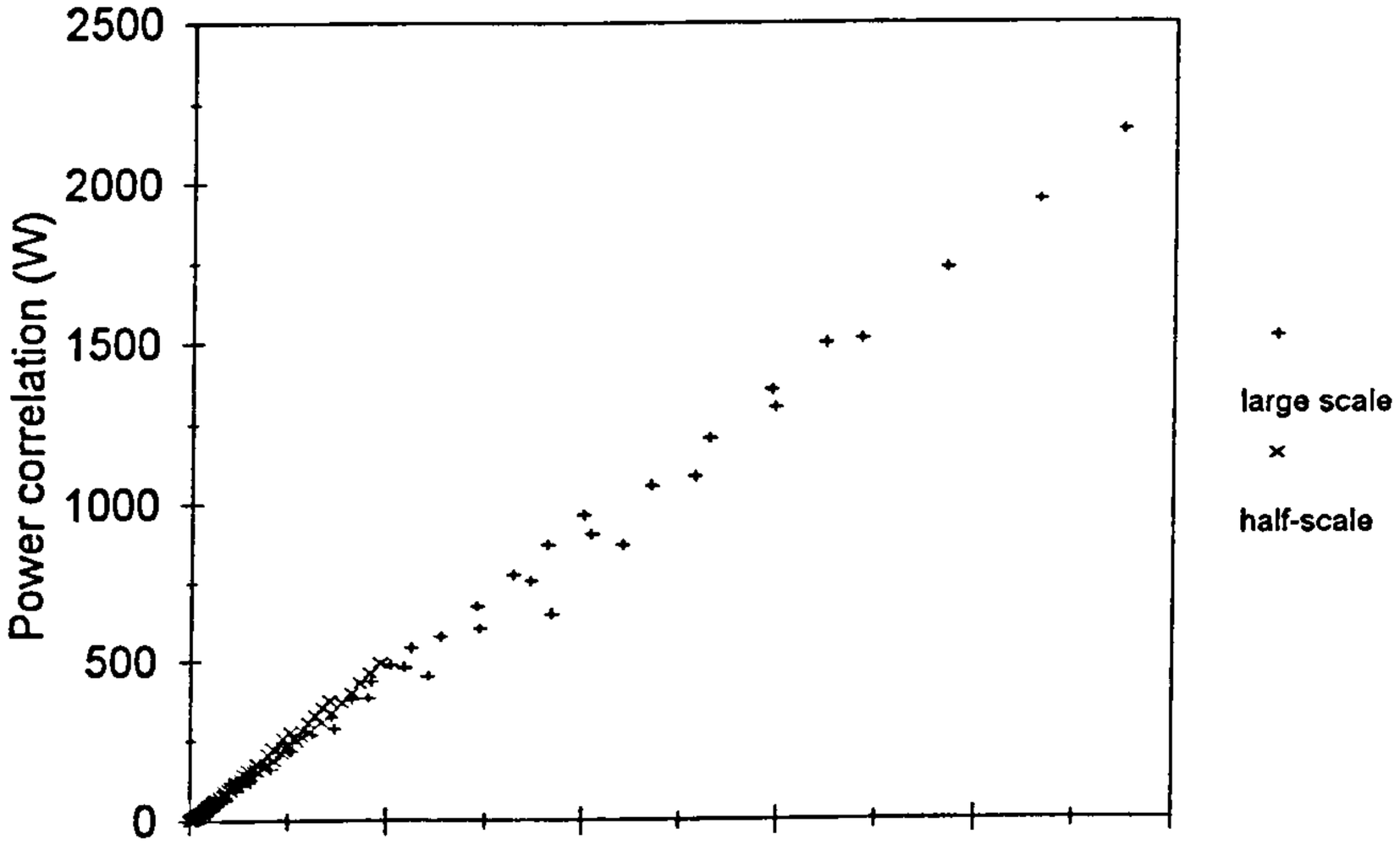

Figure 5.27 Measured values of P_{FLUID} versus values predicted using Equation 5.10

From the overall power balance (Equation 2.37), the shaft power for a rotor-stator mixer can be estimated using:

$$P_{SHAFT} \approx 10\rho N^2 D^2 Q + 24.8 N^3 D^4 (D + 5E) + P_{MECH} \qquad (5.11)$$

Use of Equation 5.11 requires knowledge of the mechanical losses, but as an approximation it is useful for estimating the motor power requirement when the flow through a rotor-stator mixer is to be imposed using an upstream pump (and controlled with a valve).

Where the rotor-stator is acting as the only pump in a pipe-line, the flow rate will probably be proportional to the shaft speed and the rotor diameter cubed (Streeter and Wylie, 1983):

$$Q \propto ND^3 \tag{5.12}$$

Bourne and Garcias-Rosas (1986) found that the flow rate through their rotor-stator unit was proportional to the rotational speed. In this case, combining Equations 5.10 and 5.12 gives:

$$P_{FLUID} \propto Po'N^3D^5 \tag{5.13}$$

where *Po'* (the power number) has different values to those given in Table 5.4.

Power measurements were undertaken for the half-scale unit and corresponding large scale unit (**r/18/50/123.34** & **s/18/50/123.8**) when the flow rate was zero (i.e. when the flow control valve was shut). Analysis of these shaft power data showed that Equation 5.13 fitted approximately (with an exponent on N of 3.45 and an exponent on D of 4.74; $R^2 = 0.939$).

5.1.7 Energy dissipation

Using Equation 5.10, it is now possible to calculate the power supplied to the fluid by the rotor. It was assumed that this power is supplied to the fluid in a small region of the rotor-stator (encompassing the rotor teeth, the stator teeth and the shear gap) For the toothed designs this region has a volume of approximately 0.07 l (0.07 kg of water) so that the power per unit mass, Φ, is given by:

$$\Phi = \frac{P_{FLUID}}{0.07} \tag{5.14}$$

It was assumed further that a proportion of this power is dissipated through turbulence, given by:

$$\eta_{TURB} = \frac{\varepsilon}{\Phi} \qquad (5.15)$$

where η_{TURB} is the turbulence factor.

There is no information in the literature on the turbulence efficiency factor for a rotor-stator. For this study it was assumed initially that 1/3 of the power supplied to the fluid by the rotor goes to turbulence dissipation. With a Kenics HEV in-line static mixer around 80% of the total power dissipated is dissipated through turbulence (Hearn, 1995). When compared to the HEV mixer efficiency the estimate of 1/3 seems conservative, but the rotor-stator mixer has many more metal surfaces than an HEV mixer which may lead to higher direct friction losses. The above assumptions give $\varepsilon \sim 5000$ W kg^{-1} at 3000 rpm and 3.0 l.s^{-1} for the toothed rotor-stator. This is a value averaged over the rotor-stator region, not the full mixer.

If ε has this value, then the corresponding engulfment time, t_E, for water at 25°C is 0.2 ms. This would mean that rotor-stator mixers could be used for competitive reactions where the reaction time is of this order. The diazo-coupling experiments were performed to estimate ε from the product distribution and these are presented in Section 5.5. The method for producing estimates for ε presented here was used in the design of these diazo-coupling tests.

It is also constructive to consider the effect of the static loss on this estimate for ε when the mixer is operated at a point where the mixer is over-run ('drowned suction', Section 5.1.2). Under these circumstances the static losses, as liquid is forced through the mixer, can become large compared with the power input to the

system by the rotor. The static losses also contribute to mixing (as in a 'static mixer'). Here, it will be assumed that the turbulent energy dissipation rate is contributed to by both P_{FLUID} and P_{STATIC}:

$$\varepsilon = \eta_{TURB}\Phi + \eta'_{TURB}\Phi' \qquad (5.16)$$

where η'_{TURB} is a turbulence efficiency factor for the static loss and Φ' is the power per unit mass due to static losses:

$$\Phi' = \frac{P_{STATIC}}{0.07} \qquad (5.17)$$

Figures 5.28 and 5.29 show Φ and Φ' plotted against flow rate for the Toothed and half-scale toothed units (plotted using Equations 5.4 and 5.10). These plots show that, assuming that $\eta'_{TURB} \approx \eta_{TURB}$, for the large unit, Φ' (the static loss) is not significant compared to Φ (given the accuracy of other assumptions) until flow rates of greater than 3 $l.s^{-1}$. The diazo-coupling work was done with flow rates below 3.0 $l.s^{-1}$ (with two exceptions), so the static loss component was not considered when estimating ε nor when designing and analysing experiments.

However, for the half-scale unit, Φ' is significant compared to Φ over the whole range and dominates as the flow rate increases. This would have important implications when using the half-scale rotor-stator as a chemical reactor under these conditions. However, it is likely that as much, if not more, power would be consumed in pumping the liquid through as is used to run the mixer. It was possible to operate the half-scale mixer at these conditions only because the unit was fitted into the flow loop designed for the large unit - it is unlikely that rotor-stator mixers in industry are operated so far past their 'positive pumping' region.

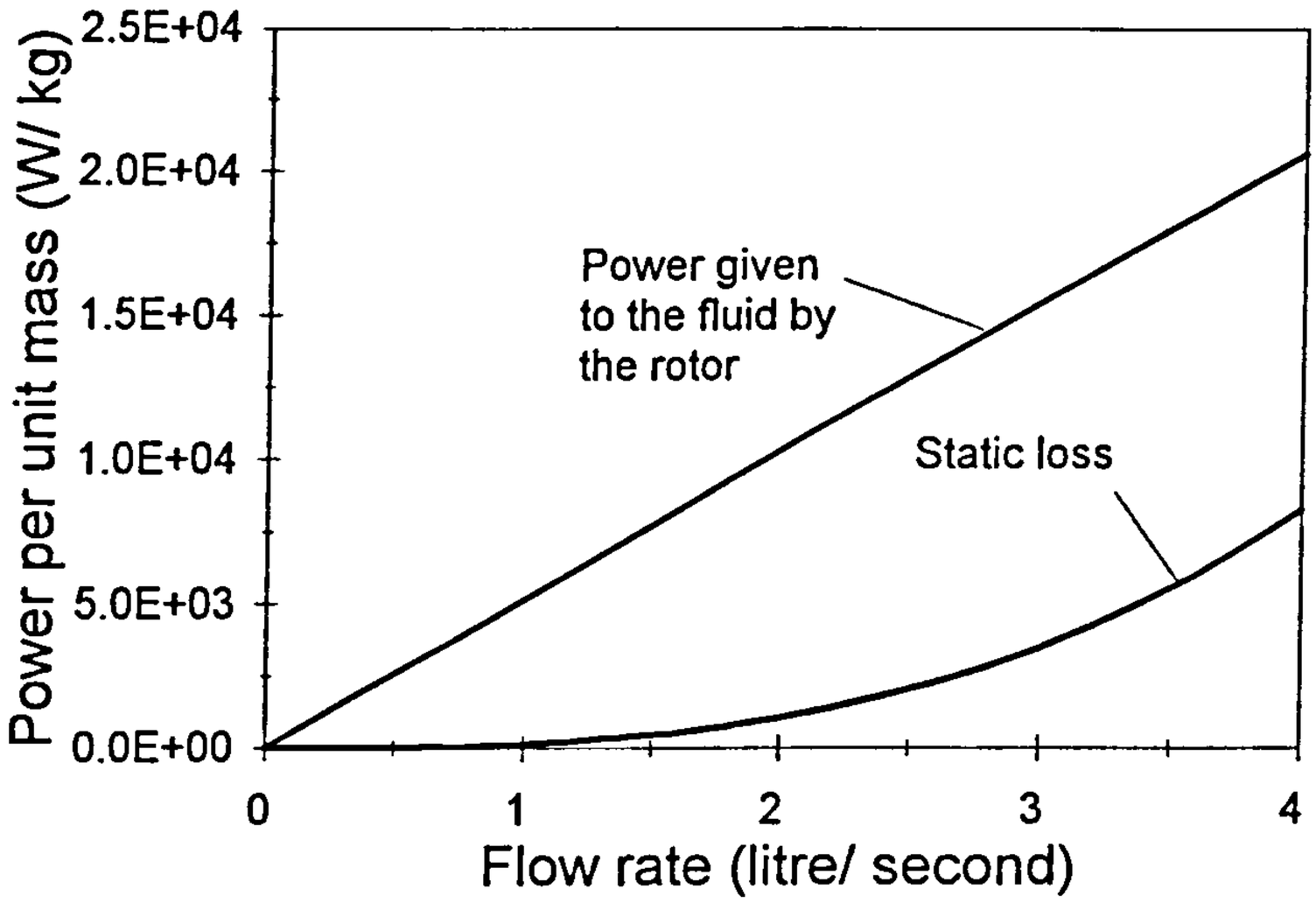

Figure 5.28 Φ (Equations 5.10 & 5.15) and Φ'(Equations 5.4 & 5.16) versus flow rate for a toothed rotor-stator unit (e.g. **r/18/50/121.45 & s/18/50/123.8**) at 3000 rpm.

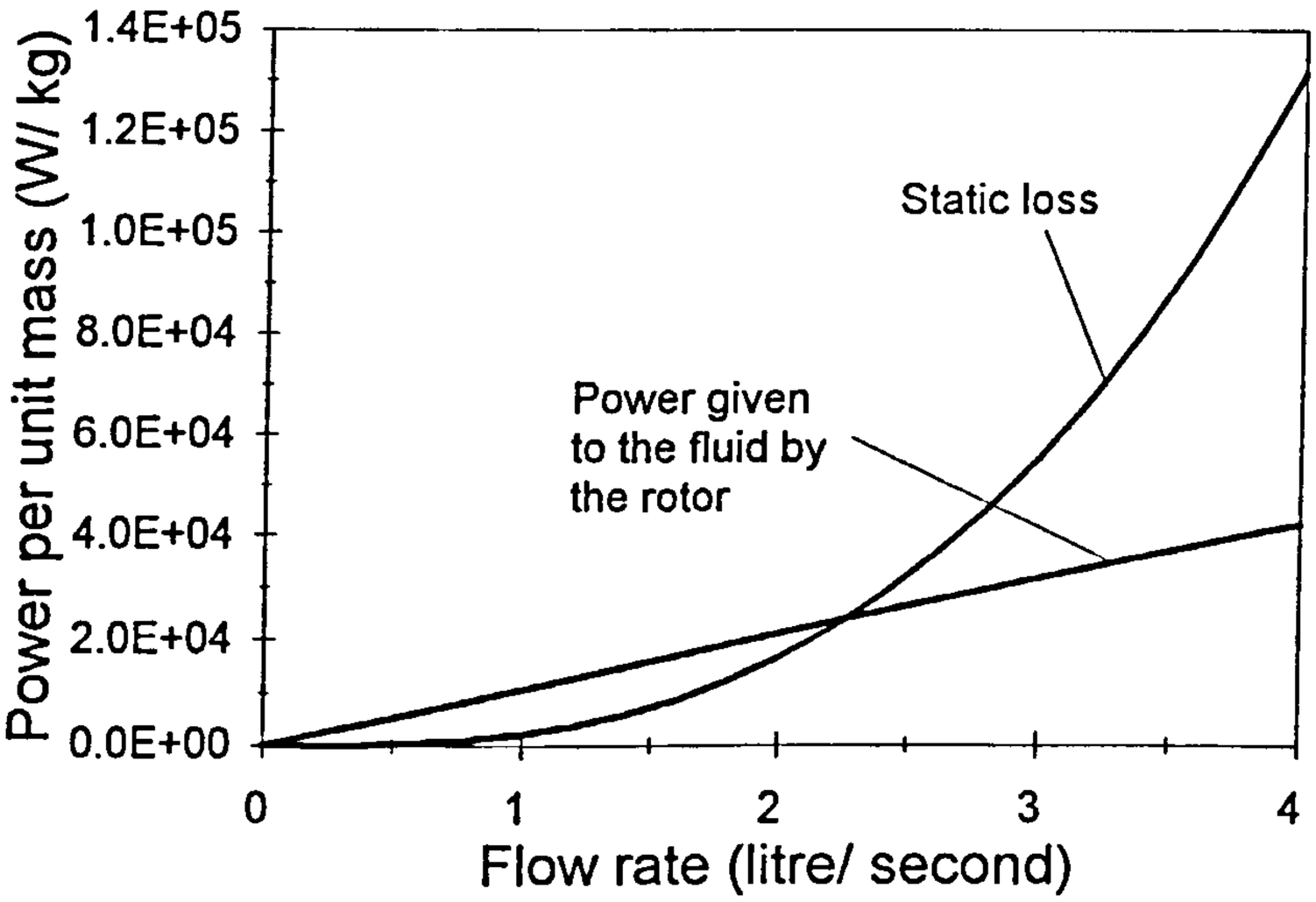

Figure 5.29 Φ (Equations 5.10 & 5.15) and Φ'(Equations 5.4 & 5.16) versus flow rate for the half-scale toothed rotor-stator unit (**r/18/50/61.44 & s/18/50/61.9**) at 3000 rpm.

5.1.8 Accuracy of results

Figures 5.30 and 5.31 show shaft torque and differential pressure results from repeat experiments (with **r/18/50/119.6 & s/18/50/123.8**). These data were taken with rotors, stators and casing made with a variety of combinations of materials (when a clear acrylic rotor, stator and casing were made for flow visualisation). The results reproduce well, with a slight deviation at low and high flow rates.

It was concluded that the material used to make the rotor and stator units did not affect the measured power and that results taken are reproducible.

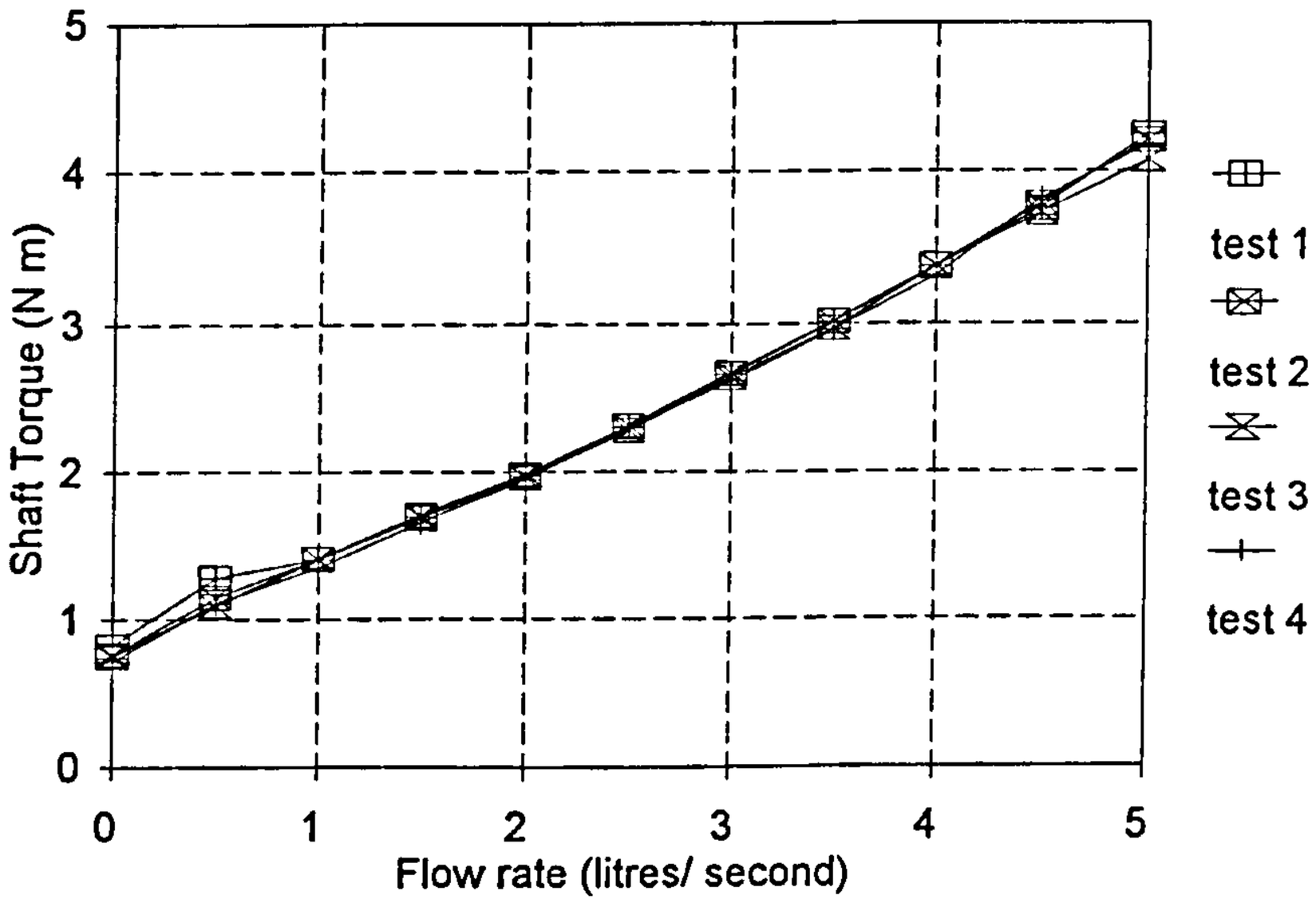

Figure 5.30 Repeat shaft torque data

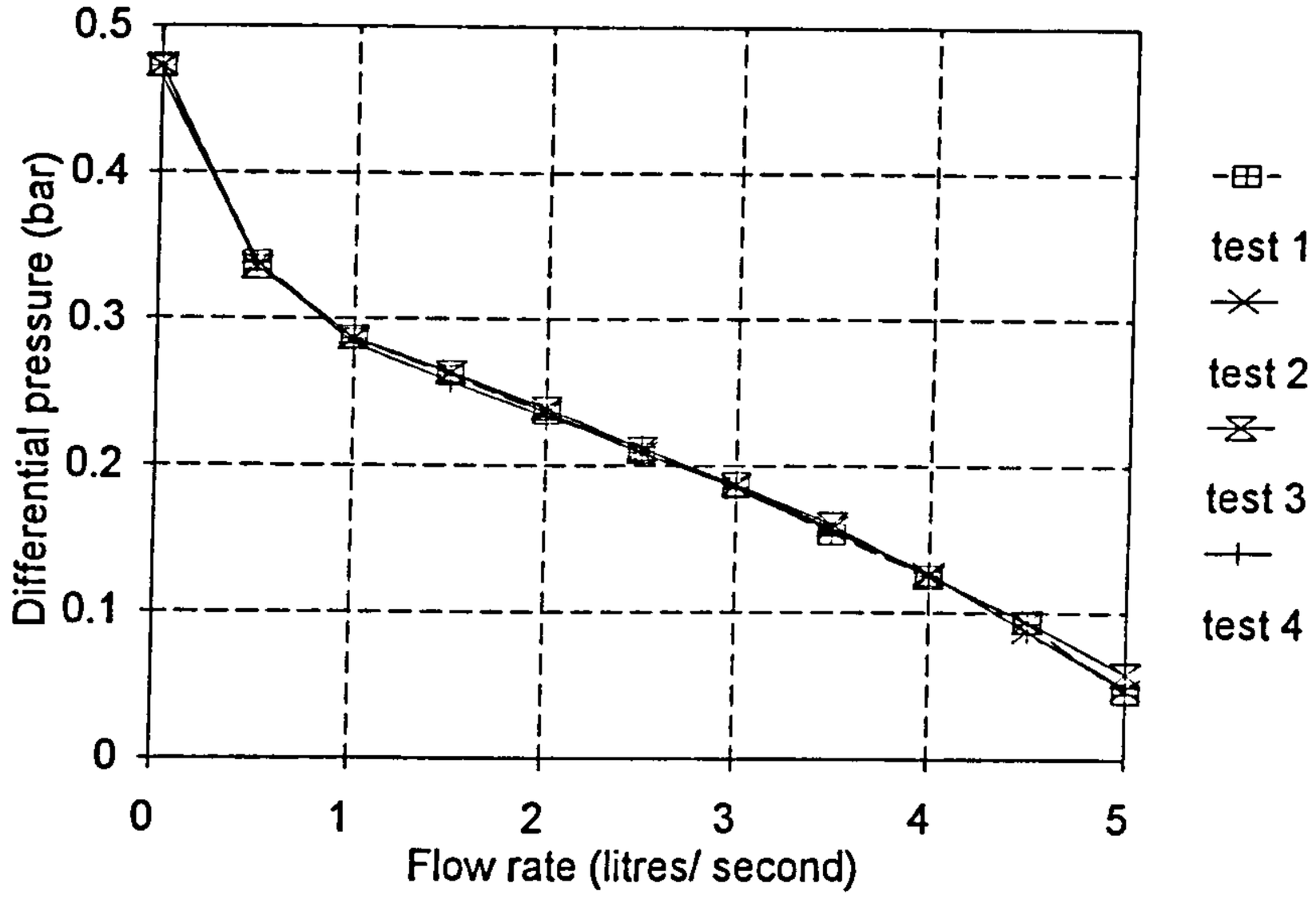

Figure 5.31 Repeat differential pressure data

5.2 Flow visualisation

The findings of the flow visualisation work, performed as described in Sections 3.5.3 and 4.2, are discussed in the following sections. During the presentation of these results, reference will be made to nominal flow parameters (e.g. average velocities, residence times etc.). Following this, results obtained using computational fluid dynamics (CFD) are discussed and compared with the visualisation results.

5.2.1 Inlet pipe

The inlet pipe contains swirling fluid caused by the effects of the spinning rotor disk propagating up the inlet pipe (Figure 5.32). There was no observable change in the flow in the inlet pipe with operating condition (N and Q) and, while this flow pattern may modify the RTD and measured pumping power, it should not affect the flows

in the immediate vicinity of the rotor-stator teeth.

It would not be good practice to feed into the inlet pipe when the process being undertaken in the mixer requires fast and immediate mixing, for example, competitive chemical reactions (Bourne and Garcias-Rosas, 1986). For this reason, no further work was done on the flow pattern in this region.

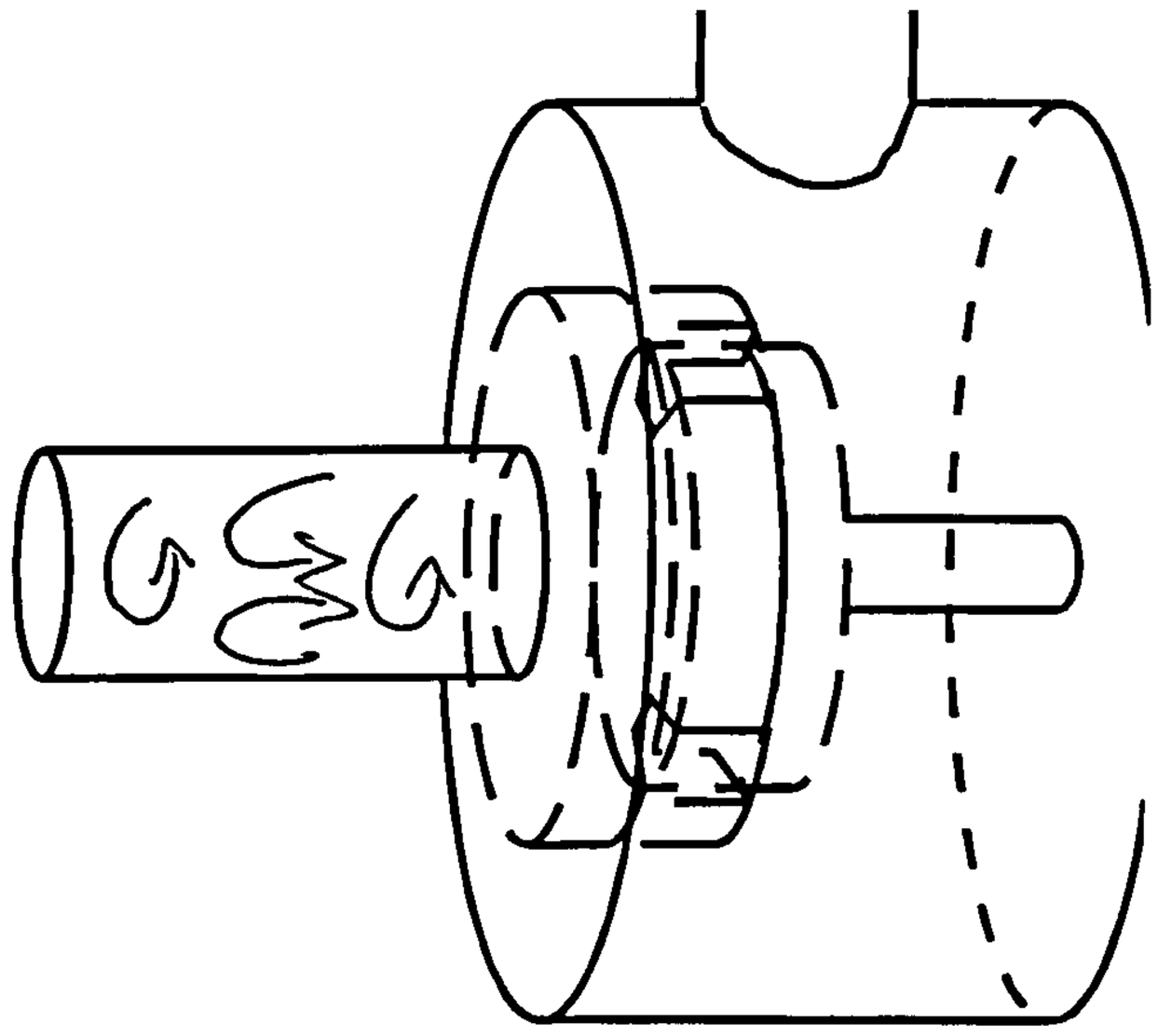

Figure 5.32 Inlet pipe swirl

5.2.2 Rotor

Water entering the rotor region was accelerated tangentially by the rotor. The flow pattern in the region upstream of the rotor teeth was characterised by swirl generated as fluid followed the rotor face. As with the flow pattern in the inlet pipe, there was little dependency of this flow on the operating condition.

Tracer introduced upstream of the rotor teeth and into the rotor teeth (Feed positions

I and II, Figure 3.12), followed the rotor teeth. This is shown schematically in Figure 5.33. Tracer was transported a significant distance around the rotor circumference, leading to an interaction between the plumes from adjacent feeds (Figure 5.34). Reactant plume interaction could dramatically change the outcome of some processes as products from the reaction occurring due to one feed meet fresh products from another feed..

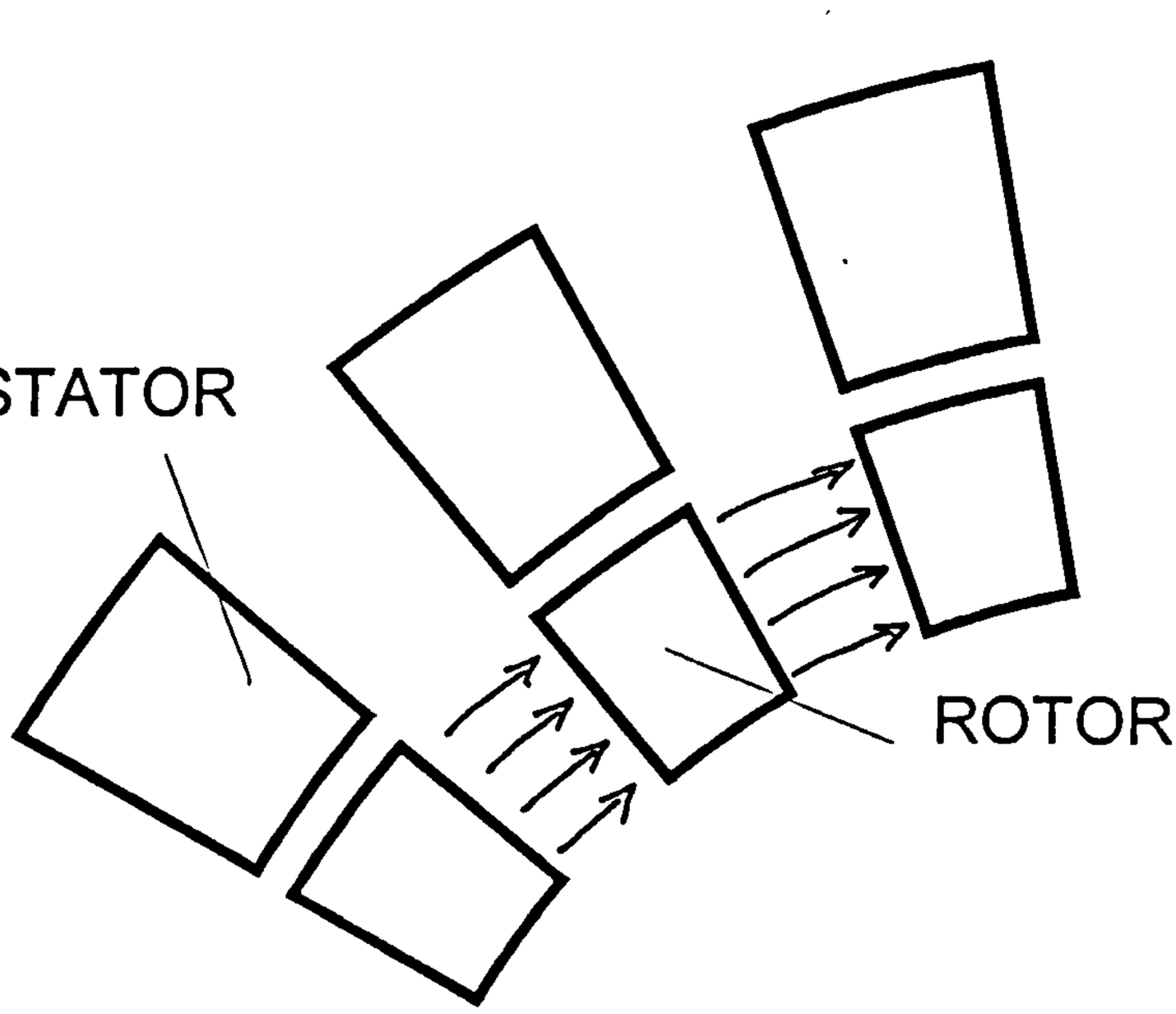

Figure 5.33 Schematic diagram of flow in the rotor teeth

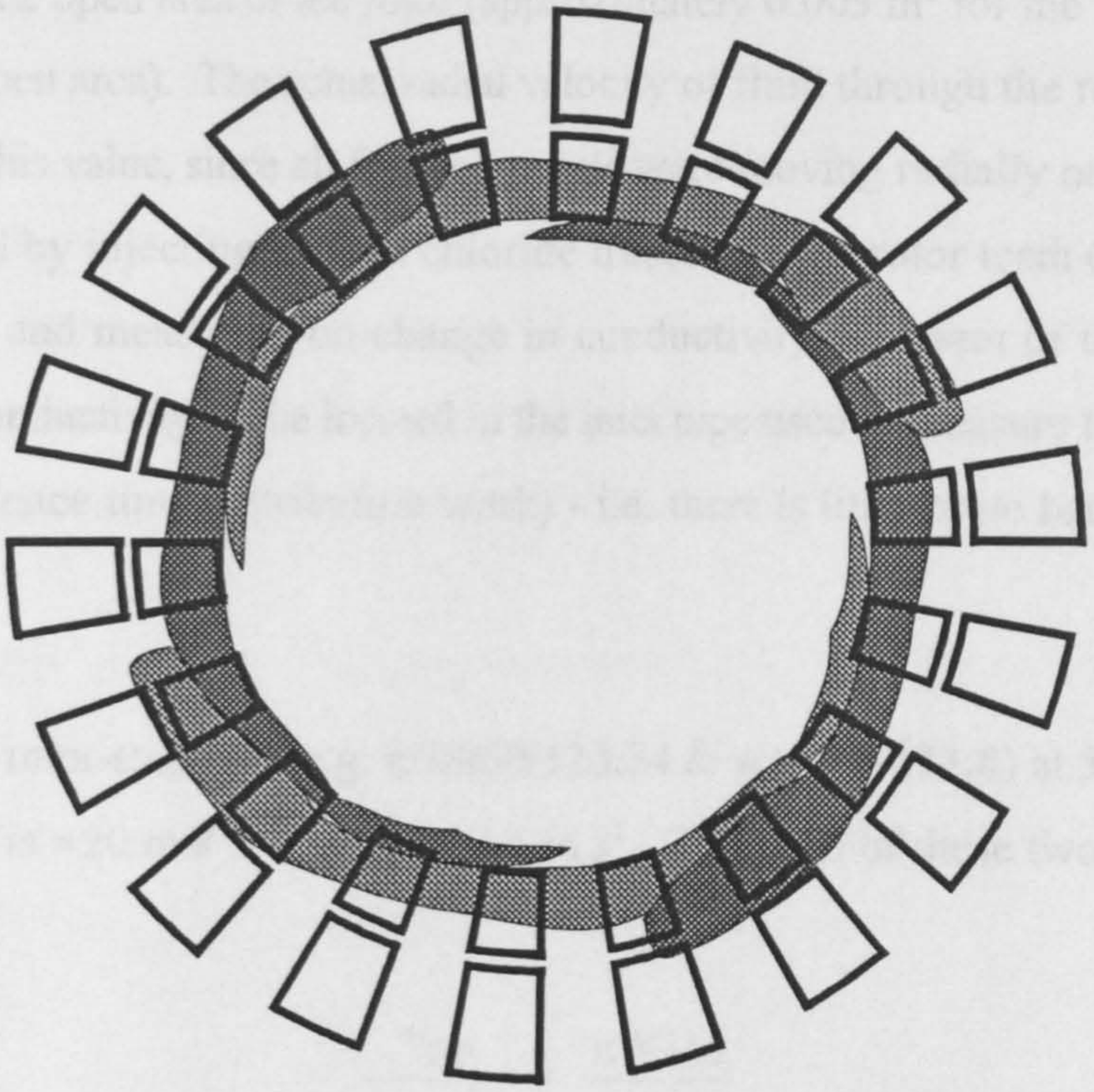

Figure 5.34 Trajectory of plumes produced during acid-base decolourisation experiments

Consideration of values of nominal velocities and residence times shows that the flow in the rotor teeth might be expected to behave as reported above. Firstly, as the fluid is shown to follow the rotor teeth, then the velocity of fluid at the rotor tip, v_{TIP}, will be the same as the tip speed of the rotor:

$$v_{TIP} = \pi ND \tag{5.18}$$

where N is the shaft speed (s^{-1}) and D is the rotor diameter (m).

The trajectory of fluid through the rotor region (in the absence of any dispersion) is indicated by v_{TIP} and the nominal radial velocity, v_{RADIAL}:

$$v_{RADIAL} = \frac{Q}{A} \tag{5.19}$$

where A is the open area of the rotor (approximately 0.003 m^2 for the toothed rotors with 50% open area). The actual radial velocity of fluid through the rotor teeth will be close to this value, since all fluid elements were moving radially outwards. This was checked by injecting sodium chloride tracer into the rotor teeth (through Feed Position II) and measuring no change in conductivity upstream of the rotor teeth (using the conductivity probe located in the inlet pipe used to measure the inlet pulse for the residence time distribution work) - i.e. there is little or no back flow in the region.

For a typical rotor-stator set (e.g. **r/18/50/123.34 & s/18/50/123.8**) at 3000 rpm and 3.0 l s^{-1}, v_{TIP} is ≈20 m s^{-1} and v_{RADIAL} ≈ 1 m s^{-1}. The ratio of these two quantities is given by:

$$\frac{v_{TIP}}{v_{RADIAL}} = \frac{\pi NDA}{Q} \qquad (5.20)$$

This ratio can be used to estimate the tangential spreading of fluid in the rotor. In the above example, fluid introduced into the mixer just upstream of the rotor teeth is required to move approximately 15 mm radially to reach the shear gap. In the time required to move this distance radially, the fluid will (on average) move a distance of 300 mm tangentially (~0.75 of the rotor circumference). This predicts that reaction plumes from neighbouring feeds will interact, as was observed.

It is also possible, knowing the nominal radial velocity through a region and the radial length of that region, d_{RADIAL}, to calculate the nominal residence time of fluid in that region:

$$\tau = \frac{d_{RADIAL}}{v_{RADIAL}} \qquad (5.21)$$

This can be used to compare with the intrinsic rate of the process that is occurring in the rotor-stator region (e.g. chemical reaction time) and will be useful when determining the rotor type and size required for a particular process. In the above example, this gives a nominal residence time in the rotor teeth, τ_{ROTOR} of ~0.015 s (very short compared to the nominal residence time for the overall unit of ~0.5 s). A similar calculation can be used to calculate the nominal residence time in other regions of the mixer, for example the residence time in the stator.

A final parameter indicates the length to which fluid blobs, passing through the rotor, are reduced by the chopping action of the rotor, once again without diffusion or back-mixing. The length of such blobs is given by the nominal radial velocity divided by the tooth passing frequency:

$$L_0 = \frac{v_{RADIAL}}{Nn} \tag{5.22}$$

where n is the number of teeth on the rotor. This length will be adopted as the initial scale of segregation when considering meso-mixing rates in Section 5.4.

5.2.3 Shear gap

It was very difficult to observe the flow pattern in the shear gap region, because of the scale over which effects in the shear gap occur (<1 mm) and the rotor teeth passing at high speed. However, the effect of the shear gap size on leakage flows between stator tooth slots was observed (Figure 5.35). With the thickest shear gap there was significant leakage between tooth slots.

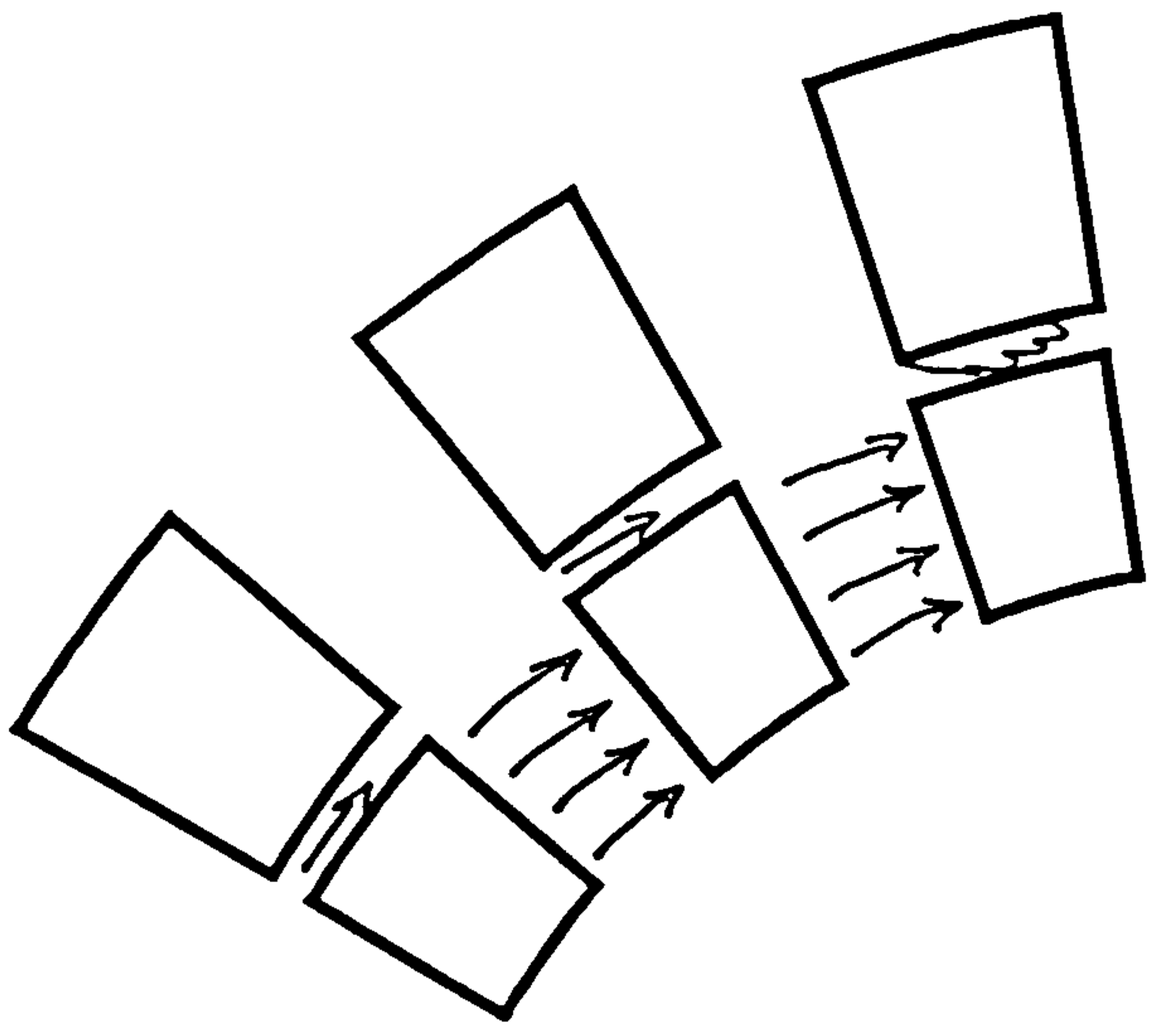

Figure 5.35 Leakage between stator slots and gas cavity formation.

It was expected that pulsation should occur because of rotor-stator interaction, particularly with the thinnest shear gap and the 18/18 or 18/19 rotor-stator combinations. However, this could not be observed directly.

With the thinnest shear gap there was evidence of gas cavities forming at the leading edge of the stator teeth (also shown in Figure 5.35).

5.2.4 Stator

In the stator region, fluid discharging from the rotor - with high circumferential velocity - is abruptly turned by the upstream face of the stator teeth, to emerge radially (Figure 5.36). A fast stream follows the leading edge of the stator and this

is accompanied by a region of recirculation.

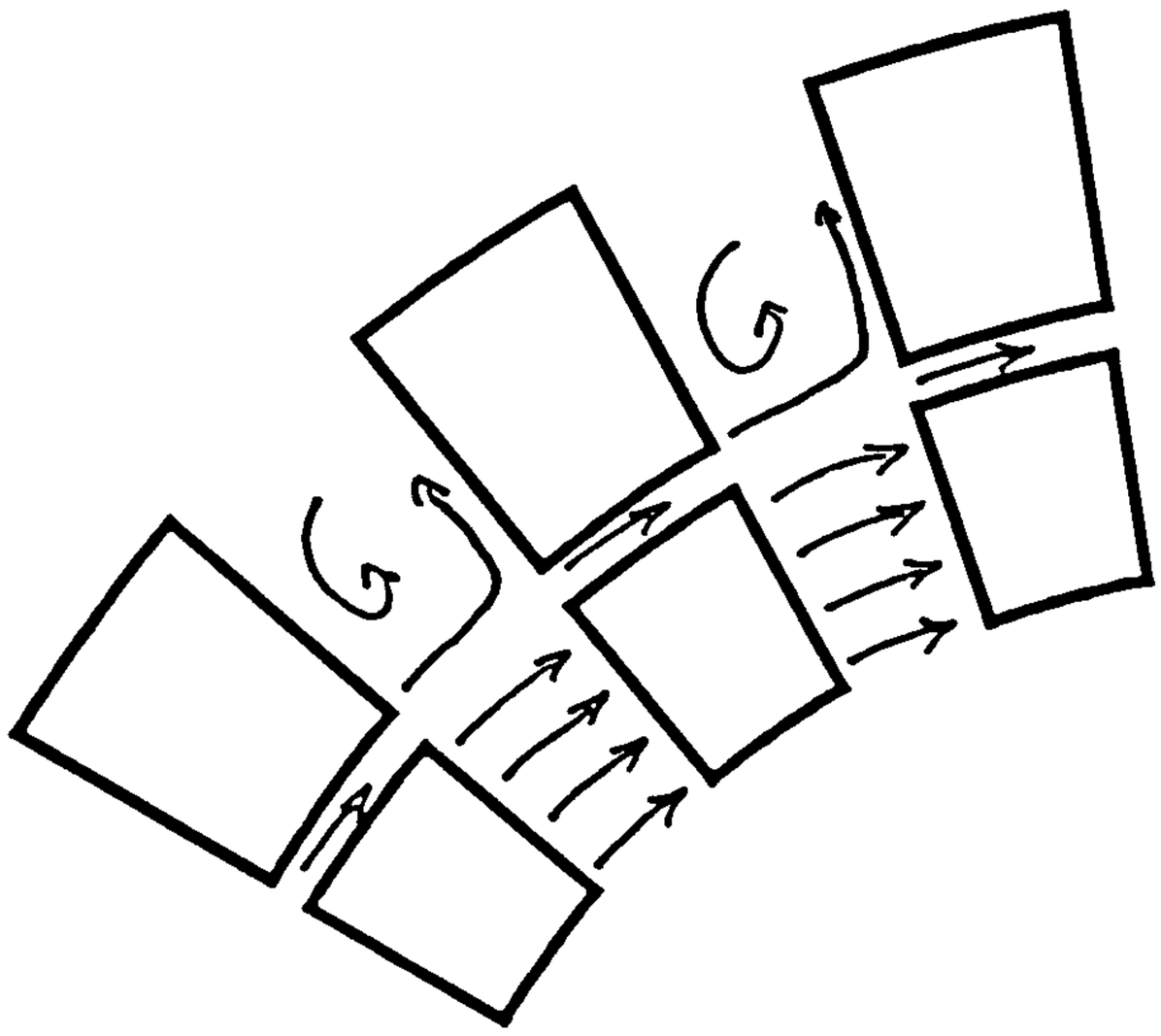

Figure 5.36 Flow pattern through the stator

In this region, the tangential kinetic energy given to the fluid by the rotor is transformed to pumping power, skin friction losses and turbulent losses. The magnitude and distribution of the losses cannot be determined by flow visualisation, but it is likely that the point where the abrupt turn in the flow takes place (the upstream face of the stator) is where these losses are greatest.

5.2.5 Volute

In general, the flow in the volute was dis-ordered and the general features of this flow are described here and shown in Figure 3.37. Behind the rotor, recirculating flows were observed (Detail A) and any air in the volute tended to accumulate around the seal spring on the rotor shaft.

The flow discharged from the stator radially (Detail B), as was also shown in Figure 3.36. The outlet pipe contained swirling flow, as the liquid passes from the large volute, as shown by Detail C.

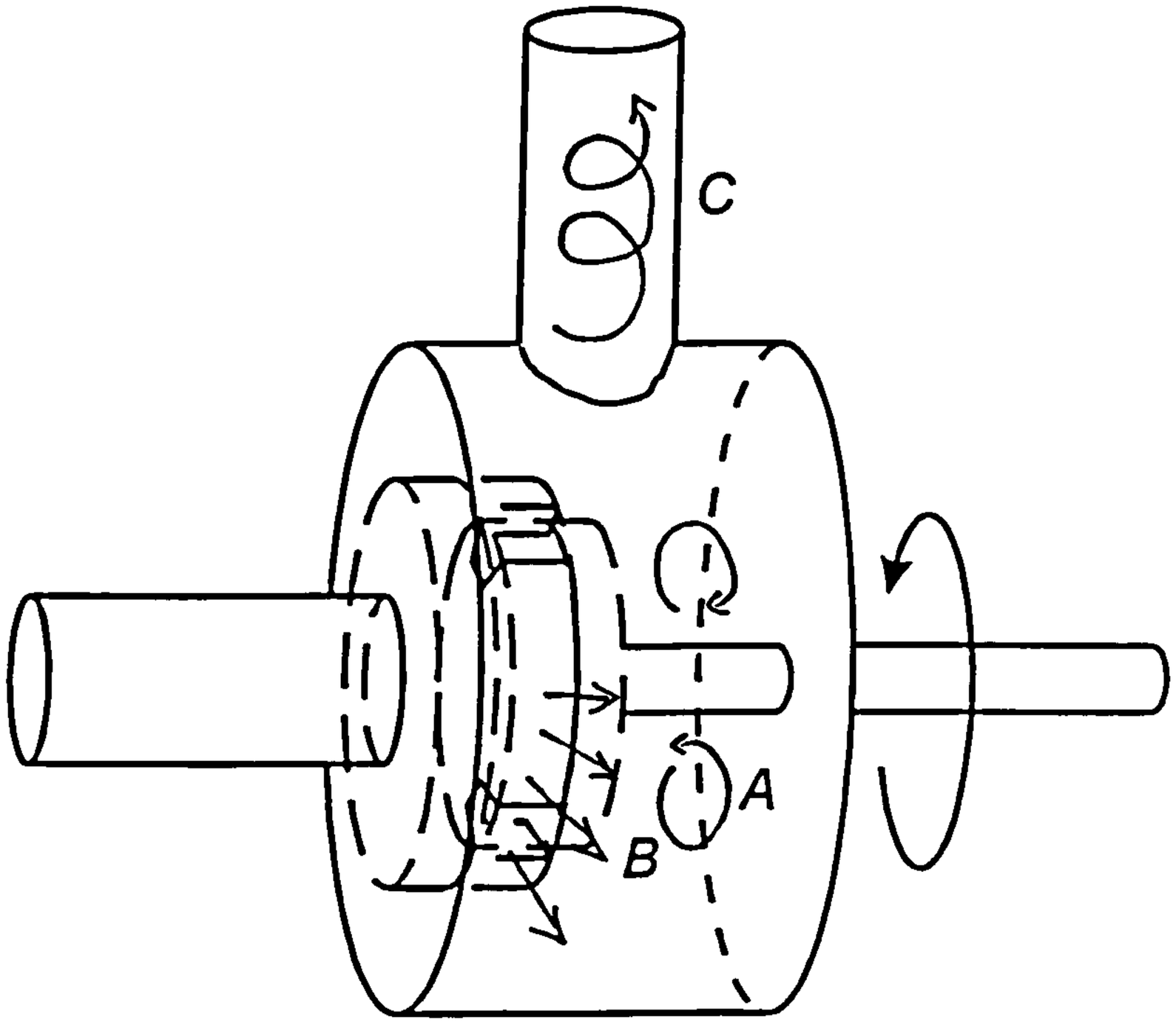

Figure 5.37 Flow pattern in the volute

It is likely that the overall residence time distribution characteristics of the mixer were determined by the flows in the volute (since the volume of the volute is much greater than the volume of the inlet and outlet pipes and rotor-stator regions). These features were observed for all rotor-stator combinations, but no change with operating condition (either N or Q) could be detected.

5.2.6 Computational fluid dynamics

During the period of this work, developments in hardware and software made computational fluid dynamics (CFD) an increasingly useful tool for the analysis of

fluid engineering problems. A CFD study was used, towards the end of the work, to check the findings from the flow visualisation. CFD produces a great deal of information about a particular flow situation, for example the velocity and pressure fields as well as the distribution and intensity of turbulence, but requires careful validation before results can be used with the fullest confidence. Such validation was not undertaken during this work, but a qualitative comparison between visualisation and CFD results was performed.

The modelling of turbulence phenomena is difficult and models must be used to represent the effect of turbulence on a flow. For this study, the standard k-ε turbulence model was used (Jones and Launder, 1972). The quantity ε produced by this model is the turbulent energy dissipation rate, the same quantity discussed in this thesis when discussing micro-mixing and the E-model. However, ε is modelled as being related to mean velocity gradients, an assumption that does not take into account the fine scale structure of turbulence, but one which is necessary because of the still limited power of computers. It has been shown that some of the assumptions behind this model (e.g. isotropic turbulence) can lead to inaccuracy when modelling swirling flows (Hannon, 1992). More elaborate turbulence models, for example differential stress models that model Reynolds stresses explicitly, have been shown to produce more accurate solutions (Esfandiari, 1996). However, this CFD analysis was intended as a preliminary study and therefore the k-ε model was used for its ease of implementation and greater speed than, e.g., the Reynolds stress model.

Sliding mesh techniques are now available on commercially available codes (including Harwell Flow3D which was used for this work), allowing a fixed mesh to be used for the stator with a rotating mesh for the rotor. Little progress was made in this study using these techniques, so the rotor was not modelled explicitly.

Instead, the discharge from the rotor was estimated and used as a boundary condition for a simulation of the flow through the stator. Flow visualisation of the flows in the rotor showed that the fluid followed the rotor teeth (i.e the tangential velocity of the rotor discharge is equal to the tip speed) and the radial velocity of fluid in the rotor discharge will be ~v_{RADIAL}. It was further assumed that the discharge of the rotor was constant (i.e. the possible effect of pulsation caused by rotor-stator interaction was not modelled). Given that no radial pulsation could be detected with flow visualisation this is a valid assumption.

The rotor-stator combinations **r/18/50/119.6 & s/18/50/123.8** and **r/18/50/123.34 & s/18/50/123.8** were modelled. The simulations were conducted using the physical properties of water at 25℃ and it was assumed that the flow was incompressible and isothermal. The inlet boundary condition was a nominal radial velocity of 0.5 m s^{-1} and the tangential velocity was 19 m.s^{-1}. These values represented a shaft speed of 3000 rpm and a flow rate of 1.5 l.s^{-1}. The flow geometry was set up using a 2-dimensional grid in cylindrical co-ordinates (16,416 cells) (Figure 5.38). Hybrid differencing was used (AEA, 1995). Approximately 8000 iterations were required to give a converged solution for the simulation with the 2.1 mm shear gap but the solution for the 0.23 mm case did not converge fully.

Figures 5.39 and 5.40 show velocity vectors for the 2.1 and 0.23 mm shear gaps. The vectors in Figure 5.39 are coloured to show local values of ε and the vectors in Figure 5.40 are coloured to show the local fluid speed. Qualitatively, these flow patterns are similar to those observed during visualisation. The fluid discharging from the rotor impinges on to the upstream face of the stator tooth and is turned abruptly to follow the upstream face of the stator tooth. Finally, it discharges radially into the volute. A similar recirculation to that visualised (Figure 5.34) is apparent in both of the CFD plots. This will bring some reaction products back into

the reaction zone, possibly increasing the amount of by-products formed.

The results were processed to give values of ε, the turbulent energy dissipation rate. The highest value for ε for the 2.1 mm shear gap is approximately 45,000 $W.kg^{-1}$ and while this is much higher than the mean value for ε, estimated using the overall power balance measurements, it is a reasonable figure given the expected inhomogeneity of the distribution of ε. In stirred tanks, local values of ε that were as much as twenty times greater than the tank average were measured by Wu and Patterson (1989).

However, in the simulation of the 0.23 mm shear gap unit, a maximum turbulent energy dissipation rate of approximately 10×10^{6} $W.kg^{-1}$ was modelled. This is a very high value indeed and, while there may be much higher local values with the thinner shear gap, it is possible that the values produced by the simulation are a consequence of the non-convergence of the solution. In both cases, these values occur over a comparatively small volume and this may have important implications when trying to make use of this energy dissipation for mixing. According to the CFD results, the highest energy dissipation rates occur (for both shear gap thicknesses) as the fluid expands from the shear gap into the stator tooth slot. It was suggested in Section 5.2.4 that ε will be highest on the upstream edge of the stator teeth. It is possible that the deficiencies of the standard k-ε turbulence models cause this discrepancy between the suggestion made about energy dissipation from flow visualisation and the CFD results. Further work, with different turbulence models, is needed to investigate this. In addition, closer examination of the flow (possibly using laser doppler anemometry) would be necessary to map the distribution of turbulent energy dissipation.

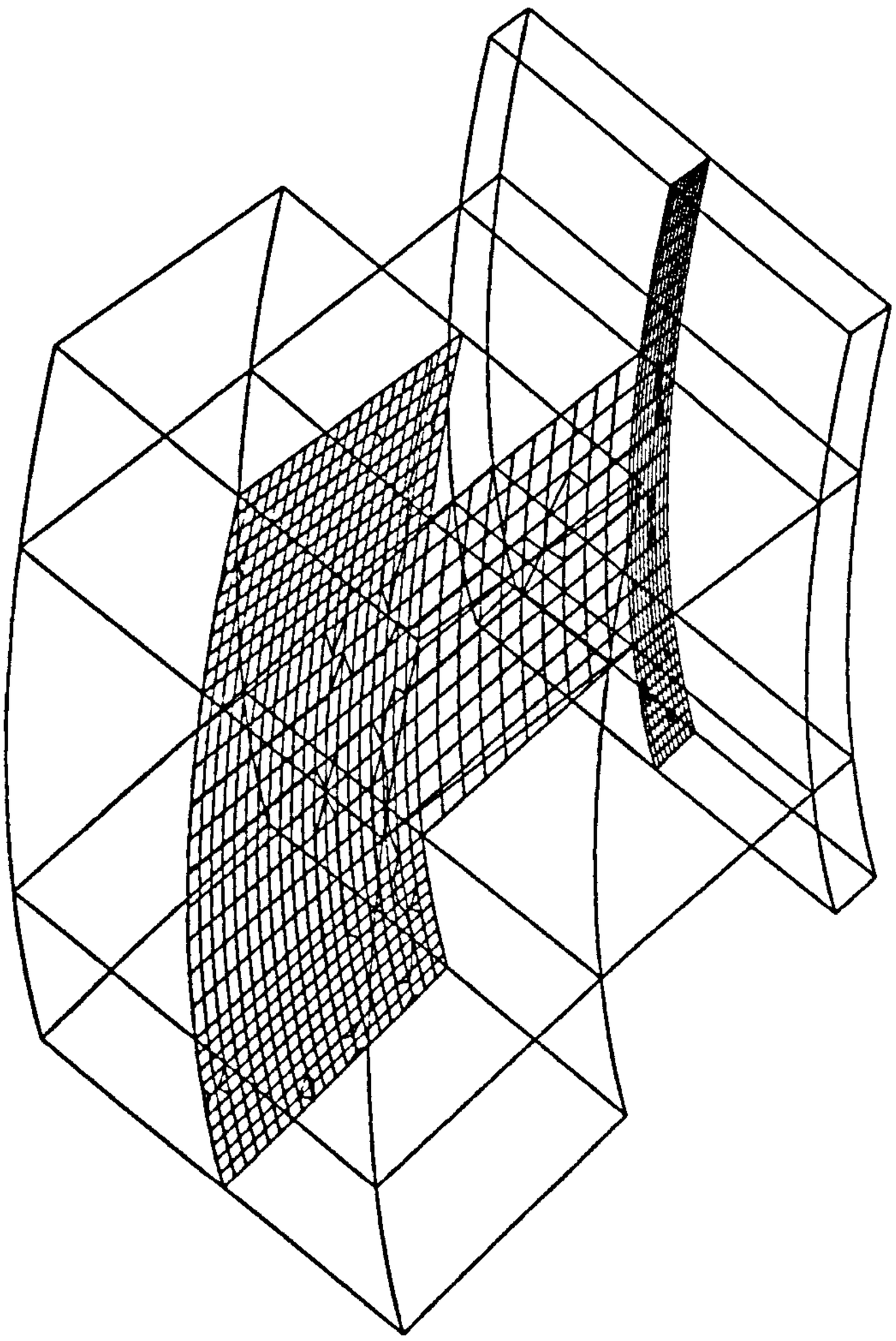

Figure 5.38. The computational grid used

There would appear to be a great deal of work that could be done in the optimisation of rotor-stator design using CFD. There is need of substantial validation before the results obtained using CFD can be used with confidence, but the initial results presented here and elsewhere (Ruszkowski, 1995 and Le Clair, 1995) are promising. Further developments in CFD technology, including sliding grids and improved turbulence models, should increase the applicability of CFD to this field.

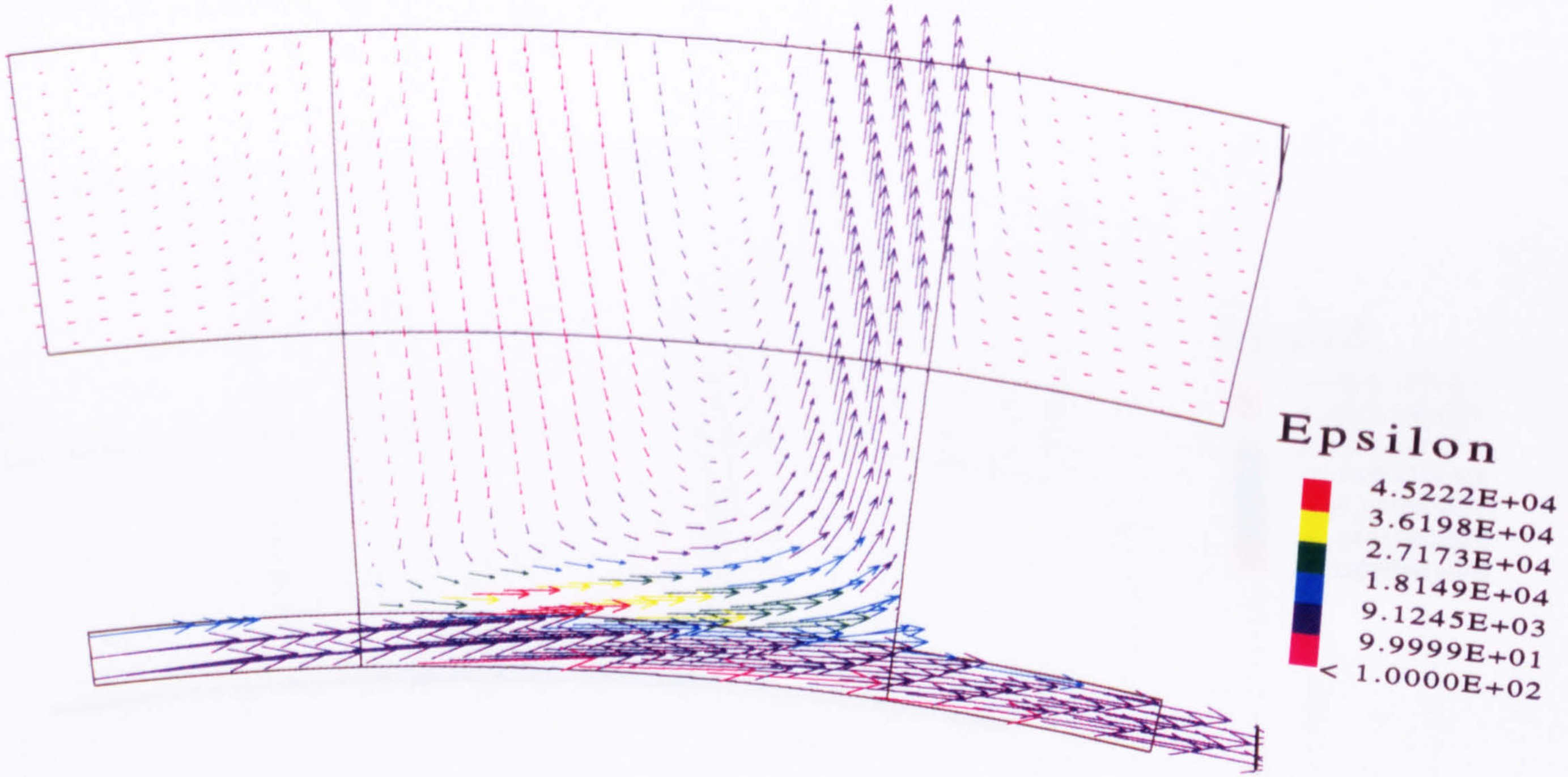

Figure 5.39 CFD results for the 2.1 mm shear gap

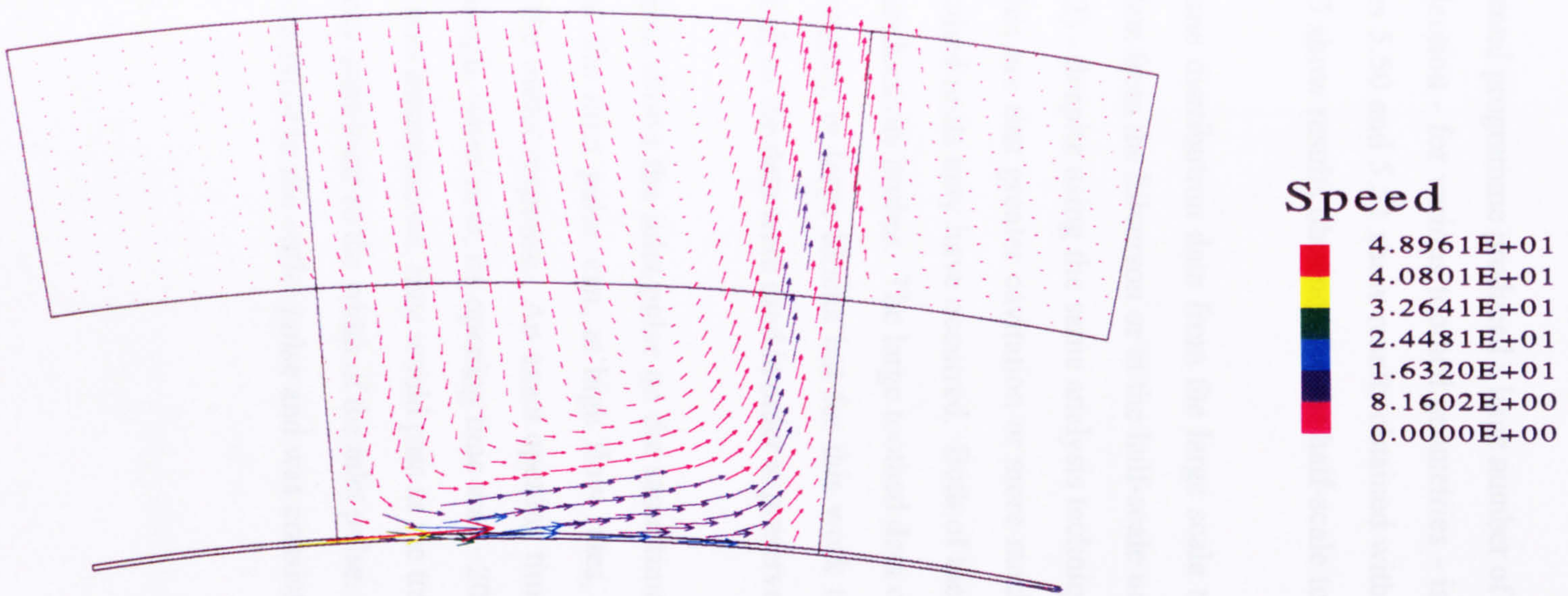

Figure 5.40 CFD results for the 0.23 mm shear gap

5.3 Residence time distribution

The experimental programme produced a large number of residence time distribution curves, a selection - for various toothed geometries - is shown in Figures 5.41 to 5.49. Figures 5.50 and 5.51 show results obtained with the Silverson and Figures 5.52 and 5.53 show results obtained for the half-scale toothed.

Residence time distribution data from the large scale toothed units tended to be noisier than data from the Silverson or at the half-scale unit (compare Figures 5.41, 5.50 and 5.52) - despite using the same analysis techniques for all units. Possible reasons for this are that greater cavitation or more mechanical vibration with the large scale toothed units may have occurred. Both of these phenomena could have affected the conductivity probes. The large toothed data could have been smoothed by block averaging in large blocks but for this work the same data preparation techniques for all of the data were used in order to preserve the shapes of the curves.

Figure 5.41 also shows the inlet pulse on the same time axis as the outlet curve, indicating that the inlet pulse can, at high flow rates, have a significant width compared to the outlet response. An exact opening time for the injector was not measured although, when new, its opening time was ~20 ms (Hearn, 1992). Even if the opening was instantaneous, time would pass as the tracer was flushed from the unit and this may contribute to the width of the inlet pulse. However, the inlet pulse was narrow compared to the outlet pulse and was consistent from test to test.

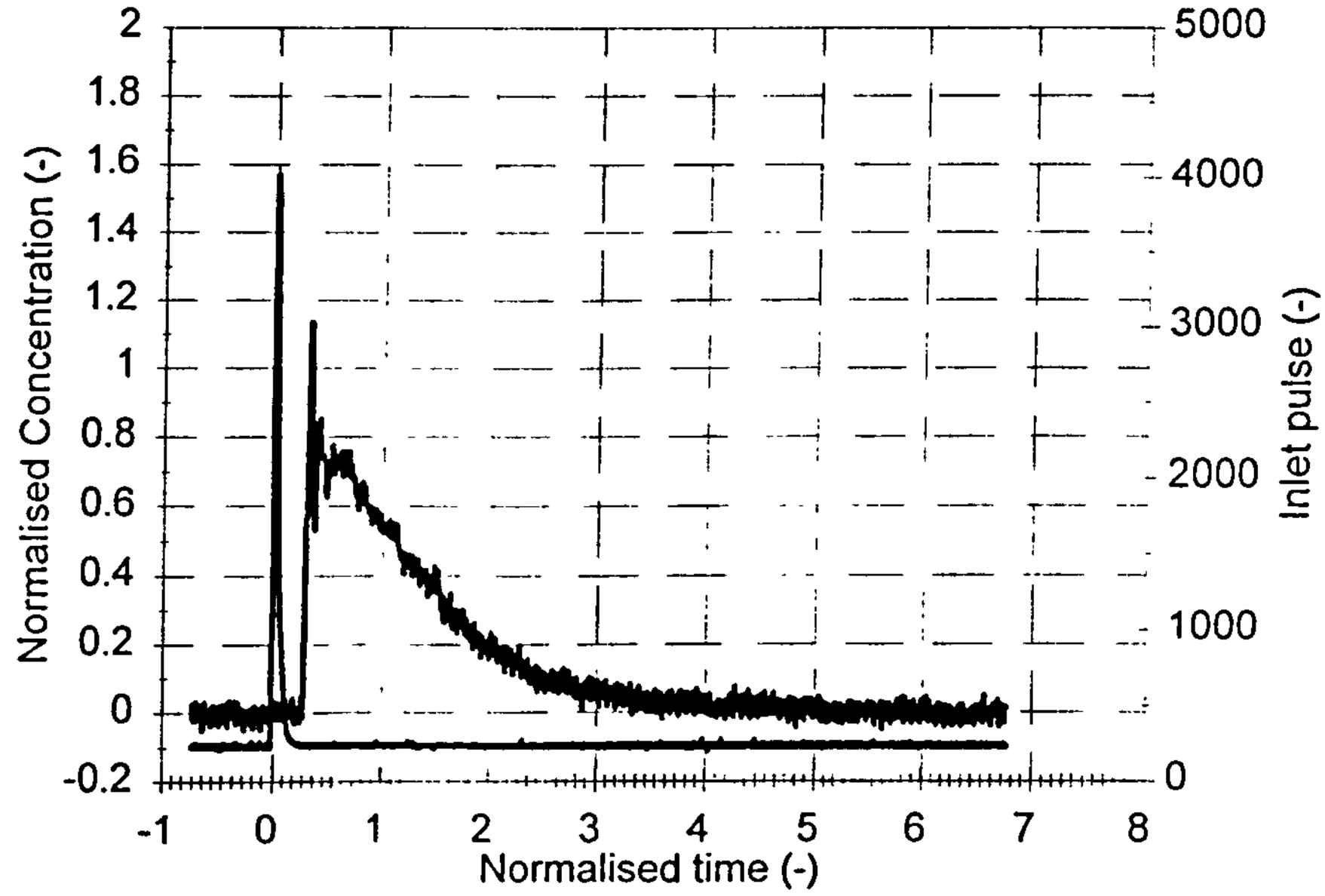

Figure 5.41 Residence time distribution (**r/18/50/123.34 & s/18/33/123.8**) 2.0 $l.s^{-1}$ and 3000 rpm

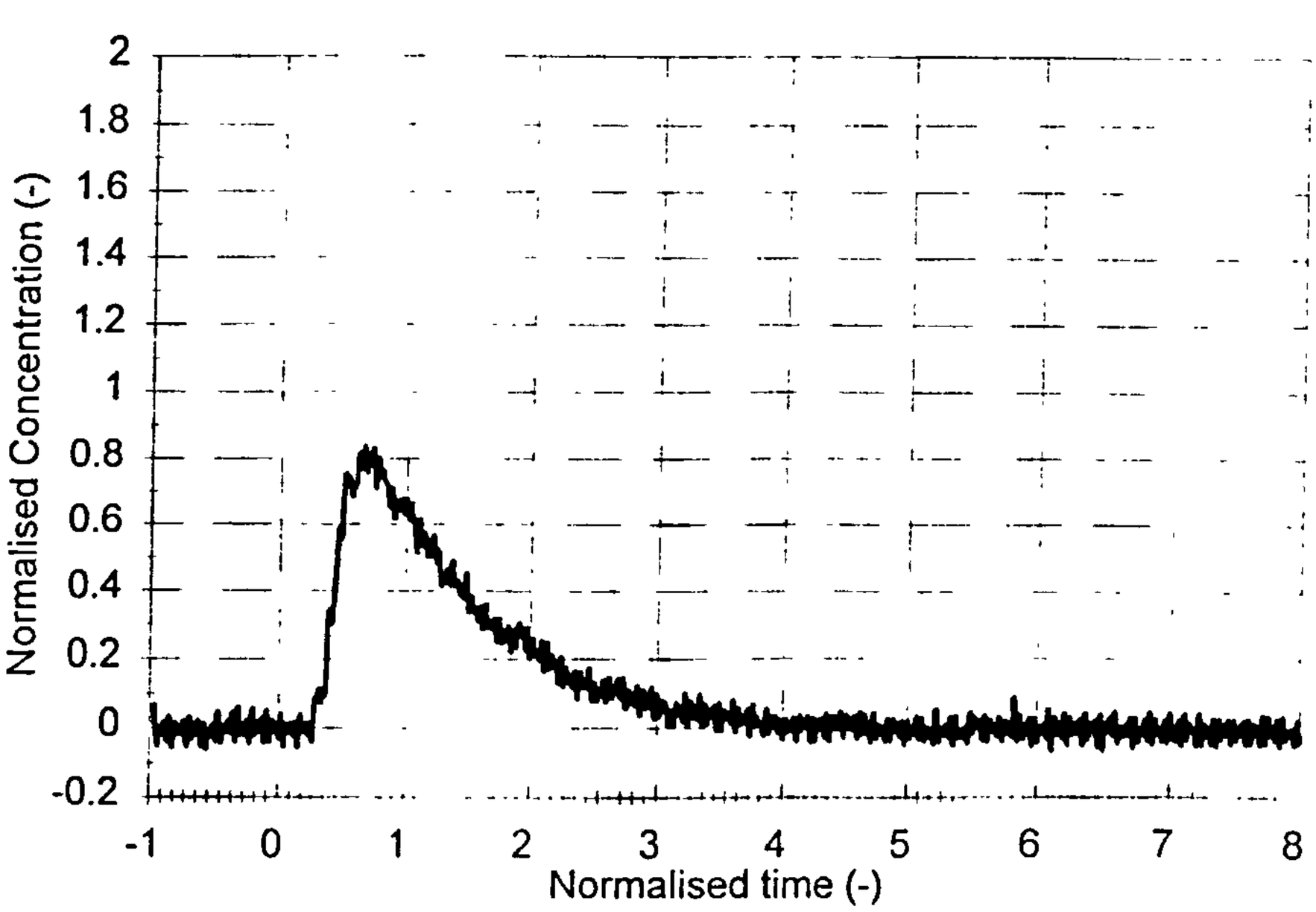

Figure 5.42 Residence time distribution (**r/18/50/123.34 & s/18/33/123.8**) 3.0 $l.s^{-1}$ and 3000 rpm

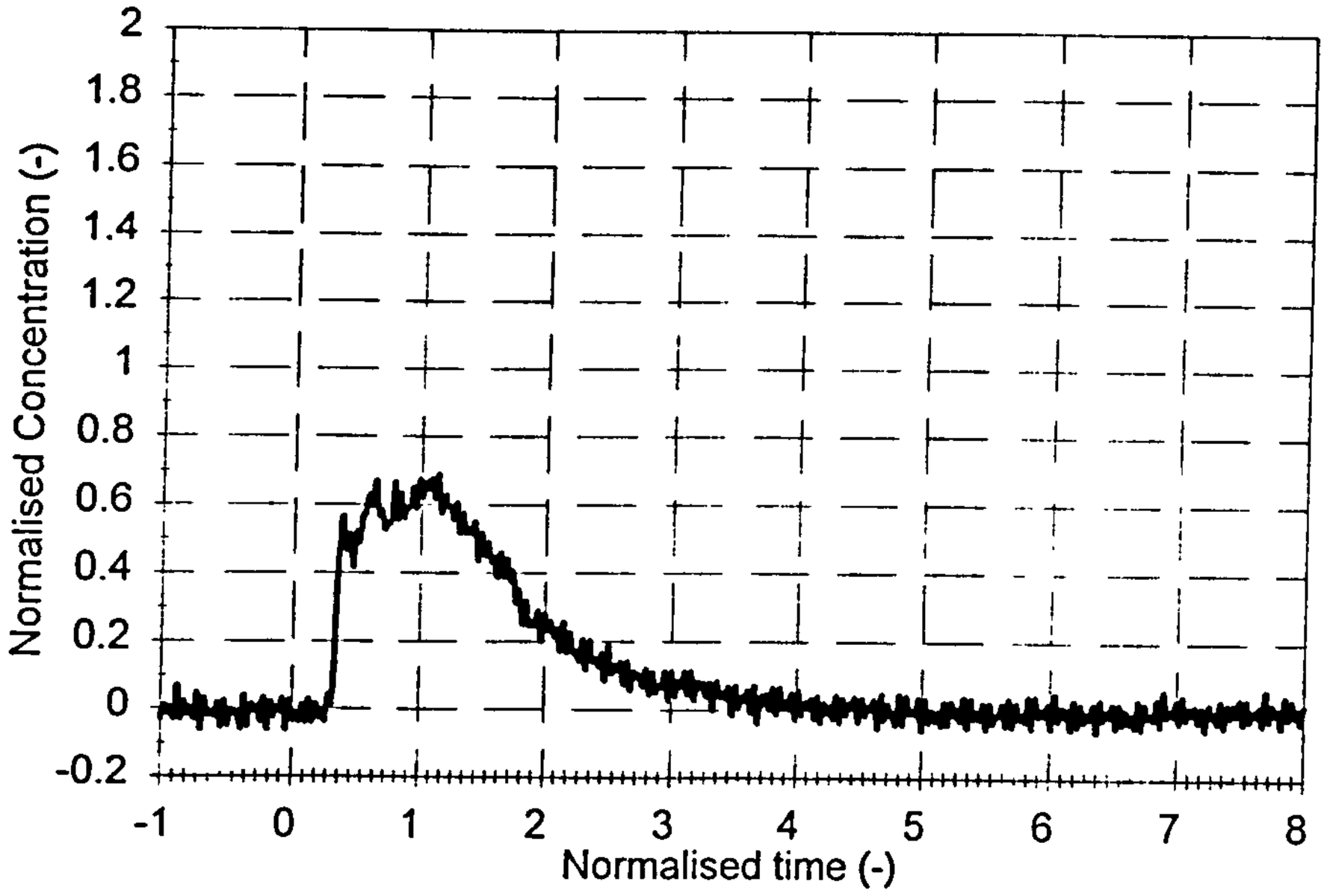

Figure 5.43 Residence time distribution (**r/18/50/123.34 & s/18/33/123.8**) 4.0 $l.s^{-1}$ and 3000 rpm

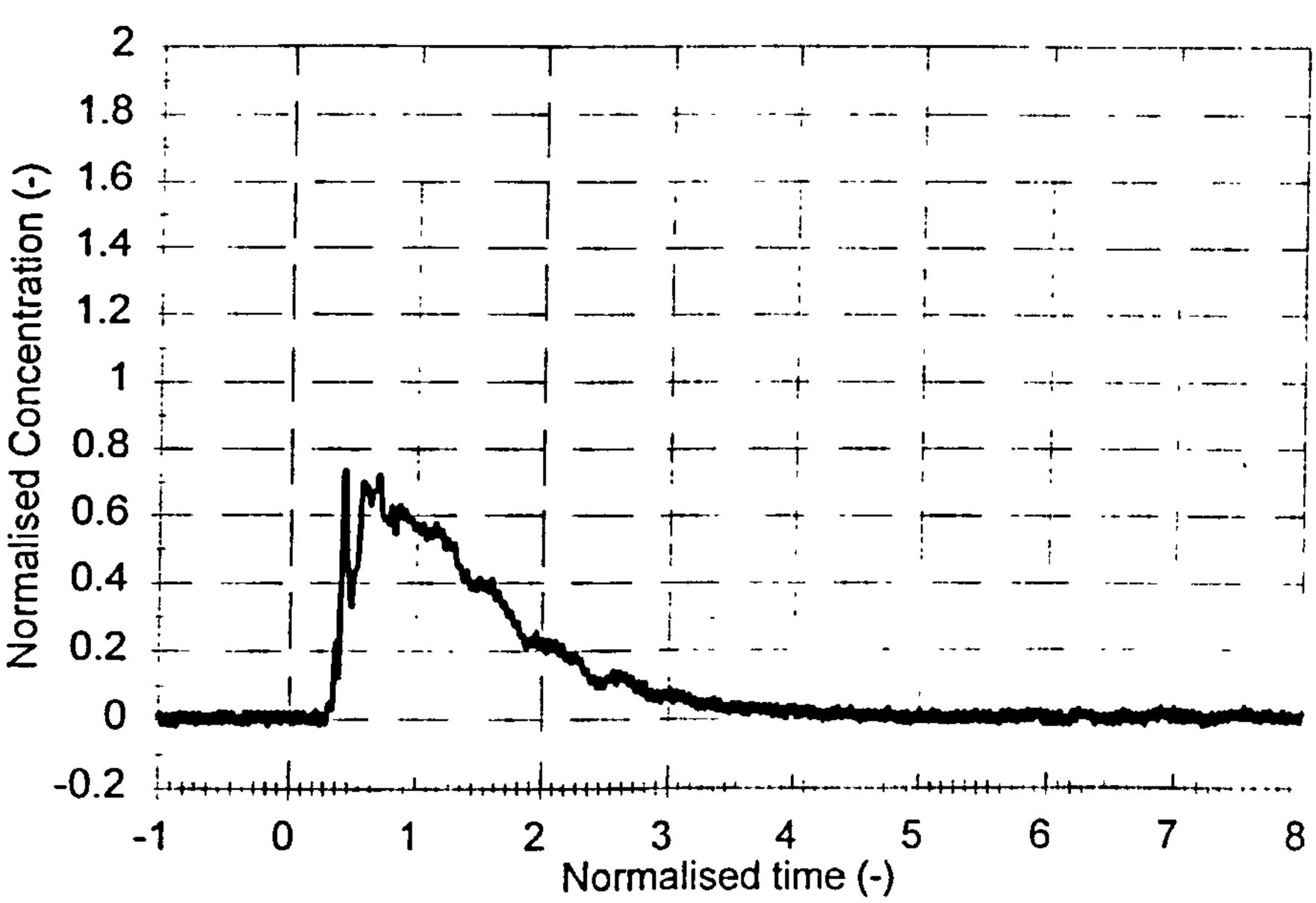

Figure 5.44 Residence time distribution (**r/18/50/123.34 & s/18/33/123.8**) 3.0 $l.s^{-1}$ and 1000 rpm

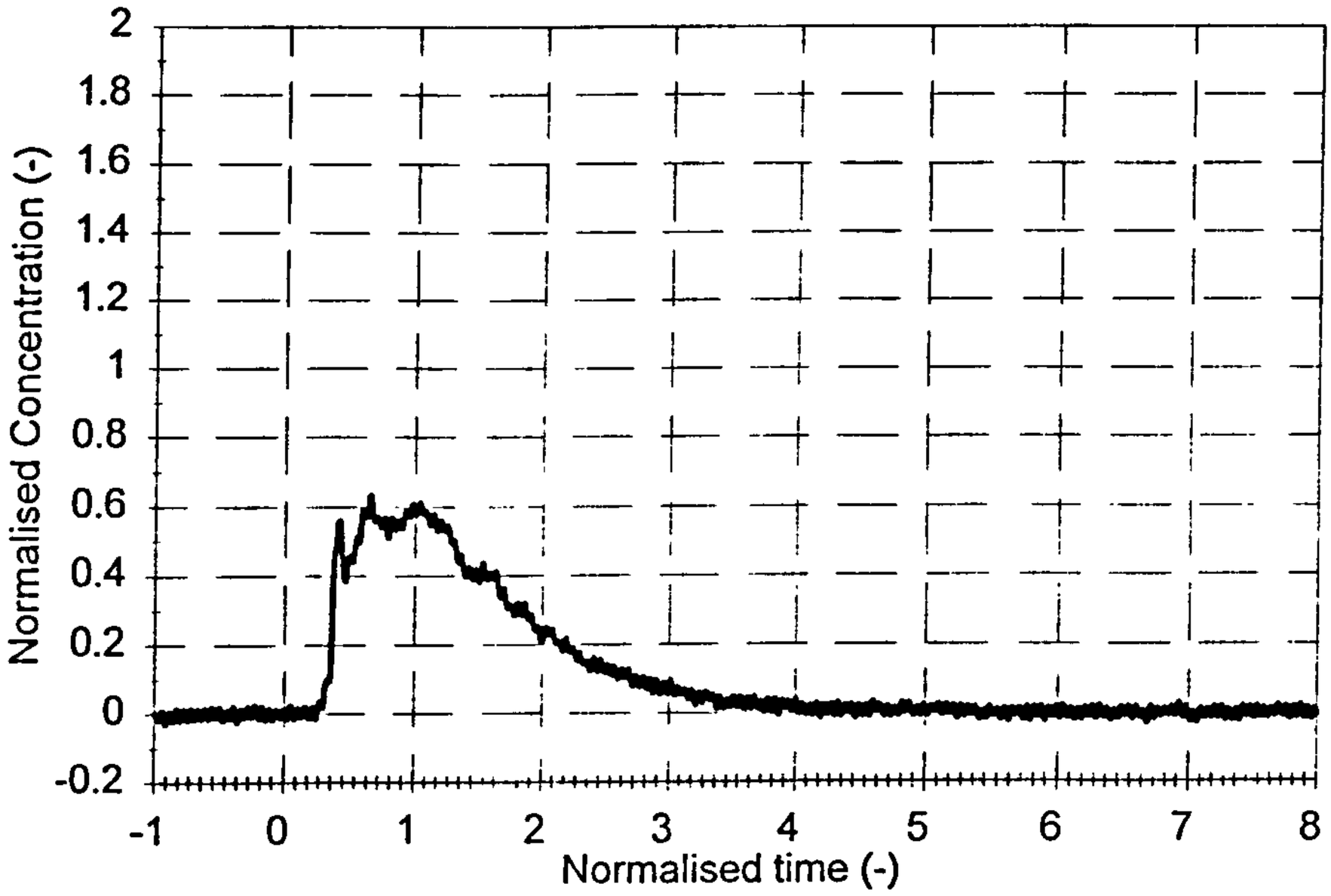

Figure 5.45 Residence time distribution (**r/18/50/123.34 & s/18/33/123.8**) 3.0 $l.s^{-1}$ and 2000 rpm

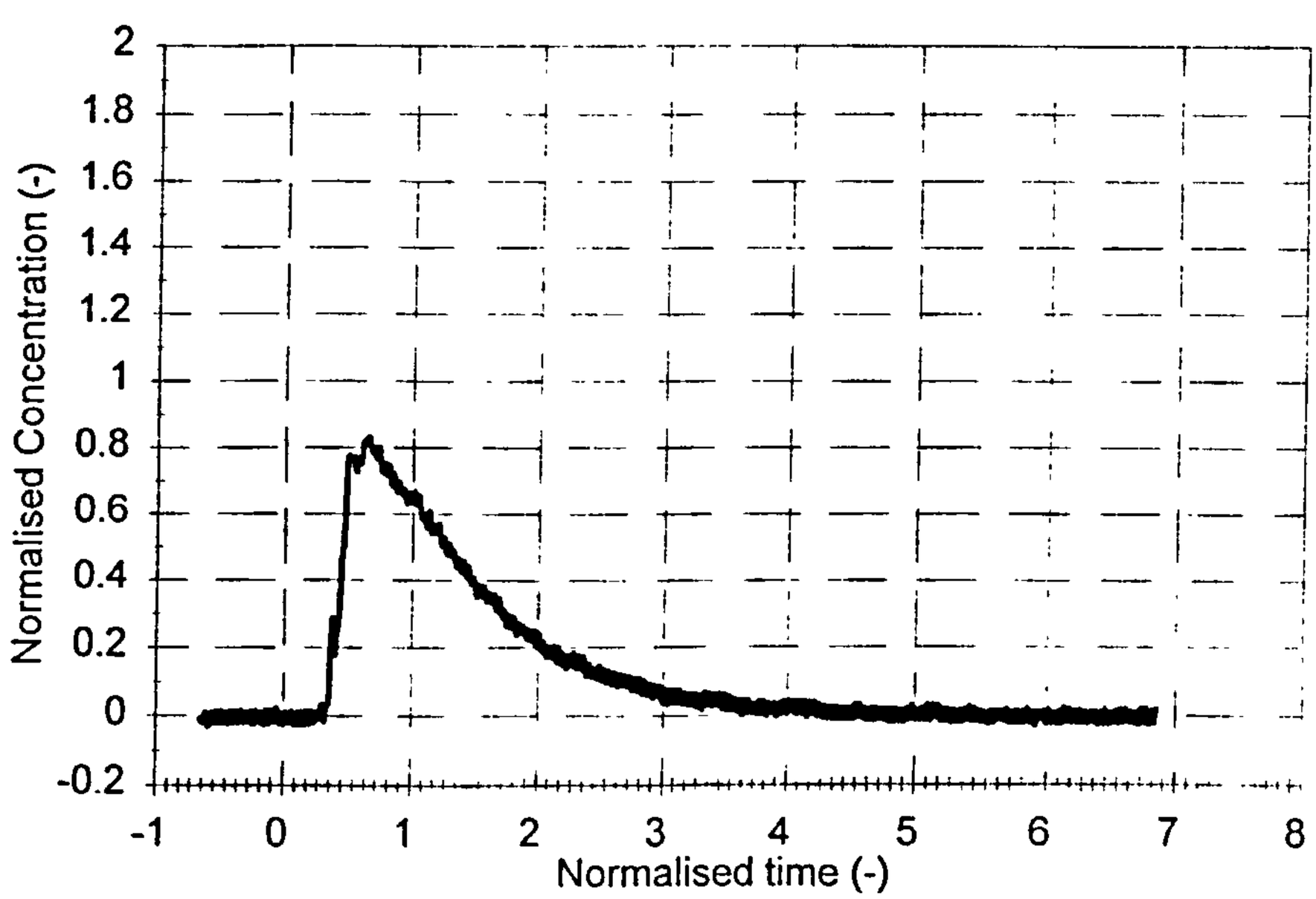

Figure 5.46 Residence time distribution (**r/12/50/121.45 & s/18/33/123.8**) 2.0 $l.s^{-1}$ and 3000 rpm

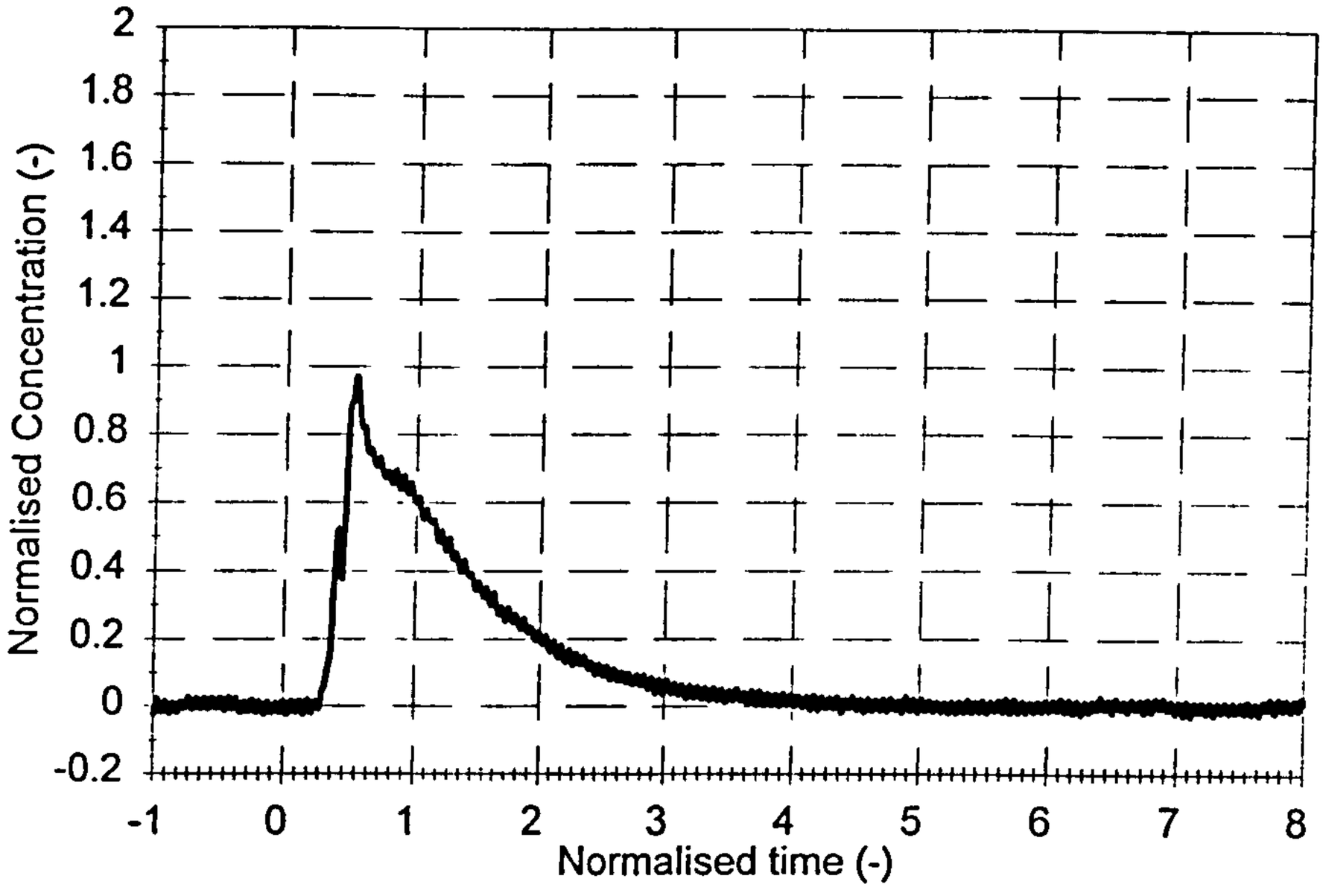

Figure 5.47 Residence time distribution (**r/12/50/121.45 & s/18/33/123.8**) 3.0 $l.s^{-1}$ and 3000 rpm

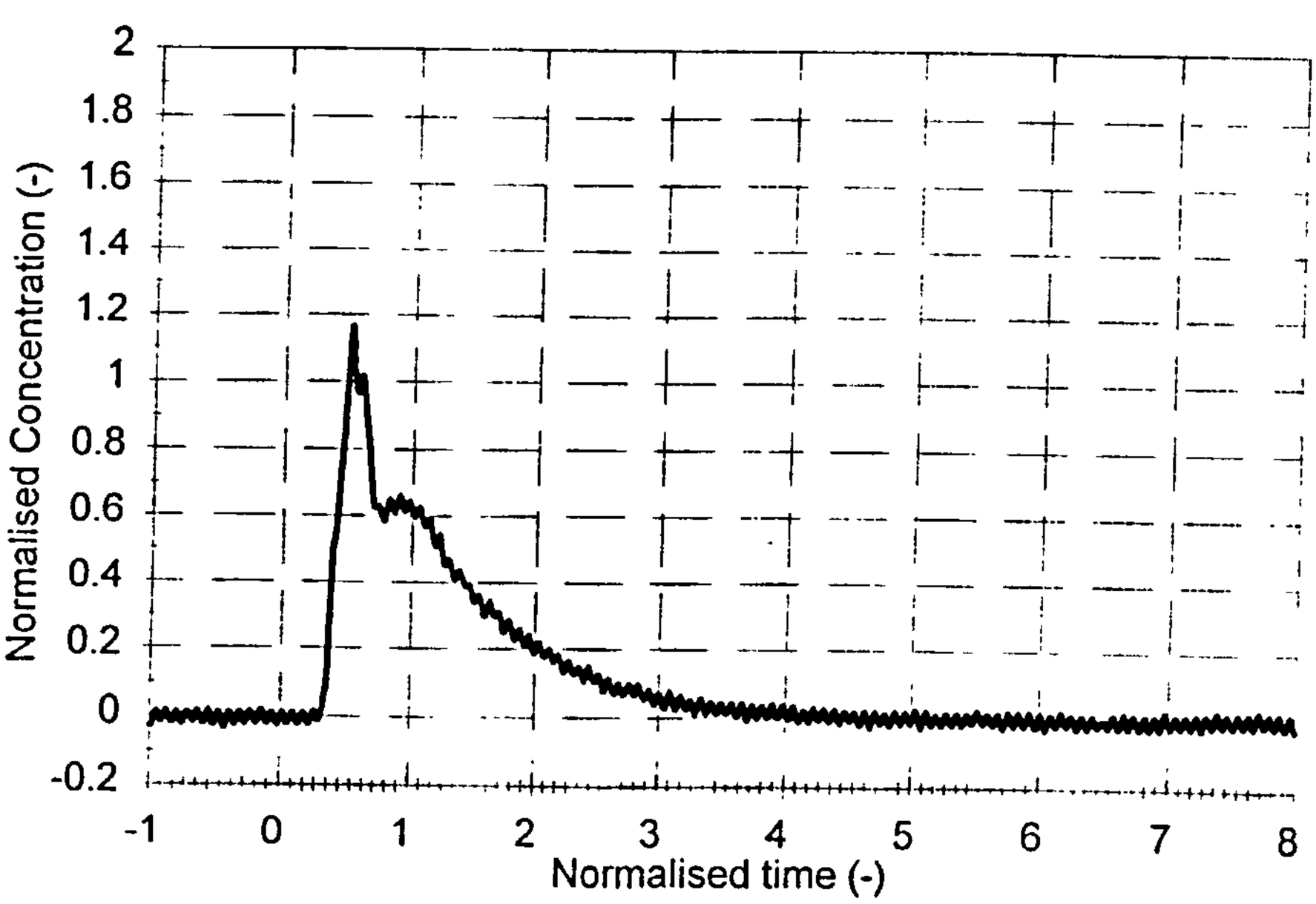

Figure 5.48 Residence time distribution (**r/12/50/121.45 & s/18/33/123.8**) 4.0 $l.s^{-1}$ and 3000 rpm

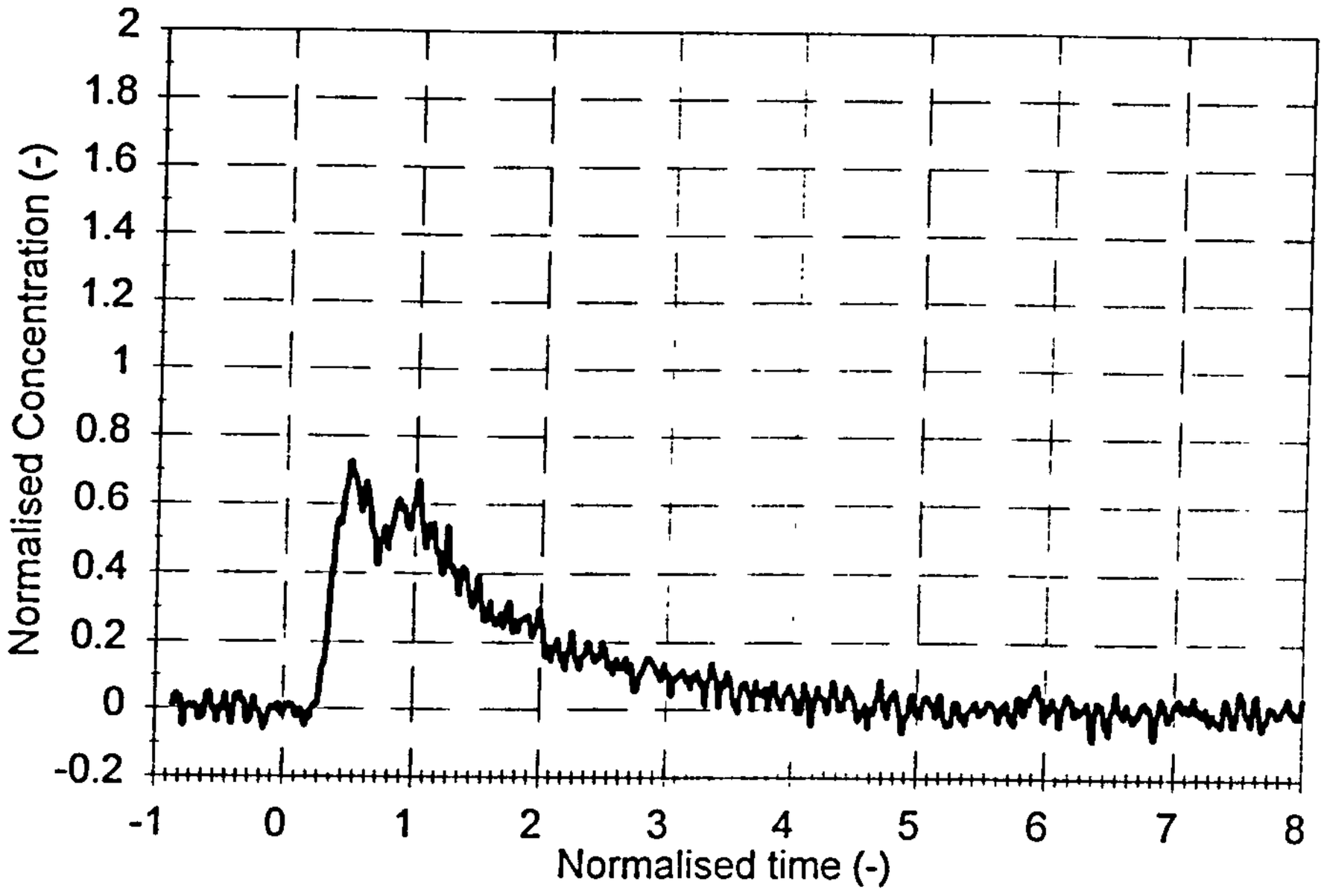

Figure 5.49 Residence time distribution (r/18/50/123.34 & s/19/50/123.8) 3.0 $l.s^{-1}$ and 3000 rpm

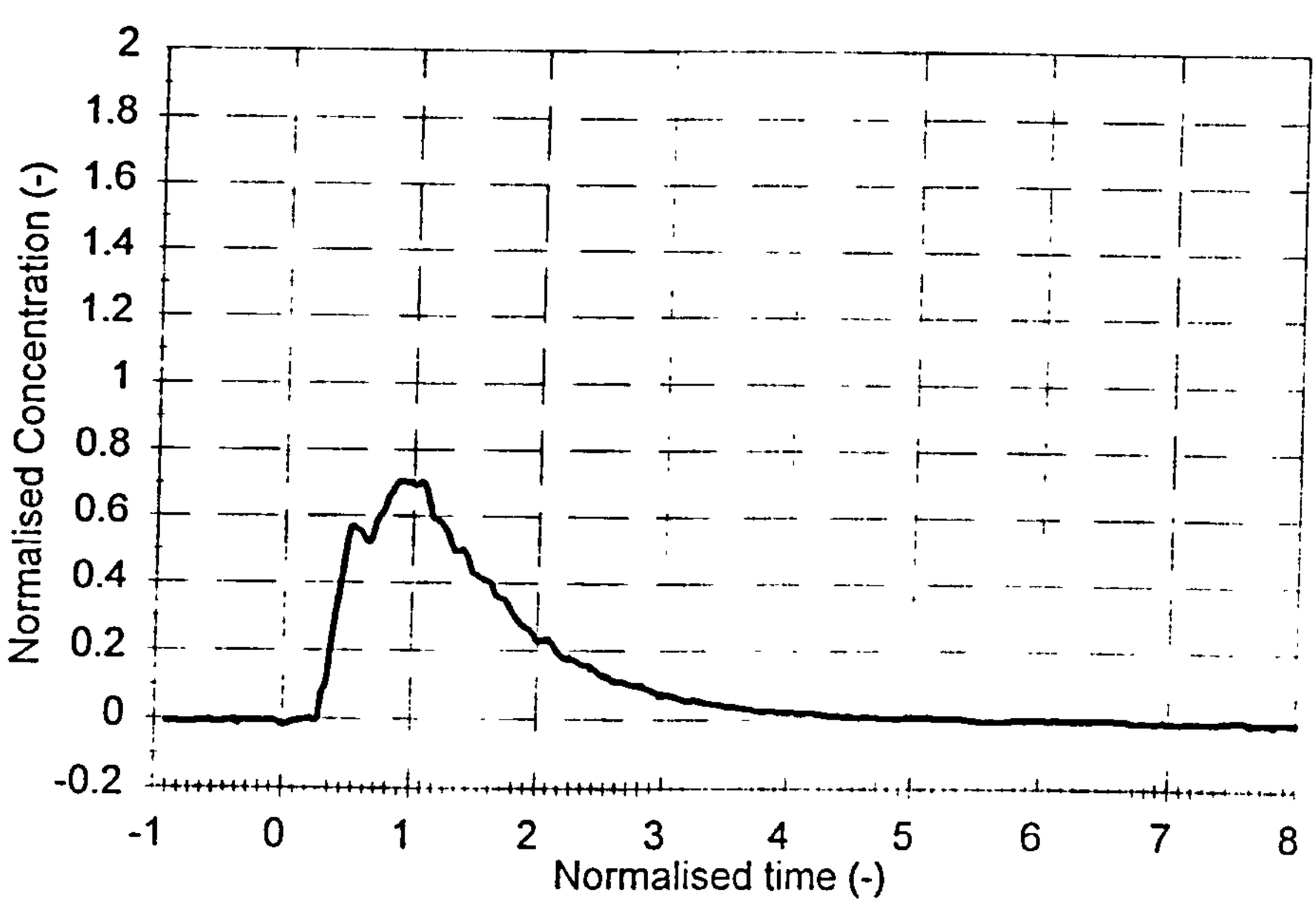

Figure 5.50 Residence time distribution (Silverson) 3.0 $l.s^{-1}$ and 3000 rpm

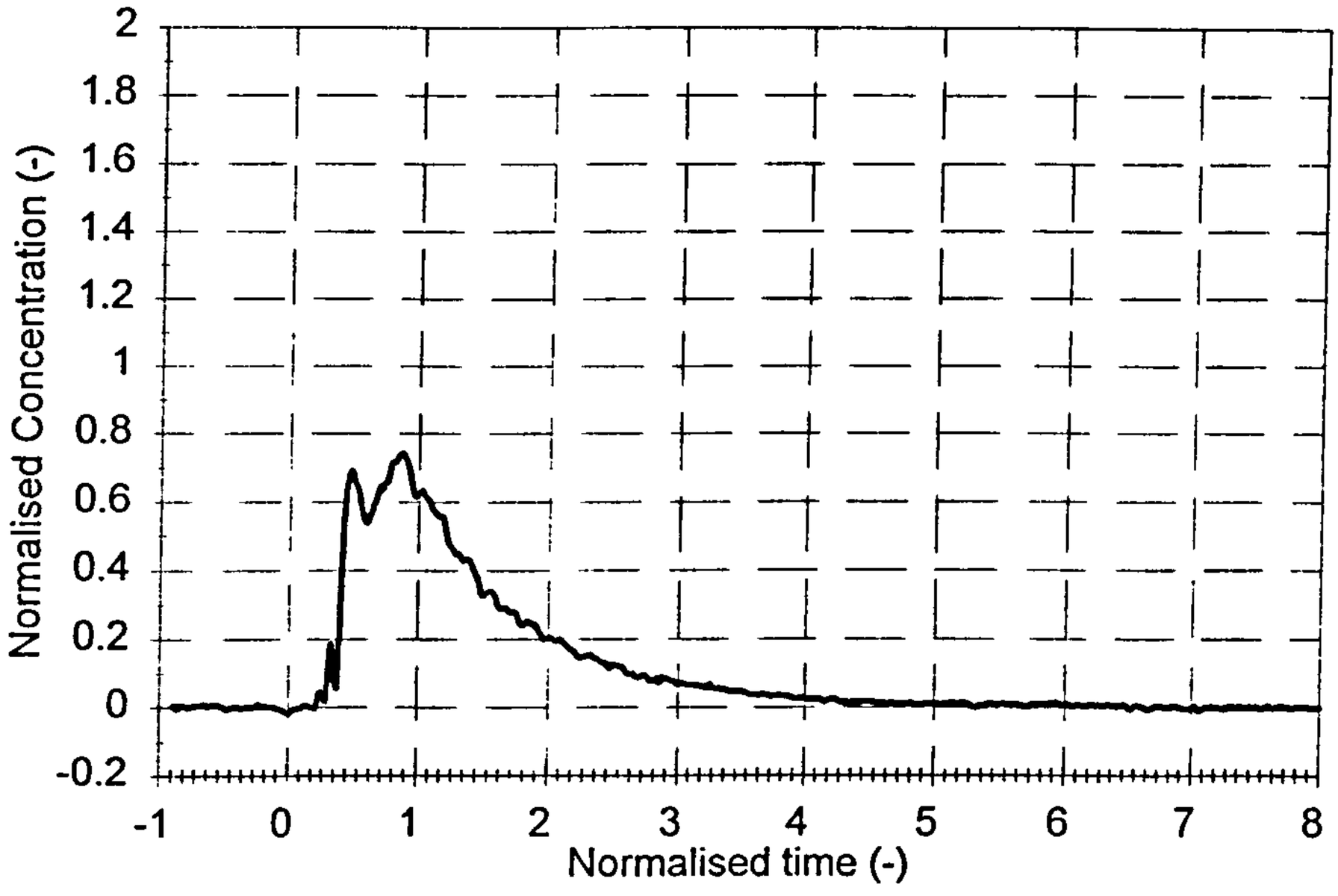

Figure 5.51 Residence time distribution (Silverson) 2.0 $l.s^{-1}$ and 2000 rpm

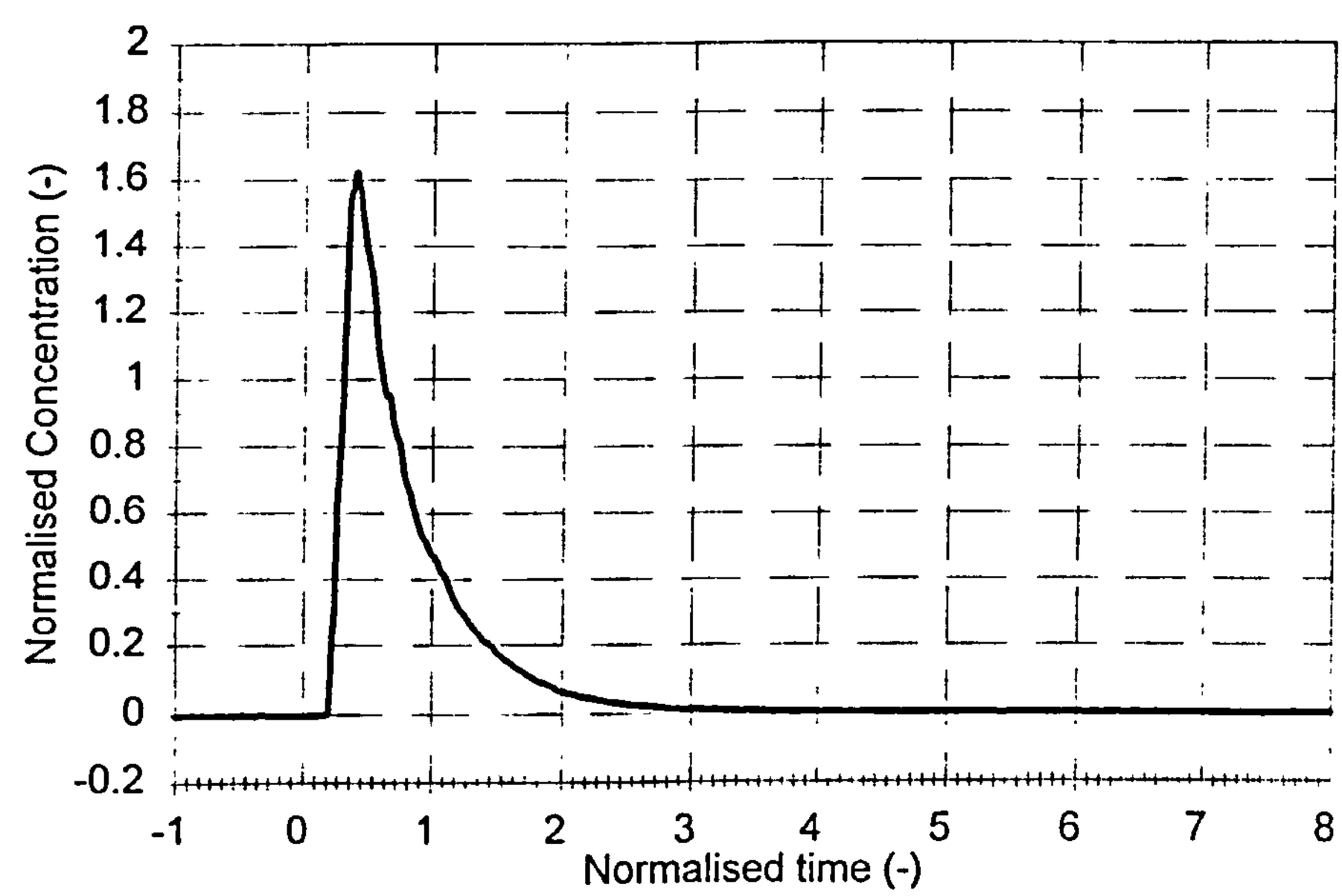

Figure 5.52 Residence time distribution (half-scale unit) 0.4 $l.s^{-1}$ and 3500 rpm

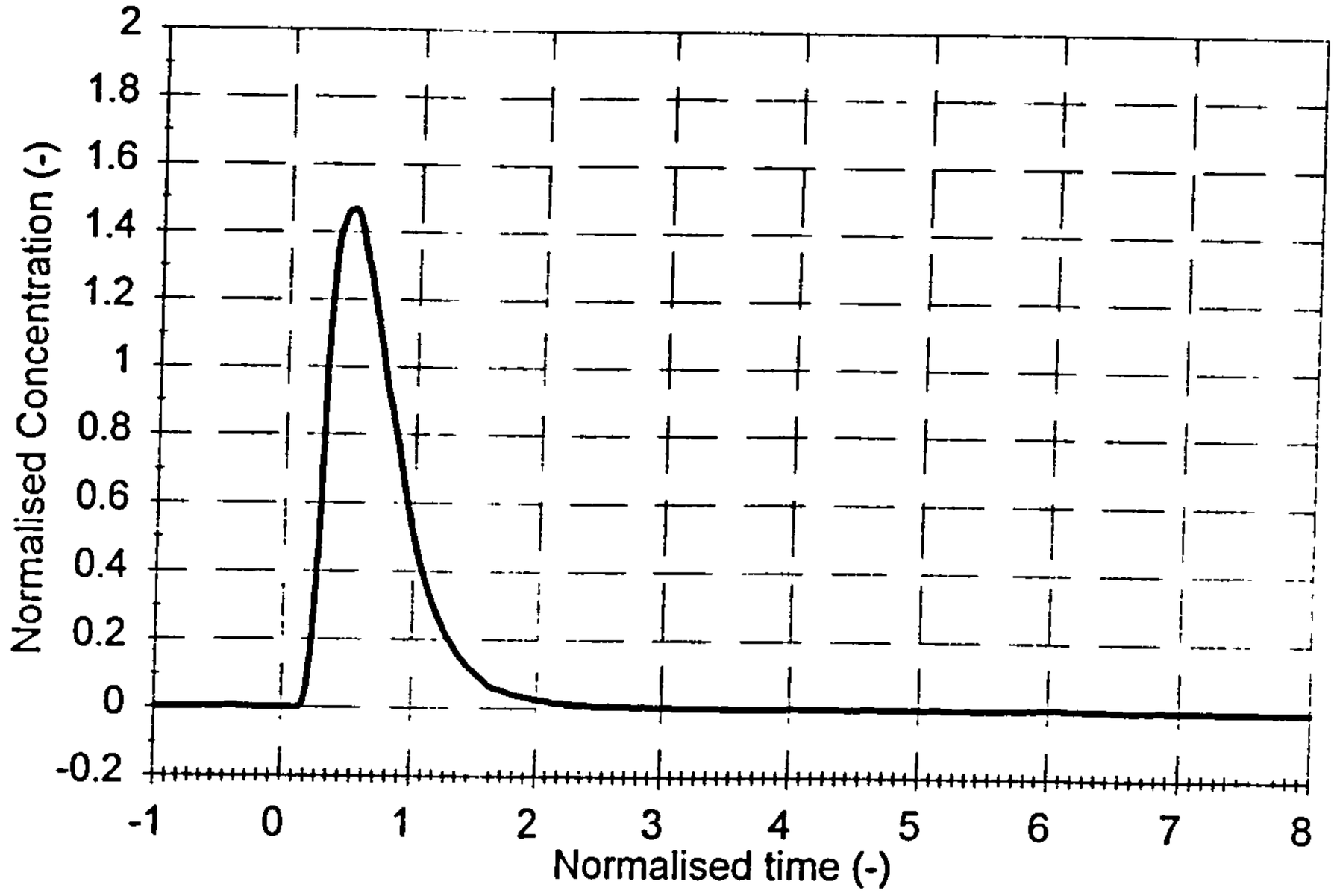

Figure 5.53 Residence time distribution (half-scale unit) 3.0 $l.s^{-1}$ and 3500 rpm

With the exception of Figure 5.53, which was taken for a flow rate much greater than the best efficiency flow rate (Section 5.2), all of the curves have similar characteristics - delay followed by a rapid rise, a peak at about 0.5 to 0.6 of a mean residence time and tailing up to about 4 or 5 residence times. The design of the toothed rotor-stator units had very little effect on the RTD shape, with the tails of the residence time distributions for all combinations of geometry having similar characteristics.

Some of the curves produced with the toothed units showed a cropped peak, e.g. Figures 5.43 and 5.45, while others had a short peak before the main peak (e.g. Figure 5.48) or a double peak (e.g. Figure 5.49). These changes in the characteristic of the peak were not reproducible and did not depend upon the geometry of the unit tested. These changes in the shape of the peak may indicate short circuiting through the volute (the early peak) or a slow moving recirculation in the volute (the double peak).

Further, the residence time distribution for the Silverson (Figures 5.50 and 4.51) is very similar to that for the toothed designs, albeit smoother. This adds to the suggestion given in Section 5.2 that the overall shape of the RTD is determined by the flow through the volute.

There was very little change in RTD with operating condition (e.g. Q, Figures 5.41 to 5.43 or N, Figures 5.42, 5.44 and 5.45). This, once again appears to support the finding that the RTD is determined by the flow in the volute.

However, there are some differences in the RTDs produced at the large scale and half-scale toothed units. The half-scale RTDs shows a higher peak and a steeper descent from this peak, showing that much of the tracer is flushed out rapidly. The differences in the RTDs between the two scales may be due to the scaling compromises. At the smaller scale the relative volume of the volute is smaller, because the same shaft and seal arrangements are used, leading to the more rapid flushing that is observed. The tail of the RTD still persists for up to about 4 - 5 residence times and this may be due to a small amount of tracer becoming trapped in the chamber that houses the seal.

At the half-scale, the BEP can be exceeded greatly (using the flow loop described in Section 3.1) and when this is done, the RTD shows much less tailing as the tracer is flushed from the volute more effectively (Figure 5.53). This is probably due to the radial velocity discharging from the stator being much greater, modifying the flow pattern in the volute. The BEP at the shaft speed shown in Figure 5.53 is ~0.3 to 0.4 $l.s^{-1}$ and this curve was measured at 3.5^{1} l.s . The time at which the concentration returns to zero (the maximum residence time) changes from ~3.5 (Figure 5.52) to ~2.5 nominal residence times. This change in RTD shape obtained as the flow rate was increased may also signify a change of the flow pattern in the

rotor-stator tooth region. In this case, the ratio v_{TIP}:v_{RADIAL} is much lower that at the BEP and therefore, reagents will not be transported as far around the rotor before entering the stator region. This may in turn affect the amount of interaction between neighbouring reaction zones. Diazo-coupling tests would be required to investigate the effect of operating a rotor-stator mixer at a flow rate well above its BEP.

5.3.1 Modelling of residence time distribution curves

The plug flow-well mixed tanks in series model (Levenspiel, 1972) was used to model the RTDs:

$$C = \left(\frac{V}{V_m}\right) e^{\left[\frac{-V}{V_m}\left(t - \frac{V_p}{V_m}\right)\right]} \qquad (2.24)$$

where V_P and V_M are the volumes of plug and mixed flow regions. It is reasonable to use this model because the flow visualisation results suggest that the inlet and outlet pipes and flow up to and through the stator might be considered to be plug flow (albeit dispersed plug flow) whereas the volute can be considered to be well mixed.

Figure 5.54 shows the model curve for a plug flow well to mixed region volume ratio of 0.4. This fits the RTD obtained close to the BEP at the half-scale well (Figure 5.52) and it is therefore likely that flow through the rotor-stator mixer fits the physical basis of the model - a region of plug flow and a larger region of well mixed flow in series.

Further investigation of the RTD data is not reported here, because the RTDs that were measured showed the behaviour of the total volume of each unit they were of

limited use for the investigation of the performance of the rotor-stator for fast chemical reactions. This was because the critical region for mixing (the immediate vicinity of the rotor-stator teeth) occupies a small proportion of the overall volume.

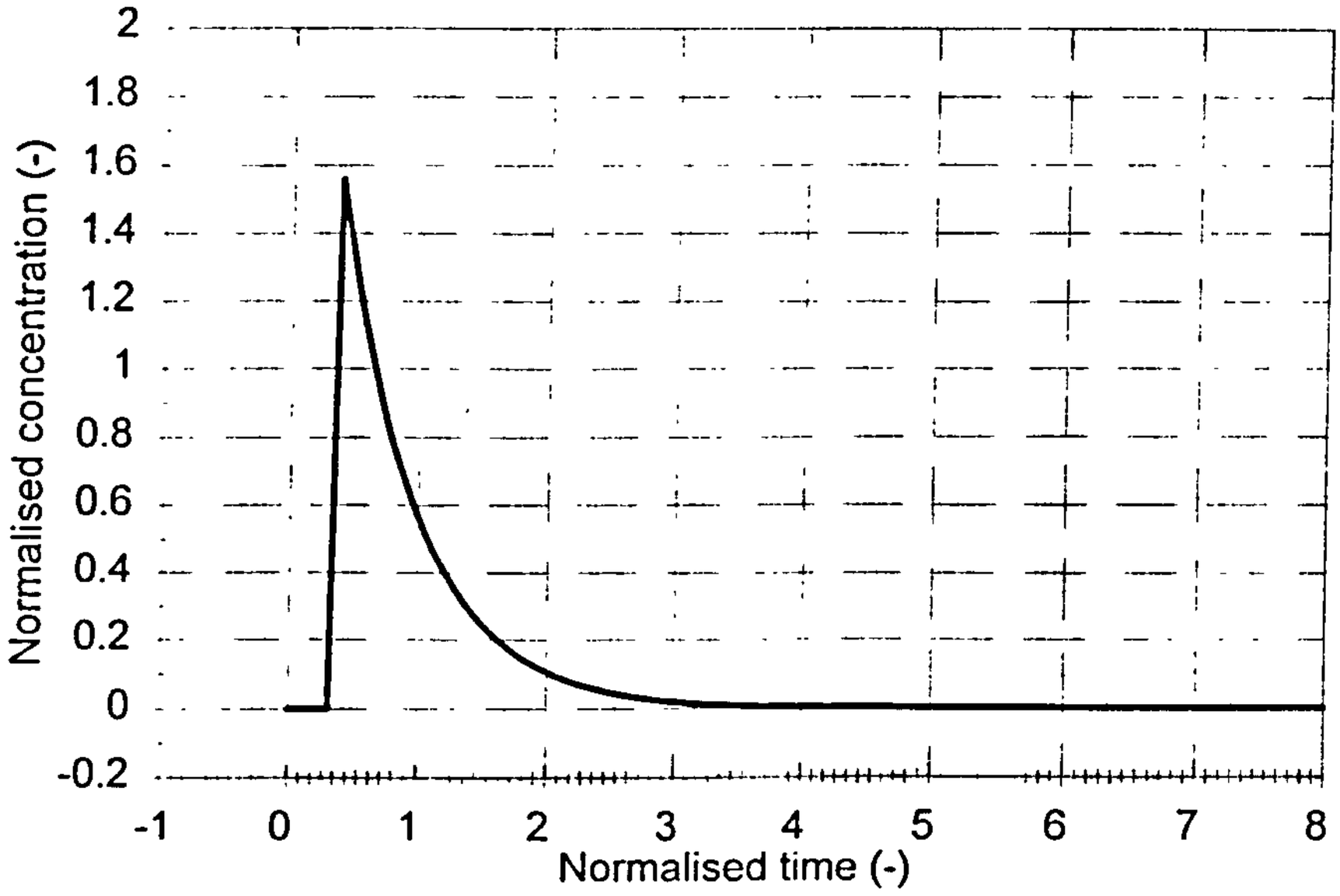

Figure 5.54 Residence time distribution modelled using Equation 2.24, with $V_P:V_M = 0.4$

5.4 Mixing mechanisms and design of diazo-coupling experiments

5.4.1 Background and experimental design

In attempting to make micro-mixing limit the overall mixing rate, estimates of characteristic micro-mixing and meso-mixing times for quantitative comparison were required.

A characteristic timescale for meso-mixing is given by Equation 2.3 (Corrsin, 1964):

$$t_{MESO} \sim \left(\frac{L_0^2}{\varepsilon} \right)^{1/3} \tag{2.3}$$

This gives the time required for coarse scale distribution of reagents in terms of an initial scale of segregation, L_0, and ε. Here, L_0 will be taken as the length scale that was identified in Section (5.2) i.e:

$$L_0 = \frac{v_{RADIAL}}{nN} \tag{5.20}$$

where n is the number of teeth on the rotor (L_0 is a measure of the initial eddy size that is generated by the rotor teeth chopping the fluid that passes through the rotor-stator). At 3000 rpm and 3.0 $l.s^{-1}$ for an 18 toothed rotor, L_0 is of the order of 1 mm.

A corresponding timescale for micro-mixing in low viscosity systems is the engulfment time:

$$t_E \approx 17 \left(\frac{\mu}{\rho \varepsilon} \right)^{1/2} \tag{2.5}$$

Micro-mixing will be the rate controlling mechanism when $t_{MACRO} \ll t_{MICRO}$. Figure 5.55 is a plot comparing the meso and micro-mixing timescales, given by these expressions, versus flow rate with N = 3000 rpm and ν=0.89 cP (i.e water at 25°C, using Equation 5.15 and assuming that η_{TURB} = 1/3 to give ε). It shows that micro-mixing is slower (greater time) at very low flow rates (about 0.1 l/ s), but at higher flow rates, the meso-mixing time is larger. The implication of this result is that meso-mixing might limit the overall rate of mixing for the diazo-coupling experiments that were conducted. However, Equation 2.3 is sometimes given in the literature with a constant of proportionality and therefore this analysis is only

approximate.

The viscosity of the solution was increased for the later diazo-coupling experiments that were conducted, as this should slow the micro-mixing step without affecting the meso-mixing time. Figure 5.56 shows the effect of viscosity on the comparison between the meso and micro-mixing timescales at a higher viscosity (5 cP). Here, the micro-mixing rate is greater and therefore micro-mixing is more likely to limit the overall mixing rate.

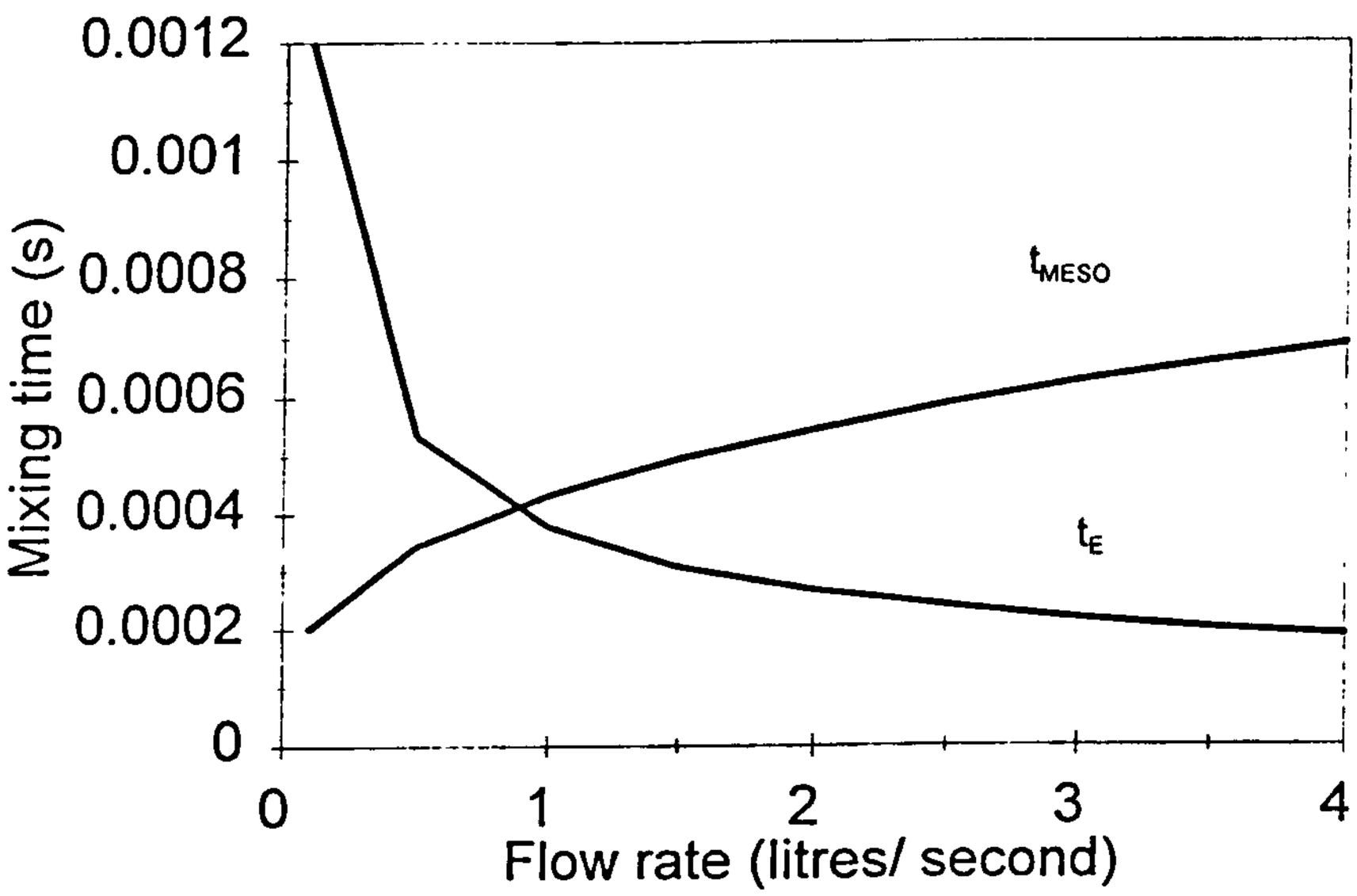

Figure 5.55 Comparison of micro and proposed meso-mixing times (ν=0.89 cP)

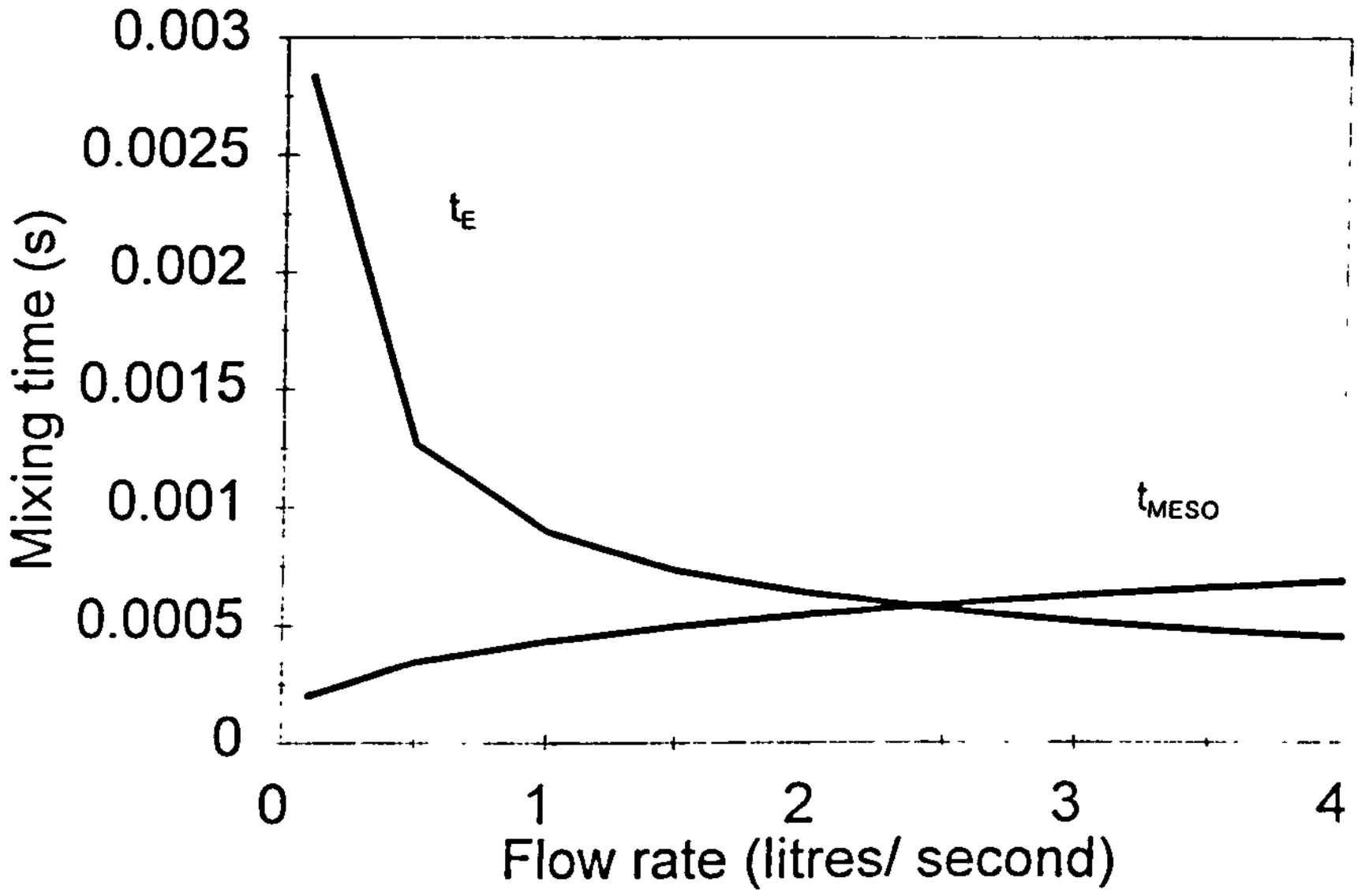

Figure 5.56 Comparison of micro and proposed meso-mixing times ($\nu = 5$ cP)

5.5 Diazo-coupling experiments

Results from the diazo-coupling experiments, described in Sections 3.5.4 and 4.4 are given in the following sections. These are analysed to give qualitative information, e.g. effect of feed position and operating condition (N, Q) and qualitative information on the turbulent energy dissipation rate (using the E-model).

5.5.1 Experimental results

The experimental results from diazo-coupling Runs 1, 2 and 3 are given in Tables 5.5 to 5.7.

Mass balances (calculated using Equation 3.9) are generally close to 1.0. The

exceptions were at the low flow rates of B solution, when it is possible that pulsations from the peristaltic pump (that was rotating more slowly at low flow rates) caused the flow rate of B to vary. However, most of the mass balances are satisfactory. In addition, the reproducibility of results was good (e.g. Run 2, Samples 8,9; Run 3, Samples 11,12). The analytical error in X_Q using the spectrophotometer is approximately ±0.005 (Bourne et. al., 1992).

The concentration of S, c_S, is small and the very small negative values obtained are an artifact of the multiple regression used (Equation 3.8). In the following analysis it was assumed that c_S was zero.

Table 5.5 Results from diazo-coupling Run 1 - using r/18/50/119.6 & s/18/50/123.8, ν = 0.89 cP

Test no.	N	Q_A $l\,s^{-1}$	Q_B $l\,s^{-1}$	a	Feed position	No. of feeds	c_{R+T}	c_S	c_Q	X_Q	Mass Balance
1	3000	3.0	6.0E-4	5000	I	1	0.003429	-4.70E-05	0.000748	0.179076	1.09
2	3000	3.0	6.0E-4	5000	II	1	0.002599	-4.30E-05	0.000545	0.173346	1.45
3	3000	3.0	6.0E-4	5000	III	1	0.003411	-5.60E-05	0.000733	0.176882	1.10
4	3000	3.0	6.0E-4	5000	IV	1	0.003492	-3.30E-05	0.000622	0.151191	1.10

Table 5.6 Results from diazo-coupling Run 2 - using r/18/50/123.34 & s/18/50/123.8, ν = 5.9 cP

Test no.	N	Q_A $l\,s^{-1}$	Q_B $l\,s^{-1}$	a	Feed position	No. of feeds	c_{R+T}	c_S	c_Q	X_Q	Mass Balance
1	3000	3.0	1.67E-4	18000	IV	1	0.001147	-1.70E-05	0.000424	0.269892	0.80
2	3000	3.0	3.33E-4	9000	IV	2	0.002116	-4.30E-05	0.000620	0.226608	0.92
3	3000	3.0	6.67E-4	4500	IV	2	0.003872	-7.90E-05	0.001233	0.241528	0.99
4	3000	3.0	5.0E-4	6000	IV	3	0.002903	-7.30E-05	0.000762	0.207913	1.03
5	3000	4.0	5.0E-4	8000	IV	3	0.002279	-5.70E-05	0.000615	0.212509	0.98
9	3000	3.0	7.5E-4	4000	I	1	0.004319	-9.30E-05	0.001317	0.233676	1.01
10	3000	3.0	1.5E-3	2000	I	2	0.007691	-1.68E-04	0.002949	0.277162	1.07
11	3000	3.0	1.5E-3	2000	I	4	0.007725	-1.64E-04	0.003034	0.281996	1.06
12	3000	3.0	1.5E-3	2000	I	4	0.007727	-1.66E-04	0.003081	0.285067	1.05
13	3000	4.0	1.5E-3	2667	I	4	0.005940	-1.34E-04	0.002304	0.279476	1.03
14	3000	2.0	1.5E-3	1333	I	4	0.010561	-2.14E-04	0.005770	0.353316	1.04

Table 5.7 Results from diazo-coupling Run 3 - using r/18/50/123.34 & s/18/50/123.8, ν = 4.0 cP

Test no.	N	Q_A l s^{-1}	Q_B l s^{-1}	a	Feed position	No. of feeds	c_{R+T}	c_S	c_Q	X_Q	Mass Balance
1	1573	2.0	1.12E-4	18000	IV	1	0.001048	-1.30E-05	0.000396	0.274238	0.87
2	1573	2.0	2.27E-4	9000	IV	2	0.002012	-1.10E-05	0.000655	0.245594	0.95
3	2079	2.0	2.27E-4	9000	IV	2	0.002161	-3.10E-05	0.000539	0.199630	0.94
4	2501	2.0	2.27E-4	9000	IV	2	0.002020	-2.40E-05	0.000489	0.194898	1.01
5	2970	2.0	2.27E-4	9000	IV	2	0.002089	-3.60E-05	0.000429	0.170373	1.00
6	2970	2.0	2.27E-4	9000	IV	1	0.002149	-4.70E-05	0.000427	0.165761	0.98
7	2970	3.0	3.33e-4	9000	IV	2	0.002246	-6.20E-05	0.000373	0.142421	0.96
8	2970	3.0	7.5E-4	4000	I	1	0.004497	-8.60E-05	0.001037	0.187387	1.03
9	2970	3.0	7.5E-4	4000	I	1	0.004408	-8.10E-05	0.001028	0.189110	1.05
10	2970	2.0	5.0E-4	4000	I	1	0.004416	-7.80E-05	0.001055	0.192835	1.04
11	2970	2.0	5.0E-4	4000	I	1	0.004342	-6.90E-05	0.001074	0.198301	1.05
12	2970	2.0	5.0E-4	4000	I	2	0.004514	-7.40E-05	0.001105	0.196654	1.01
13	2970	2.0	1.0E-3	2000	I	4	0.008084	-1.08E-04	0.002783	0.256096	1.05
14	2043	2.0	1.0E-3	2000	I	4	0.007674	-9.90E-05	0.003265	0.298473	1.04
15	1509	2.0	1.0E-3	2000	I	4	0.007575	-9.20E-05	0.003616	0.323117	1.02

5.5.2 General findings from diazo-coupling data

(a) Effect of rotor speed, *N*

Increasing the rotor speed and keeping everything else constant gives lower X_Q values, see Figures 5.57 and 5.58, indicating improved mixing in the reaction zones. This is consistent with the turbulent energy dissipation rate increasing with N (Equation 5.19).

The ratio of tip speed to nominal radial velocity and therefore the trajectory of fluid elements through the mixer is important. An increased rotor speed means that fluid is dragged further around by the rotor teeth before discharging into the stator.

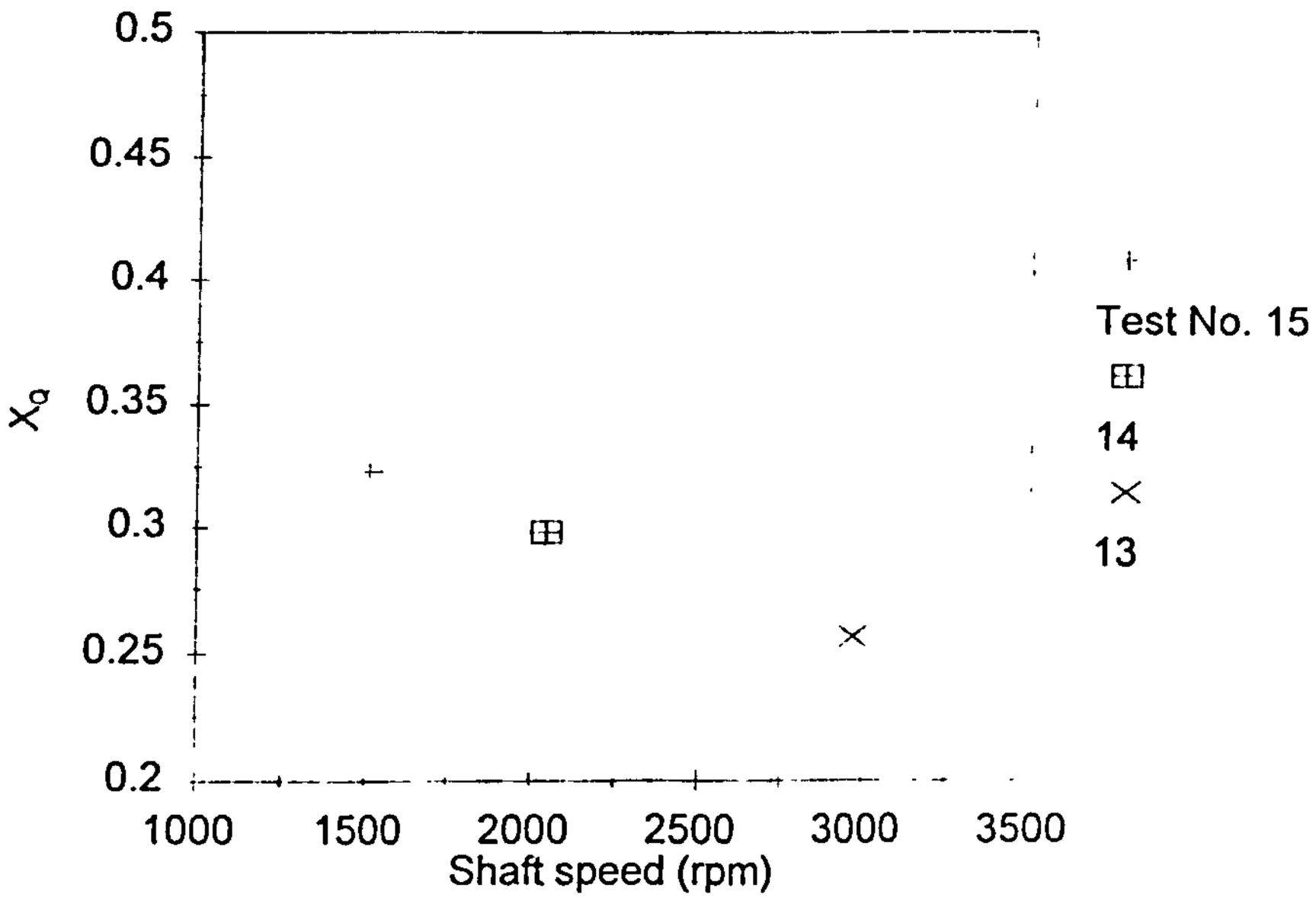

Figure 5.57 X_Q versus shaft speed (Run 3, Test Nos 13, 14, 15)

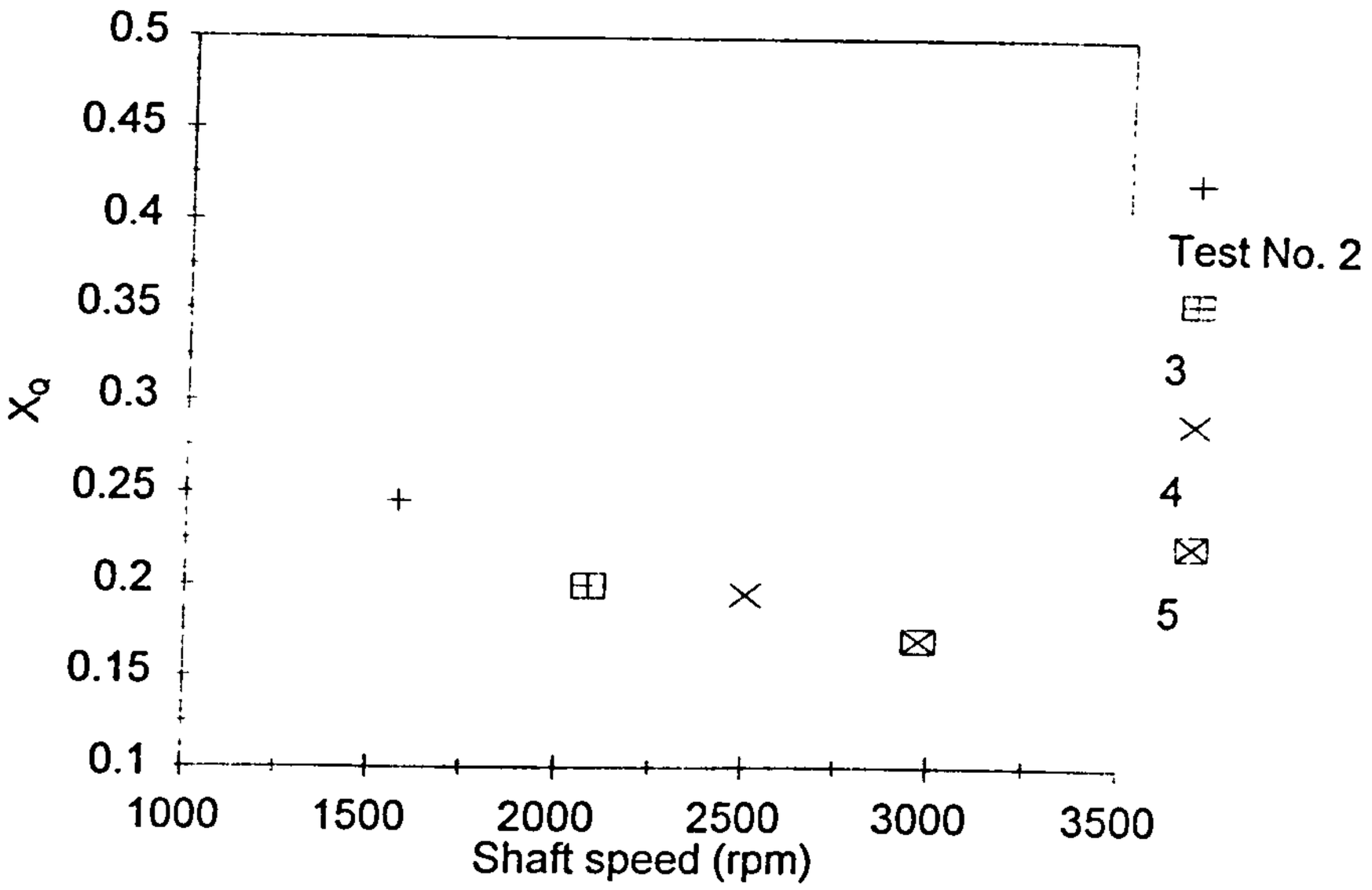

Figure 5.58 X_Q versus shaft speed (Run 3, Test Nos 2, 3, 4, 5)

(b) Effect of carrier flow rate (Q_{A+C})

Test Nos. 5 and 7 from Run 3 (Table 5.7) show the effect of increasing Q_{A+C}, at constant flow rate ratio, a. At 2.0 $l.s^{-1}$ and 3.0 $l.s^{-1}$, X_Q = 0.170 and 0.142 respectively. Increased flow rate gives lower X_Q values indicating improved mixing; this is consistent with Equation 5.10.

However, changing Q_{A+C} also modifies the nominal radial velocity and therefore the trajectory of reactants through the mixer, and so some of the change in X_Q may be due to macro-scale effects if micro-mixing is not limiting these results.

(c) Effect of feed position

Results from Run 1 (Table 5.6) showed that Feed Position IV gave the lowest X_Q values, possibly indicating that energy dissipation rates are highest in the immediate vicinity of the shear gap.

(d) Effect of number of feed positions

Test Nos. 10 and 11 from Run 2 and Samples 11 and 12 from Run 4 show the effect of doubling the number of feed positions (in Feed Position I), keeping the flow rate of A+C solution and B solution constant. In both cases, X_Q was not affected by the number of feed tubes.

These tests showed that increasing the number of feeds does not have a significant effect on X_Q. This could mean that the reaction was micro-mixing controlled (since improving macro-mixing by a better distribution of B solution throughout the rotor-stator ring did not affect X_Q) or that the reaction zones from the feed tubes did not interact. Consideration of velocity ratios and residence times as given in Section 5.2 and the flow visualisation results support the conclusion that micro-mixing is the controlling mechanism (since these show that the reaction plumes from adjacent feed tubes do interact - e.g. Figure 5.32).

When the number of feed tubes (in Feed Position I) and the total flow of B are doubled, X_Q increases (Run 2, Test Nos 9 and 10 shown in Table 5.6; Run 3, Test Nos 12 and 13, Table 5.7). This also indicates that the reaction zones are interacting (i.e. they are not isolated, in which case X_Q would not be affected).

(e) Estimation of turbulent energy dissipation rates per unit mass - use of the E-model

Given the above evidence that results obtained when feeding via Feed Position I were micro-mixing limited, the E-model can be used here to estimate ε.

From Run 3, Test No 13 (2970 rpm and 2.0 l.s^{-1}) gave $X_Q = 0.256 \pm 0.005$. Using the E-model yields a value for ε of 105 W.kg^{-1}, with a lower bound error of 96 ($X_Q = 0.251$) and an upper bound error of 115 W.kg^{-1} ($X_Q = 0.261$). The E-model was also used to calculate the appropriate ε for Test Nos 14 and 15 and the results are shown in Table 5.8. Table 5.8 also shows Φ, the total power supplied to the fluid in the rotor-stator region by the rotor (calculated using Equation 5.10 and the value for *Po* from Table 5.4) and the calculated value of η_{TURB} (calculated using Equation 5.15).

Table 5.8 Analysis of results from Run 3

Test No.	N	P_{FLUID}	Φ	X_Q	ε	η_{TURB}
13	2970	849	12130	0.2561	105	0.0087
14	2043	402	5740	0.2985	52	0.0091
15	1509	219	3131	0.3231	35.5	0.0113

The average value of η_{TURB} is 0.0097 and when this is used in Equation 5.15, the resulting estimated values of ε can be used to plot the experimental data against the E-model curve (Figure 5.59). The correspondence is good, a further indication that micro-mixing did limit the reaction. However, the values of η_{TURB} that are given by this analysis are very low indeed (implying that less than 1% of the power supplied to the fluid by the rotor is dissipated through turbulence).

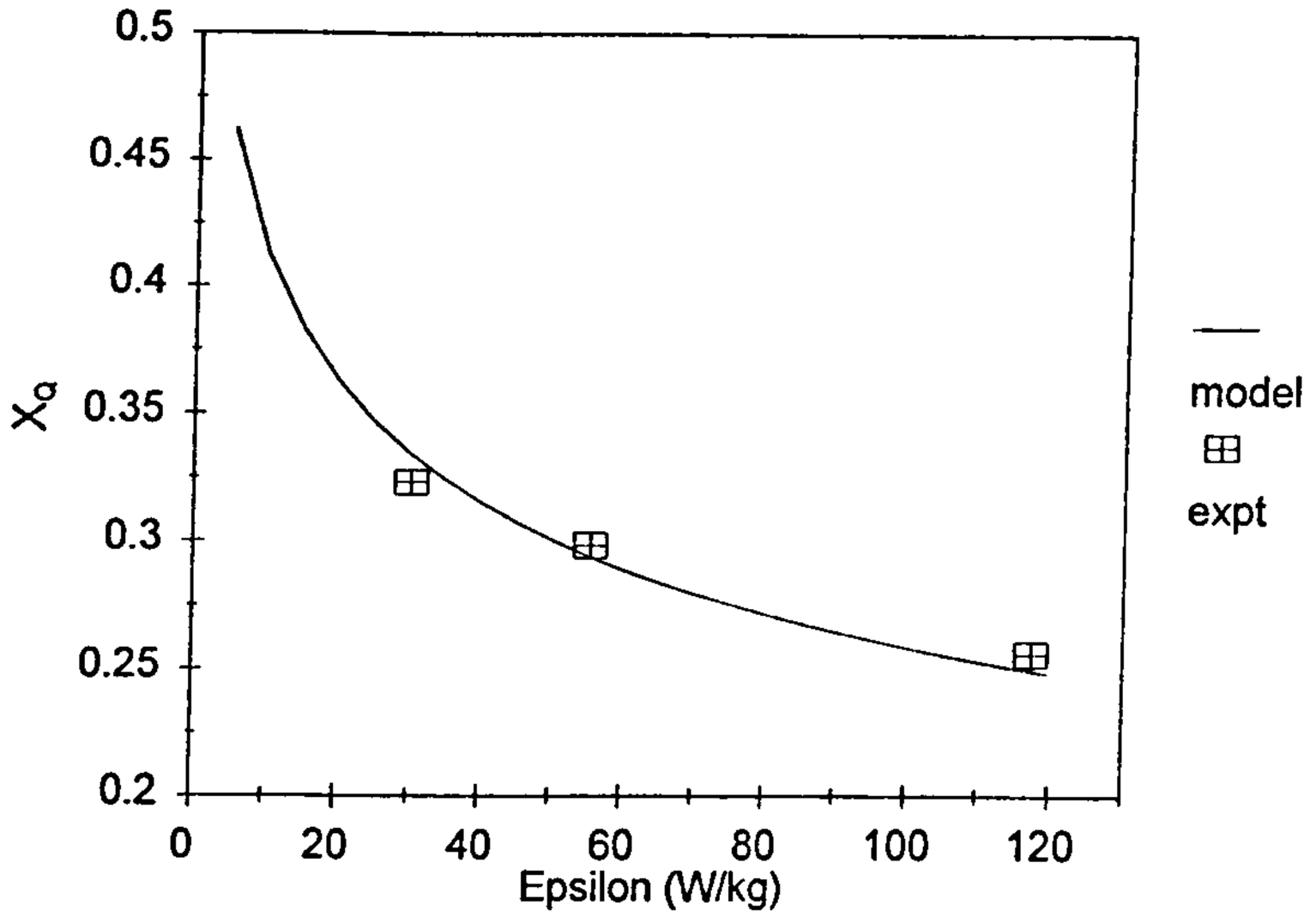

Figure 5.59 Comparison of measured X_Q and results obtained with the E-model with $\eta_{TURB} = 0.0097$

For Run 3, Test No 13, further analysis is given here to estimate the extent of the reaction zone. The nominal radial velocity, v_{RADIAL}, at these conditions is given by:

$$v_{RADIAL} = \frac{Q}{A} \tag{5.19}$$

where A is the open area of the rotor ($= 2.91 \times 10^{-3}$ m^2 at the outer radius of the rotor, assumed to be constant in the rotor-stator region). Therefore, $v_{RADIAL} \approx 0.7$ m.s^{-1} and, since the radial distance from the feed tubes to the outer radius of the stator is approximately 25 mm, the nominal residence time for fluid elements in the rotor-stator region is ≈ 0.03 s. The E-model yields a value for T, the number of fluid engulfments required for the reaction to go to completion (Equation 2.15) and for these conditions (i.e. 105 W.kg^{-1}) it gave a value of $T = 13.8$. The time for one engulfment, t_E, is given by Equation (2.5) and is 0.0033 s, giving a reaction time ($t_E \times T$) of 0.046 s. Therefore, according to this analysis, the reaction did not go to

completion in the rotor-stator region and the reaction zone entered the volute. However, most of the reaction occurred in the rotor-stator region and still the high values for ε were not found.

It is possible that by-passing through the rotor-stator region accounts for this discrepancy. If, as was suggested by the CFD simulations presented in Section 5.2.6, there is significant inhomogeneity in the distribution of ε then it is possible that many fluid elements do not see the high values of ε.

5.5.3 Effect of feed arrangement

It has been shown that the optimal feed tube position for reactive mixing applications is in the locality of the shear gap region - Feed Position IV (although the precise position has not been established). It also been shown by flow visualisation (Section 5.2) that a large number of feed tubes is necessary for two reasons:

(I) to make use of the turbulent energy that is dissipated all of the way around the rotor-stator ring,

(ii) to ensure that all of the carrier flow (*A*+*C* in the reactive mixing tests) meets reagents (*B*) fed into the mixer in the region of high energy dissipation.

A two-piece stator was machined with a groove connecting stator tooth feeds that went to each tooth (Figure 3.14). This was fitted into the rig and a diazo-coupling Run was performed to assess the performance of Feed Position IV versus Feed Position I and to estimate ε in the vicinity of the shear gap.

5.5.4 Diazo-coupling experiments performed using the 18 feed stator - Run 4.

Results obtained using the 18 feed manifold-stator are given in Table 5.9.

(a) General findings

The mass balances for this run were poor compared to those obtained in Runs 1,2 and 3. In particular, the mass balances for Test Nos. 1 and 12 are very poor and these results were not used in the subsequent analysis. In addition, some of the points taken at repeat conditions (e.g. Test Nos. 1 and 4) do not reproduce as well as in previous runs. Explanations for the reduction in quality of the results are: experimental error or it is possible that the 18 toothed manifold was not working correctly (i.e. the flow rate of *B* solution was not constant). However, while the quality of the data appear to be lower than before, these data were used below to examine the performance of the 18 toothed manifold feed arrangement.

The value of X_Q decreased with increasing flow rate (e.g. Test Nos. 5, 6, 7) and this is, once again, to be expected from Equation 5.10. Figure 5.60 shows the effect of flow rate on X_Q for Test Nos 5, 6, 7.

It is not possible to make a firm comparison with the data from Runs 2 & 3, since the viscosities of the liquids used are not equal and this will affect micro-mixing rates. However, the difference in viscosity is small and so a brief comparison can be made. This shows that, in general, lower values of X_Q (and therefore improved yield, if Q is a waste product) are obtained when reagents are fed through the 18 feed holes. This is illustrated by, for example, comparing Run 4, Test 16 (X_Q=0.2087) and Run 2, Tests 11 & 12 (X_Q=0.2820 & 0.2851) where the operating conditions are very similar. Also this trend is shown by Run 4, Test 6 (X_Q=0.2575) and Run 3,

Test 14 (X_Q=0.2985). An exception is Run 4, Test 15 (X_Q=0.2726) and Run 3, Test 13 (X_Q=0.2561); however, in this case the mass balance for Run 4, Test 15 is poor. It is concluded that the feed manifold performs better, for this particular reaction. It is likely that this will apply to other fast reaction schemes.

Table 5.9 Results from diazo-coupling Run 4 - using r/18/50/123.34 & s/18/50/123.8, ν = 6.6 cP

Test no.	N	Q_A $l\,s^{-1}$	Q_B $l\,s^{-1}$	a	Feed position	No. of feeds	c_{R+T}	c_S	c_Q	X_Q	Mass Balance
1	1515	1	5.0E-4	2000	IV	18	0.005369	-1.25E-04	0.001839	0.255133	1.58
2	1515	2	1.0E-3	2000	IV	18	0.006712	-7.80E-05	0.002946	0.305032	1.18
3	1515	3	1.5E-3	2000	IV	18	0.007302	-1.71E-04	0.002788	0.276313	1.13
4	1515	1	5.0E-4	2000	IV	18	0.007384	-1.67E-04	0.003543	0.324243	1.04
5	1992	1	5.0E-4	2000	IV	18	0.007369	-1.61E-03	0.002847	0.278681	1.11
6	1992	2	1.0E-3	2000	IV	18	0.007348	-1.66E-04	0.002548	0.257478	1.15
7	1992	3	1.5E-3	2000	IV	18	0.007248	-1.70E-04	0.002576	0.262215	1.16
8	2517	1	5.0E-4	2000	IV	18	0.008575	-1.76E-04	0.00522	0.378398	0.82
9	2517	3	1.5E-3	2000	IV	18	0.007640	-1.66E-04	0.002423	0.240783	1.13
10	2517	2	1.0E-3	2000	IV	18	0.007773	-1.66E-04	0.002725	0.259573	1.08
11	2958	1	5.0E-4	2000	IV	18	0.008177	-1.28E-04	0.00337	0.291851	0.98
12	2958	1	6.67E-4	1500	IV	18	0.007890	-1.51E-04	0.002741	0.257831	1.43
13	2958	1	4.0E-4	2500	IV	18	0.007111	-1.39E-04	0.002037	0.222672	0.99
14	2958	1	3.33E-4	3000	IV	18	0.005977	-1.57E-04	0.001232	0.170897	1.05
15	2958	2	1.0E-3	2000	IV	18	0.009099	-2.20E-04	0.003409	0.272546	0.91
16	2958	3	1.5E-3	2000	IV	18	0.007618	-1.83E-04	0.002009	0.208684	1.18
17	1490	1	5.0E-4	2000	IV	18	0.006809	-1.66E-04	0.003202	0.319848	1.14
18	2017	1	5.0E-4	2000	IV	18	0.006933	-1.59E-04	0.002608	0.273347	1.19
19	2539	1	5.0E-4	2000	IV	18	0.007263	-1.63E-04	0.002919	0.286682	1.12

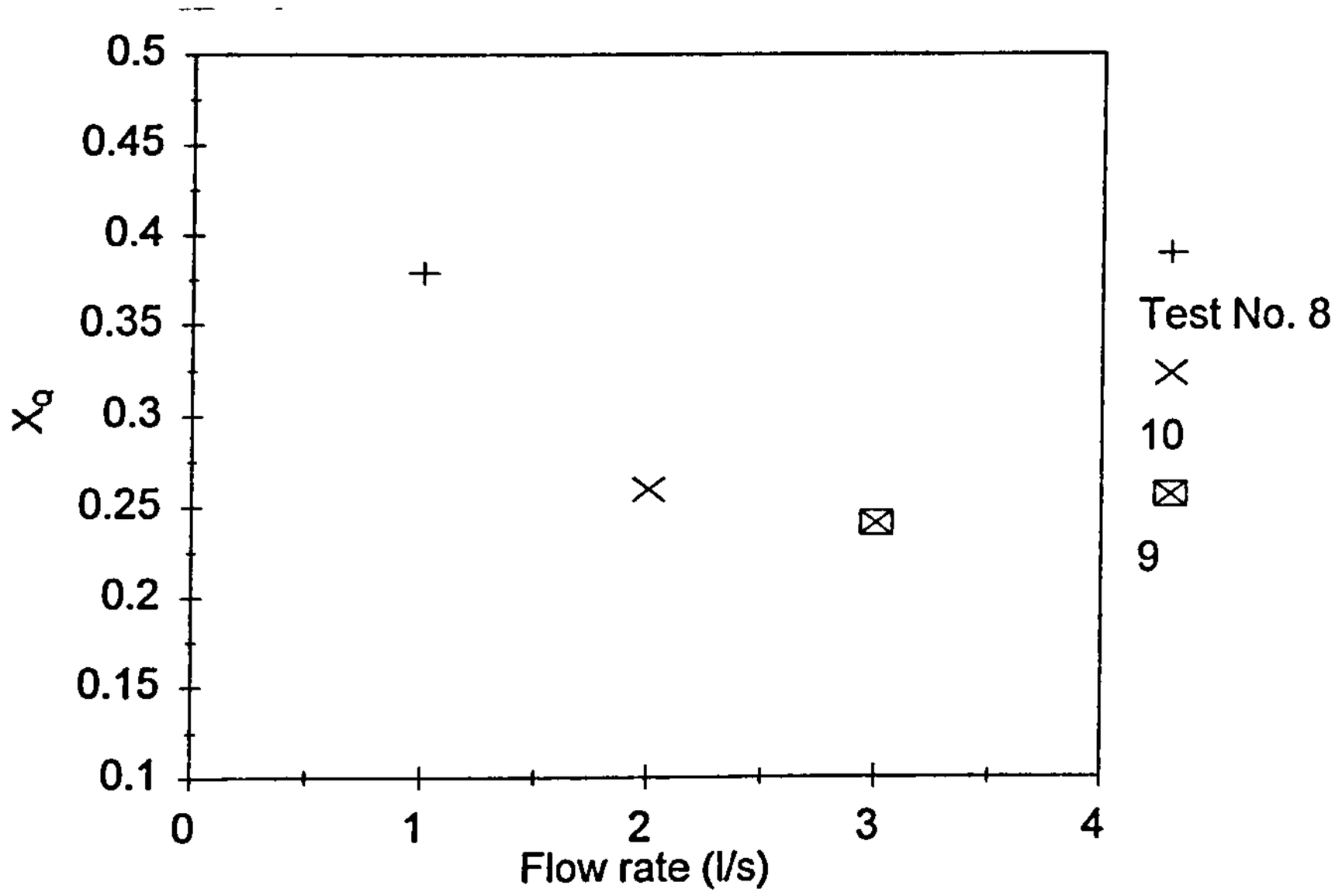

Figure 5.60 X_Q versus flow rate (Run 4, Test Nos 8, 10, 9)

(b) Analysis with the E-model

A similar analysis to that for Run 3 was also conducted for the results from Run 4 (Test Nos 16, 9, 7 and 3). For this run, *B* solution was fed through all 18 stator teeth into the shear gap (Figure 3.13) and there was no direct evidence that micro-mixing was limiting the reaction, since the number of feed tubes was not varied, but the analysis was undertaken to give an indication of the lower bound for ε (i.e. if micro-mixing did limit the reaction outcome then the value given would be accurate, if macro/meso-mixing effects were important then ε could be much higher than the values estimated using the E-Model).

Table 5.10 Analysis of diazo-coupling Run 4 data

Test No.	N	P_{FLUID}	Φ	X_Q	ε	η_{TURB}
16	2958	1263	18049	0.2087	445	0.0247
9	2517	915	13068	0.2408	231	0.0177
7	1992	573	8185	0.2622	157	0.0192
3	1515	331	4735	0.2763	122	0.0258

Figure 5.61 is a plot of the experimental data (using $\eta_{TURB} = 0.0219$) versus the E-model curves. As with Figure 5.59, the correspondence between model and experimental values is good. Since the results follow the micro-mixing model well, this is once again a good indication that micro-mixing limits the reaction outcome.

The analysis of the extent of the reaction zone shows that it entered the volute, with the residence time in the stator being ~12 ms (the Reagent B was fed into the shear gap so the radial distance to the end of the stator was ≈12 mm and v_{RADIAL} was ≈1 $m.s^{-1}$). The engulfment time was 2.1 ms and the number of engulfments required for reaction to go to completion was given by the E-model as 18.33. Therefore $t_{REACTION}$ was 38 ms. The reaction zone therefore entered a significant distance into the

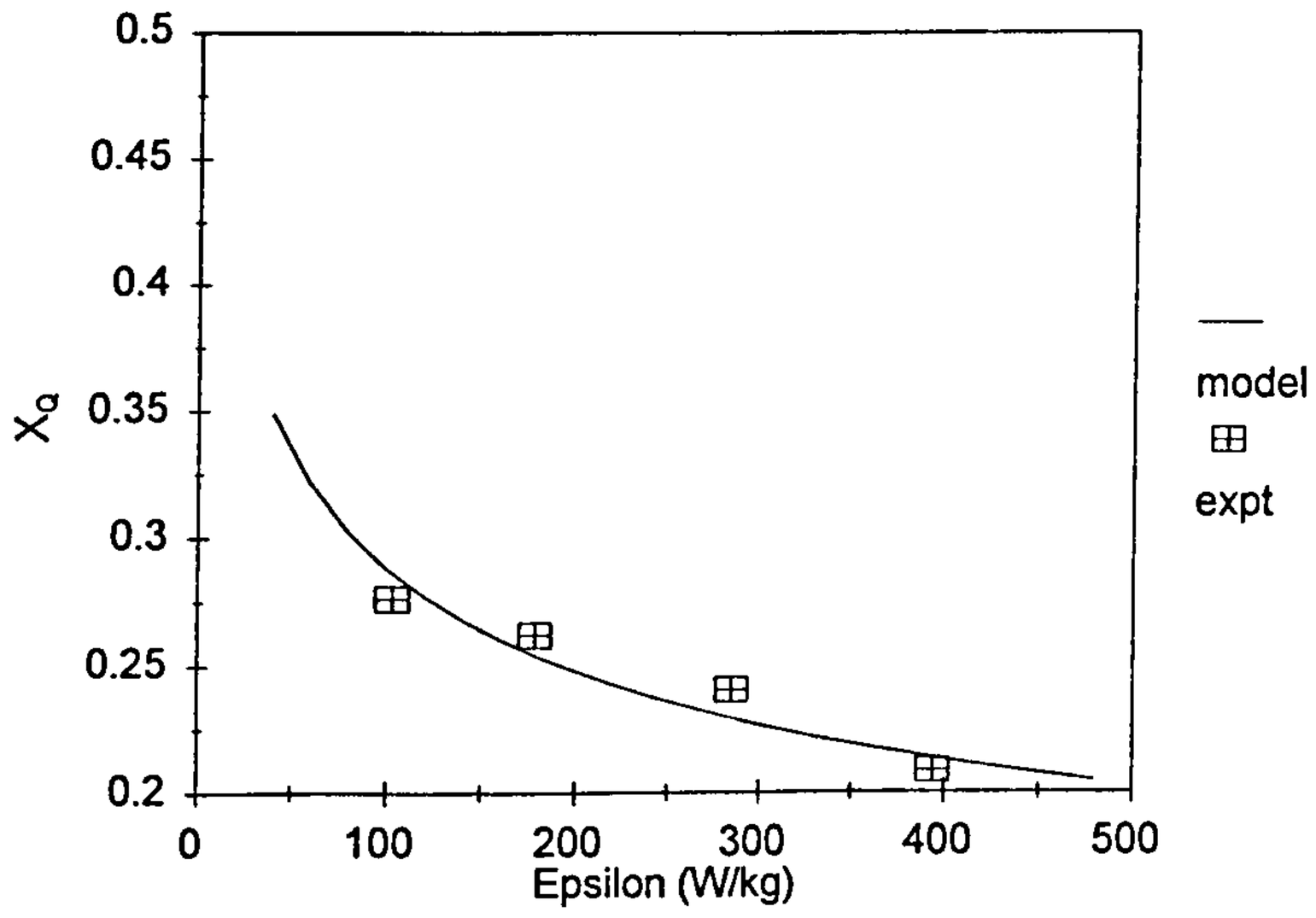

Figure 5.61 Comparison of measured X_Q and results obtained with the E-model with $\eta_{TURB} = 0.0219$

volute, where the turbulence dissipation rate will be diminishing. The reactive mixing tests indicate the average energy dissipation rate in the reaction zone (Bourne, 1995a), so it is possible that the measured ε could be increased by designing experiments in which the reaction zone does not enter the volute.

The value of η_{TURB} (~2%) is higher than that obtained when feeding upstream of the rotor teeth, confirming that, for this particular reaction, Feed Position IV gives the best reaction yield.

The proportion of the total energy input to the system that manifests itself as 'useful' energy dissipation is small. The decay of turbulent energy in the system may persist through the volute and continue for a distance along the outlet pipe. The assumption made earlier in this thesis, that power given to the fluid by the rotor is dissipated through turbulent energy dissipation in the rotor-stator region (Section 5.1.7),

appears to not be borne out by the finding that η_{TURB} is of order 0.01 to 0.02. This value is much lower than the equivalent for motionless mixers. The implication is that the turbulent energy dissipation is spread throughout the system downstream of the rotor-stator teeth (the analysis of the extent of the reaction zone given in Sections 5.5.1 and 5.5.4 showed that a large proportion of the reaction occurred in the volute).

While it is likely that the turbulent energy dissipation field is highly inhomogeneous, with the highest energy dissipation in the region of the rotor-stator, it may be useful to consider the energy dissipation occurring throughout the volute. The volume of liquid in the volute of the large toothed unit is 1.59 litres, approximately 23 times greater than the volume assumed when designing the experiments. This gives a value for η_{TURB} of order 0.25 to 0.50 for the rotor-stator system. This value is closer to the expected value (assumed to be 0.33 when designing the experiments).

The assumption, that the turbulent energy is dissipated throughout the volute, does not take account of the inhomogeneity in ε that is expected (Section 5.2.4). However, values of ε calculated using η_{TURB} of 0.25 to 0.50 are much closer to the energy dissipation rates determined using the diazo-coupling technique. Values for epsilon determined using the diazo-coupling technique are averaged over the extent of the reaction zone (Bourne & Studer, 1992).

Further work using the diazo-coupling technique would be required to increase understanding of the turbulence field in the rotor-stator mixer.

5.6 Flow and mixing in rotor-stator mixers

The findings from the experimental work and analysis is used here to comment on

the use of rotor-stator mixers.

5.6.1 General remarks on rotor-stator mixers

Rotor-stator mixers supply a large amount of power to the fluid passing through, within a very small region (~4% of the total volume). However, from the results of the diazo-coupling experiments, it is estimated that a only small percentage (<3%) of the power that is supplied to the fluid by the rotor is dissipated through turbulence in the rotor-stator region. It appears that it is difficult to utilise the energy dissipation in a rotor-stator mixer because of by-passing and inhomogeneity in the turbulence field. The by-passing and inhomogeneity mean that a proportion of the fluid passing through the mixer may not experience the high energy dissipation rates.

Feed Position IV (Figure 3.13) was found to give the best performance from the diazo-coupling data. It is probable that feeding directly into the shear gap is the best way to feed reagents for fast competitive chemical reactions, although it is possible that the precise location might be optimised (e.g. closer to the leading edge of the stator tooth).

In order to ensure that a greater proportion of the flow 'sees' the high energy dissipation rates, two routes are suggested. The first is to design rotor-stators that reduce the inhomogeneity. The Silverson design has a much lower nominal radial velocity through the rotor than the toothed designs (it has a larger open area) and it is possible that this may reduce the short circuiting. Also, the 36-toothed stator and 19-toothed designs may reduce by-passing. Further diazo-coupling experiments are required using these geometries to investigate this further.

The second way to improve the utilisation of the power supplied to the fluid may be

to recycle the process fluid through the device (i.e. to operate in semi-batch mode). Therefore, if (say) only 20% of the fluid passing through the device experiences the peak ε, then after a certain number of passes it could be assumed that all (or >95%, say) of the fluid has experienced the peak ε. Pedrocchi and Widmer (1989), studying emulsification in a rotor-stator device, found that up to 50 passes through the unit were required for their emulsion to reach an equilibrium drop size distribution. This result may have been as a consequence of the characteristics of their particular emulsion, or it may have been due to by-passing. Similar experiments to those conducted by Pedrocchi and Widmer could be used on the rotors and stators investigated here to complement the findings from this work.

5.6.2 Silverson units as chemical reactors

No diazo-coupling tests were done with the Silverson unit. However, using results produced with the toothed unit, and extending the analysis of these it is possible to comment on the likely performance of the Silverson unit as a chemical reactor.

Assuming that the turbulence production mechanism is primarily the same (rapid, inefficient transformation of tangential kinetic energy) and occurs in a similar volume, then estimates of P_{FLUID} (Equation 5.10) for the Silverson will be similar to those for the toothed unit (albeit lower in this case, because of the slightly smaller diameter of the Silverson). This would imply that the turbulent energy dissipation rate is of the same order as in toothed rotor-stator mixers. However, there are some differences in the flow through the Silverson, particularly through the rotor which has a greater open area and so a lower v_{RADIAL}. This means that, when estimating the path of reagents through the rotor-stator region, the ratio v_{TIP}:v_{RADIAL} will be higher and, at the same operating conditions (N and Q), reagents fed upstream of the shear gap will be transported further around the rotor-stator ring before emerging through

the stator. It is not clear what effect this will have on the performance of the Silverson unit as a chemical reactor and therefore experiments would be required in order to investigate.

For this study, the stator used with the Silverson unit (shown in Figure 3.9 and Plate 3.3) consisted of solid stainless steel with 13 holes. Other stators in the Silverson range are made up from fine grids, which may act differently as turbulence generators and therefore also merit investigation.

5.6.3 Scale up of a rotor-stator process

Process development usually takes place on small scale equipment. The developer has the challenge of scaling processes up to pilot scale or production scale predictably. Delays and uncertainty in commissioning can have a significant bearing on the commercial success of a process. Studer (1990) recommends that constant tip speed be used as a rule for scale-up of micro-mixing controlled reactions.

Here, scale-up is considered for a rotor-stator system, assuming that a process has been successfully developed at small scale. It is assumed that scale up depends upon keeping the residence time, in the region of intense mixing, constant and ensuring that the same limiting mixing time-scale (i.e. meso/micro) applies on scale-up.

If the scaled unit has the same design then, if the scale ratio is R, the required flow rate to keep a constant residence time in the rotor-stator teeth is given by:

$$Q_{LARGE} = R^3 Q_{SMALL} \tag{5.23}$$

Using the approach outlined in Section 5.4, the rate limiting (i.e. longest mixing

time) can be determined. For example, in Figure 5.54, meso-mixing times are generally longer than the micro-mixing times and will therefore probably limit the overall mixing rate. When meso-mixing limits the overall rate (from Equations 2.3, 5.10, 5.14, 5.15 and 5.20) then the scale-up rule is constant rotor speed. When micro-mixing limits then the scale-up rule (from Equations 2.5, 5.10, and 5.14) is constant tip speed (as was found by Studer, 1990).

However, if the scale-up rule of constant tip speed is used, then the ratio v_{TIP}:v_{RADIAL} is modified, which may affect the mixing performance.

Further work is required to check the scale-up rules suggested in this section.

CHAPTER 6

CONCLUSIONS AND RECOMMENDATIONS

6.1 Conclusions

The conclusions from this study are given in the following sections.

6.1.1 Experimental rig

The rig and rotor-stator units produced in this work allowed measurement of the overall power balance, flow pattern, residence time distribution and product selectivity from diazo-coupling tests to a good degree of accuracy.

Repeat energy balance data are shown in Figures 5.30 and 5.31.

6.1.2 Energy Balance, flow visualisation and residence time distribution work on the toothed/Silverson units.

The power supplied to the fluid by the rotor, with turbulent flow conditions, is given by Equation 5.10:

$$P_{FLUID} = Po\rho N^2 D^2 Q$$

where *Po* is give in Table 5.4 and is ~10 for all rotor-stator geometries tested here (including half-scale toothed).

The Silverson unit draws more shaft power, but is a more efficient pump.

The flow pattern in the rotor is predominantly tangential, with a much lower radial component. The flow through the stator is predominantly radial. An abrupt transformation from tangential to radial flow occurs on the upstream faces of the stator teeth. The overall residence time distribution of the rotor-stator mixers tested was due mainly to the disordered, mixed, flow in the volute.

The residence time distribution data taken confirmed the finding of Studer (1990) of predominantly backmixed behaviour. Significant tailing (long residence times) were also observed. The residence time distribution characteristics of the toothed and Silverson units were insensitive to operating condition or even mixer geometry.

6.1.3 Energy Balance and residence time distribution work on the half-scale toothed unit.

It was possible to force fluid through the half-scale toothed unit at flow rates well above those where the unit could give a positive pumping effect. Under these circumstances ('drowned suction'), the total pressure losses across the mixer (which contribute to mixing) can exceed the shaft power input.

Under drowned suction conditions, the residence time distribution characteristics of the half-scale toothed unit changed (the peak approaches one residence time and the length of the tail on the distribution shortened).

6.1.4 Reactive mixing experiments on the toothed unit.

Feed Position IV (feeding into the shear gap through a stator tooth) gave the best yield for the diazo-coupling reaction scheme used for this work. It is likely that this will be true for other fast competitive reaction schemes.

The value for ε, estimated using the results from diazo-coupling experiments is proportional to P_{FLUID} and is of order 500 W.kg^{-1} at 3000 rpm and 3.0 l.s^{-1} in the toothed unit. If it is assumed that the power given to the rotor is dissipated through turbulence in the immediate vicinity of the rotor-stator teeth then 500 W.kg^{-1} represents a small proportion of the power dissipation per unit mass (giving a turbulence efficiency factor, η_{TURB} of <3%). However if it is assumed that the power given to the rotor is dissipated through turbulence throughout the mixer volute then η_{TURB} is of order 25 to 50%.

Further work is required to investigate the turbulence field throughout the rotor-stator mixer.

6.1.5 Description of the flow and mixing characteristics of rotor-stator mixers

The description of the flow pattern, residence time distribution and turbulence characteristics presented in this thesis is not complete, but does provide information that can be used to locate feed positions, size motors, estimate the magnitude of the turbulent energy dissipation rate etc. It appears difficult to take full advantage of the high energy dissipation produced in rotor-stator mixers for fast chemical reaction applications, but the turbulent energy dissipation rates measured are still high and rotor-stator mixers should be considered for application to reactive mixing.

Further work is required in many areas, both specific to the flow and also with reference to particular applications.

6.2 Recommendations for future work

6.2.1 Further diazo-coupling experiments

Further diazo-coupling experiments could be used to investigate further the use of rotor-stator mixers as chemical reactors. It is possible that ways could be found to make better use of the power that is supplied to the fluid by the rotor and to map out the distribution of ε. The Silverson and other toothed (e.g. 36-toothed stator) designs should be used to perform diazo-coupling experiments to determine their performance to compare with the 18-toothed units.

Performing these experiments in semi-batch mode may increase the likelihood that all of the fluid will experience the high ε. However, the reaction zones may grow as reagents are consumed (and the concentrations and of reagents is reduced). Given that the region of high energy dissipation may be small, the growth in reaction zone size may mean that the reaction is not completed in this region and the product distribution may be affected.

The use of multi-ringed rotor-stators (e.g. Figure 2.1) will increase the time that fluid elements spend in the region of high energy dissipation, and will increase the chances of a particular fluid element experiencing the peak ε during one pass through a unit.

6.2.2 Liquid-liquid droplet size reduction

Liquid-liquid drop size reduction work could be used to determine the peak energy dissipation rates and to gauge the amount of any by-passing through the regions of high energy dissipation. The drop size distribution could be measured for water and

a small quantity of an immiscible phase (e.g. viscous oil) that is passed through a rotor-stator unit in a loop around a batch vessel. The minimum stable drop size would indicate the maximum energy dissipation rate (if enough is known about , e.g., the surface tension of the oil phase) and the number of passes through the loop that are required to reach the equilibrium could indicate the amount of by-passing.

It is possible that a bi-modal drop size distribution would be produced initially because of the expected inhomogeneity of ε in rotor-stator mixers. As the number of passes increases then this should settle to a single distribution.

6.2.3 Computational fluid dynamics (CFD)

Computational fluid dynamics could be used to improve the understanding of the flow pattern and turbulence in a rotor-stator mixer. This approach would require careful validation (e.g. laser doppler anemometry or particle image velocimetry), but once validated, CFD could be used to optimize the design of rotor-stator mixers or improve understanding of a particular process that occurs in them. In particular, sliding mesh technology lends itself well to rotor-stator mixer analysis (Luo et. al., 1993).

As computers and CFD programs become more sophisticated, it is likely that CFD will become a common tool for the design of process equipment and it is important that it is used appropriately. Work is required to determine the limits of applicability of CFD and, e.g., the turbulence models that should be used.

REFERENCES

Anderson, H. H. (1980). *Centrifugal pumps*. 3rd edition. Trade and Technical press. ISBN 85461 076 6

Baker, M. R. (1993) "Droplet breakup using in-line mixers located in recirculation loops around batch vessels". Chem. Eng. Science, Vol 48, No. 22, pp 3829-3833.

Baldyga, J. & Bourne, J. R. (1984). "A Fluid Mechanical approach to turbulent mixing and chemical reaction . Part II Micromixing in the light of turbulence theory". Chem. Eng. Commun, 28, pp 243-258

Baldyga, J. & Bourne, J. R. (1989). "Simplification of Micromixing Calculations I. Derivation and Application of New Model". Chem. Eng. J 42, 83-92

Bolzern, O. & Bourne, J. R. (1985). "Rapid chemical reactions in a centrifugal pump". Chem. Eng. Res. Des, vol 63.

Bouette, D. W. (1974). High, Medium and Low Shear Continuous Mixing Techniques. In: *1st European Conference on Mixing and Centrifugal Separation*, Paper D4.

Bourne, J. R. & Garcias-Rosas, J. (1985). Fast Chemical Reaction in High Intensity Ystral Dynamic Mixer. In *5th European Conference on Mixing*.

Bourne, J. R. & Garcias-Rosas, J. (1986). "Rotor Stator Mixers for Rapid Micromixing". Chem. Eng. Res. Des, Vol 64.

Bourne, J.R, Hilber, C. & Tovstiga, G. (1985) "Kinetics of the azo coupling reactions between 1-naphthol and diazotised sulphanillic acid". Chem Eng Comm, 37, 293.

Bourne, J. R., Kut, O. M., Lenzner, J. and Maire, H. (1990). "Kinetics of the diazo coupling between 1-naphthol and diazotised sulfanillic acid". Ind. Eng. Chem. Res. 29, p 1761.

Bourne, J. R., Lenzner, J., and Kut, O. M. (1992). "An improved reaction scheme to investigate micromixing in high intensity mixers". Ind. Eng. Chem. Res. 31, p 949.

Bourne, J. R. & Studer, M. (1992). "Fast Reactions in Rotor-stator Mixers of Different Size". Chem. Eng. Proces 31, pp 285-296

Copley, Diana. M. & Worster, R. C. (1961). Pressure measurements at the blade tips of a centrifugal pump impeller and the effects of tip profile on pump performance. BHRA report RR 710. Cranfield. U.K.

Copley, Diana. M. & Worster, R. C. & Zanker, K. J. (1962). The flow in pump volutes and its effect on performance. In: *8th Conference on Hydrodynamics*.

Corrsin, S. (1964). "The isotropic turbulent mixer: part II. Arbitrary Schmitd number". A.I.Ch.E.J vol 10.

Fraser, W. H. (1982). "Recirculation in centrifugal pumps - Part I". Indian Pumps, vol 14.

Hearn, S. (1992). Residence time distribution and pressure gain measurements in a Weir Group centrifugal pump with an open impeller. HILINE report HLP 02. BHRG Ltd, Cranfield.

Hearn, S. (1994). Personal communication to T Sparks.

Holley, W. & Weisser, H. (1982). "Dispersing Equipment and its Use in Emulsification - Part 2: The emulsification process". Z. Lebensm. Technol. Verfahrenstech. (ZFL) 33 Heft 4

Jekat, W. K. (1986) in *Pump Handbook.* 2nd edition. Edited by Karassik, I. J. Krutzsch, W. C. Fraser, W. H. & Messina, J. P. (1986). McGraw-Hill, New York. ISBN 0-07-033302-5.

Jones, W. P. and Launder, B. E. (1972). "The prediction of laminarization with a two-equation model of turbulence". Int. J. Heat Mass Transfer. Vol 15. pp 301-314.

Karassik, I. J. (1983). "Flow recirculation in centrifugal pumps: from theory to practice". World Pumps April 1983, pp 119-123.

Karassik, I. J. Krutzsch, W. C. Fraser, W. H. & Messina, J. P. eds. (1986). *Pump Handbook.* 2nd edition. McGraw-Hill, New York. ISBN 0-07-033302-5.

Levenspiel, O. (1972). *Chemical Reaction Engineering.* 2nd edition. John Wiley and sons, New York. ISBN 0-471-53019-0.

Luo, J. Y. Gosman, A. D. Issa, R. I. Middleton, J. C. and Fitzgerald, M. K.

(1993). Full flow field computation of mixing in baffled stirred vessels. In: The 1993 ICHEME RESEARCH EVENT.

Massey, B. S. (1983). *Mechanics of Fluids*. Fith edition.Van Nostrand Reinhold. UK. ISBN 0 442 305494

Miller, D. S. (1990). *Internal flow systems*. 2nd edition. BHRA, Cranfield. ISBN 0-947711-77-5

Pedrocchi, L. & Widmer, F. (1988). Formation of Emulsions in a Turbulent Shearfield. In: 6th European Conference on Mixing.

Pedrocchi, L. & Widmer, F. (1989). "Emulsionsherstellung im Turbulenten Scherfeld." -ing. -T Chem. ech. 61, Heft 1.

Rushton, J. H. Costich, E. W. & Everett, H. J. (1950). "Power characteristics of mixing impellers". Chemical Engineering Progress. Vol 46, No 8.

Ruszkowski, S. W. (1985). The FMP Method for Measuring Mixing Times. FMP Report 008. BHR Group Limited, Cranfield.

Sparks, T. G. (1993). Operational characteristics of rotor/stator mixers. MPhil thesis. Cranfield Institute of technology.

Stepanoff, A. J. (1957). *Centrifugal and axial flow pumps, theory design and application.* 2nd edition. John Wiley and Sons ISBN 0-471-82137-3.

Studer, M. (1991). Residence Time Distribution and Pressure Drop Measurements in the Kenics Mixer. HILINE Report HLC 04. BHR Group Limited, Cranfield.

Studer, M. (1990). Ablauf Scneller Reactionen in Rotor-Stator-Mischern Verschiedener Grösser. Ph.D Thesis 9037, ETH Zürich.

Summets, A. M. (1966). "Continuous Reactor-Mixer for Liquid Media". Khim. Neft. Mashinostr. 10.

Tennekes, J. H., and Lumley, I. L. *A first course in turbulence.* MIT Press. Cambridge, MA, USA. 1972.

Tovstiga, G. T. Micro mixing and fast chemical reactions in a turulent tubular reactor. PhD thesis No. 8111, ETH, Zürich. 1986

Wu, H. & Patterson, G. K. (1989). "Laser-doppler measurements of turbulent-flow parameters in a stirred mixer". Chemical Engineering Science vol 44. No 10. pp 2207-2221

Yedidiah, S. (1985). "Cause and effect of recirculation in centrifugal pumps: Parts 1 & 2". World Pumps.

APPENDIX 1

EXPERIMENTAL EQUIPMENT SUPPLIERS

Silverson in-line 425 LSM rotor/stator mixer, machine No 425LSM276
Silverson Machines Limited,
Waterside,
Chesham,
Buckinghamshire,
England HP5 1PQ.

Flygt BS 20066.171 submersible pump
ITT Flygt Limited,
Colwick,
Nottingham,
England NG4 2AN.

LABTECH NOTEBOOK version 5
Laboratories Technologies Corporation,
400 Research Drive,
Wilmington MA,
USA 01887.

T 30 FD torque transducer and KMN 902.D signal amplifier
Hottinger Baldwin Messtechnik GmbH
Postfach 4235,
Im Tiefen See 45,
D-6100 Darmstadt
Deutschland.

Druck 1 bar differential pressure transducer
Druck Limited,
Fir Tree Lane,
Groby,
Leicester,
England LE6 0FH.

HP 8452A diode array spectrophotometer
Waldbronn Analytical Division,
Hewlett Packard GmbH,
D-7517 Waldbronn 2,
Deutschland.

505S peristaltic pump drive unit and 303 pump heads
Watson-Marlow Limited,
Falmouth,
Cornwall,
England TR11 4RU.

APPENDIX 2

CALIBRATION OF TRANSDUCERS

A2.1 Shaft torque transducer

TORQUE CALIBRATION - ROTOR/STATOR MIXER

lever arm = (m) 0.35
g 9.81

Vol water	Mass kg	Newtons (N)	Torque (N m)	Meter	Torque (calc.) (N m)
0	0.000	0.000	0.000	147	0.004
84.7	0.085	0.831	0.291	308	0.292
489.4	0.489	4.801	1.680	1083	1.680
782.5	0.783	7.676	2.687	1640	2.677
1103.7	1.104	10.827	3.790	2260	3.787
1275.2	1.275	12.510	4.378	2595	4.387

Regression Output:

Constant	-0.260	
Std Err of Y Est	0.007	
R Squared	1.000	
No. of Observations	6.000	
Degrees of Freedom	4.000	
X Coefficient(s)	0.001791	(slope)
Std Err of Coef.	3.06E-06	

A2.2 Differential pressure transducer

SINGLE CHANNEL
CALIBRATION CERTIFICATE

Calibration Date: 4/11/93 Calibration Period (months): 12

Device Type: PTX 120/WL.

Serial No/Plant No: 443710.

Manufacturer: Druck

Source: "

Ambient Temperature: 20°C.

Measurement Range: 0 - 1 Bar Diff

Calibration Instruction No: C101.

INPUT UNITS Bar.	OUTPUT UNITS Volts	DISPLAY UNITS
0.000	0.000	N/A
0.200	1.003	
0.400	1.998	
0.600	2.998	
0.800	4.00	
1.000	5.00	
0.800	4.00	
0.600	3.003	
0.400	2.005	
0.200	1.005	
0.000	0.000	
Comments		

Calibrated by: J. Knopp Signed:

EC05 Rev 0

APPENDIX 3

PROCEDURE FOR DIAZO-COUPLING TESTS

The chemicals used for the diazo-coupling experiments are given in Table A3.1; all chemicals were supplied by BHD Chemicals, Poole, England.

Production of the diazotised-sulphanilic acid must take place in a fume cupboard, as some of the chemicals are harmful and some toxic nitrous gases are produced by the reaction.

Table A3.1 Chemicals used

Name	Formula	Molar mass (g mol^{-1})
sulphanilic acid	$NH_2.C_6H_4.SO_3H$	173.19
sodium nitrite	$NaNO_2$	69.00
sodium hydrogen carbonate	$NaHCO_3$	84.03
sodium carbonate	Na_2CO_3	105.99
hydrochloric acid	HCl	- (sp. gr. 1.18)
urea	$NH_2.CO.NH_2$	60.06
1-naphthol	$C_{10}H_7OH$	144.17
2-naphthol	$C_{10}H_7OH$	144.17

Naphthol (*A* + *C*) solution

The 1-naphthol and 2-naphthol were dissolved into de-ionised water and stirred for approximately 12 hours (during cold weather, these were pre-dissolved in ethanol). This solution was transferred into the delivery tank (Tank 1 in Figure 3.1). Then

solid sodium carbonate and sodium bicarbonate were added (to buffer the solution to remove pH gradients in the reaction zones). The temperature was raised to 25 °C using an immersion heater controlled by a thermostat.

Diazotised sulphanilic acid (*B* solution)

Anhydrous sodium carbonate was dissolved into de-ionised water in a conical flask. Then sulphanilic acid was added (over a period of approximately 10 to 15 minutes to avoid foaming). This solution was cooled to 0 °C by placing in an ice bath.

Sodium nitrite was dissolved in de-ionised water, in a separate flask, and also cooled to 0 °C.

Hydrochloric acid was added to a small amount of ice (made with de-ionised water) in a beaker (volume approx 3 litres), forming a slurry and stirred using a magnetic stirrer and follower.

The sodium nitrite and anhydrous sodium carbonate + sulphanilic acid solution described above were added simultaneously to the hydrochloric acid slurry and mixed vigorously. A small quantity of nitrous gas (toxic) is given off at this stage. Further ice was added to ensure that the temperature remained at 0°C. After approximately 15 minutes of stirring, urea was added to react with any excess sodium nitrite. The solution was stirred for a further 5 minutes. Following this, the solution was transferred to a measuring cylinder and made up to a half of the final volume by adding de-ionised water. De-ionised water, previously warmed to 50 °C, was added and used to adjust the temperature of the final solution to 25 °C.

Finally the resulting solution was transferred to the vessel and moved to the test rig,

where it was connected to the peristaltic pump that fed the *B* solution into the mixer.

APPENDIX 4

RAW DATA

A4.1 Differential pressure data

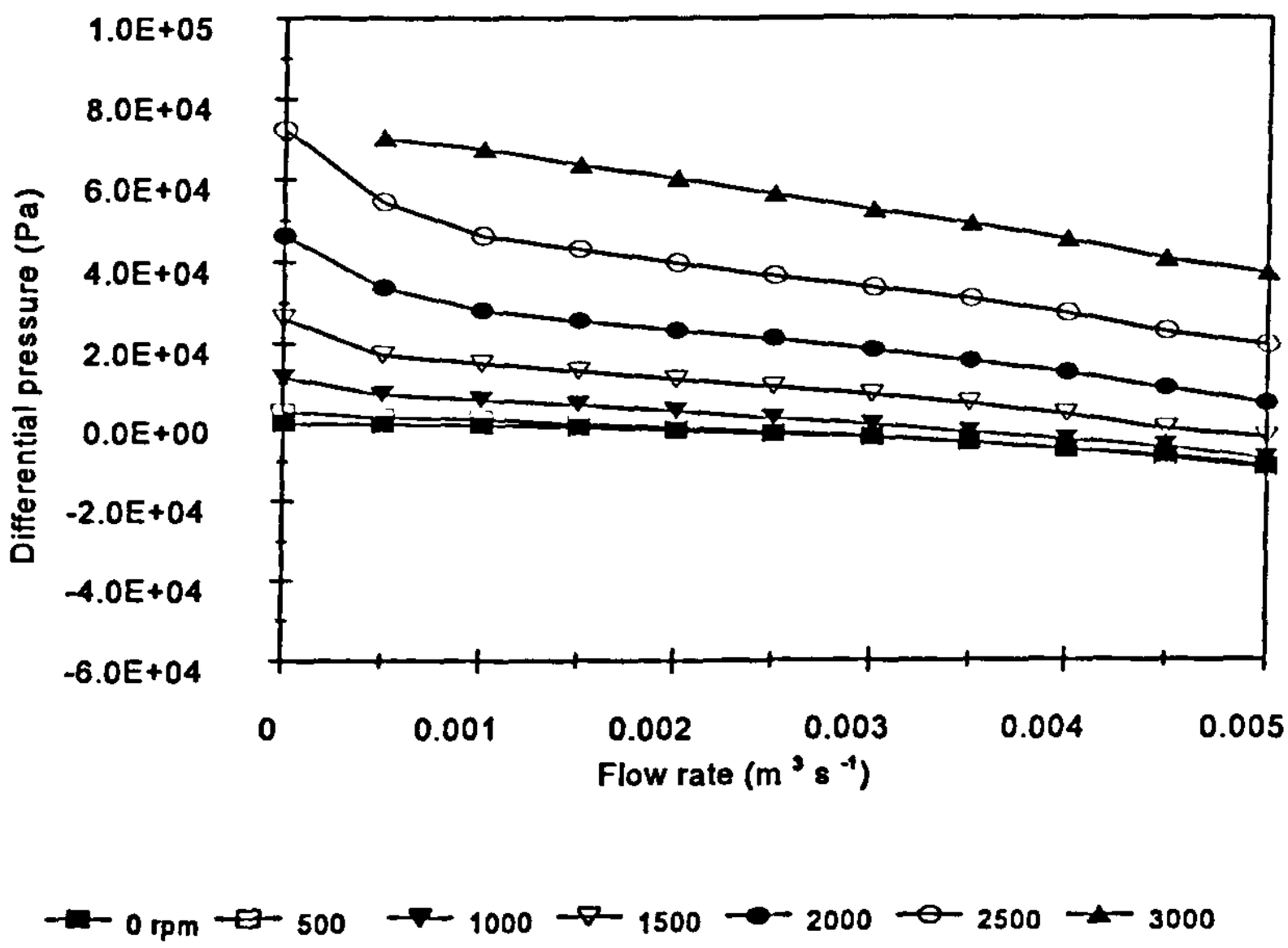

Figure A4.1 Differential pressure (r/18/50/119.6 & s/18/50/123.8)

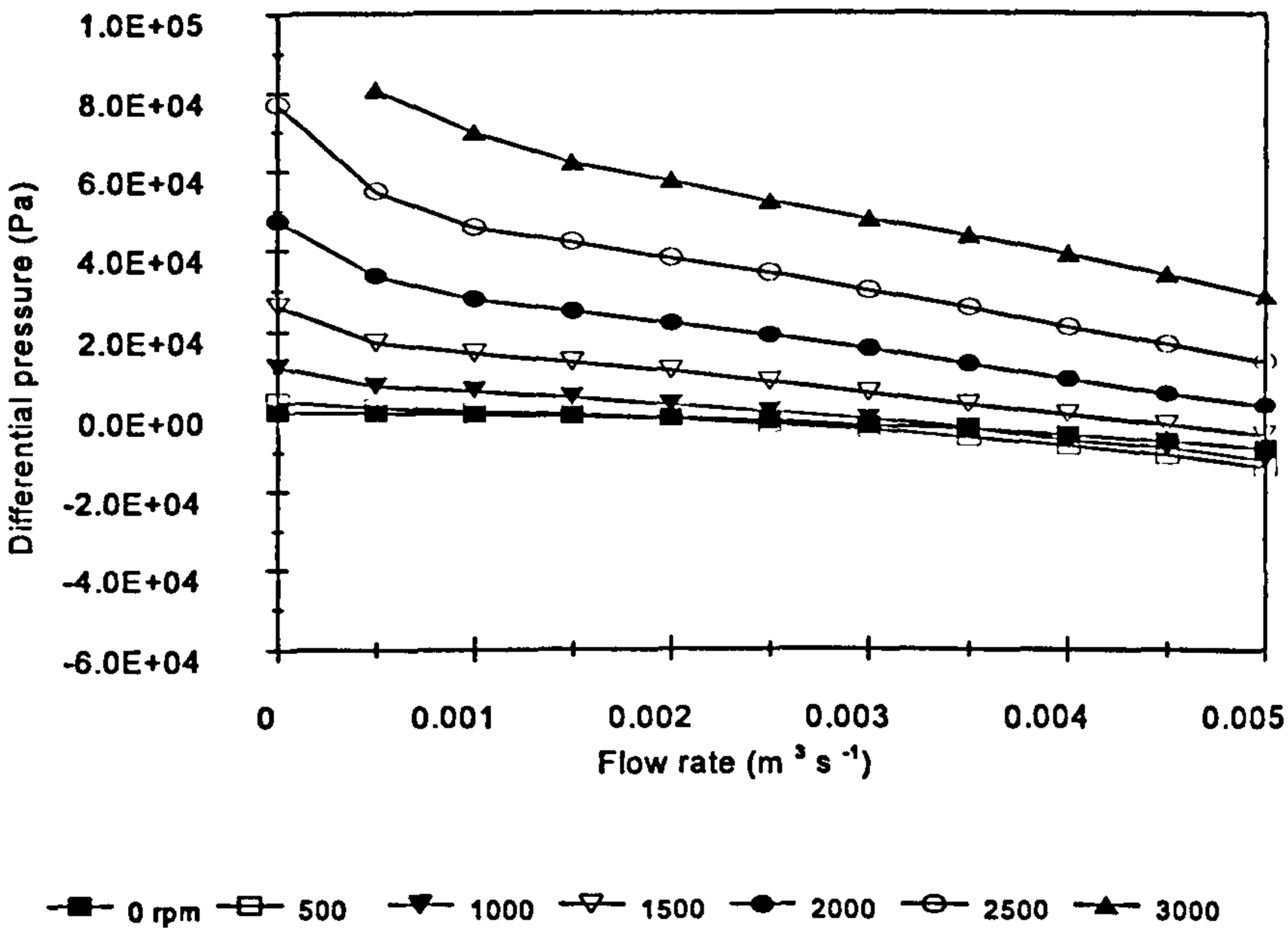

Figure A4.2 Differential pressure (r/18/50/119.6 & s/18/33/123.8)

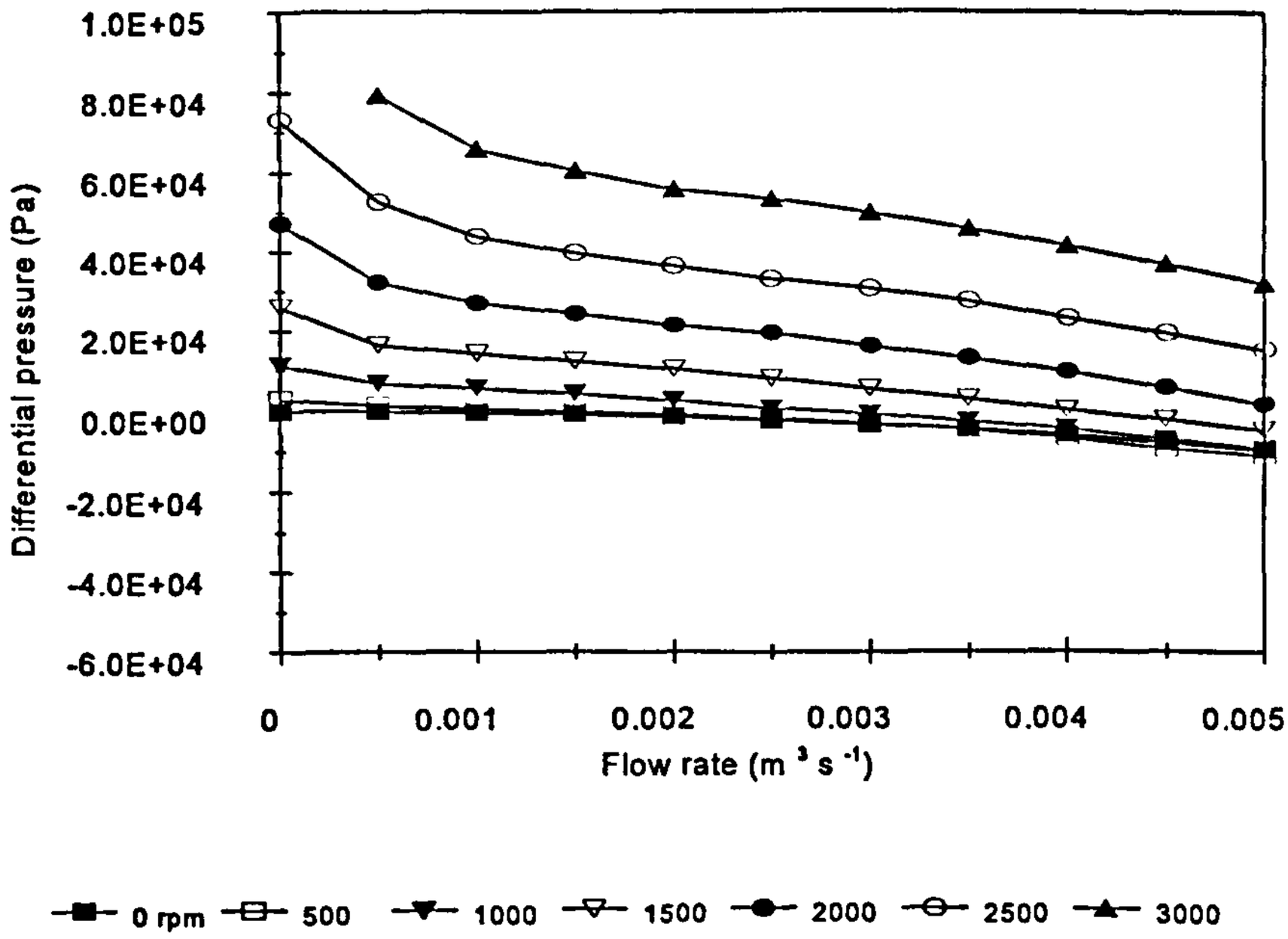

Figure A4.3 Differential pressure (r/18/50/119.6 & s/19/50/123.8)

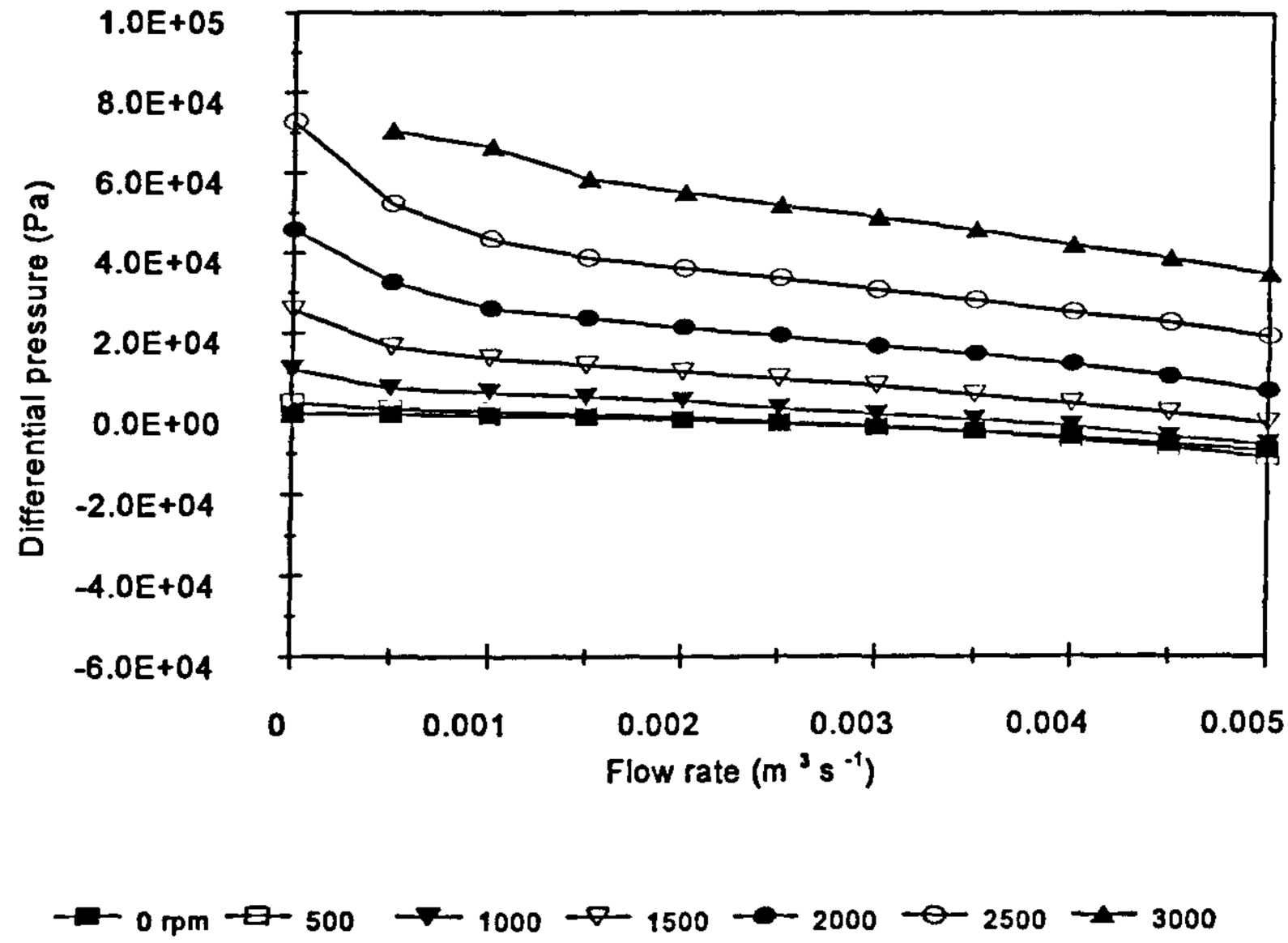

Figure A4.4 Differential pressure (r/18/50/119.6 & s/36/50/123.8)

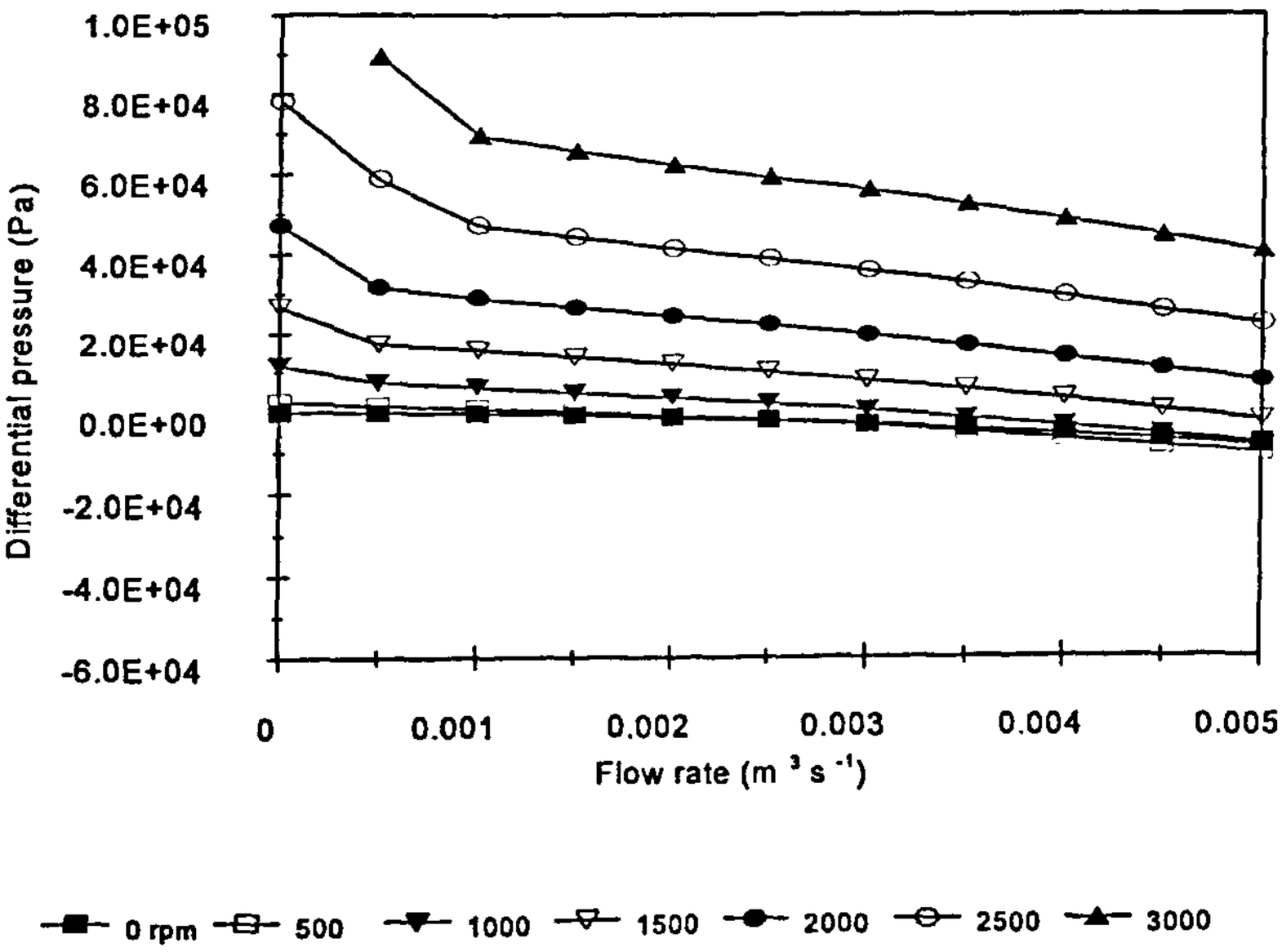

Figure A4.5 Differential pressure (r/12/67/121.45 & s/18/50/123.8)

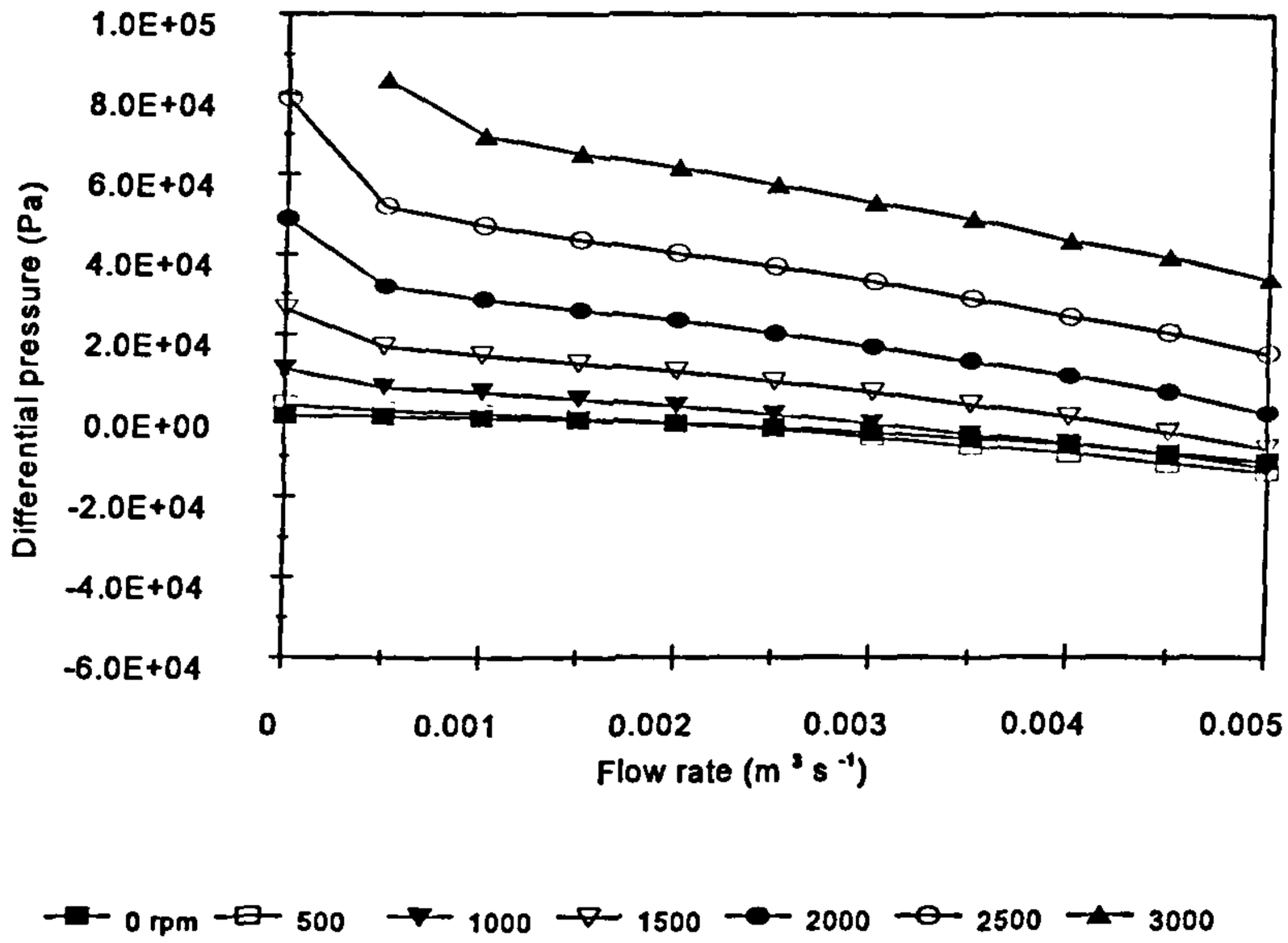

Figure A4.6 Differential pressure (r/12/67/121.45 & s/18/33/123.8)

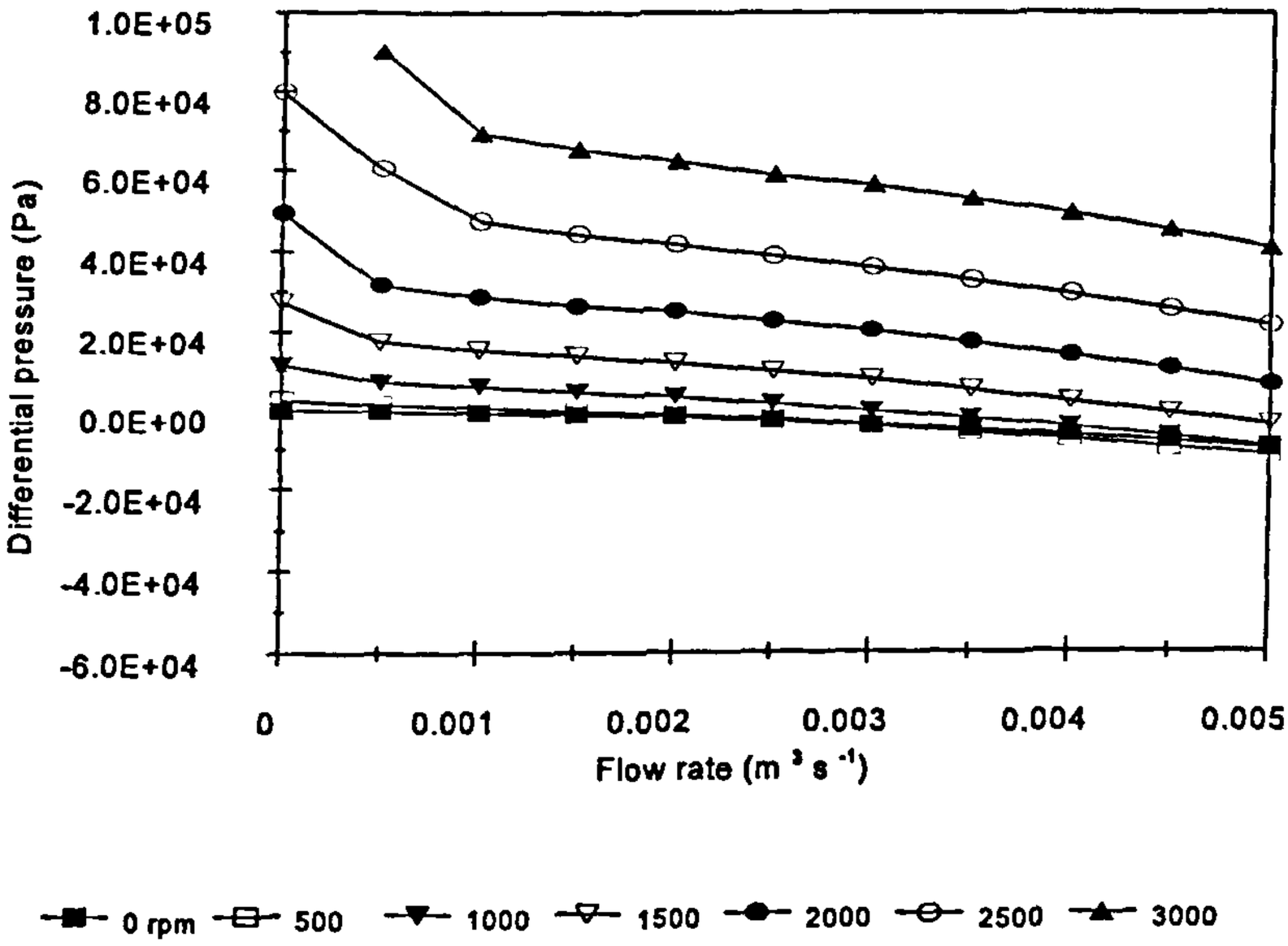

Figure A4.7 Differential pressure (r/12/67/121.45 & s/19/50/123.8)

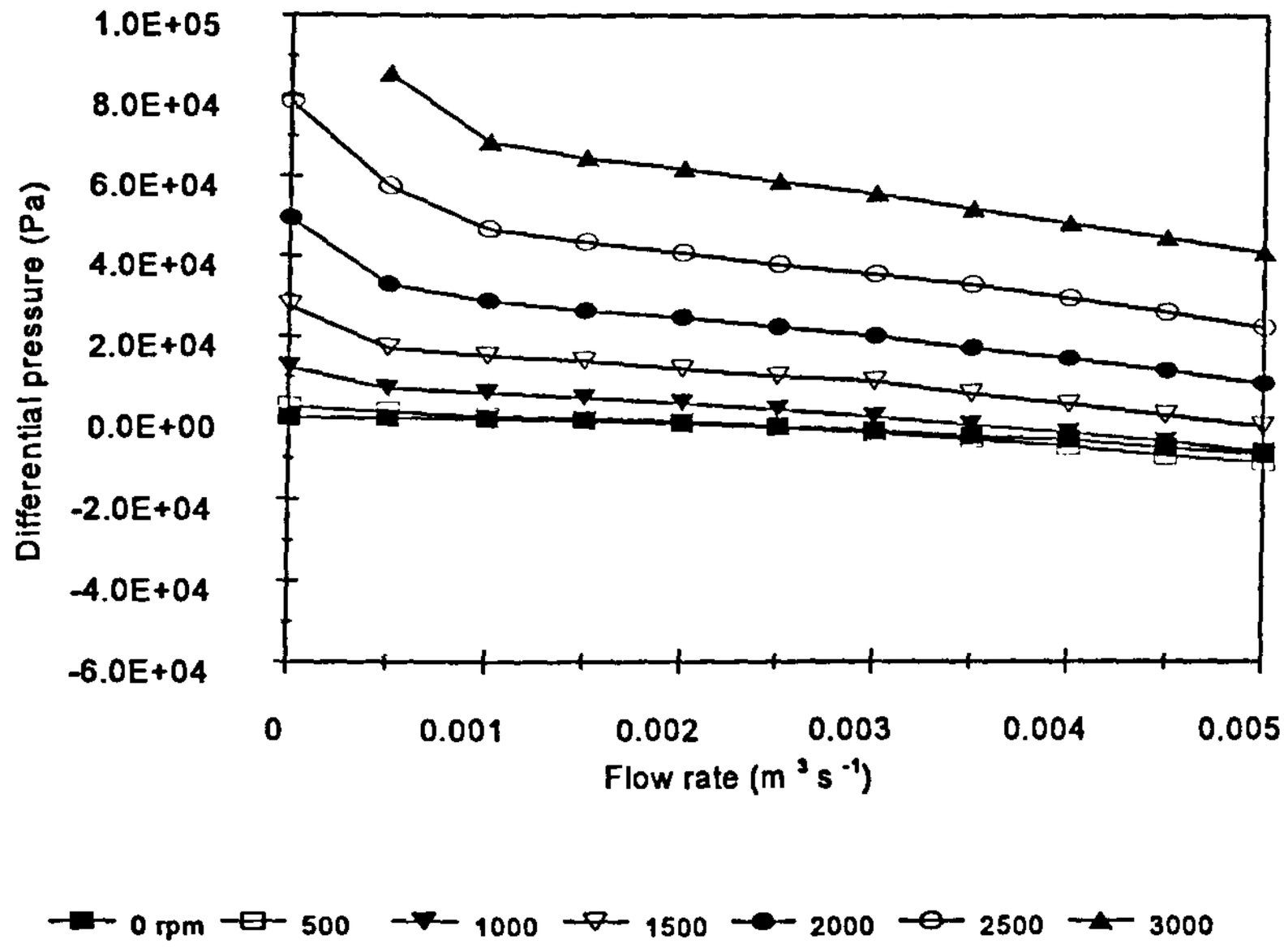

Figure A4.8 Differential pressure (r/12/67/121.45 & s/36/50/123.8)

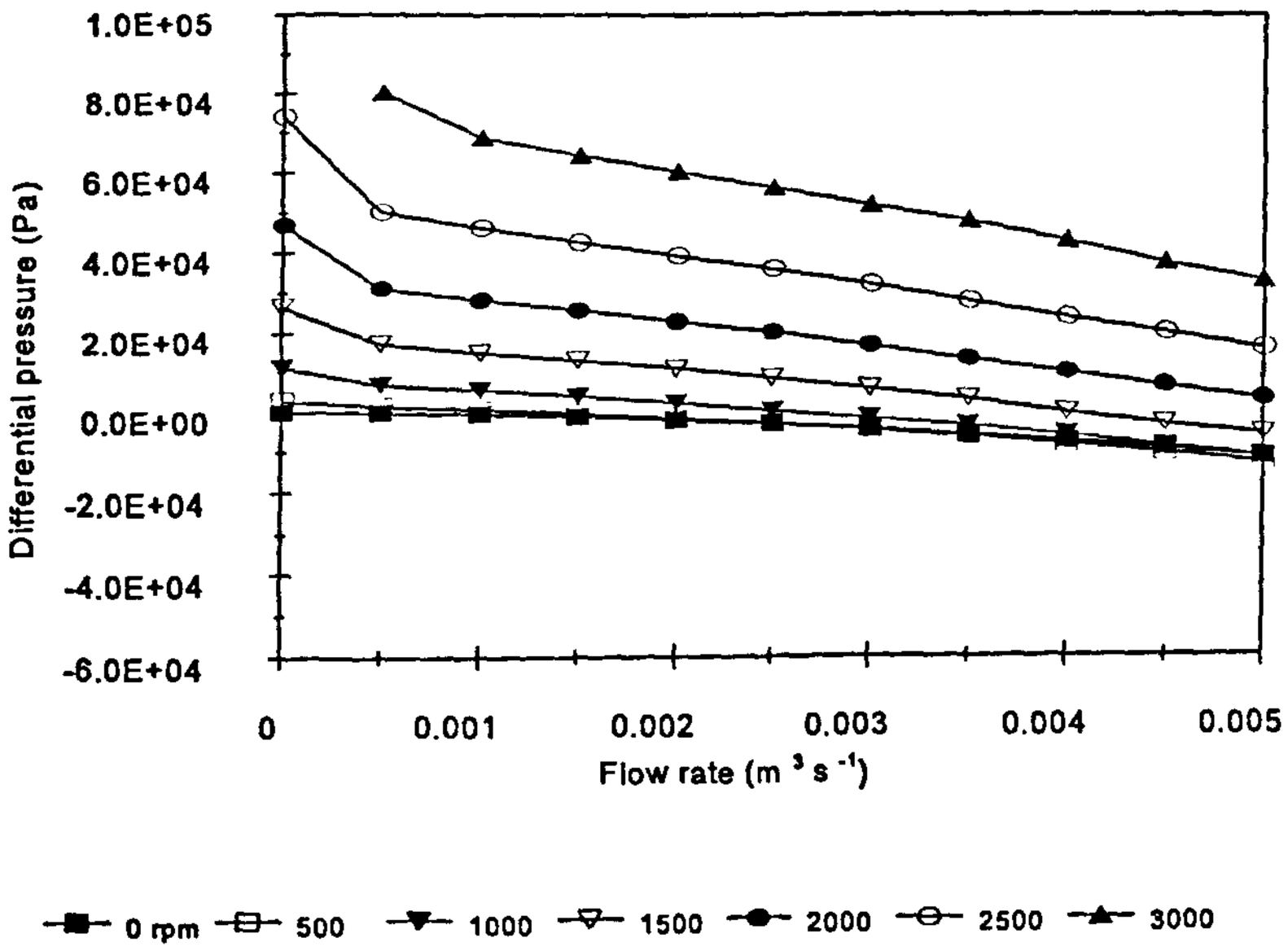

Figure A4.9 Differential pressure (r/50/50/121.45 & s/18/50/123.8)

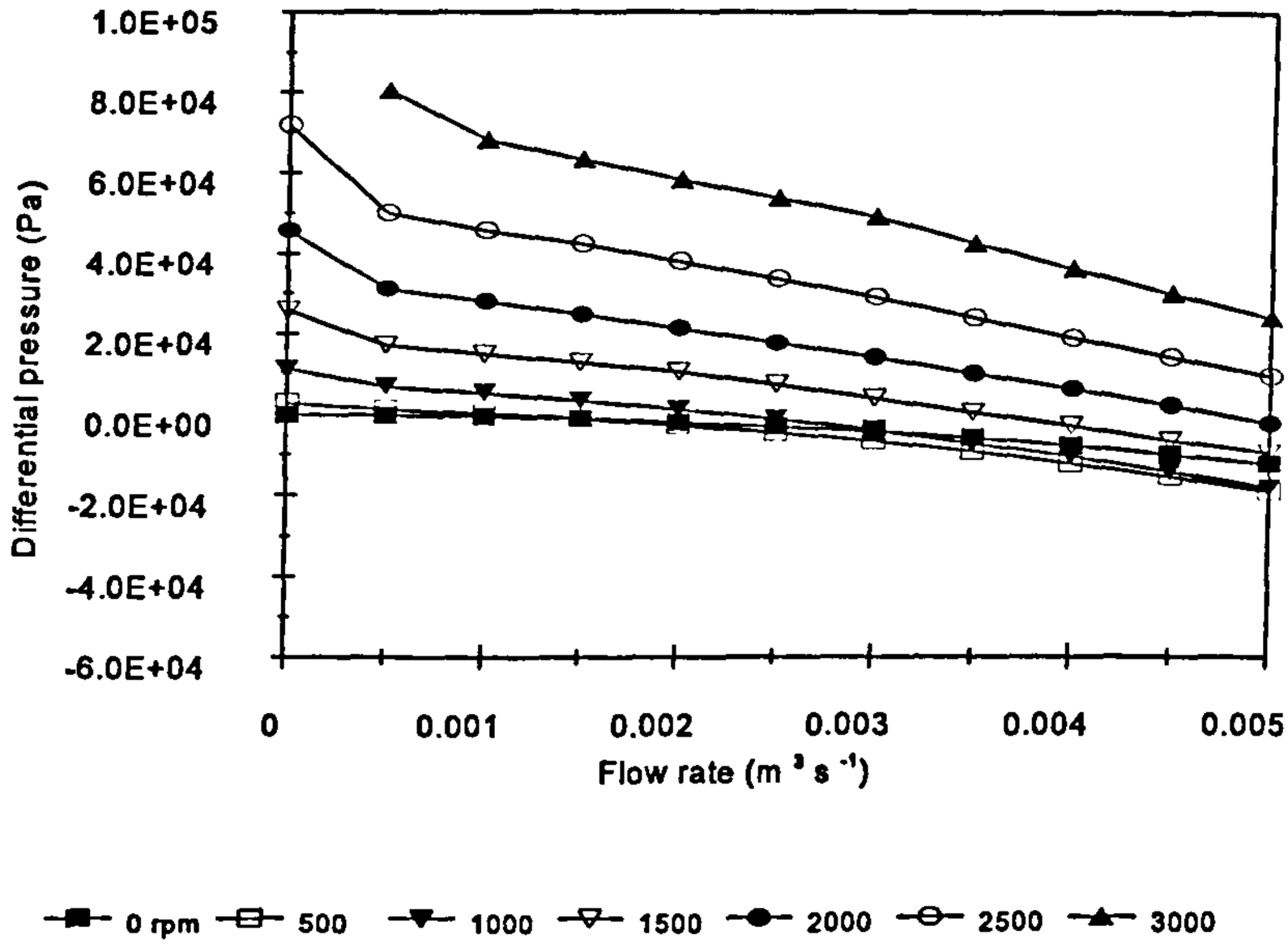

Figure A4.10 **Differential pressure (r/18/50/121.45 & s/18/33/123.8)**

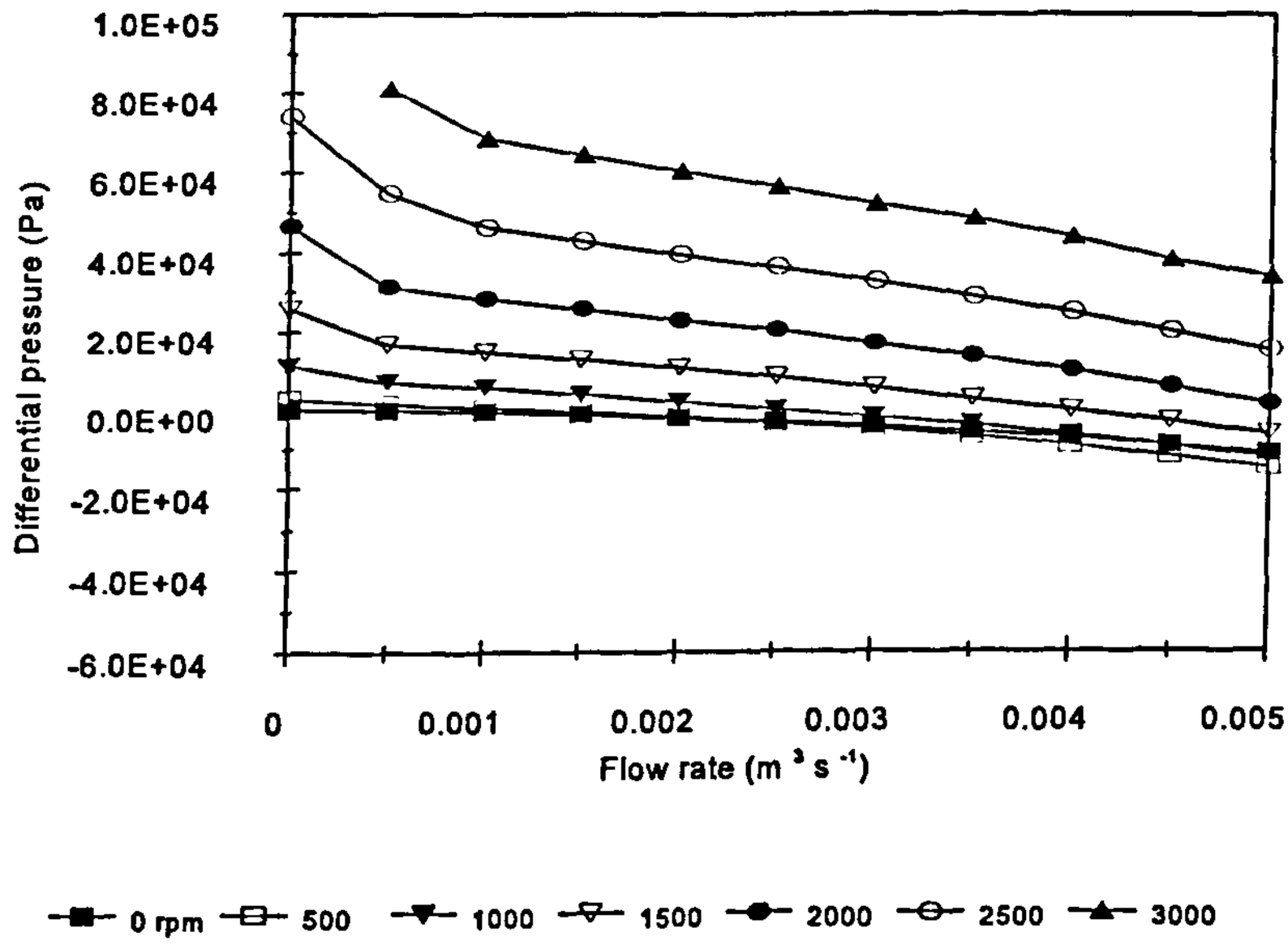

Figure A4.11 **Differential pressure (r/18/50/121.45 & s/19/50/123.8)**

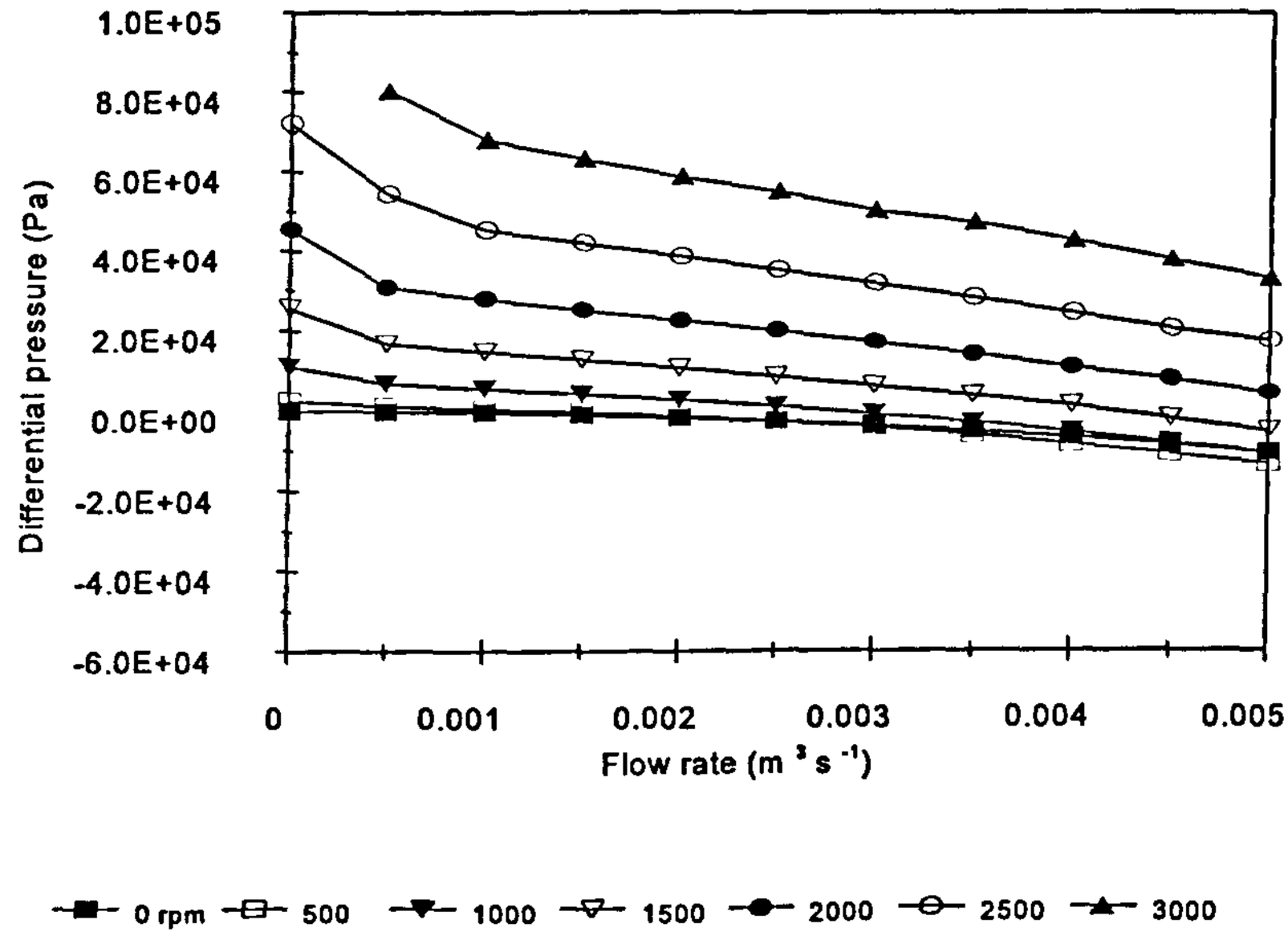

Figure A4.12 **Differential pressure (r/18/50/121.45 & s/36/50/123.8)**

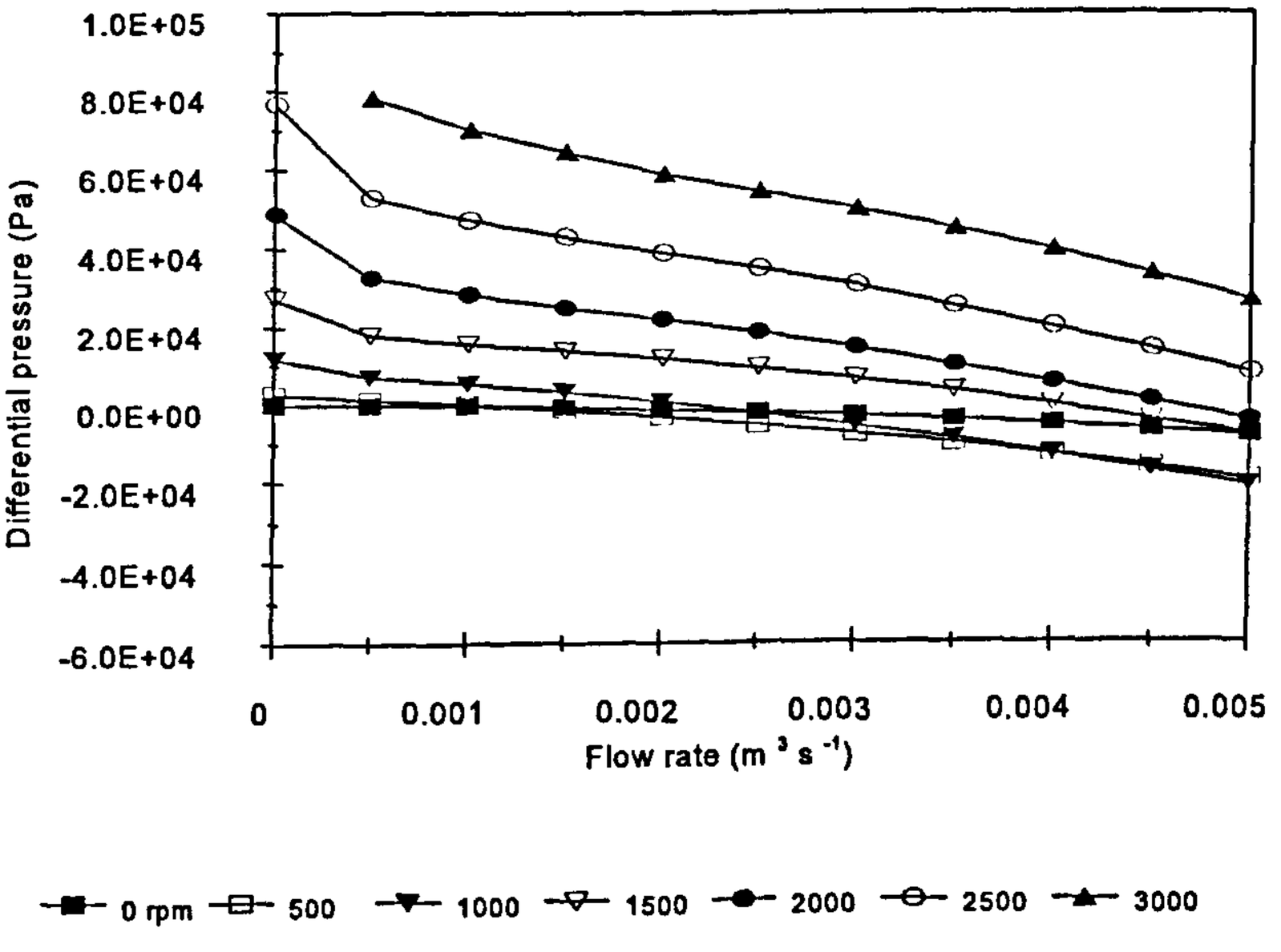

Figure A4.13 **Differential pressure (r/18/50/123.34 & s/18/50/123.8)**

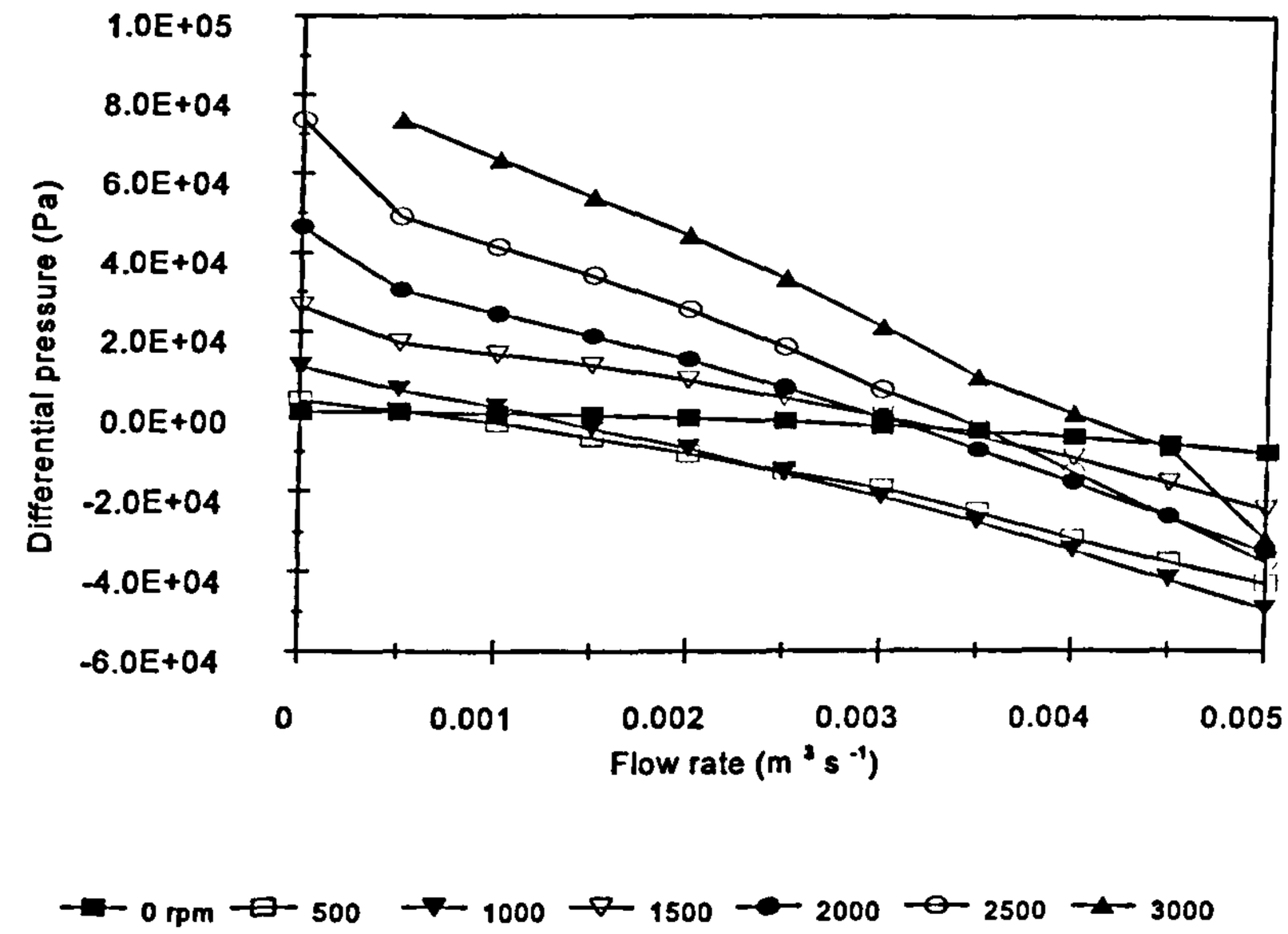

Figure A4.14 **Differential pressure (r/18/50/123.34 & s/18/33/123.8)**

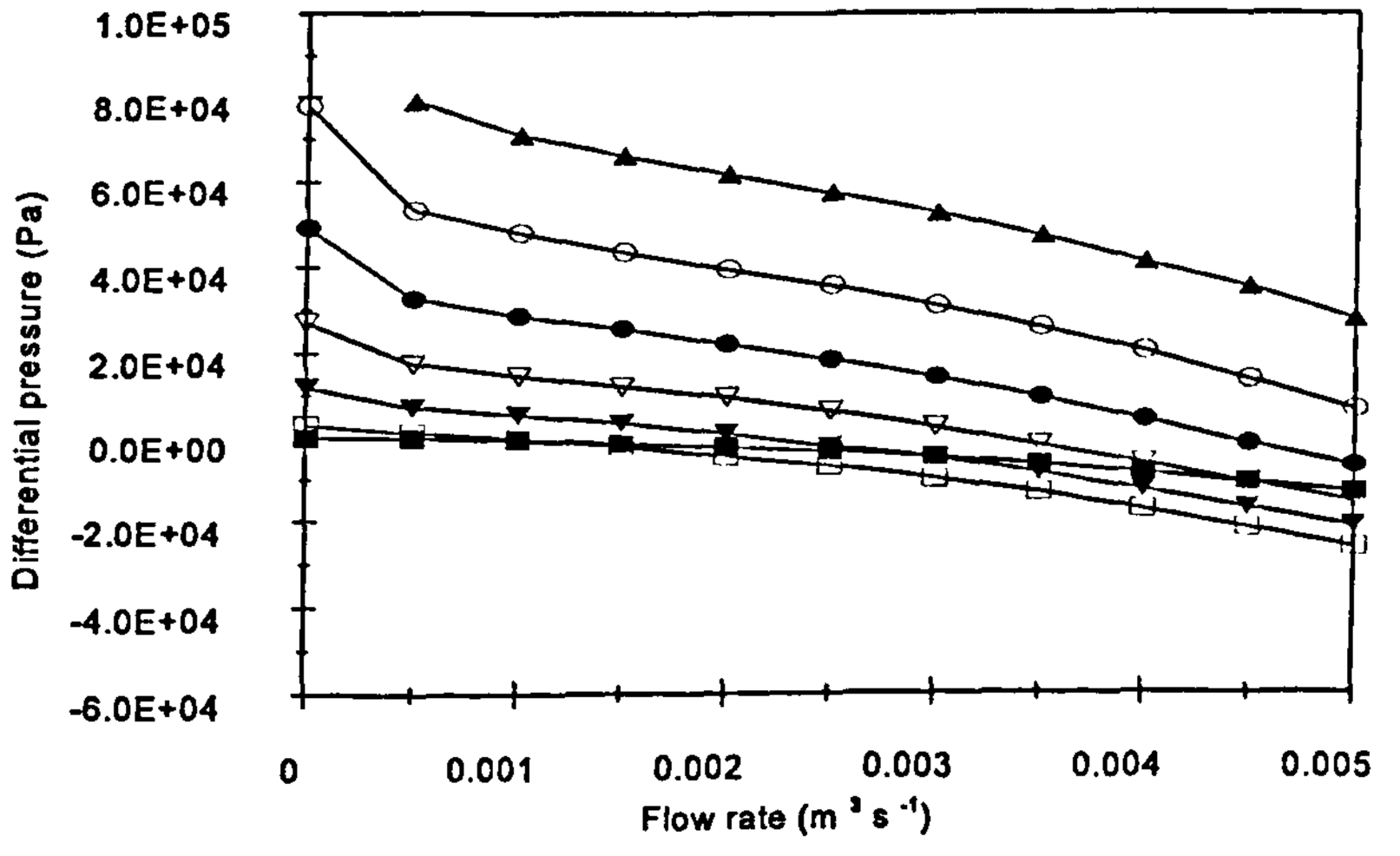

Figure A4.15 **Differential pressure (r/18/50/123.34 & s/19/50/123.8)**

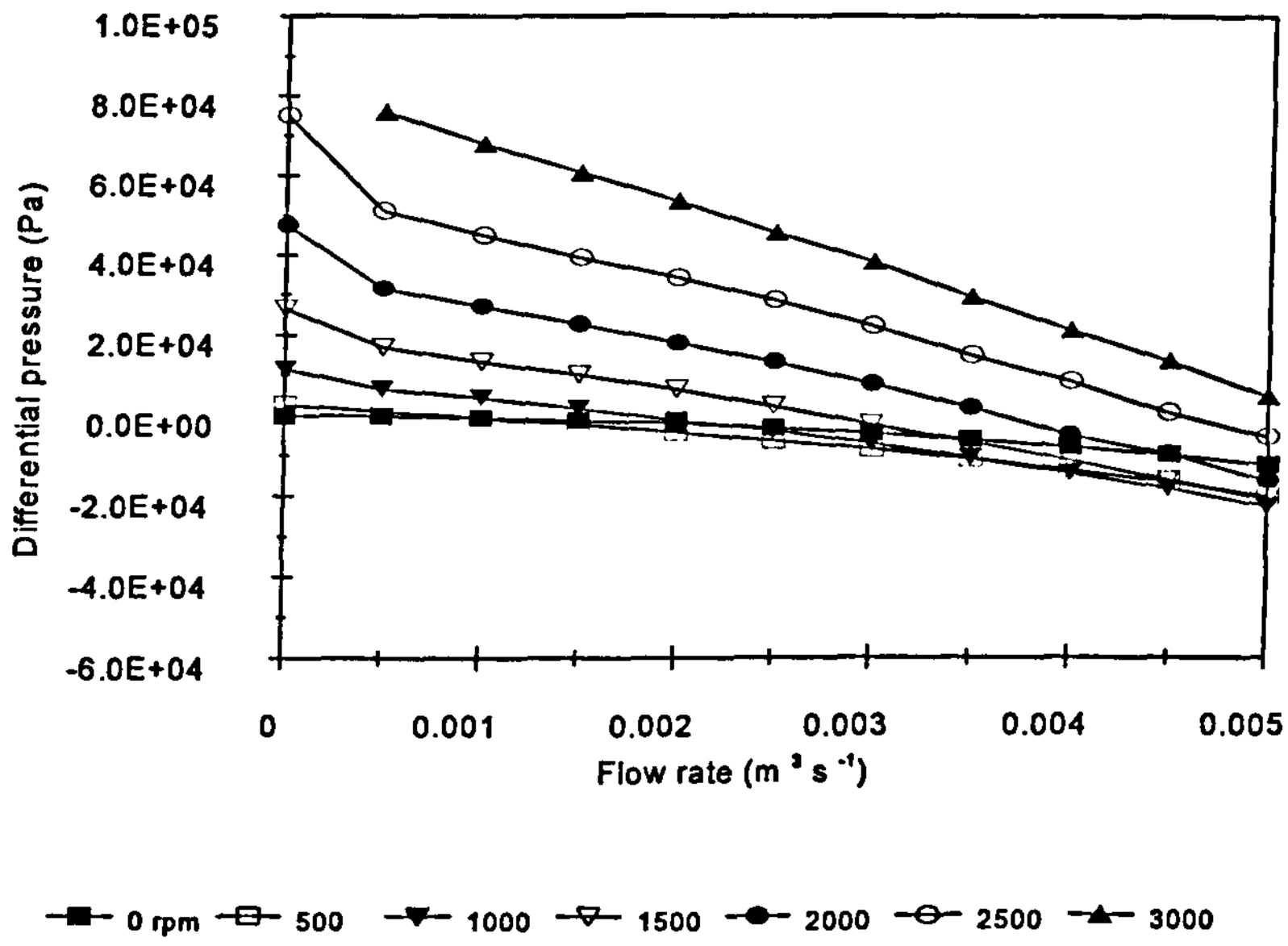

Figure A4.16 **Differential pressure (r/18/50/123.34 & s/36/50/123.8)**

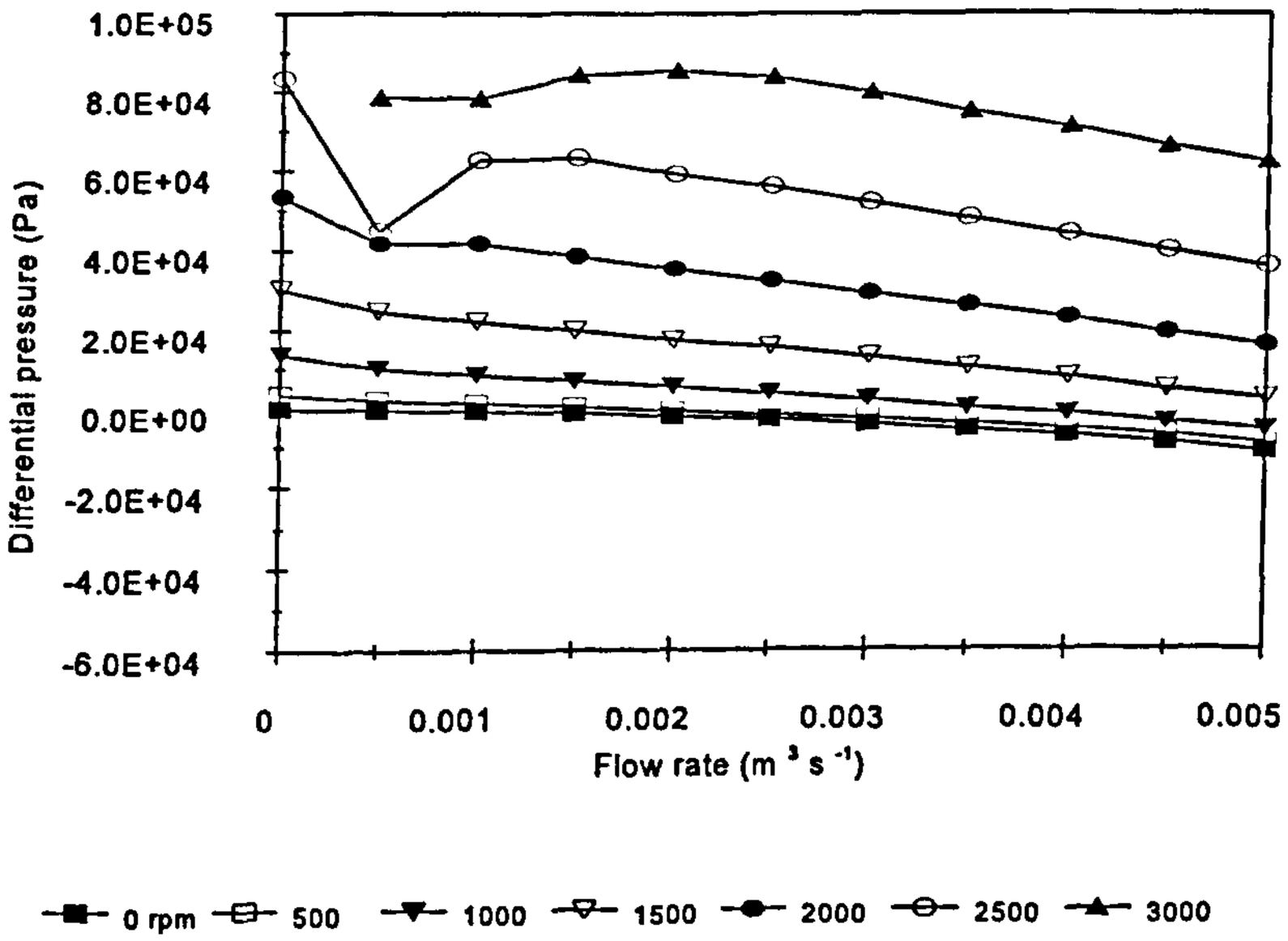

Figure A4.17 **Differential pressure (Silverson)**

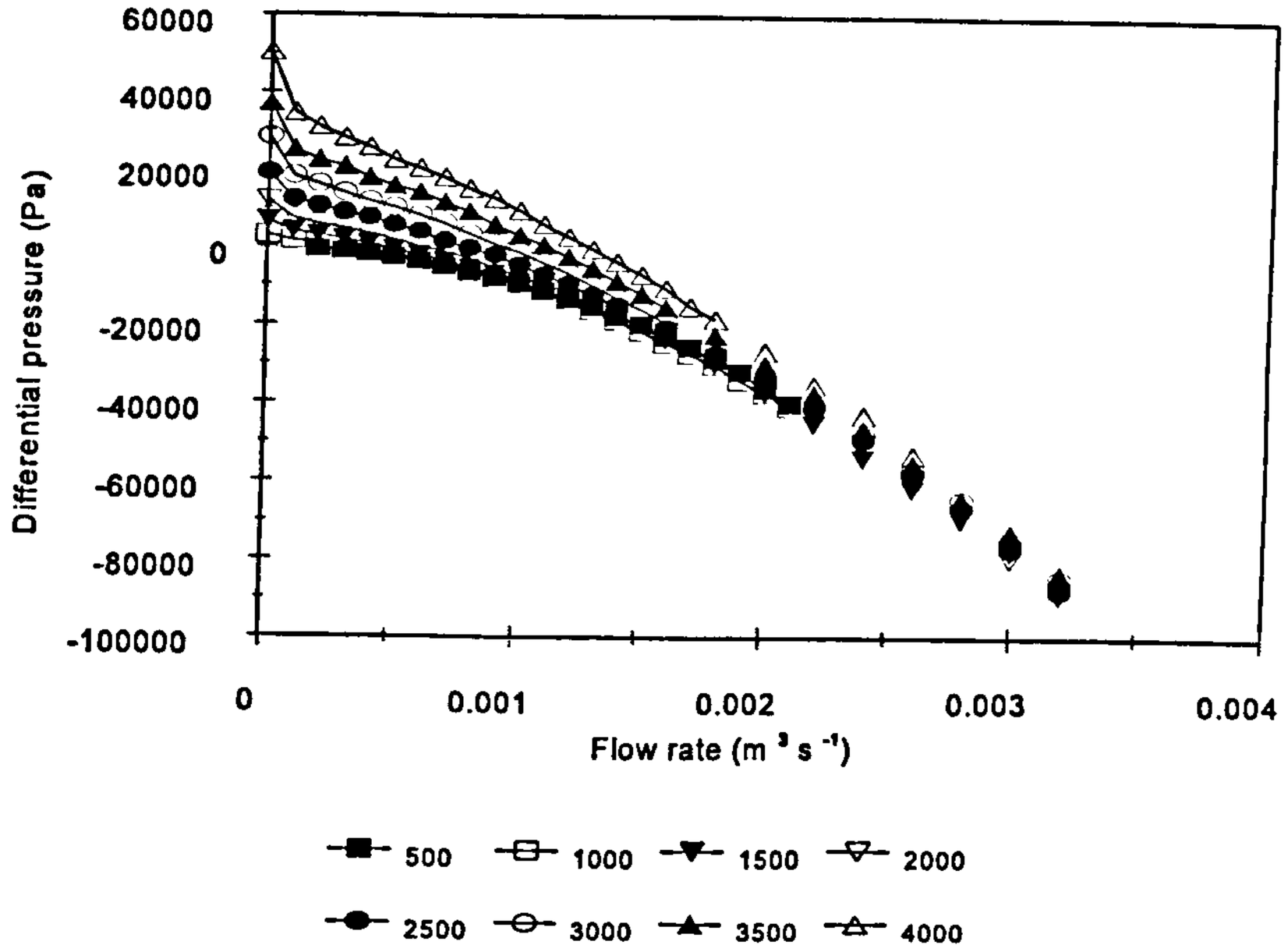

Figure A4.18 Differential pressure (Scale Toothed)

A4.2 Shaft torque data

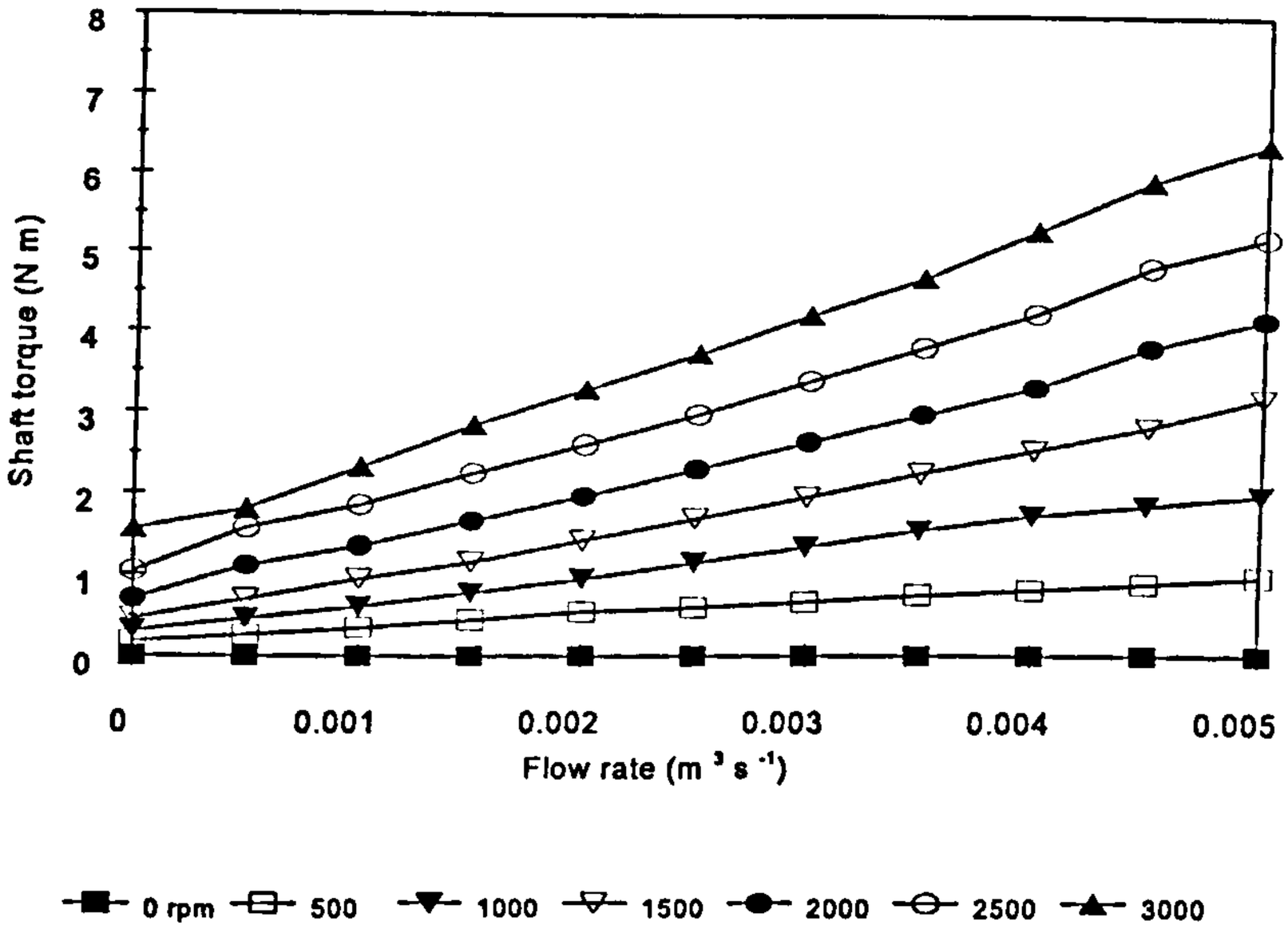

Figure A4.19 Shaft torque (r/18/50/119.6 & s/18/50/123.8)

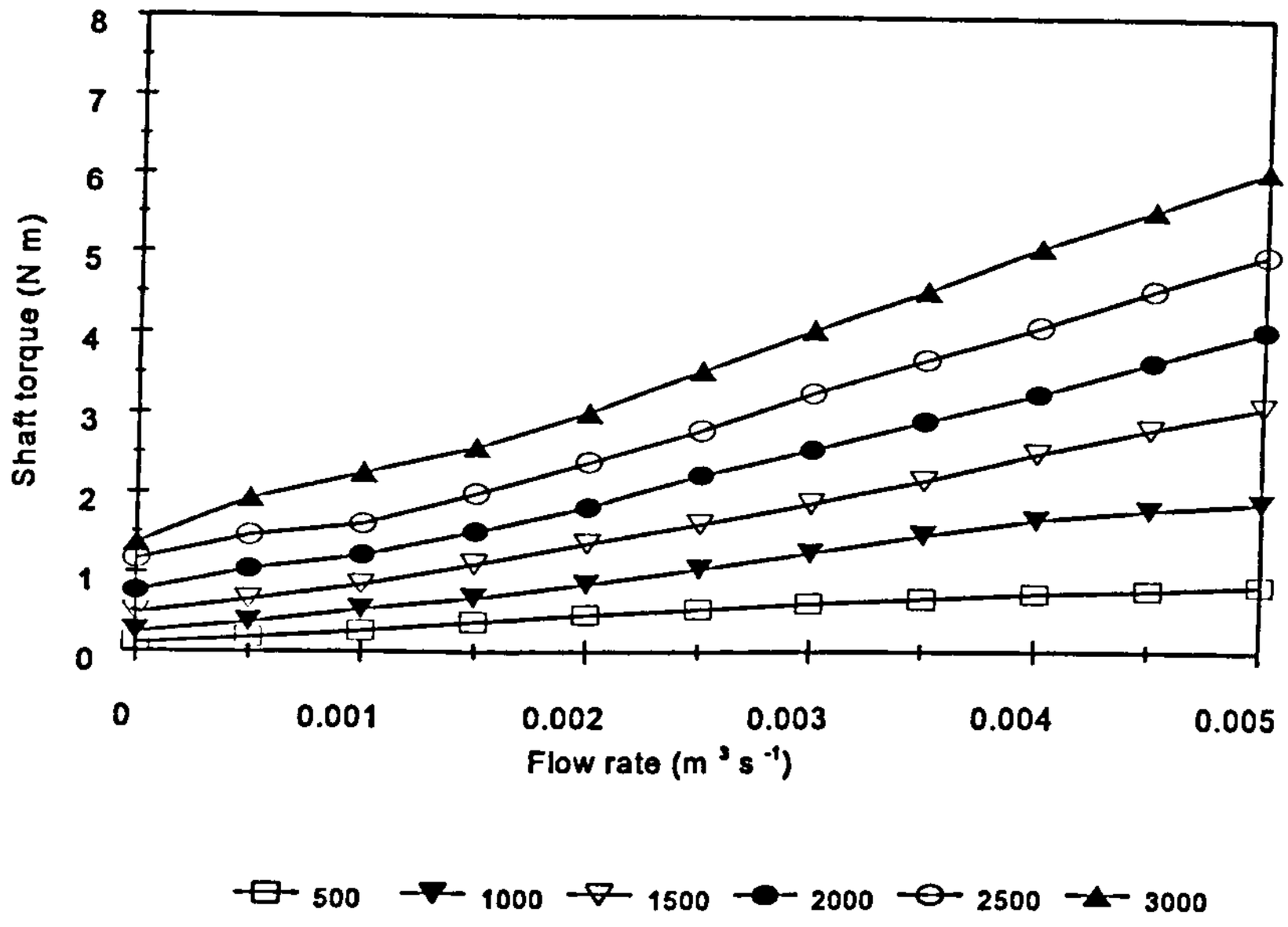

Figure A4.20 **Shaft torque (r/18/50/119.6 & s/18/33/123.8)**

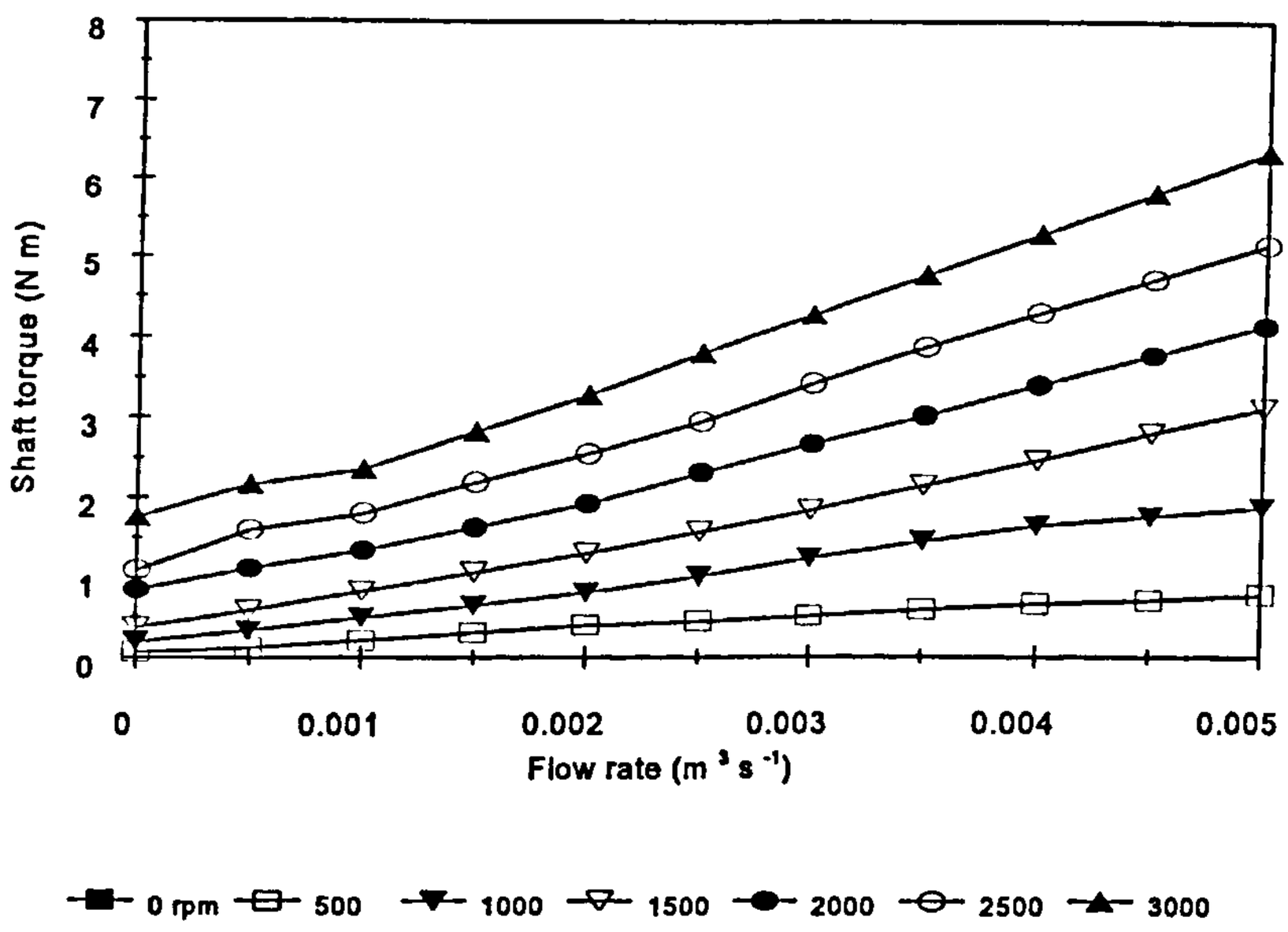

Figure A4.21 **Shaft torque (r/18/50/119.6 & s/19/50/123.8)**

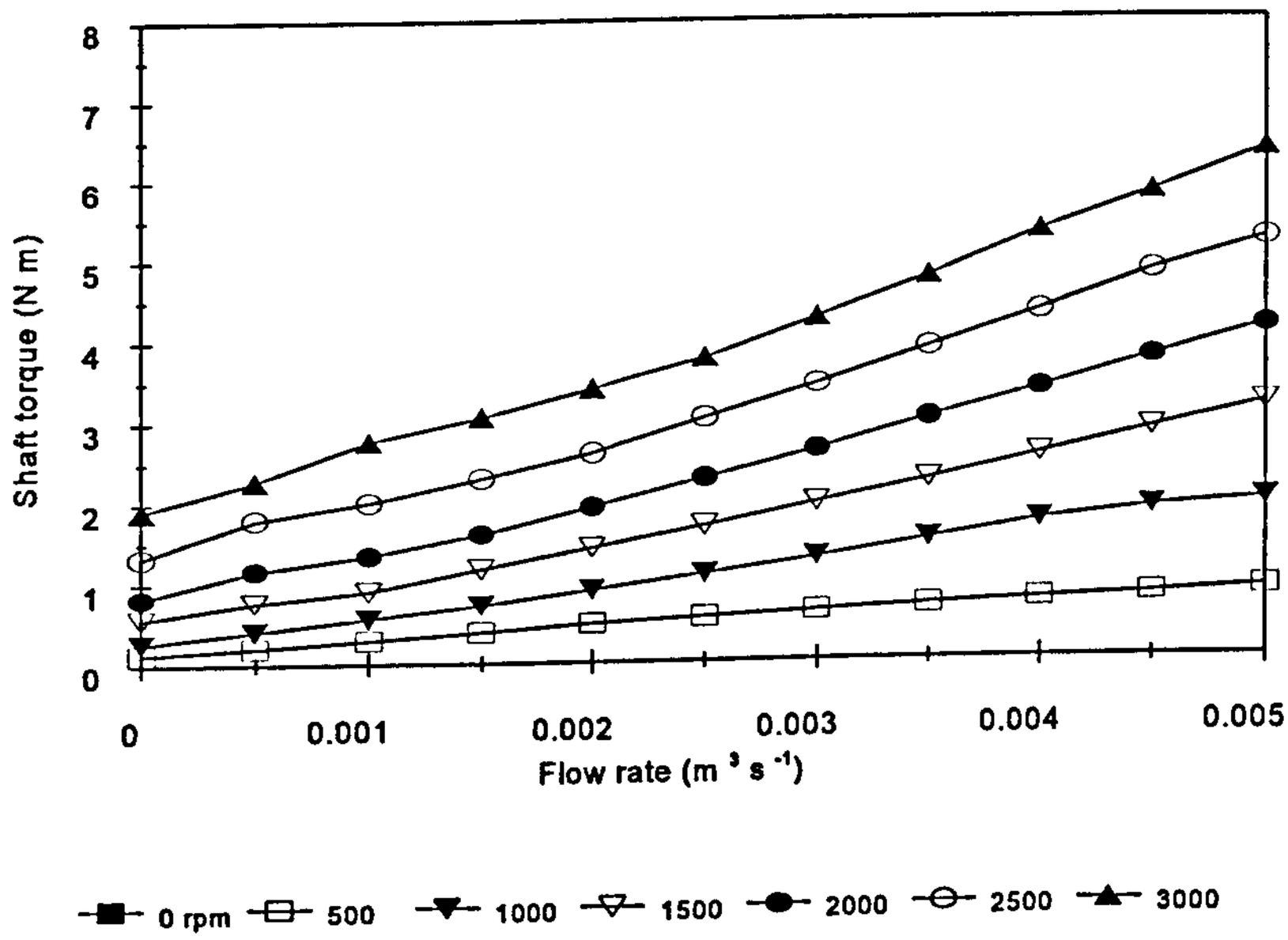

Figure A4.22 **Shaft torque (r/18/50/119.6 & s/36/50/123.8)**

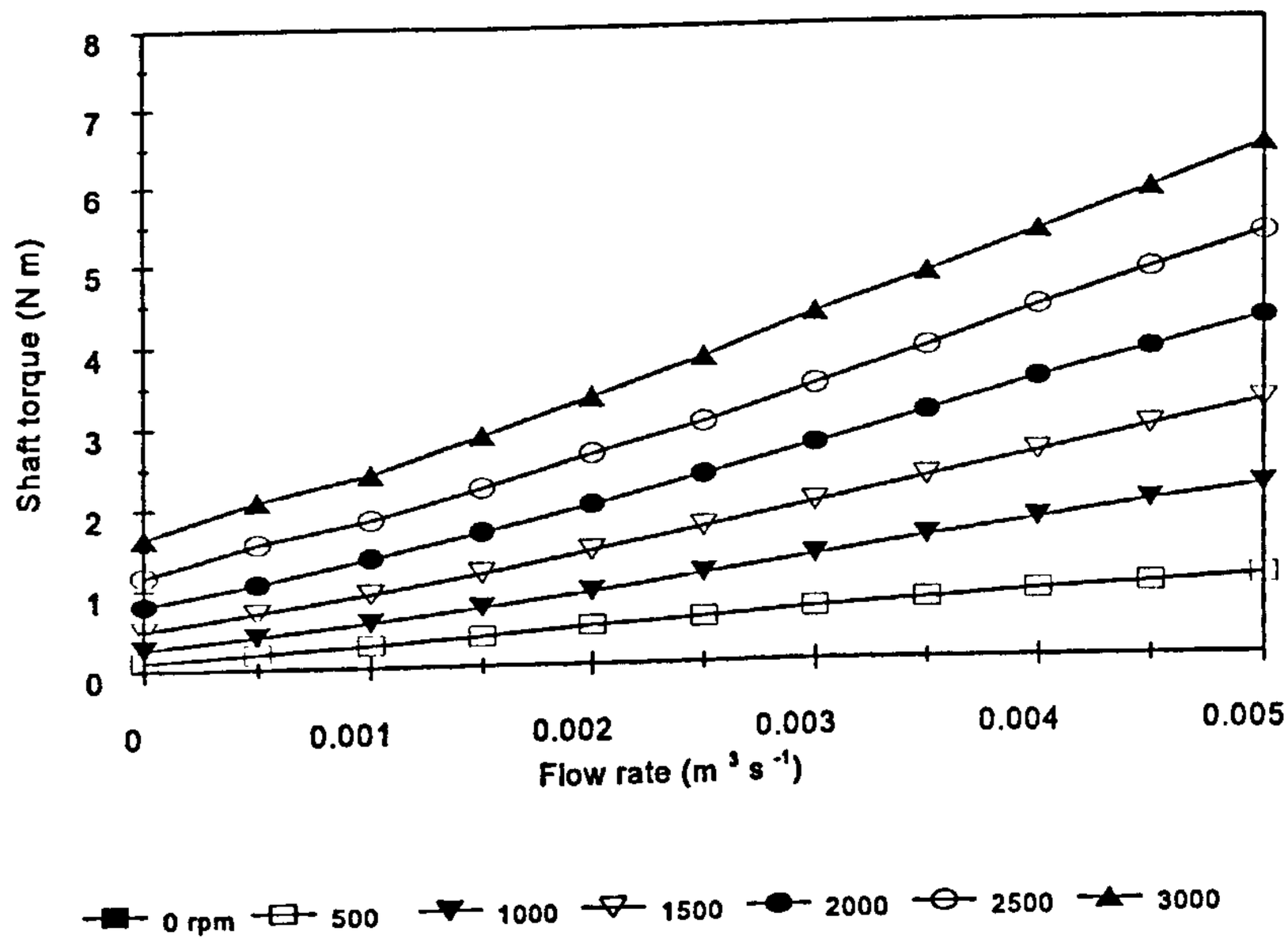

Figure A4.23 **Shaft torque (r/12/67/121.45 & s/18/50/123.8)**

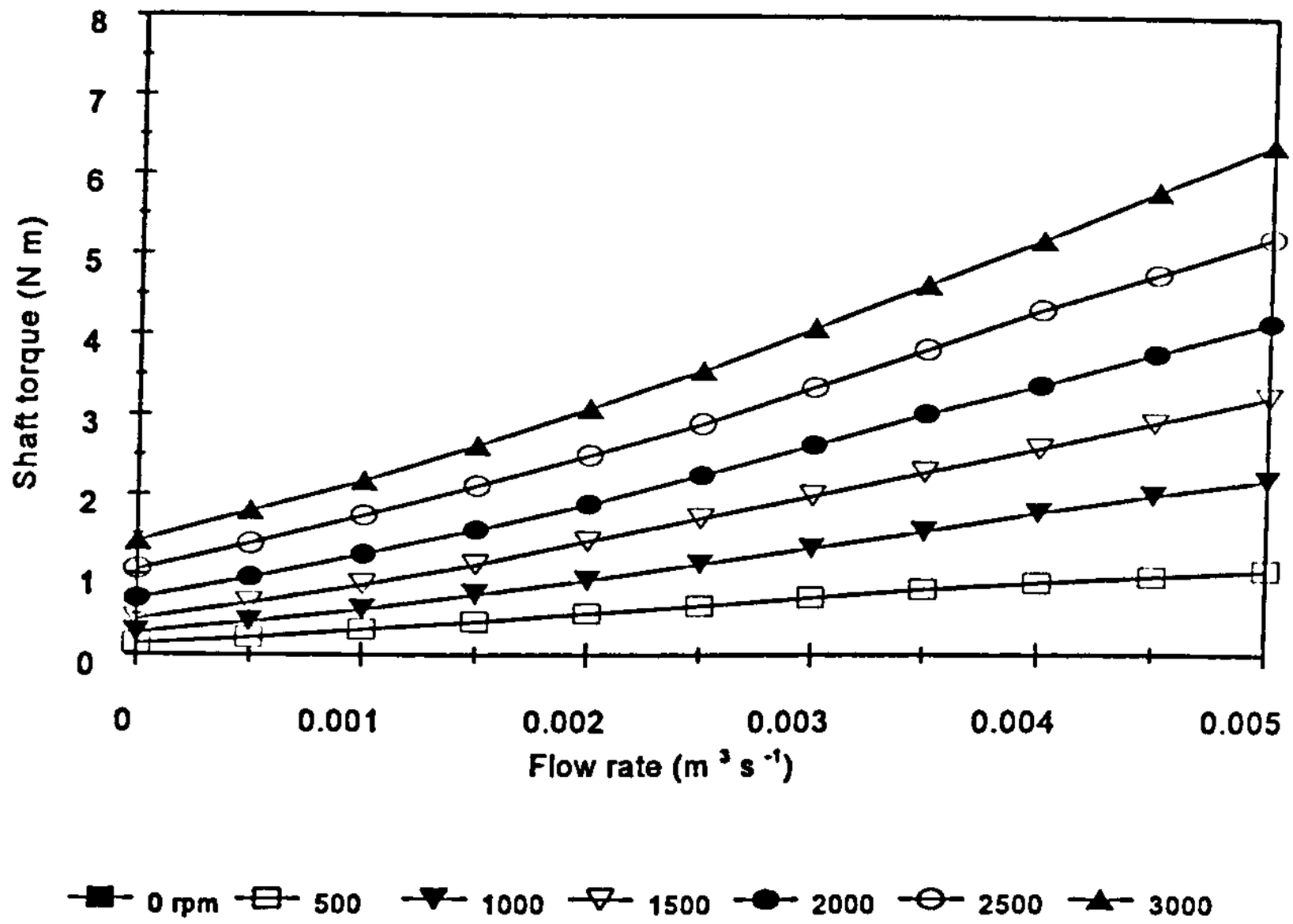

Figure A4.24 **Shaft torque (r/12/67/121.45 & s/18/33/123.8)**

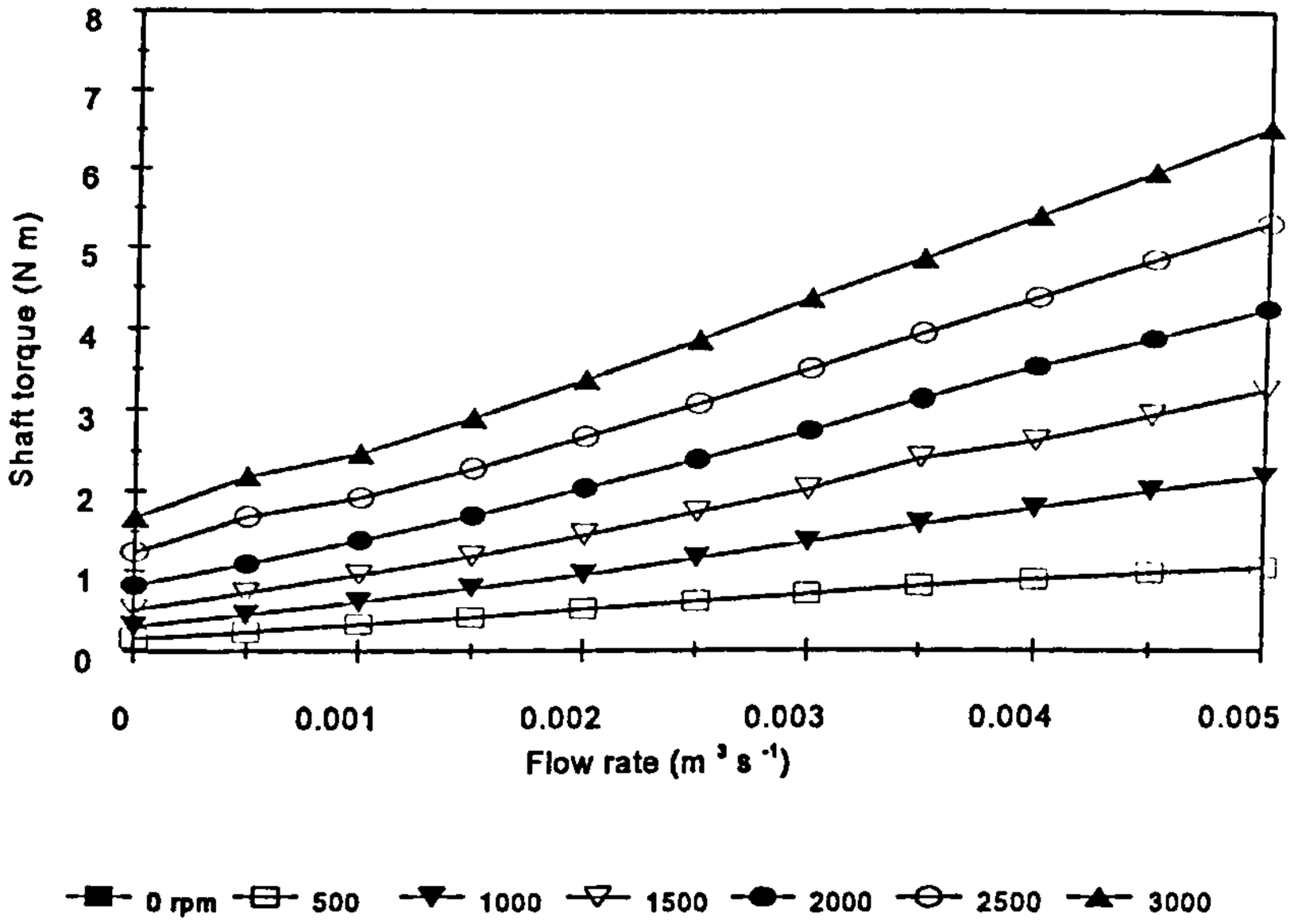

Figure A4.25 **Shaft torque (r/12/67/121.45 & s/19/50/123.8)**

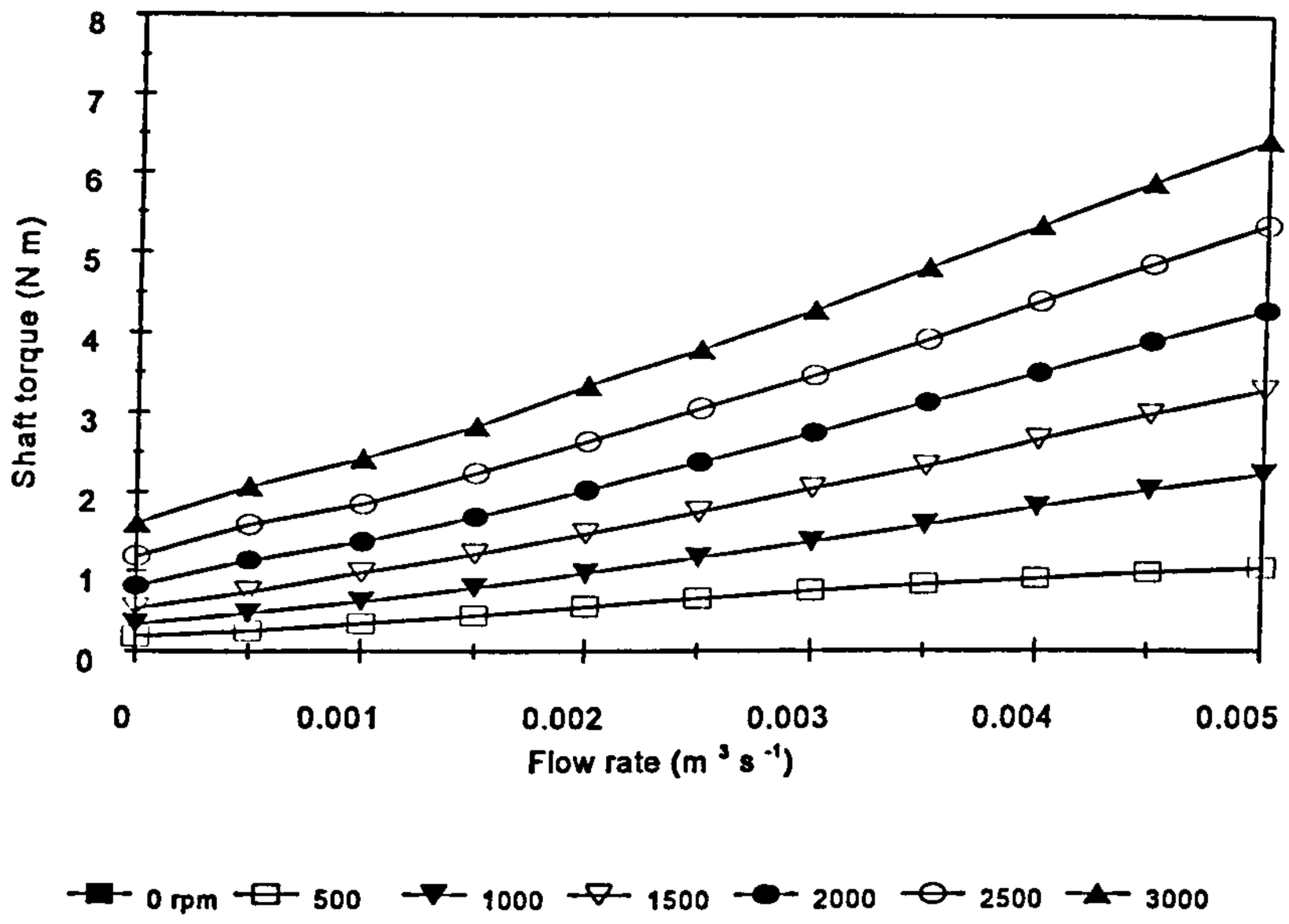

Figure A4.26 **Shaft torque (r/12/67/121.45 & s/36/50/123.8)**

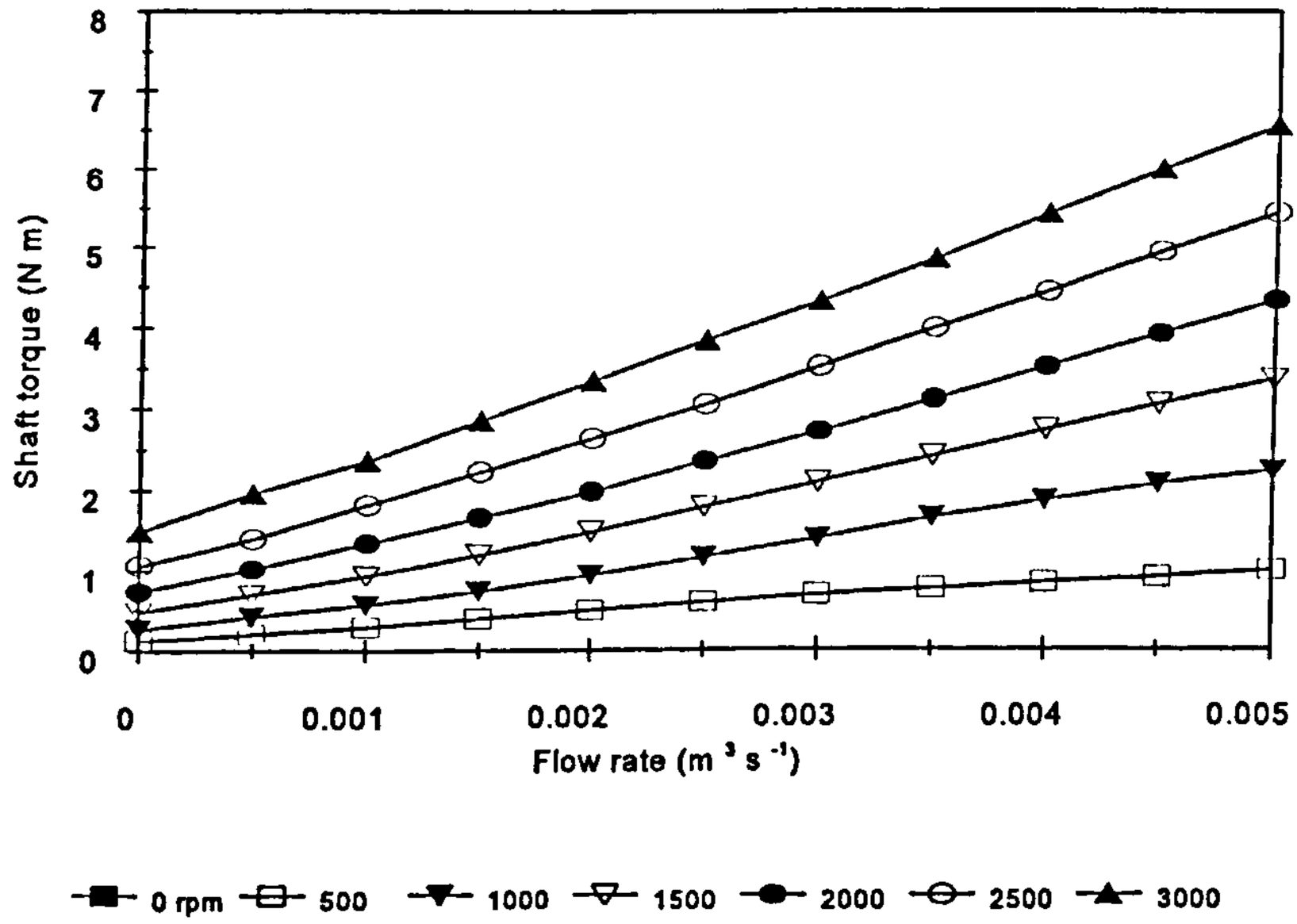

Figure A4.27 **Shaft torque (r/50/50/121.45 & s/18/50/123.8)**

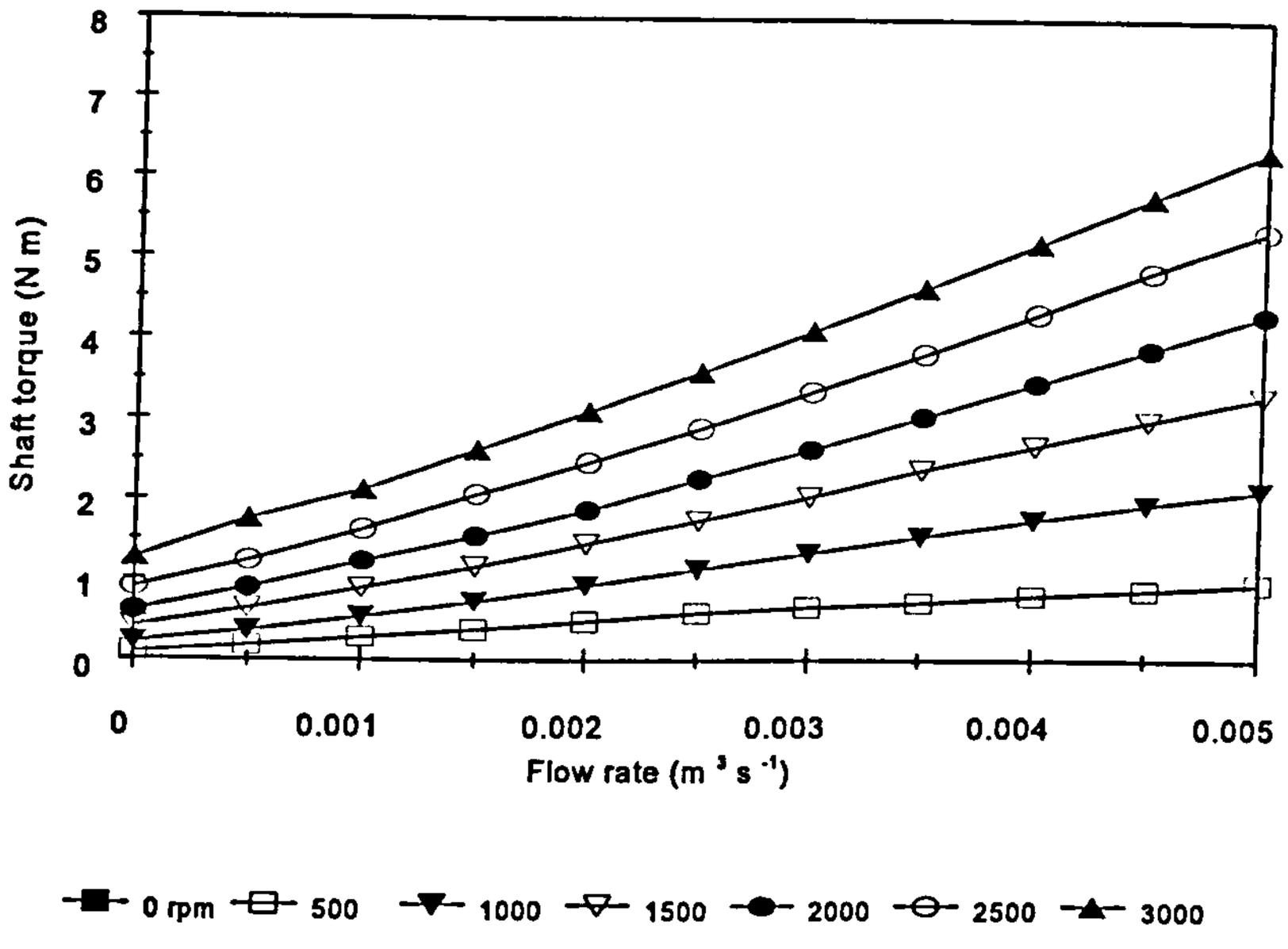

Figure A4.28 Shaft torque (r/18/50/121.45 & s/18/33/123.8)

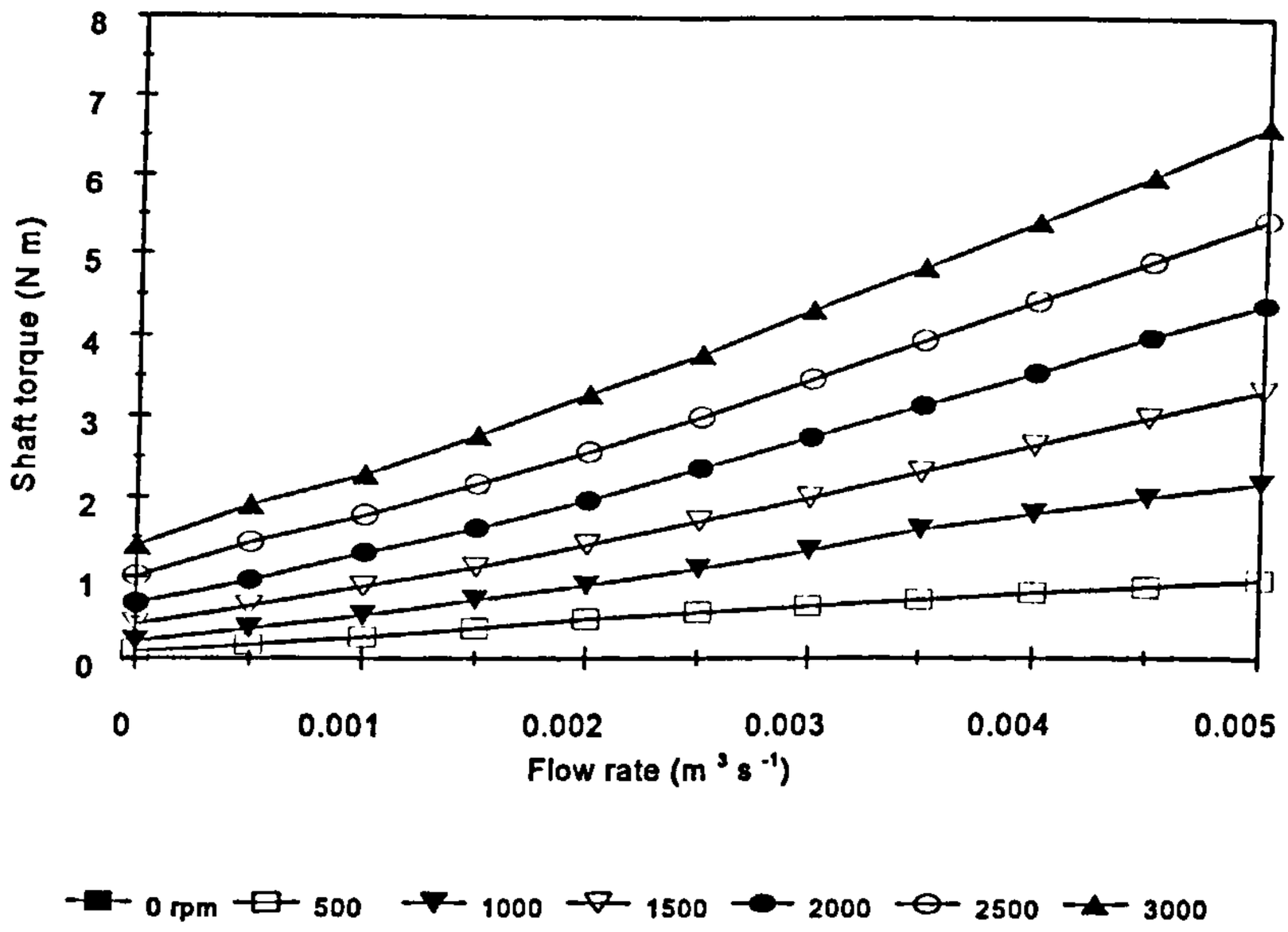

Figure A4.29 Shaft torque (r/18/50/121.45 & s/19/50/123.8)

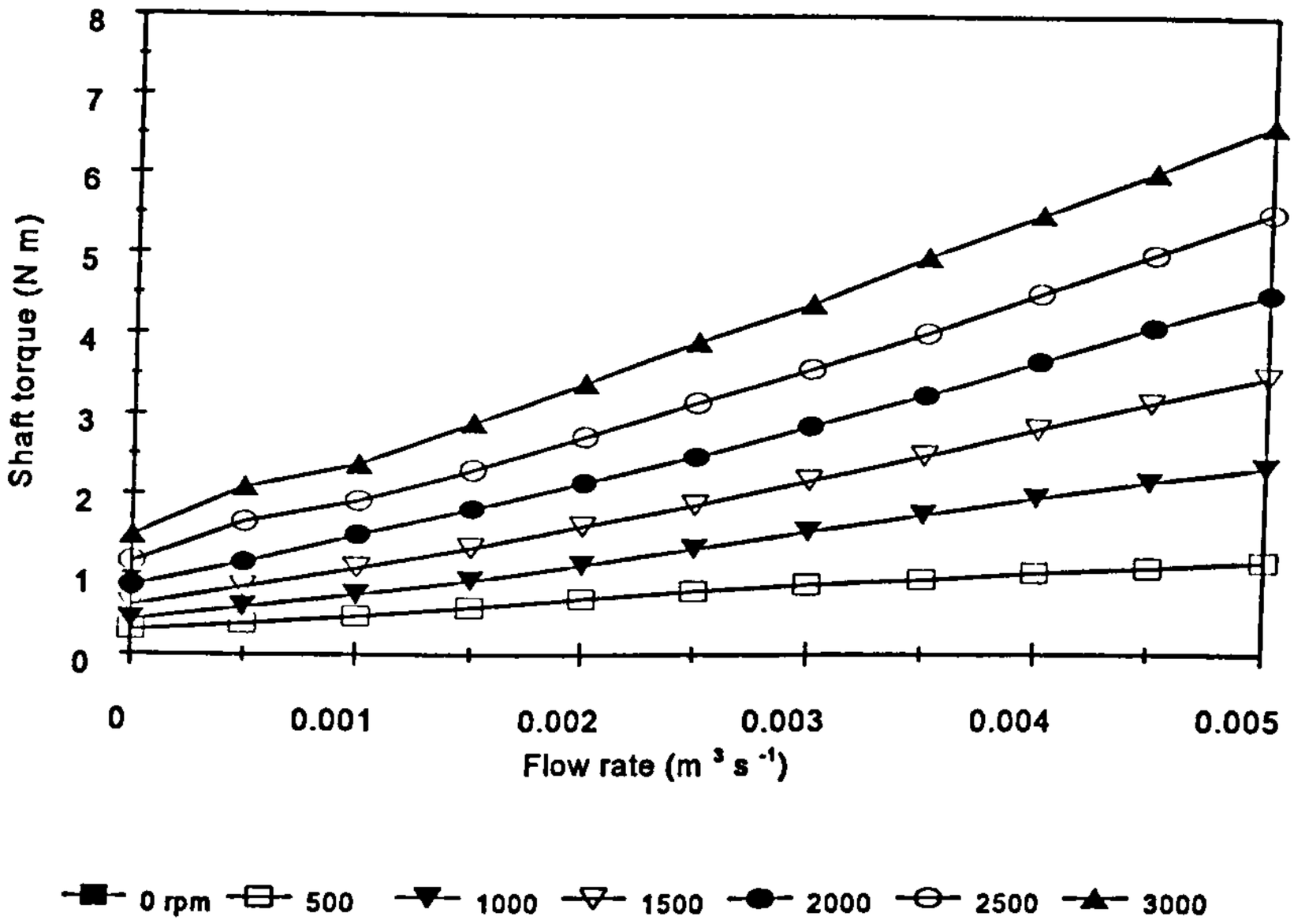

Figure A4.30 **Shaft torque (r/18/50/121.45 & s/36/50/123.8)**

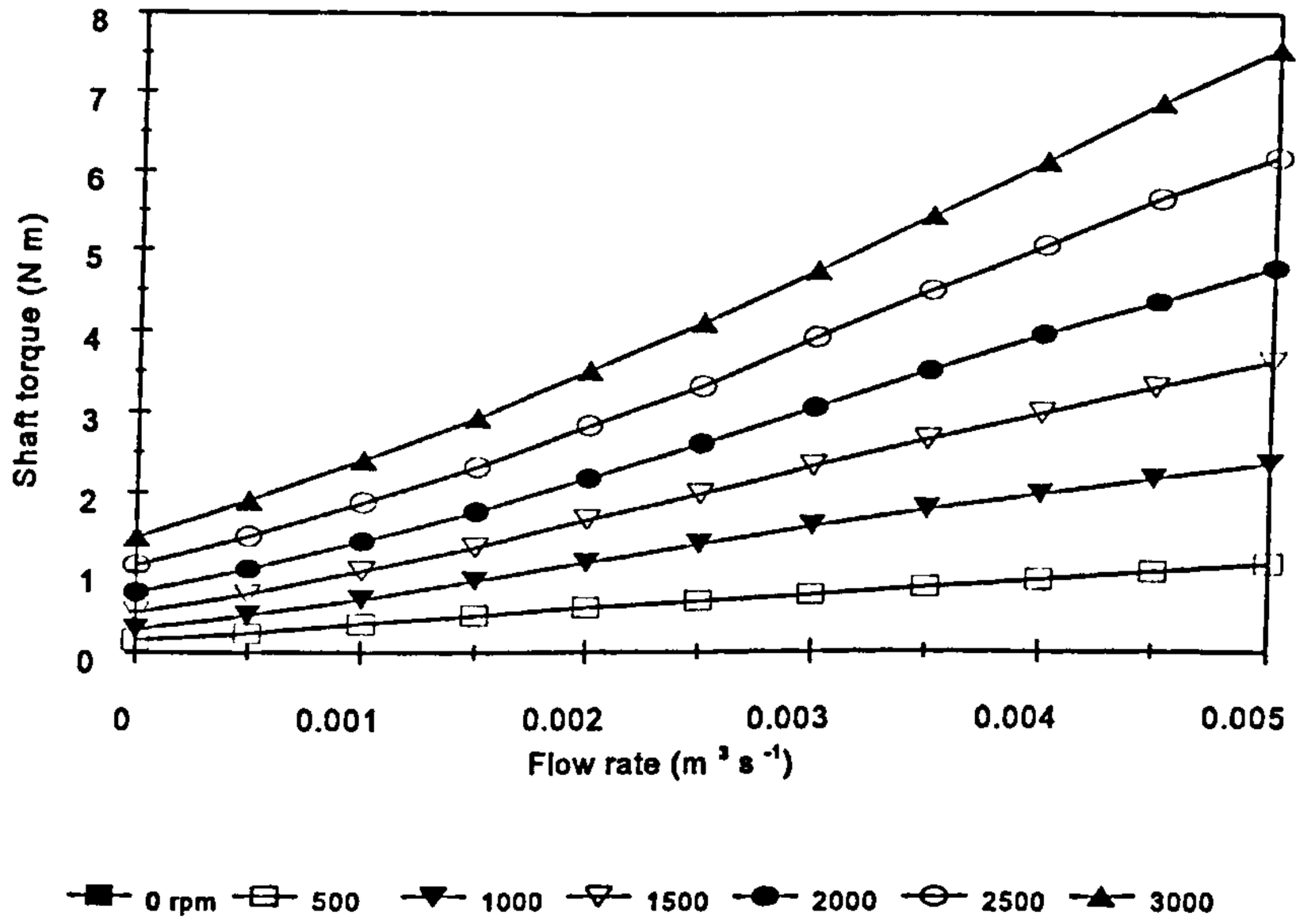

Figure A4.31 **Shaft torque (r/18/50/123.34 & s/18/50/123.8)**

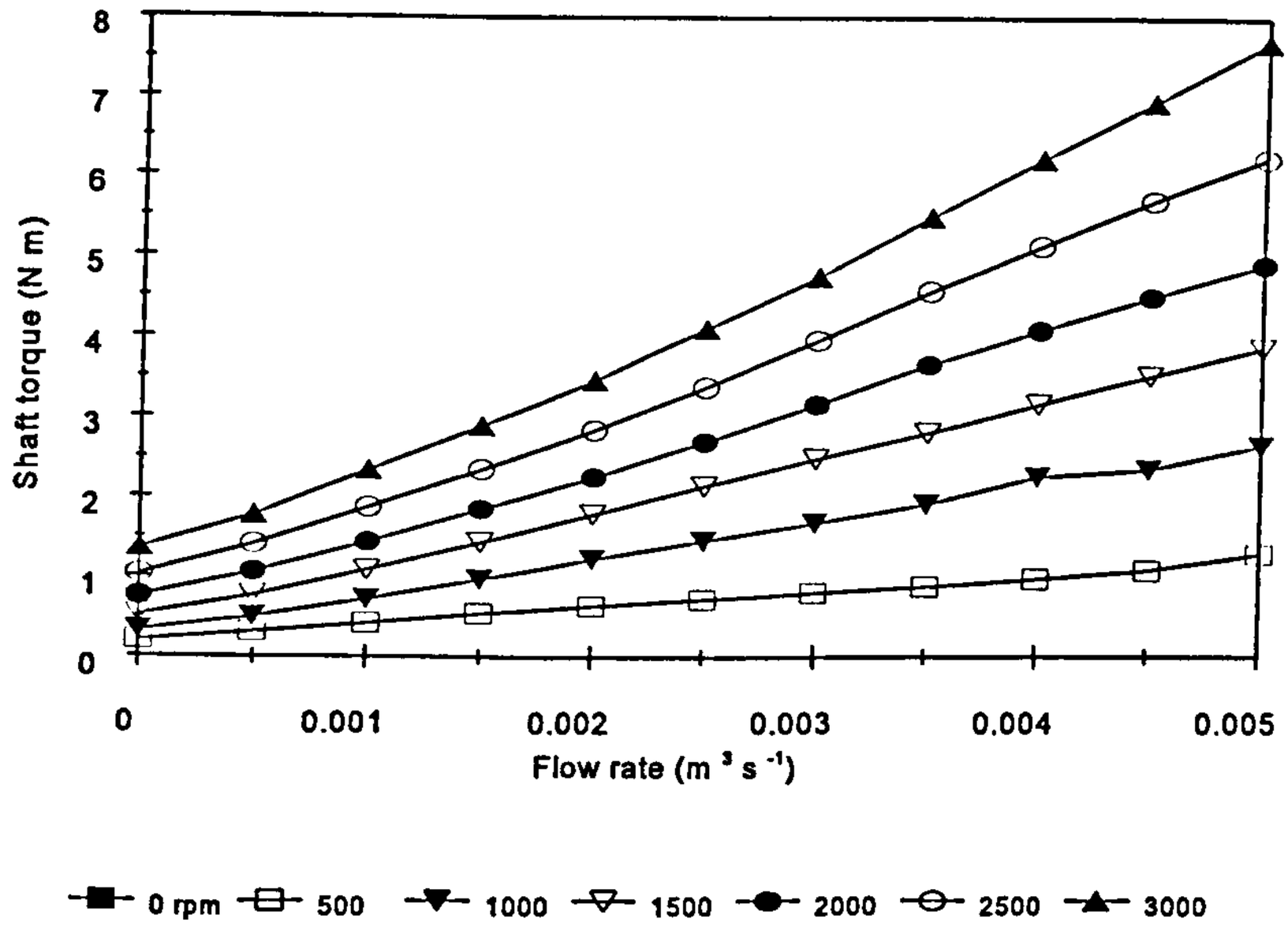

Figure A4.32 **Shaft torque (r/18/50/123.34 & s/18/33/123.8)**

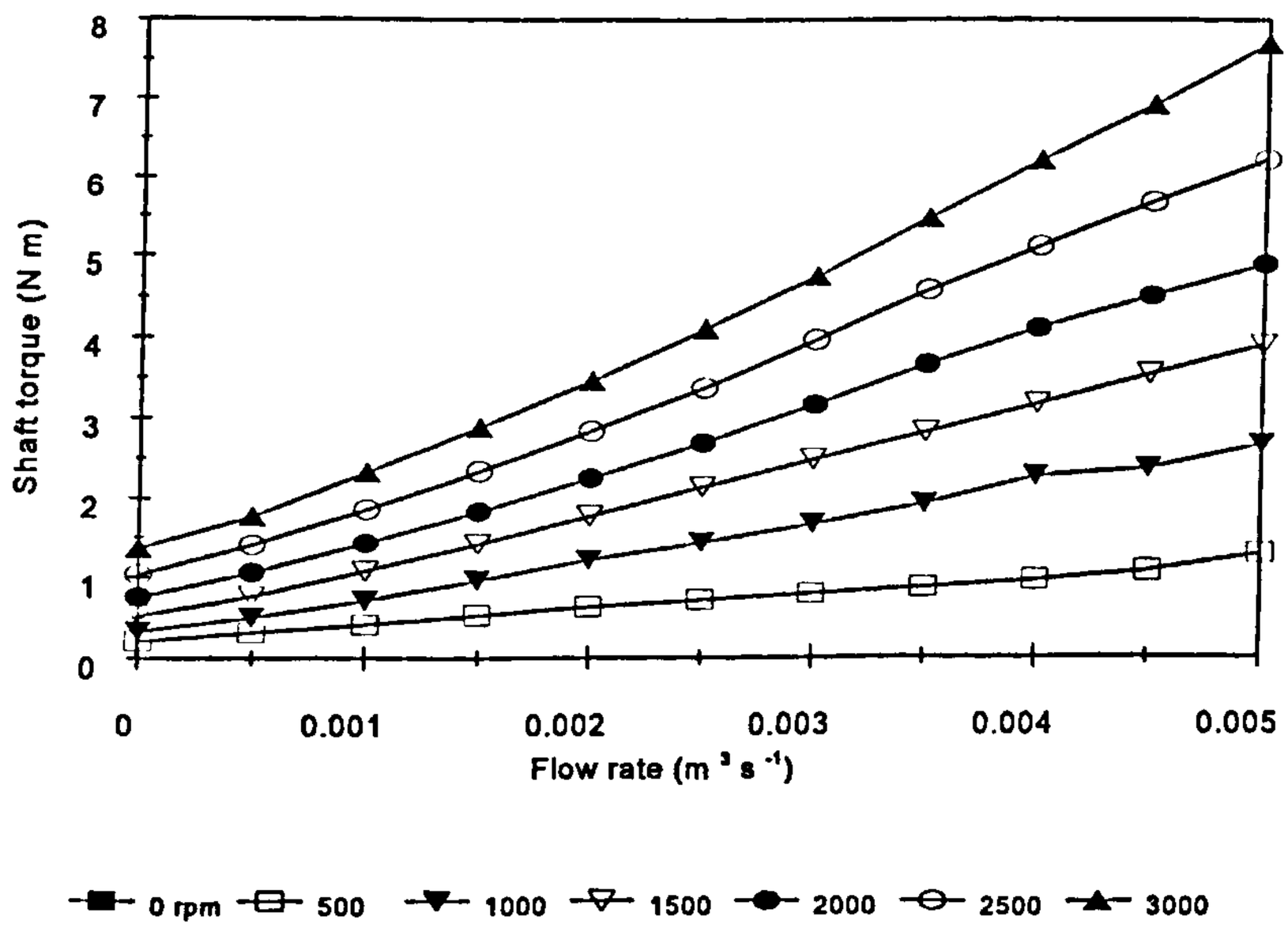

Figure A4.33 **Shaft torque (r/18/50/123.34 & s/19/50/123.8)**

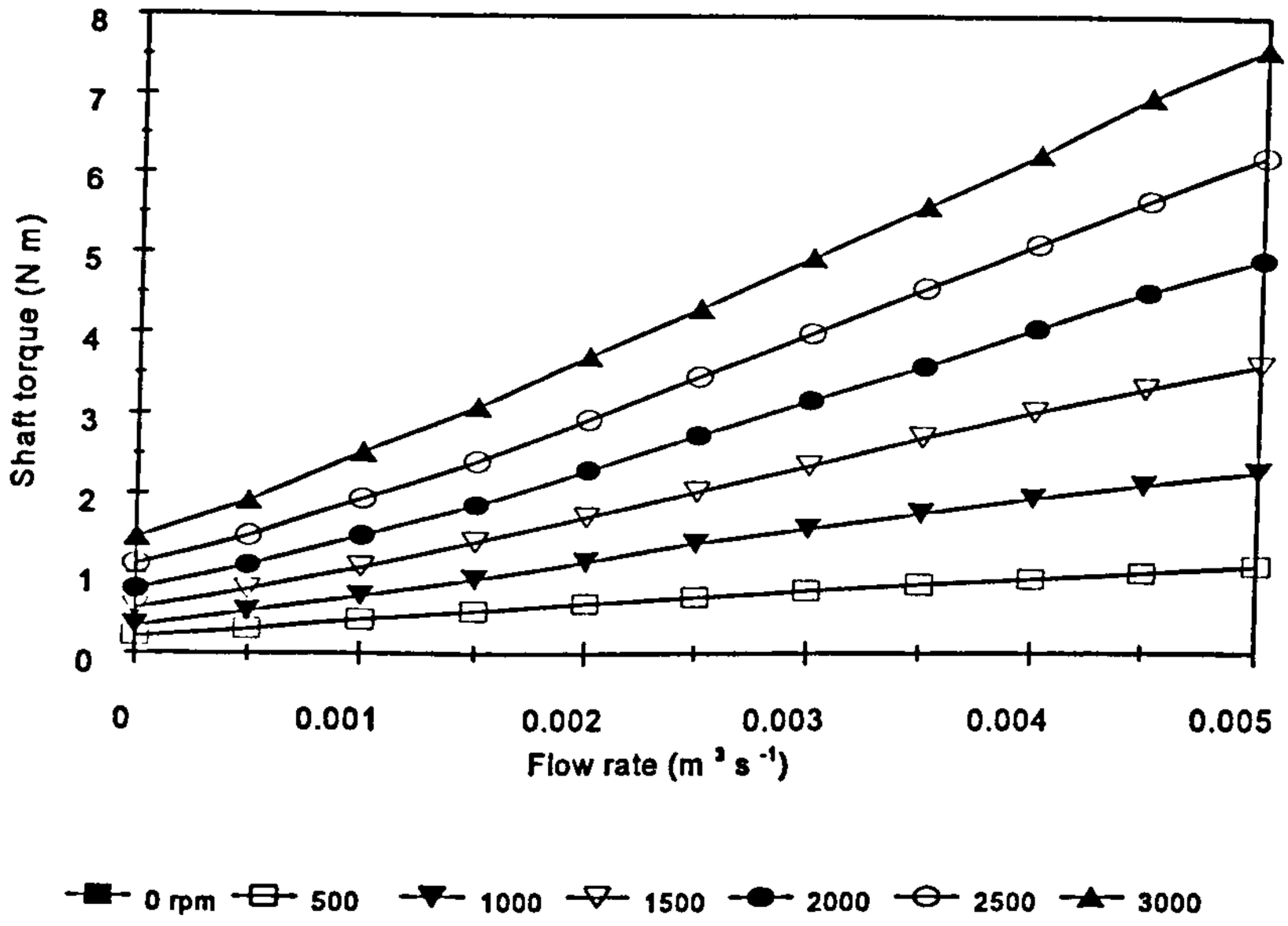

Figure A4.34 **Shaft torque (r/18/50/123.34 & s/36/50/123.8)**

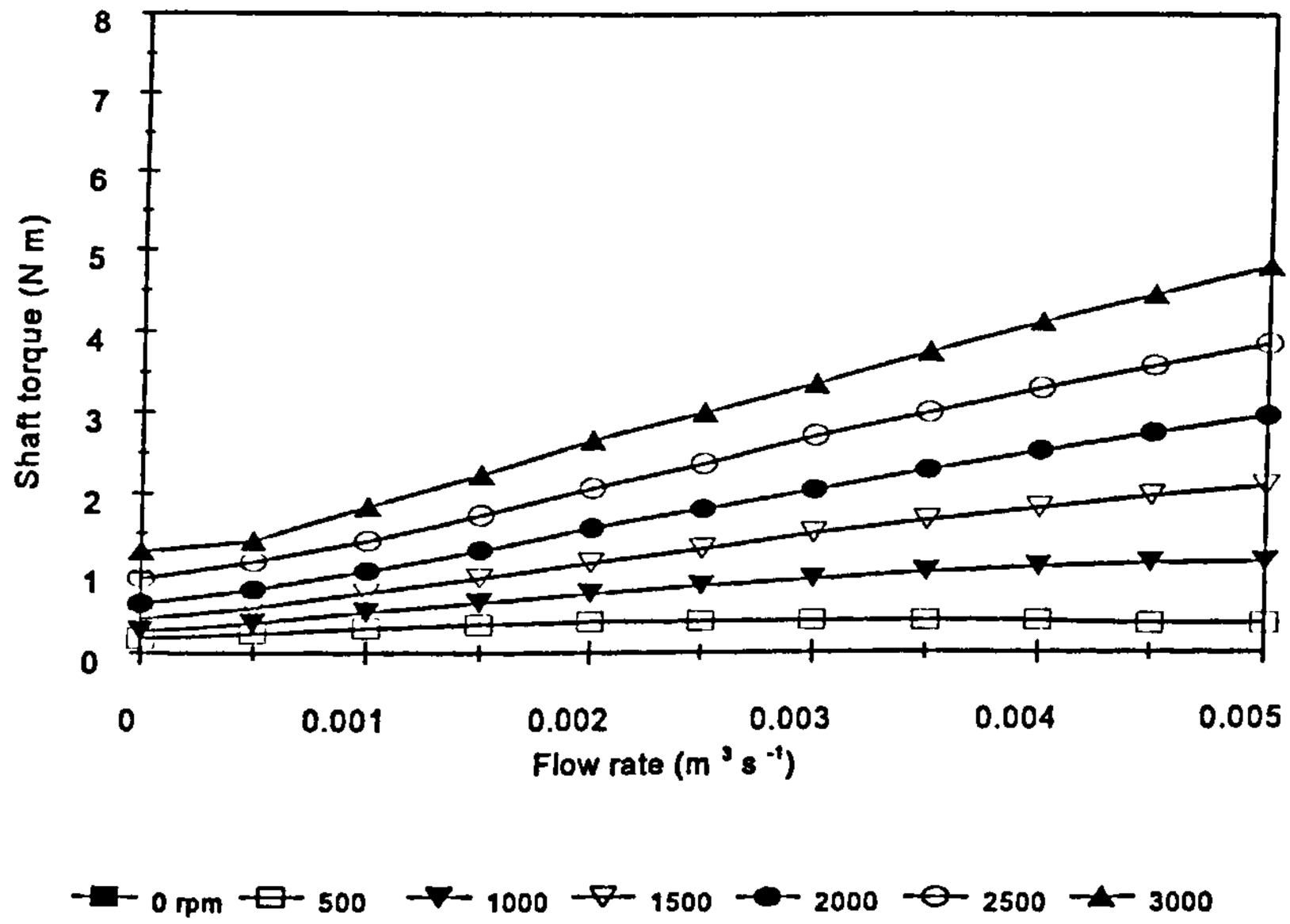

Figure A4.35 **Shaft torque (Silverson)**

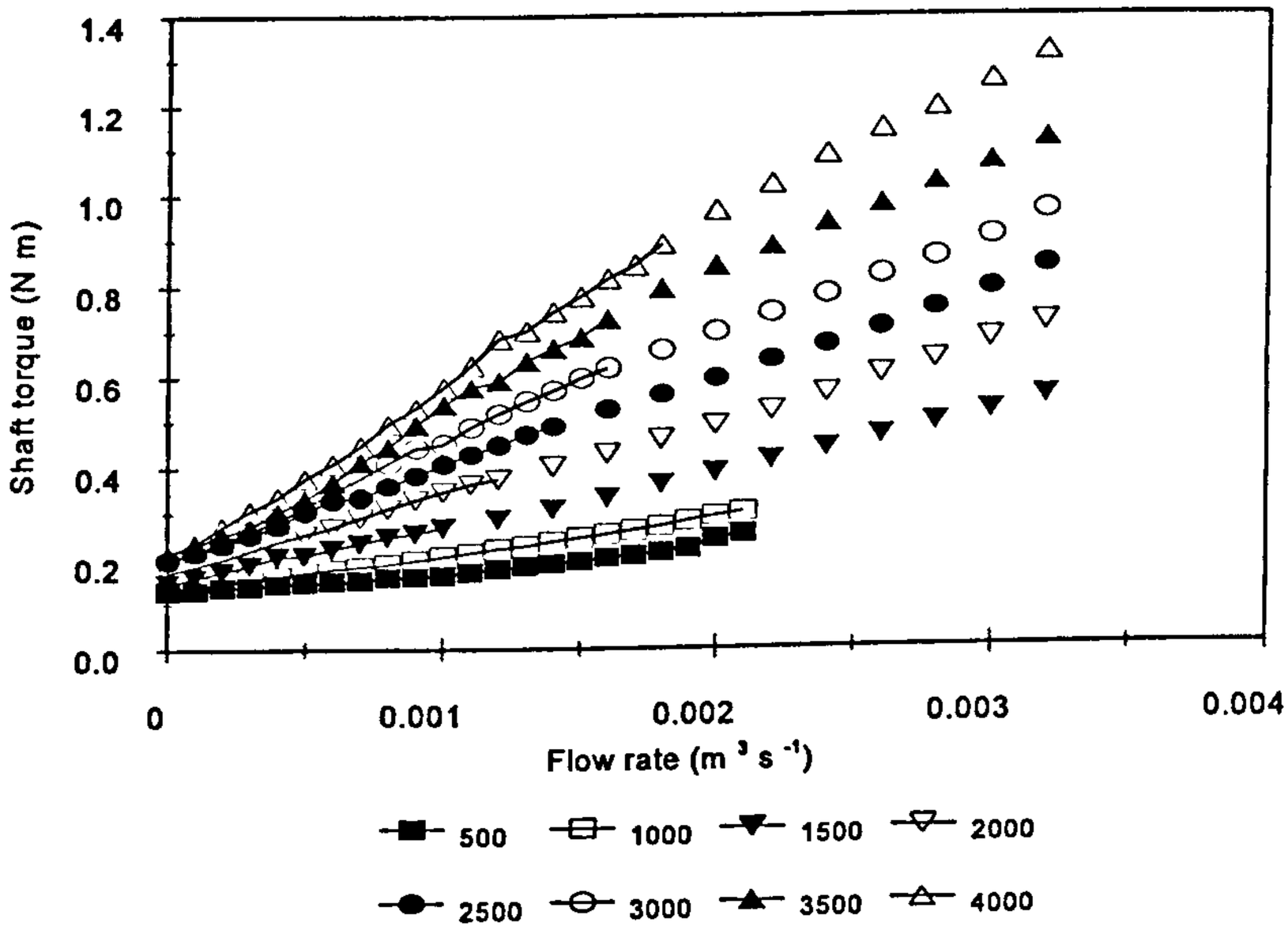

Figure A4.36 Shaft torque (Scale Toothed)

APPENDIX 5

COMPUTER PROGRAM USED TO SOLVE MODEL EQUATIONS

```
CLS
' SEMI-BATCH REACTOR - NEW REACTION SYSTEM WITH
' SELF-ENGULFMENT
' Written: ETH Group, 1991
' Modifications by BHR Group:
' By:    Date:         Detail:
' JH     April 92      To implement acceleration
' JH,SH  September 93  To implement self-engulfment
' TS,    June 1995     Changed to Quickbasic

    k1p = 12238!
    k1o = 921!
    k2p = 22.25
    k2o = 1.835
    k3 = 125!

   INPUT "FILE NAME...?", FILE$
   INPUT "DATA FILE...?", FILE1$
   PRINT ""
10 INPUT "FA?", FA
   INPUT "FAA?", FAA
   INPUT "TIME STEP?", hini
   INPUT "CONV?", conv
   INPUT "CB0?", CB0
   INPUT "VISCOSITY?", VISC
   CLS
   PRINT "FILE NAME = ", FILE$
   PRINT ""
   PRINT "FA =  ", FA
   PRINT "FAA =  ", FAA
   PRINT "TIME STEP =  ", hini
   PRINT "CONV =  ", conv
   PRINT "CB0 =  ", CB0
   PRINT "VISCOSITY =  ", VISC
   PRINT ""
   INPUT "CORRECT? ", N$
   IF UCASE$(N$) = "Y" THEN GOTO 20 ELSE GOTO 10
   PRINT ""
```

```
20 INPUT "LOWER ALPHA....?", LALPH
   INPUT "UPPER ALPHA....?", UALPH
   INPUT "STEP...?", PINC

   INPUT "LOWER ENERGY DISSIPATION RATE (EPSILON)?", LEPS
   INPUT "UPPER ENERGY DISSIPATION RATE (EPSILON)?", UEPS
   INPUT "STEP", INC

   PRINT "Calculating....."

   FOR ALPHA = LALPH TO UALPH STEP PINC

   FOR EPS = LEPS TO UEPS STEP INC

      E = .058 * SQR(EPS / VISC)
      DAM = k2o * CB0 / ((1 + ALPHA) * E)

      DA = DAM * (ALPHA + 1!)
      Z0 = 1! / (ALPHA + 1!)
      B1 = k1p / k2o
      B2 = k1o / k2o
      B3 = k2p / k2o
      B4 = B1 + B2
      B5 = k3 / k2o

      J = 1
      AAM = FA
      AAAM = FAA
      BAM = 0!
      RAM = 0!
      TAM = 0!
      QAM = 0!
      SAM = 0!
         FLAG = 0

   111   h = hini
         ABM = 0!
         AABM = 0!
         BBM = 1!
         RBM = 0!
         TBM = 0!
         QBM = 0!
         SBM = 0!
```

```
    T = 0!

121   IF INKEY$ <> "" THEN INPUT "DO YOU WANT TO STOP?", IN$
      IF UCASE$(IN$) = "Y" THEN GOTO 2000
      XB = Z0 * (EXP(T) / (1! - Z0 * (1! - EXP(T))))
      XA = 1! - XB
      ABM1 = ABM + h * ((AAM - ABM) * XA - DA * ABM * BBM * B4)
      AABM1 = AABM + h * ((AAAM - AABM) * XA - B5 * DA * AABM * BBM)
      BBM1 = BBM + h * ((BAM - BBM) * XA - DA * ABM * BBM * B4 - DA * BBM *
RBM - B3 * DA * BBM * TBM - B5 * DA * AABM * BBM)
      RBM1 = RBM + h * ((RAM - RBM) * XA + DA * BBM * (B1 * ABM - RBM))
      TBM1 = TBM + h * ((TAM - TBM) * XA + DA * BBM * (B2 * ABM - B3 * TBM))
      QBM1 = QBM + h * ((QAM - QBM) * XA + DA * B5 * AABM * BBM)
      SBM1 = SBM + h * ((SAM - SBM) * XA + DA * BBM * (RBM + B3 * TBM))
      ABM2 = (ABM + ABM1) / 2!
      AABM2 = (AABM + AABM1) / 2!
      BBM2 = (BBM + BBM1) / 2!
      RBM2 = (RBM + RBM1) / 2!
      TBM2 = (TBM + TBM1) / 2!
      QBM2 = (QBM + QBM1) / 2!
      SBM2 = (SBM + SBM1) / 2!
      XB = Z0 * (EXP(T + h / 2!) / (1! - Z0 * (1! - EXP(T + h / 2!))))
      XA = 1! - XB
      ABM = ABM + h * ((AAM - ABM2) * XA - DA * ABM2 * BBM2 * B4)
      AABM = AABM + h * ((AAAM - AABM2) * XA - B5 * DA * AABM2 * BBM2)
     BBM = BBM + h * ((BAM - BBM2) * XA - DA * ABM2 * BBM2 * B4 - DA * BBM2
* RBM2 - B3 * DA * BBM2 * TBM2 - B5 * DA * AABM2 * BBM2)
      RBM = RBM + h * ((RAM - RBM2) * XA + DA * BBM2 * (B1 * ABM2 - RBM2))
       TBM = TBM + h * ((TAM - TBM2) * XA + DA * BBM2 * (B2 * ABM2 - B3 *
TBM2))
      QBM = QBM + h * ((QAM - QBM2) * XA + DA * B5 * AABM2 * BBM2)
      SBM = SBM + h * ((SAM - SBM2) * XA + DA * BBM2 * (RBM2 + B3 * TBM2))

     ALFFA = ALPHA + J
      T = T + h
      XB = Z0 * (EXP(T) / (1! - Z0 * (1! - EXP(T))))
      VE = XB / Z0
      IF VE >= ALFFA THEN
         FLAG = 1
         VE = ALFFA
         AAM = ABM
         AAAM = AABM
         BAM = BBM
         RAM = RBM
```

```
    TAM = TBM
    SAM = SBM
    QAM = QBM
END IF

CUT = (1 - conv) / VE
IF BBM > CUT THEN GOTO 121
    IF VE >= ALFFA GOTO 222

    AAM = (AAM * (ALFFA - VE) + ABM * VE) / (ALFFA)
    AAAM = (AAAM * (ALFFA - VE) + AABM * VE) / (ALFFA)
    BAM = (BAM * (ALFFA - VE) + BBM * VE) / (ALFFA)
    RAM = (RAM * (ALFFA - VE) + RBM * VE) / (ALFFA)
    TAM = (TAM * (ALFFA - VE) + TBM * VE) / (ALFFA)
    QAM = (QAM * (ALFFA - VE) + QBM * VE) / (ALFFA)
    SAM = (SAM * (ALFFA - VE) + SBM * VE) / (ALFFA)

222  XS = 2! * SAM / (RAM + TAM + 2! * SAM + QAM)
    XQ = QAM / (RAM + TAM + 2! * SAM + QAM)
    XQ1 = QAM / (RAM + TAM)
    XR = RAM / (RAM + TAM + 2 * SAM + QAM)
    XT = TAM / (RAM + TAM + 2 * SAM + QAM)
    MB = J / (ALFFA) / (BAM + RAM + TAM + 2! * SAM + QAM) * 100!
CLS
BEEP
PRINT "DAM = "; DAM; " FA = "; FA; " FAA = "; FAA
PRINT "EPSILON = "; EPS; " ALPHA = "; ALPHA; "T = "; T
IF FLAG = 1 THEN PRINT "REACTION ZONE FILLS"
PRINT "XS = "; XS; " XQ = "; XQ; " XQ1 = "; XQ1
PRINT "XR = "; XR; " XT = "; XT
PRINT "MB = "; MB; " XB = "; XB
PRINT "Solver parameters:"
PRINT "Conv = "; conv; "Timestep = "; hini
PRINT "----------------------------------------------------"

OPEN FILE$ FOR APPEND AS #1
PRINT "SAVING TO "; FILE$
PRINT #1, "DAM = "; DAM; " FA = "; FA; " FAA = "; FAA
PRINT #1, "EPSILON = "; EPS; " ALPHA = "; ALPHA; "T = "; T
IF FLAG = 1 THEN PRINT #1, "REACTION ZONE FILLS"
PRINT #1, "XS = "; XS; " XQ = "; XQ; " XQ1 = "; XQ1
PRINT #1, "XR = "; XR; " XT = "; XT
PRINT #1, "MB = "; MB; " XB = "; XB
```

```
PRINT #1, "Solver parameters:"
PRINT #1, "Conv = "; conv; "Timestep = "; hini
PRINT #1, "-------------------------------------------------------"
PRINT #1, ""
CLOSE #1
PRINT "DONE."

OPEN FILE1$ FOR APPEND AS #2
    PRINT #2, ALPHA; EPS; XQ
    CLOSE #2

    NEXT EPS
1100  NEXT ALPHA

2000 END
```

APPENDIX 6

From proceedings of the 1st International Conference on Process Intensification for the Process Industries, Antwerp, Belgium, December 1995. Edited by C Ramshaw.

ASSESSING ROTOR/STATOR MIXERS FOR RAPID CHEMICAL REACTIONS USING OVERALL POWER CHARACTERISTICS

T. G. Sparks[1],
D. E. Brown[2],
A. J. Green[1].

Summary

Rotor/stator mixers are used extensively in the process industries, but much less research work has been reported on them than on stirred tanks or motionless mixers.

This paper considers the overall power characteristics of a rotor/stator mixer so that local energy dissipation rates (and hence mixing rates) might be estimated. These are then assessed in process intensification terms.

[1]BHR Group Limited, Cranfield, Bedford, MK43 0AJ, UK.

[2]Biotechnology Centre, Cranfield University, Bedford, MK43 0AL, UK.

NOTATION

SYMBOL	MEANING	UNITS
K	constant (used in disk friction equation)	-
L_0	initial scale of segregation	m
N	shaft speed	s^{-1}
P_{SHAFT}	shaft power	W
P_{PUMP}	pumping power	W
P_{MECH}	mechanical losses	W
P_{DISK}	disk friction losses	W
P_{LEAK}	leakage (recirculation) losses	W
$P_{HYDRAULIC}$	hydraulic losses	W
Q	flow rate	$m^3 s^{-1}$
t_E	engulfment time	s
t_{MESO}	meso mixing time	s
Δp	differential pressure	Pa
η	pumping efficiency	-
ε	turbulent energy dissipation rate	$W kg^{-1}$
Λ	shaft torque	N m
ν	kinematic viscosity	$m^2 s^{-1}$

1 BACKGROUND

This section gives a general background to rotor/stator mixers, discusses previous work and defines the power balance that will be used to characterise the rotor/stator mixer.

1.1 Rotor/stator mixers

A rotor/stator mixer contains a high speed rotor spinning close to a motionless stator. Fluid passes through the region where rotor and stator interact and experiences highly pulsating flow and shear. In-line rotor/stator mixers resemble centrifugal pumps and may contribute significantly to pumping the fluid. This is shown schematically in Figure 1 and Figure 2 shows an industrial example.

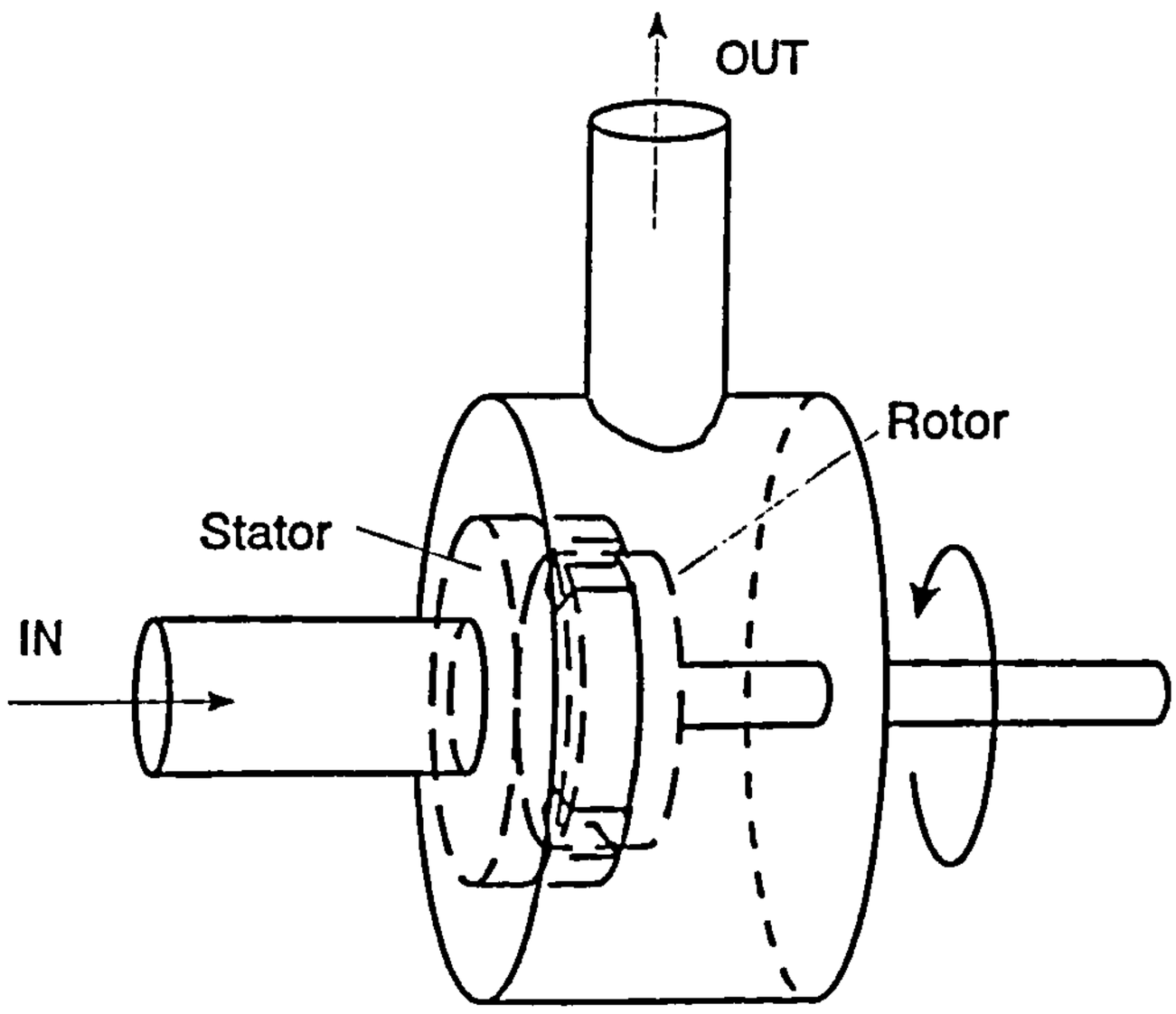

Figure 1 A rotor/stator mixer

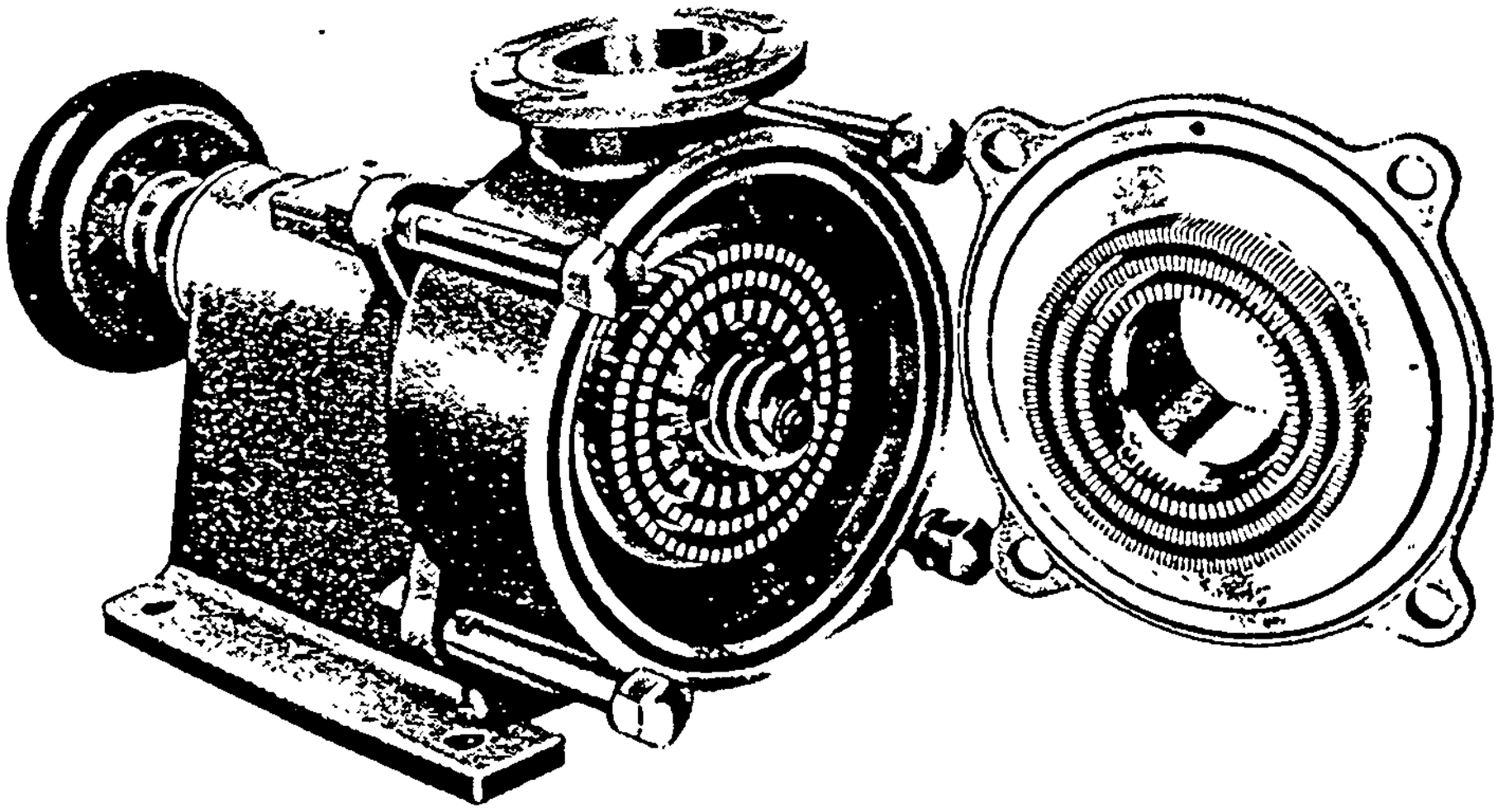

Figure 2 An industrial example of a rotor/stator mixer

1.2 Process intensification

Process intensification (PI) is a design philosophy where the fluid dynamics of a process are matched to its chemical and physical requirements. For fast (particularly fast, competitive) chemical reactions, this implies short residence time reactors with intense mixing, and continuous or semi-batch operation. In-line rotor/stator mixers appear to offer such a combination of features.

1.3 Turbulent energy dissipation rate and mixing rates

Mixing rates can affect the outcome of competitive chemical reactions, where the intrinsic rate of the reaction is comparable to the rate of mixing (Ref. 1). Several mixing timescales can be defined, any one of which might be the rate limiting step.

Micro mixing - the stage of mixing that brings about final, molecular, homogeneity - depends upon the rate of dissipation of turbulent energy. For a low viscosity liquid the micro mixing rate is given by the rate of engulfment within small turbulent eddies (Ref. 2):

$$t_E \approx 17\left[\frac{\nu}{\varepsilon}\right]^{1/2} \qquad (1)$$

Within larger turbulent eddies, 'meso mixing' (Ref. 3), reduces the scale of segregation of reactants (although not bringing about the molecular homogeneity needed for reaction - this requires micro mixing). A characteristic timescale (Ref. 4) is

$$t_{MESO} \sim \left[\frac{L_0^2}{\varepsilon}\right]^{1/3} \qquad (2)$$

where L_0 is a characteristic length for the initial scale of segregation.

To define the mixing rate for a reactor, perhaps in order to model the performance, the equations above show that the turbulent energy dissipation rate per unit mass, ε, is a crucial parameter.

1.4 Previous work on rotor/stator mixers

Bourne and Garcias-Rosas (Ref. 5) and Bourne and Studer (Ref. 6), used the product distribution of competitive diazo coupling reactions conducted in a rotor/stator mixer to determine local turbulent energy dissipation rates. They report values for ε of up to 700 W kg^{-1} (Bourne and Garcias-Rosas) and 1200 W kg^{-1} (Bourne and Studer). These correspond to a micro mixing time (in water at 25°C), t_E, of ~2×10^{-3} to 1.5×10^{-3} s, sufficiently rapid to compare with the intrinsic speed of fast competitive chemical reactions, and therefore affect their outcome.

The technique used gave local information, the diazo coupling reaction scheme can be used to infer average ε in the reaction zone. They report that removal of the stator has no effect on the outcome of these reactions - implying that the reaction is over before the shear gap (the thin region between the rotor and stator) or the stator is reached, or that the stator has no effect on the ε.

This paper attempts to infer energy dissipation rates by estimating ε in terms of measurements of the overall power balance.

1.5 Power balance for a centrifugal pump

The following power balance was adopted (Ref. 7) for a centrifugal pump and can be applied to a rotor/stator mixer:

$$P_{SHAFT} = P_{PUMP} + P_{MECH} + P_{DISK} + P_{LEAK} + P_{HYDRAULIC} \quad (3)$$

Figure 3 shows the power balance for a double suction centrifugal pump (from Ref. 8). The components of this balance are discussed below.

P_{SHAFT} - This is the shaft power input to the mixer.

P_{PUMP} - The pumping power output, this would be needed to assess whether an additional pump is needed.

P_{MECH} - The mechanical losses, in Figure 3, are the losses due to friction in the seals and bearings. Some definitions of mechanical loss include disk friction, which is not included here because the seal and bearing losses could be measured separately from the disk friction losses. Mechanical losses (and the disk friction loss) do not contribute to mixing.

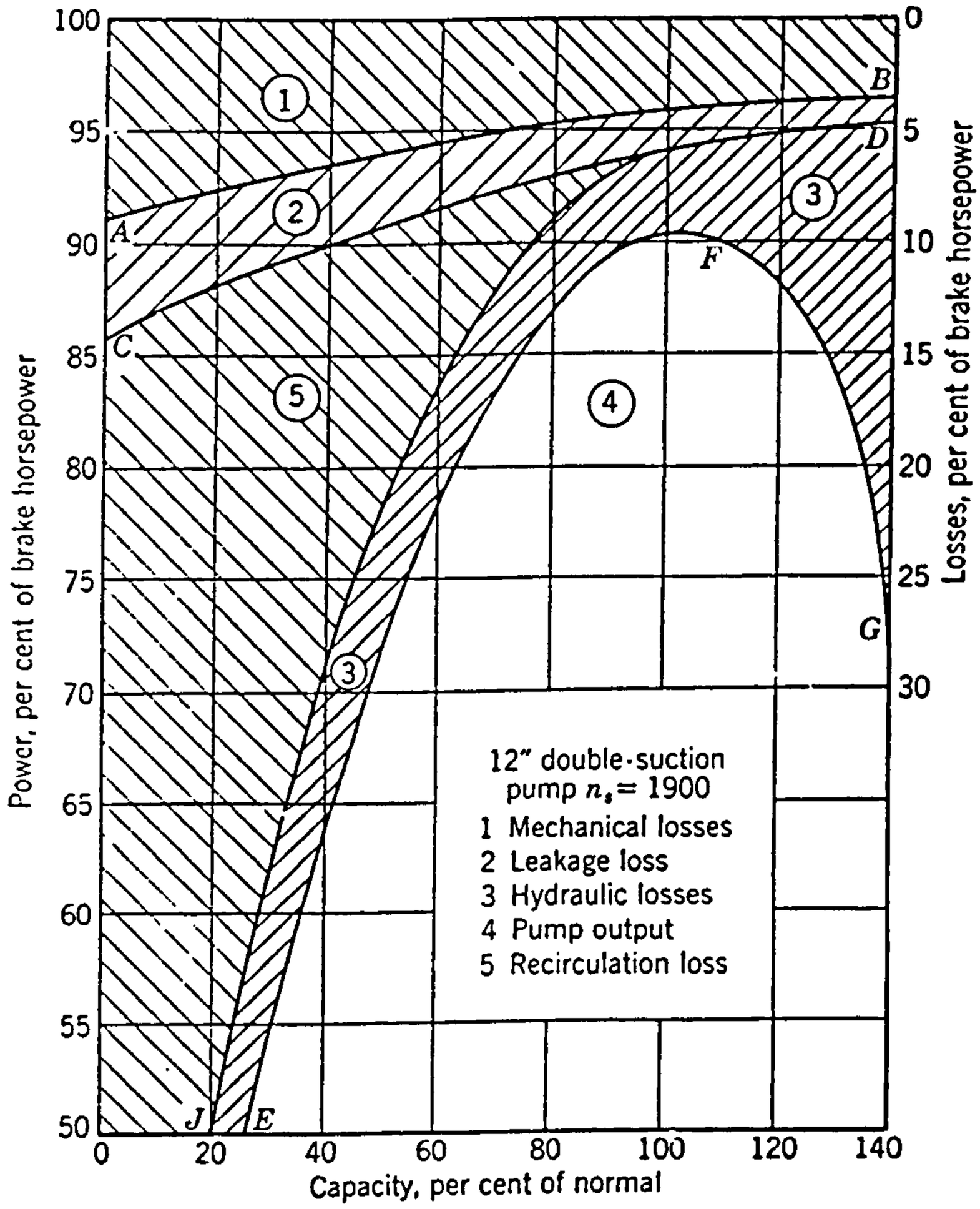

Figure 3 Power balance for a double suction centrifugal pump (Ref. 8)

P_{DISK} - Disk friction losses are caused by frictional drag on the solid surfaces of the rotor, and are analogous to the skin friction losses in a motionless mixer. Disk friction losses are significant in pumps and they are accounted for in this work.

P_{LEAK} - The leakage loss can mean the loss due to leakage through seals or, as it is in this work, the loss due to fluid not passing through in the required direction. An example of this type of leakage (or recirculation) loss is fluid passing back from the high pressure (downstream) side of the impeller to the low pressure (upstream) side. This is a macro mixing mechanism (reducing coarse scale concentration fluctuations) and will influence the residence time distribution.

$P_{HYDRAULIC}$ - Hydraulic losses (turbulent losses) are the losses that contribute to micro mixing.

2 EXPERIMENTAL DETAILS

2.1 Rig/ methods

A rotor/ stator mixer, based upon a Silverson machine, was placed in a flow loop - see

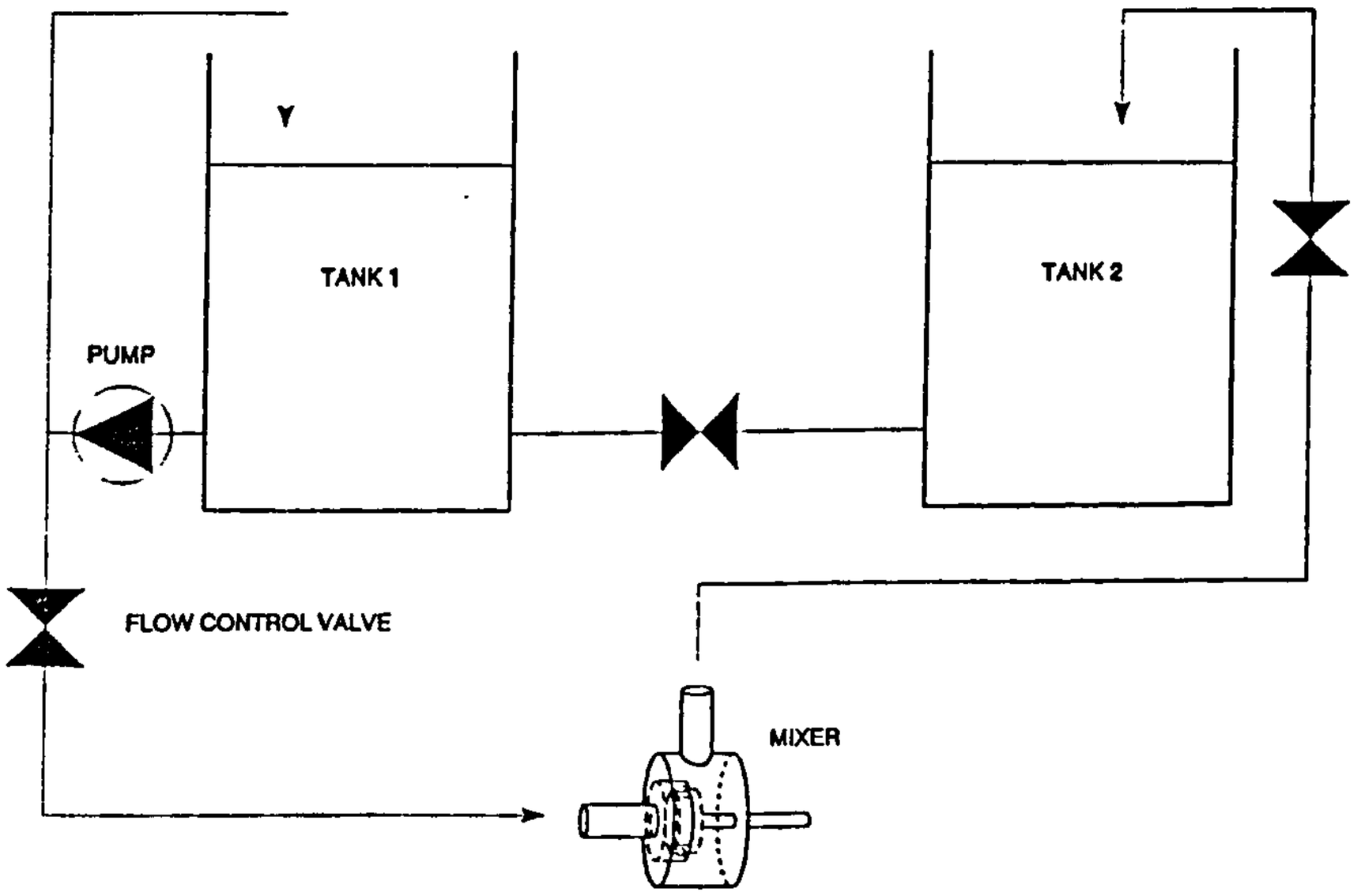

Figure 4 Test loop (Ref. 9)

Figure 4. Shaft torque, shaft speed and differential pressure were measured. The machine contained a mixer unit designed by the author to model a typical toothed rotor/stator type, see Figure 5. The rotor diameter was 121.45 mm and the inner diameter of the stator teeth was 123.8 mm, both rotor and stator had 18 teeth and a tooth open area of 50%.

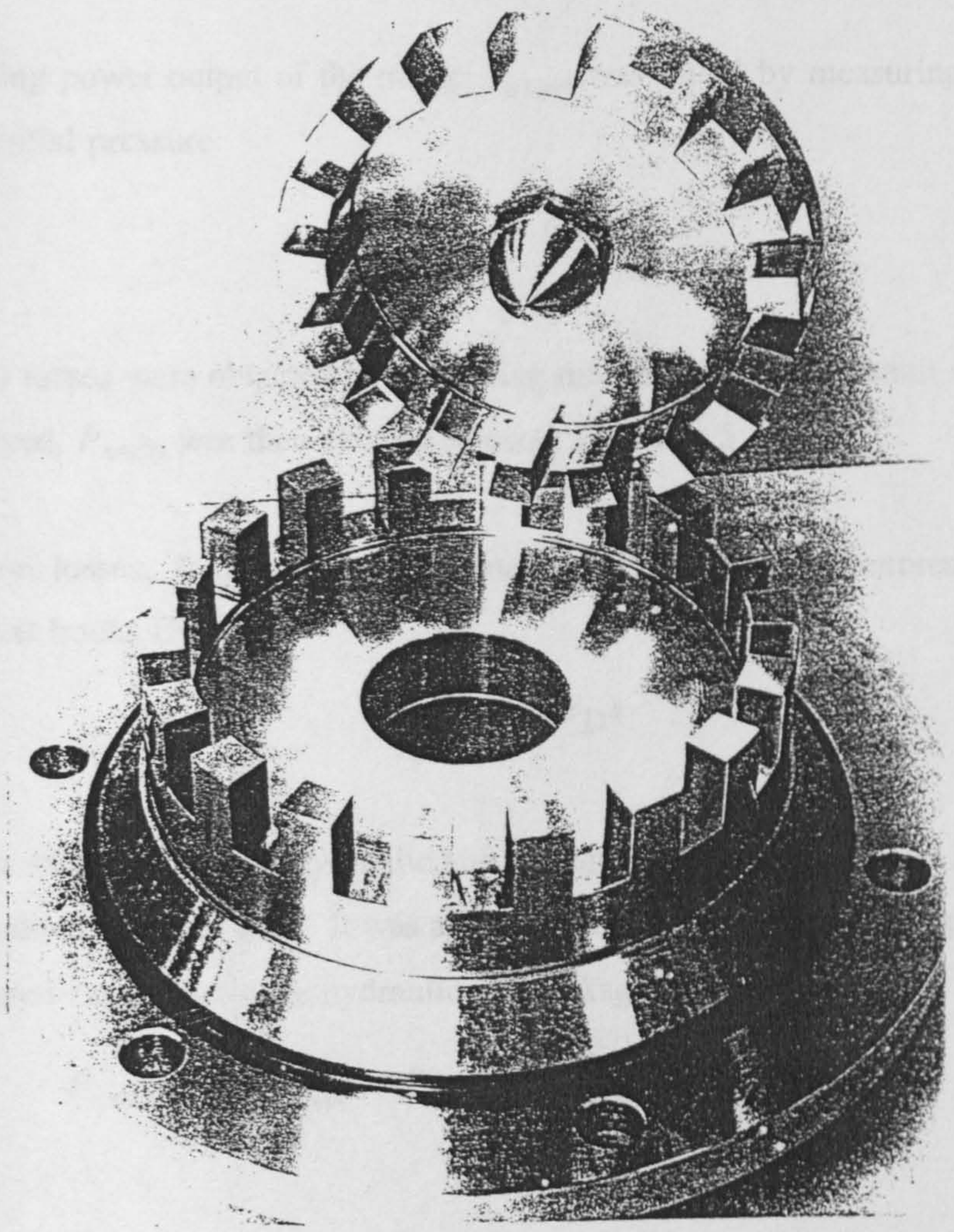

Figure 5 Toothed rotor/stator

The following paragraphs show how components of the power balance, see Equation 1, were measured or estimated.

Shaft power, P_{SHAFT}, was determined by measuring the shaft torque and the rotational speed and calculated using:

$$P_{SHAFT} = 2\pi N\Lambda \tag{4}$$

The pumping power output of the mixer, P_{PUMP}, was found by measuring the flow rate and differential pressure:

$$P_{PUMP} = Q\Delta p \tag{5}$$

Mechanical losses were obtained by measuring the shaft torque and shaft speed with the rotor removed, P_{MECH} was then calculated using Equation 5.

Disk friction losses, P_{DISK}, were determined using an empirical expression given in pumping text books (Ref. 10):

$$P_{DISK} = KN^3D^5 \tag{6}$$

It was not possible to measure hydraulic and leakage losses ($P_{HYDRAULIC}$ and P_{LEAK}) directly with the methods outlined here. It was assumed that the remainder of the power balance (not accounted for above)is the hydraulic and leakage losses combined:

$$P_{HYDRAULIC} + P_{LEAK} = P_{SHAFT} - (P_{PUMP} + P_{DISK} + P_{MECH}) \tag{7}$$

3 RESULTS/ DISCUSSION

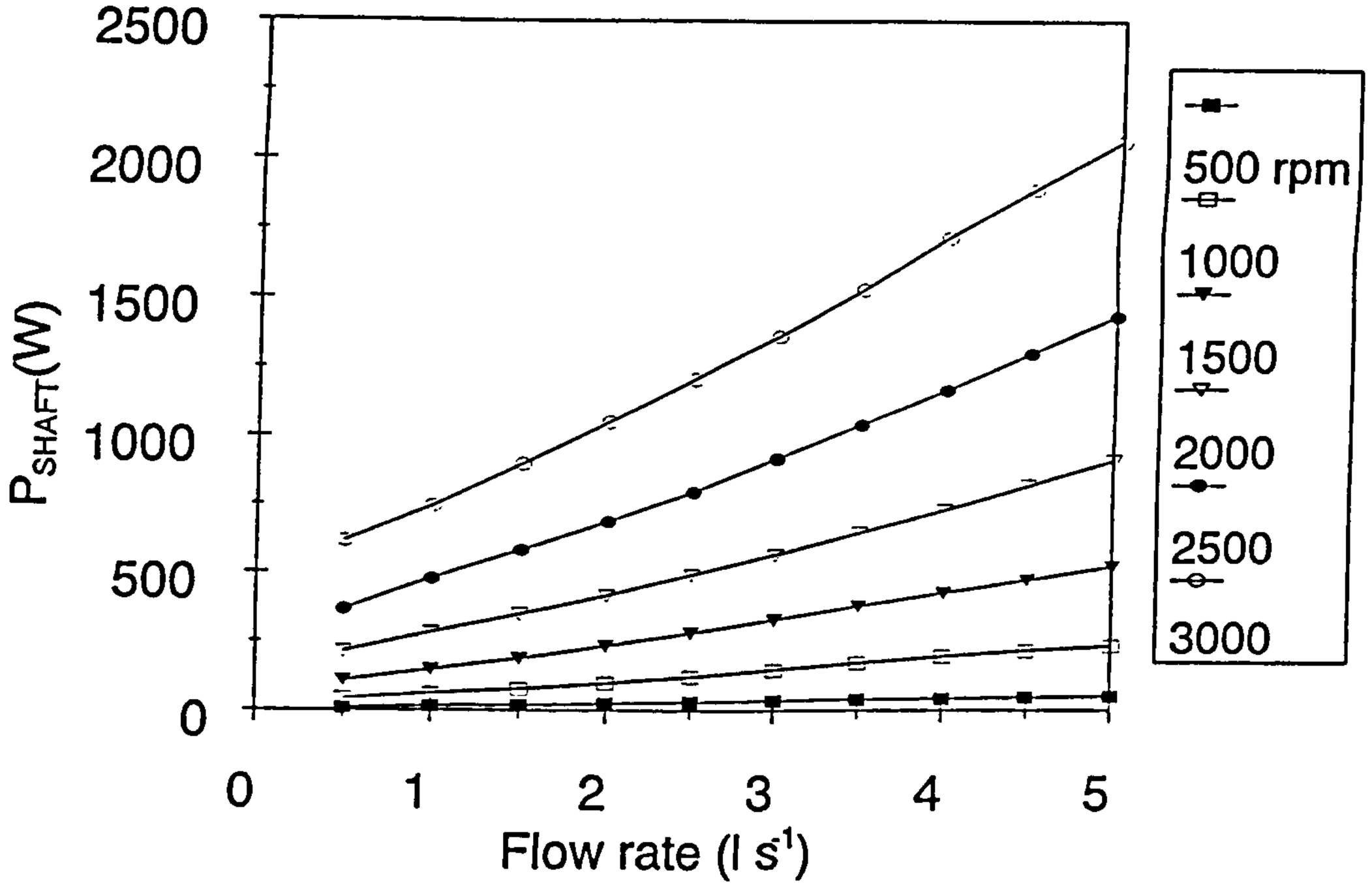

Figure 6 Shaft power against flow rate for a range of shaft speeds

Figures 6 and 7 show shaft power and pumping power data, and Figure 8 shows the overall energy balance for the mixer at 3000 rpm.

Figure 6 shows that shaft power rises approximately with flow rate and that, at maximum flow rate and shaft speed the shaft power is approximately 2 kW. The proportion of this power going to turbulence and mixing will be considered later. Each curve in Figure 7, the pumping power curves, shows a maximum; in fact at low shaft speeds and high flow rates there is a nett pressure drop across the mixer. This is because the differential pressure across the mixer shows the combined effects of pressure rise due to the rotor and the 'static' losses that occur in the system.

3.1 Power balance

The power balance, Figure 8, summarises the power dissipation and transformation in the mixer at 3000 rpm. It shows that the mechanical and disk friction losses account for

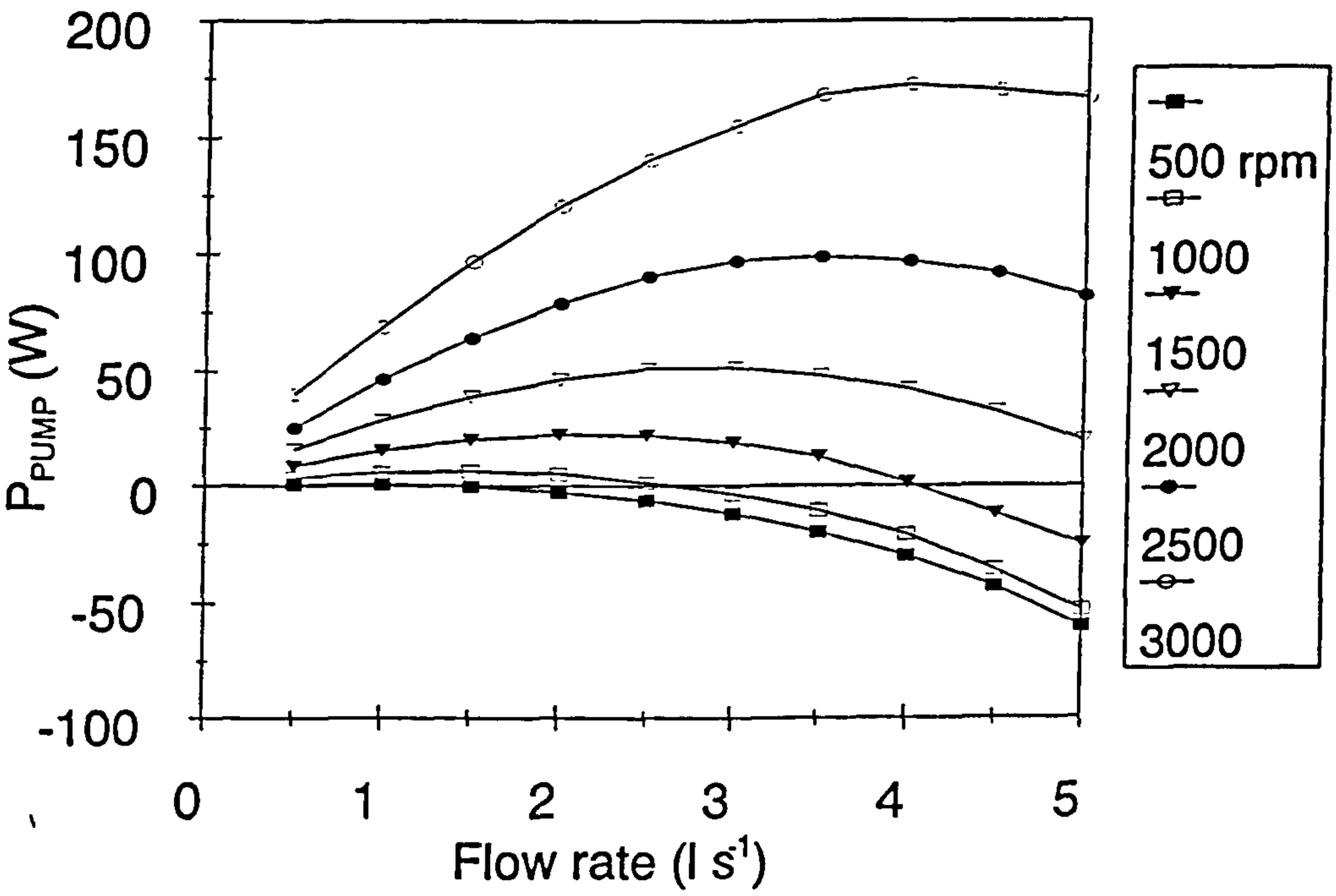

Figure 7 Pumping power against flow rate

about 25% of the shaft power input at low flow rates but at high flow rates, the overall shaft power increases. The mechanical and disk friction losses (which do not depend on flow rate) therefore account for a lower proportion of the total shaft power input. The remainder of the power balance is discussed in the following sections.

3.1.1 Pumping efficiency

The pumping efficiency of this unit is very much lower than that for a centrifugal pump (it was not designed to pump):

$$\eta = \frac{Q\Delta p}{P_{SHAFT}} \tag{8}$$

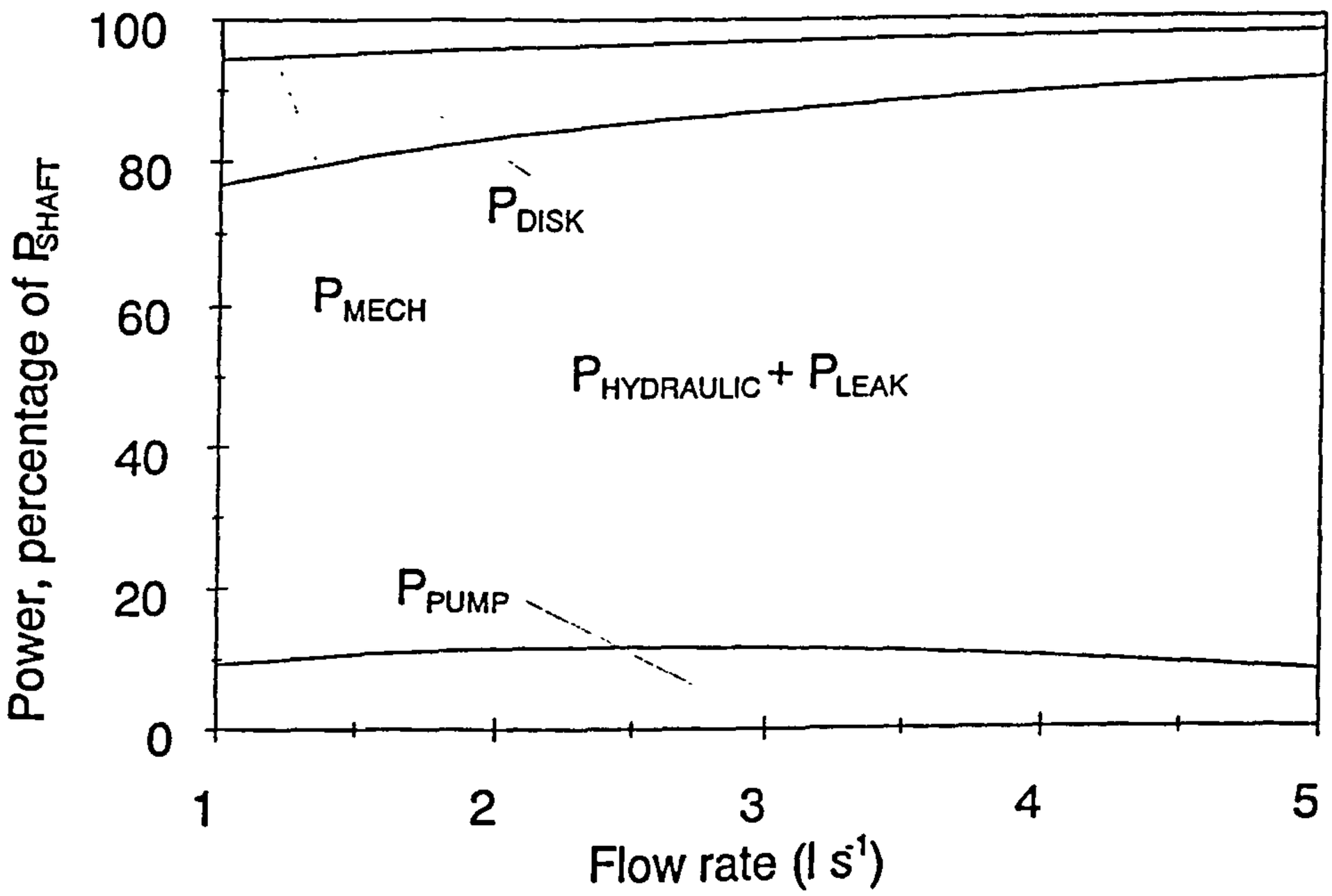

Figure 8 Power balance at 3000 rpm

With centrifugal pumps this value might be as high as 90%. In the power balance shown here it is ~10-15% at the best efficiency point.

There is a basic hydrodynamic reason for the best efficiency point (BEP) in a pump, which occurs when the tip speed of the rotor matches the speed of the flow in the volute. In the rotor/stator mixer, where the rotor and the volute are effectively separated by the stator, there is not a simple set of conditions that accompany the BEP.

3.1.2 $P_{HYDRAULIC}$ and P_{LEAK}

Most of the shaft power input (~70%) is not accounted for by the other components of the power balance, it is therefore concluded that this power is dissipated through hydraulic and leakage losses combined.

Using these techniques it is not possible to measure ε directly. It is assumed that approximately 1/3 of the hydraulic and leakage losses combined is dissipated to turbulence and that this occurs in the immediate vicinity of the rotor/stator teeth.

At 3.0 l s^{-1} and 3000 rpm, the shaft power is approximately 1.2 kW (Figure 6). If 1/3 of this (400 W) is dissipated through turbulent energy dissipation within the rotor/stator teeth (in this case fluid mass ~0.07 kg) this gives ε~5500 W kg^{-1}.

This value, an estimate averaged over the extent of the rotor/stator teeth and including the shear gap, is somewhat higher than that obtained using the chemical reaction technique used by Bourne and co-workers (in smaller mixers). This could be explained by their result that the removal of the stator had no effect - it is probable that energy dissipation rates in the shear gap and stator are higher than those in the rotor.

Further, the energy balance shows that the proportion of power going to hydraulic and leakage losses is relatively insensitive to flow rate. The power balance for the pump showed that the hydraulic losses (component 3 in Figure 3) increase rapidly as the best pumping efficiency point is passed. In fact the BEP is not as well defined as for the

pump. The drop in efficiency above the BEP arises due to increasing 'static' losses in the mixer (in fact, at high flow rates there could be a nett pressure drop across the mixer).

3.2 Implications for mixing performance

Turbulent energy dissipation rates of 5500 W kg^{-1} correspond to a micro mixing time (in water) of 7×10^{-4} s and a meso mixing time (acting upon an initial scale of segregation of 1 mm and calculated using Equation 2) of ~6×10^{-4} s.

These indicate extremely rapid mixing and, provided it is known how best to exploit these mixing rates (feed tube location etc.), then rotor/stator mixers will create suitable conditions for the intensification of processes.

3.3 Conclusions

i Rotor/stator mixers are inefficient pumps (10 - 15%).

ii Approximately 70% of the shaft power input to a rotor/stator mixer is dissipated through hydraulic and leakage losses.

iii This proportion is relatively insensitive to small changes in flow rate (it appears to depend more upon shaft speed), so the mixer can be used in a loop where small changes in flow rate may occur.

iv At 3000 rpm ε, the turbulent energy dissipation rate per unit mass is estimated to be approximately 5500 W kg^{-1}. This corresponds to a micro mixing timescale of approximately 7×10^{-4} s in water at room temperature.

v The rotor/stator mixer would appear to be a suitable device for chemical reactions with intrinsic rates ~10^{-3} s.

4 REFERENCES

1. **Baldyga, J. & Bourne, J. R.** "A Fluid Mechanical approach to turbulent mixing and chemical reaction." Part II Micro mixing in the light of turbulence theory. Chem. Eng. Commun 28 (1984). pp 243-258.

2. **Baldyga, J. & Bourne, J. R.** "Simplification of Micro mixing Calculations I. Derivation and Application of New Model." Chem. Eng. J 42, 83-92 (1989). pp 83-92.

3. **Baldyga, J., Bourne, J.R., Dubuis, B., Etchells, A. W. Gholap, R. V. and Zimmerman, B.** "Jet reactor scale-up for mixing controlled reactions." Trans IChemE, Vol 73, Part A, July 1995. pp 497-502.

4. **Corrsin, S.** "The isotropic turbulent mixer: part II. Arbitrary Schmidt number." A.I.Ch.E.J vol 10 (1964). p 870.

5. **Bourne, J. R. & Garcias-Rosas, J.** "Rotor Stator Mixers for Rapid Micro mixing." Chem. Eng. Res. Des, Vol 64. (1986). pp 11-17.

6. **Bourne, J. R. & Studer, M.** "Fast Reactions in Rotor/stator Mixers of Different Size." Chem. Eng. Process 31, (1992). pp 285-296.

7. **Anderson, H. H.** "Centrifugal pumps." 3rd edition. Trade and technical press. ISBN 85461 076 6. (1980).

8. **Stepanoff, A. J.** "Centrifugal and axial flow pumps, theory design and application." 2nd edition. John Wiley and Sons ISBN 0-471-82137-3. (1957).

9. **Sparks, T. G.** "Power balance and residence time distribution tests on a rotor/stator mixer." HILINE interim report number HLP05, BHR Group Limited. December 1994.

10. **Karassik, I. J. Krutzsch, W. C. Fraser, W. H. and Messina, J. P. eds.** "Pump Handbook." 2nd edition. McGraw -Hill, New York. ISBN 0-07-033302-5. (1986).